
Elements of

X-RAY

DIFFRACTION

SECOND EDITION

B. D. CULLITY

Department of Metallurgical Engineering and Materials Science
University of Notre Dame



ADDISON-WESLEY PUBLISHING COMPANY INC.

Reading, Massachusetts - Menlo Park, California
London - Amsterdam - Don Mills, Ontario - Sydney

This book is in the
Addison-Wesley Series in Metallurgy and Materials

Morris Cohen
Consulting Editor

Copyright © 1978, 1956 by Addison-Wesley Publishing Company, Inc. Philippines copyright 1978 by Addison-Wesley Publishing Company, Inc.

All rights reserved. No part of this publication may be reproduced, stored in a retrieval system, or transmitted, in any form or by any means, electronic, mechanical, photocopying, recording, or otherwise, without the prior written permission of the publisher. Printed in the United States of America. Published simultaneously in Canada. Library of Congress Catalog Card No. 77-73950.

ISBN 0-201-01174-3

24 25 26 27 28 29 30 MA 959493

Preface

X-ray diffraction is a tool for the investigation of the fine structure of matter. This technique had its beginnings in von Laue's discovery in 1912 that crystals diffract x-rays, the manner of the diffraction revealing the structure of the crystal. At first, x-ray diffraction was used only for the determination of crystal structure. Later on, however, other uses were developed, and today the method is applied not only to structure determination, but to such diverse problems as chemical analysis and stress measurement, to the study of phase equilibria and the measurement of particle size, to the determination of the orientation of one crystal or the ensemble of orientations in a polycrystalline aggregate.

The purpose of this book is to acquaint the reader who has no previous knowledge of the subject with the theory of x-ray diffraction, the experimental methods involved, and the main applications. Because the author is a metallurgist, the majority of these applications are described in terms of metals and alloys. However, little or no modification of experimental method is required for the examination of nonmetallic materials, inasmuch as the physical principles involved do not depend on the material investigated. This book should therefore be useful to metallurgists, chemists, physicists, ceramists, mineralogists, etc., namely, to all who use x-ray diffraction purely as a laboratory tool for the sort of problems already mentioned.

Members of this group, unlike x-ray crystallographers, are not normally concerned with the determination of complex crystal structures. For this reason the rotating-crystal method and space-group theory, the two chief tools in the solution of such structures, are described only briefly.

This is a book of principles and methods intended for the student, and not a reference book for the advanced research worker. Thus no metallurgical data are given beyond those necessary to illustrate the diffraction methods involved. For example, the theory and practice of determining preferred orientation are treated in detail, but the reasons for preferred orientation, the conditions affecting its development, and actual orientations found in specific metals and alloys are not described, because these topics are adequately covered in existing books. In short, x-ray diffraction is stressed rather than metallurgy.

The book is divided into three main parts: fundamentals, experimental methods, and applications. The subject of crystal structure is approached through, and based on, the concept of the point lattice (Bravais lattice), because the point lattice of a substance is so closely related to its diffraction pattern. X-ray diffraction

phenomena are rather sharply divisible into those effects that are understandable in terms of the Bragg law and those that require a more advanced treatment, based on the reciprocal lattice. This book is written entirely in terms of the Bragg law and can be read without any knowledge of the reciprocal lattice. My experience with teaching x-ray diffraction to senior students in metallurgy, for many of whom this book represents a terminal course in the subject, is that there is insufficient time to attain both a real facility for "reciprocal thinking" and a good knowledge of the many applications of diffraction. I therefore prefer the Bragg-law approach for a first course. Those instructors who wish to introduce the reciprocal lattice at the beginning can interpose Appendix 1, which contains the rudiments of the subject, between Chapters 2 and 3.

Chapters on chemical analysis by x-ray diffraction and x-ray spectroscopy are included because of the industrial importance of these analytical methods. Electron and neutron diffraction are treated in appendices.

This second edition includes an account of new developments made possible by the semiconductor detector and pulse-height analysis, namely, energy-dispersive spectrometry and diffractometry. Applications of position-sensitive detectors are also described.

A new section is devoted to x-ray topography and other x-ray methods of assessing the quality of single crystals. Other additions include a quantitative treatment of the temperature factor and descriptions of the Auger effect, micro-cameras and Guinier cameras, and microanalysis in the electron microscope. References to original papers are now given, and the tables of wavelengths and absorption coefficients have been expanded.

This edition contains more material on the measurement of preferred orientation and residual stress than the first edition, but the former chapter on chemical analysis by x-ray absorption has been dropped, as being of minor interest to most readers.

The first edition carried the following acknowledgements:

Like any author of a technical book, I am greatly indebted to previous writers on this and allied subjects. I must also acknowledge my gratitude to two of my former teachers at the Massachusetts Institute of Technology, Professor B. E. Warren and Professor John T. Norton: they will find many an echo of their own lectures in these pages. Professor Warren has kindly allowed me to use many problems of his devising, and the advice and encouragement of Professor Norton has been invaluable. My colleague at Notre Dame, Professor G. C. Kuczynski, has read the entire book as it was written, and his constructive criticisms have been most helpful. I would also like to thank the following, each of whom has read one or more chapters and offered valuable suggestions: Paul A. Beck, Herbert Friedman, S. S. Hsu, Lawrence Lee, Walter C. Miller, William Parrish, Howard Pickett, and Bernard Waldman. I am also indebted to C. G. Dunn for the loan of illustrative material and to many graduate students, August Freda in particular, who have helped with the preparation of diffraction patterns. Finally, but not perfunctorily, I wish to thank Miss Rose Kunkle for her patience and diligence in preparing the typed manuscript.

In the preparation of the second edition I have been helped in many ways by Charles W. Allen, A. W. Danko, Ron Jenkins, Paul D. Johnson, A. R. Lang, John W. Mihelich, J. B. Newkirk, Paul S. Prevey, B. E. Warren, Carl Cm. Wu, and Leo Zwell. To all these, my best thanks.

*Notre Dame, Indiana
November 1977*

B. D. Cullity

Contents

FUNDAMENTALS

Chapter 1 Properties of X-rays

1–1	Introduction	3
1–2	Electromagnetic radiation	3
1–3	The continuous spectrum	6
1–4	The characteristic spectrum	8
1–5	Absorption	13
1–6	Filters	19
1–7	Production of x-rays	21
1–8	Detection of x-rays	27
1–9	Safety precautions	29

Chapter 2 Geometry of Crystals

2–1	Introduction	32
2–2	Lattices	32
2–3	Crystal systems	34
2–4	Symmetry	37
2–5	Primitive and nonprimitive cells	39
2–6	Lattice directions and planes	41
2–7	Crystal structure	47
2–8	Atom sizes and coordination	56
2–9	Crystal shape	58
2–10	Twinned crystals	59
2–11	The stereographic projection	63

Chapter 3 Diffraction I: Directions of Diffracted Beams

3–1	Introduction	81
3–2	Diffraction	82
3–3	The Bragg law	86
3–4	X-ray spectroscopy	88
3–5	Diffraction directions	91
3–6	Diffraction methods	92
3–7	Diffraction under nonideal conditions	99

Chapter 4 Diffraction II: Intensities of Diffracted Beams

4-1	Introduction	107
4-2	Scattering by an electron	107
4-3	Scattering by an atom	111
4-4	Scattering by a unit cell	115
4-5	Some useful relations	121
4-6	Structure-factor calculations	121
4-7	Application to powder method	126
4-8	Multiplicity factor	127
4-9	Lorentz factor	127
4-10	Absorption factor	132
4-11	Temperature factor	135
4-12	Intensities of powder pattern lines	139
4-13	Examples of intensity calculations	140
4-14	Measurement of x-ray intensity	143

EXPERIMENTAL METHODS**Chapter 5 Laue Photographs**

5-1	Introduction	149
5-2	Cameras	150
5-3	Specimens and holders	155
5-4	Collimators	156
5-5	The shapes of Laue spots	158

Chapter 6 Powder Photographs

6-1	Introduction	161
6-2	Debye-Scherrer method	162
6-3	Specimen preparation	166
6-4	Film loading	167
6-5	Cameras for special conditions	168
6-6	Focusing cameras	170
6-7	Seemann-Bohlin camera	170
6-8	Back-reflection focusing cameras	172
6-9	Pinhole photographs	175
6-10	Microbeams and microcameras	177
6-11	Choice of radiation	178
6-12	Background radiation	179
6-13	Crystal monochromators	180
6-14	Guinier cameras	183
6-15	Measurement of line position	184
6-16	Measurement of line intensity	185

Chapter 7 Diffractometer and Spectrometer Measurements

7-1	Introduction	188
7-2	General features	189

Fundamentals

- 1. Properties of X-Rays**
- 2. Geometry of Crystals**
- 3. Diffraction I: Directions of Diffracted Beams**
- 4. Diffraction II: Intensities of Diffracted Beams**

Properties of X-rays

1-1 INTRODUCTION

X-rays were discovered in 1895 by the German physicist Roentgen and were so named because their nature was unknown at the time. Unlike ordinary light, these rays were invisible, but they traveled in straight lines and affected photographic film in the same way as light. On the other hand, they were much more penetrating than light and could easily pass through the human body, wood, quite thick pieces of metal, and other "opaque" objects.

It is not always necessary to understand a thing in order to use it, and x-rays were almost immediately put to use by physicians and, somewhat later, by engineers, who wished to study the internal structure of opaque  objects. By placing a source of x-rays on one side of the object and photographic film on the other, a shadow picture, or *radiograph*, could be made, the less dense portions of the object allowing a greater proportion of the x-radiation to pass through than the more dense. In this way the point of fracture in a broken bone or the position of a crack in a metal casting could be located.

Radiography was thus initiated without any precise understanding of the radiation used, because it was not until 1912 that the exact nature of x-rays was established. In that year the phenomenon of x-ray *diffraction* by crystals was discovered, and this discovery simultaneously proved the wave nature of x-rays and provided a new method for investigating the fine structure of matter. Although radiography is a very important tool in itself and has a wide field of applicability, it is ordinarily limited in the internal detail it can resolve, or disclose, to sizes of the order of 10^{-1} cm. Diffraction, on the other hand, can indirectly reveal details of internal structure of the order of 10^{-8} cm in size, and it is with this phenomenon, and its applications to metallurgical problems, that this book is concerned. The properties of x-rays and the internal structure of crystals are here described in the first two chapters as necessary preliminaries to the discussion of the diffraction of x-rays by crystals which follows.

1-2 ELECTROMAGNETIC RADIATION

We know today that x-rays are electromagnetic radiation of exactly the same nature as light but of very much shorter wavelength. The unit of measurement in the x-ray region is the angstrom (\AA), equal to 10^{-8} cm, and x-rays used in diffraction have wavelengths lying approximately in the range 0.5–2.5 \AA , whereas the wavelength of visible light is of the order of 6000 \AA . X-rays therefore occupy the region

4 Properties of x-rays

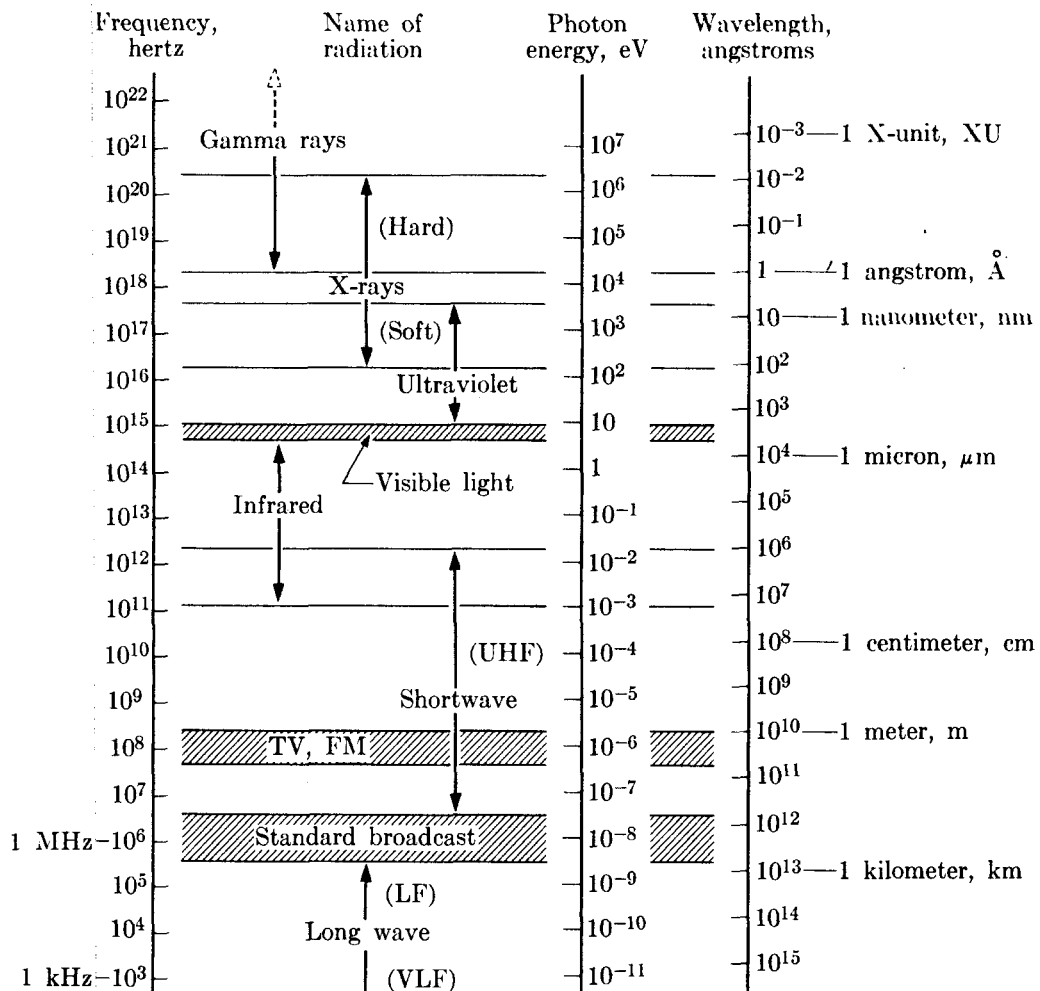


Fig. 1-1 The electromagnetic spectrum. The boundaries between regions are arbitrary, since no sharp upper or lower limits can be assigned. (H. A. Enge, M. R. Wehr, J. A. Richards, *Introduction to Atomic Physics*, Addison-Wesley Publishing Company, Inc., Reading, Mass., 1972).

between gamma and ultraviolet rays in the complete electromagnetic spectrum (Fig. 1-1). Other units sometimes used to measure x-ray wavelength are the X unit (XU) and the kilo X unit ($k\text{X} = 1000 \text{ XU}$). The $k\text{X}$ unit, whose origin will be described in Sec. 3-4, is only slightly larger than the angstrom. The approved SI unit for wavelengths in the x-ray region is the nanometer:

$$1 \text{ nanometer} = 10^{-9} \text{ m} = 10 \text{ \AA}.$$

This unit has not become popular.

It is worth while to review briefly some properties of electromagnetic waves. Suppose a monochromatic beam of x-rays, i.e., x-rays of a single wavelength, is traveling in the x direction (Fig. 1-2). Then it has associated with it an electric field \mathbf{E} in, say, the y direction and, at right angles to this, a magnetic field \mathbf{H} in the z direction. If the electric field is confined to the xy -plane as the wave travels along, the wave is said to be plane-polarized. (In a completely unpolarized wave, the

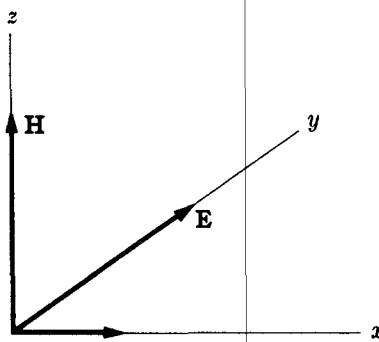


Fig. 1-2 Electric and magnetic fields associated with a wave moving in the x -direction.

electric field vector \mathbf{E} and hence the magnetic field vector \mathbf{H} can assume all directions in the yz -plane.) The magnetic field is of no concern to us here and we need not consider it further.

In the plane-polarized wave considered, \mathbf{E} is not constant with time but varies from a maximum in the $+y$ direction through zero to a maximum in the $-y$ direction and back again, at any particular point in space, say $x = 0$. At any instant of time, say $t = 0$, \mathbf{E} varies in the same fashion with distance along the x -axis. If both variations are assumed to be sinusoidal, they may be expressed in the one equation

$$\mathbf{E} = A \sin 2\pi \left(\frac{x}{\lambda} - vt \right), \quad (1-1)$$

where A = amplitude of the wave, λ = wavelength, and v = frequency. The variation of \mathbf{E} is not necessarily sinusoidal, but the exact form of the wave matters little; the important feature is its periodicity. Figure 1-3 shows the variation of \mathbf{E} graphically. The wavelength and frequency are connected by the relation

$$\lambda = \frac{c}{v}, \quad (1-2)$$

where c = velocity of light = 3.00×10^8 m/sec.

Electromagnetic radiation, such as a beam of x-rays, carries energy, and the rate of flow of this energy through unit area perpendicular to the direction of motion of the wave is called the *intensity* I . The average value of the intensity is proportional to the square of the amplitude of the wave, i.e., proportional to A^2 . In absolute units, intensity is measured in joules/m²/sec, but this measurement is a difficult one and is seldom carried out; most x-ray intensity measurements are made on a relative basis in arbitrary units, such as the degree of blackening of a photographic film exposed to the x-ray beam.

An accelerated electric charge radiates energy. The acceleration may, of course, be either positive or negative, and thus a charge continuously oscillating about some mean position acts as an excellent source of electromagnetic radiation. Radio waves, for example, are produced by the oscillation of charge back and forth in the broadcasting antenna, and visible light by oscillating electrons in the atoms

6 Properties of x-rays

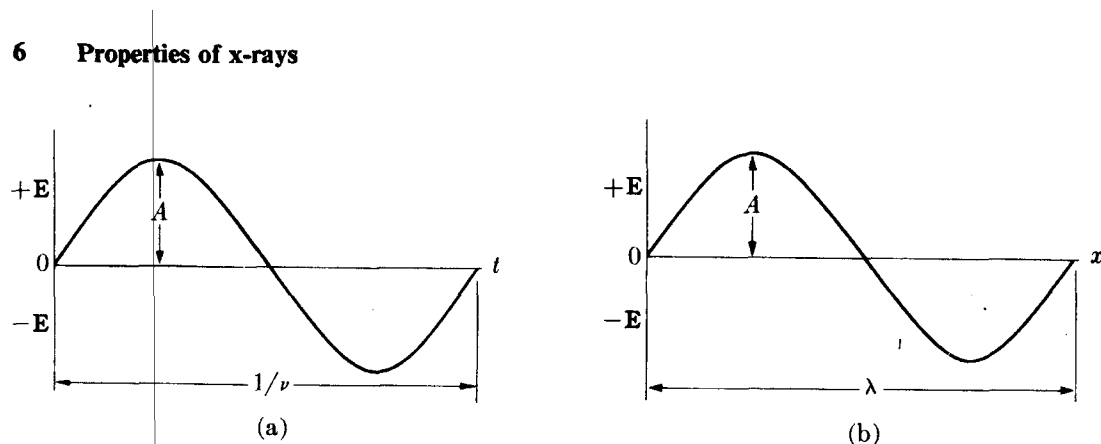


Fig. 1-3 The variation of E , (a) with t at a fixed value of x and (b) with x at a fixed value of t .

of the substance emitting the light. In each case, the frequency of the radiation is the same as the frequency of the oscillator which produces it.

Up to now we have been considering electromagnetic radiation as *wave* motion in accordance with classical theory. According to the quantum theory, however, electromagnetic radiation can also be considered as a stream of *particles* called quanta or photons. Each photon has associated with it an amount of energy hv , where h is Planck's constant (6.63×10^{-34} joule·sec). A link is thus provided between the two viewpoints, because we can use the frequency of the wave motion to calculate the energy of the photon. Radiation thus has a dual wave-particle character, and we will use sometimes one concept, sometimes the other, to explain various phenomena, giving preference in general to the classical wave theory whenever it is applicable.

1-3 THE CONTINUOUS SPECTRUM

X-rays are produced when any electrically charged particle of sufficient kinetic energy is rapidly decelerated. Electrons are usually used for this purpose, the radiation being produced in an *x-ray tube* which contains a source of electrons and two metal electrodes. The high voltage maintained across these electrodes, some tens of thousands of volts, rapidly draws the electrons to the anode, or *target*, which they strike with very high velocity. X-rays are produced at the point of impact and radiate in all directions. If e is the charge on the electron (1.60×10^{-19} coulomb) and V the voltage across the electrodes, then the kinetic energy (in joules) of the electrons on impact is given by the equation

$$KE = eV = \frac{1}{2}mv^2, \quad (1-3)$$

where m is the mass of the electron (9.11×10^{-31} kg) and v its velocity in m/sec just before impact. At a tube voltage of 30,000 volts, this velocity is about one-third that of light. Most of the kinetic energy of the electrons striking the target is converted into heat, less than 1 percent being transformed into x-rays.

When the rays coming from the target are analyzed, they are found to consist

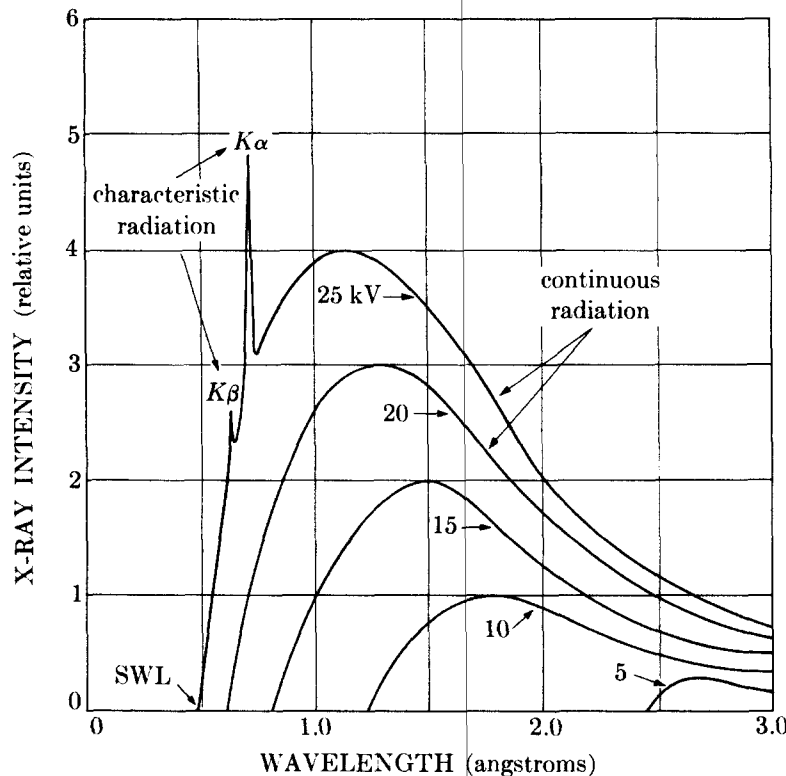


Fig. 1-4 X-ray spectrum of molybdenum as a function of applied voltage (schematic). Line widths not to scale.

of a mixture of different wavelengths, and the variation of intensity with wavelength is found to depend on the tube voltage. Figure 1-4 shows the kind of curves obtained. The intensity is zero up to a certain wavelength, called the *short-wavelength limit* (λ_{SWL}), increases rapidly to a maximum and then decreases, with no sharp limit on the long wavelength side. When the tube voltage is raised, the intensity of all wavelengths increases, and both the short-wavelength limit and the position of the maximum shift to shorter wavelengths. We are concerned now with the smooth curves in Fig. 1-4, those corresponding to applied voltages of 20 kV or less in the case of a molybdenum target. The radiation represented by such curves is called *heterochromatic, continuous, or white* radiation, since it is made up, like white light, of rays of many wavelengths. White radiation is also called *bremsstrahlung*, German for "braking radiation," because it is caused by electron deceleration.

The continuous spectrum is due to the rapid deceleration of the electrons hitting the target since, as mentioned above, any decelerated charge emits energy. Not every electron is decelerated in the same way, however; some are stopped in one impact and give up all their energy at once, while others are deviated this way and that by the atoms of the target, successively losing fractions of their total kinetic energy until it is all spent. Those electrons which are stopped in one impact will give rise to photons of maximum energy, i.e., to x-rays of minimum wave-

8 Properties of x-rays

length. Such electrons transfer all their energy eV into photon energy and we may write

$$eV = h\nu_{\max},$$

$$\lambda_{SWL} = \lambda_{\min} = \frac{c}{\nu_{\max}} = \frac{hc}{eV},$$

$$\lambda_{SWL} = \frac{(6.626 \times 10^{-34})(2.998 \times 10^8)}{(1.602 \times 10^{-19}) V} \text{ meter,}$$

$$\lambda_{SWL} = \frac{12.40 \times 10^3}{V}.$$

(1-4)

This equation gives the short-wavelength limit (in angstroms) as a function of the applied voltage V . If an electron is not completely stopped in one encounter but undergoes a glancing impact which only partially decreases its velocity, then only a fraction of its energy eV is emitted as radiation and the photon produced has energy less than $h\nu_{\max}$. In terms of wave motion, the corresponding x-ray has a frequency lower than ν_{\max} and a wavelength longer than λ_{SWL} . The totality of these wavelengths, ranging upward from λ_{SWL} , constitutes the continuous spectrum.

We now see why the curves of Fig. 1-4 become higher and shift to the left as the applied voltage is increased, since the number of photons produced per second and the average energy per photon are both increasing. The total x-ray energy emitted per second, which is proportional to the area under one of the curves of Fig. 1-4, also depends on the atomic number Z of the target and on the tube current i , the latter being a measure of the number of electrons per second striking the target. This total x-ray intensity is given by

$$I_{\text{cont. spectrum}} = AiZV^m, \quad (1-5)$$

where A is a proportionality constant and m is a constant with a value of about 2. Where large amounts of white radiation are desired, it is therefore necessary to use a heavy metal like tungsten ($Z = 74$) as a target and as high a voltage as possible. Note that the material of the target affects the intensity but not the wavelength distribution of the continuous spectrum.

1-4 THE CHARACTERISTIC SPECTRUM

When the voltage on an x-ray tube is raised above a certain critical value, characteristic of the target metal, sharp intensity maxima appear at certain wavelengths, superimposed on the continuous spectrum. Since they are so narrow and since their wavelengths are characteristic of the target metal used, they are called *characteristic lines*. These lines fall into several sets, referred to as K , L , M , etc., in the order of increasing wavelength, all the lines together forming the *characteristic spectrum* of the metal used as the target. For a molybdenum target the K lines have wavelengths of about 0.7 Å, the L lines about 5 Å, and the M lines still longer wavelengths. Ordinarily only the K lines are useful in x-ray diffraction,

the longer-wavelength lines being too easily absorbed. There are several lines in the K set, but only the three strongest are observed in normal diffraction work. These are the $K\alpha_1$, $K\alpha_2$, and $K\beta_1$, and for molybdenum their wavelengths are approximately:

$$\begin{aligned}K\alpha_1 &: 0.709 \text{ \AA}, \\K\alpha_2 &: 0.714, \\K\beta_1 &: 0.632.\end{aligned}$$

The α_1 and α_2 components have wavelengths so close together that they are not always resolved as separate lines; if resolved, they are called the $K\alpha$ doublet and, if not resolved, simply the $K\alpha$ line.* Similarly, $K\beta_1$ is usually referred to as the $K\beta$ line, with the subscript dropped. $K\alpha_1$ is always about twice as strong as $K\alpha_2$, while the intensity ratio of $K\alpha_1$ to $K\beta_1$ depends on atomic number but averages about 5/1.

These characteristic lines may be seen in the uppermost curve of Fig. 1-4. Since the critical K excitation voltage, i.e., the voltage necessary to excite K characteristic radiation, is 20.01 kV for molybdenum, the K lines do not appear in the lower curves of Fig. 1-4. An increase in voltage above the critical voltage increases the intensities of the characteristic lines relative to the continuous spectrum but *does not change their wavelengths*. Figure 1-5 shows the spectrum of molybdenum at 35 kV on a compressed vertical scale relative to that of Fig. 1-4; the increased voltage has shifted the continuous spectrum to still shorter wavelengths and increased the intensities of the K lines relative to the continuous spectrum but has not changed their wavelengths.

The intensity of any characteristic line, measured above the continuous spectrum, depends both on the tube current i and the amount by which the applied voltage V exceeds the critical excitation voltage for that line. For a K line, the intensity is given approximately by

$$I_{K \text{ line}} = Bi(V - V_K)^n, \quad (1-6)$$

where B is a proportionality constant, V_K the K excitation voltage, and n a constant with a value of about 1.5. (Actually, n is not a true constant but depends on V and varies from 1 to 2.) The intensity of a characteristic line can be quite large: for example, in the radiation from a copper target operated at 30 kV, the $K\alpha$ line has an intensity about 90 times that of the wavelengths immediately adjacent to it in the continuous spectrum. Besides being very intense, characteristic lines are also very narrow, most of them less than 0.001 Å wide measured at half their maximum intensity, as indicated in Fig. 1-5. The existence of this strong sharp $K\alpha$ line is what makes a great deal of x-ray diffraction possible, because many diffraction

* The wavelength of an unresolved $K\alpha$ doublet is usually taken as the weighted average of the wavelengths of its components, $K\alpha_1$ being given twice the weight of $K\alpha_2$, since it is twice as strong. Thus the wavelength of the unresolved Mo $K\alpha$ line is

$$\frac{1}{3}(2 \times 0.709 + 0.714) = 0.711 \text{ \AA}.$$

10 Properties of x-rays

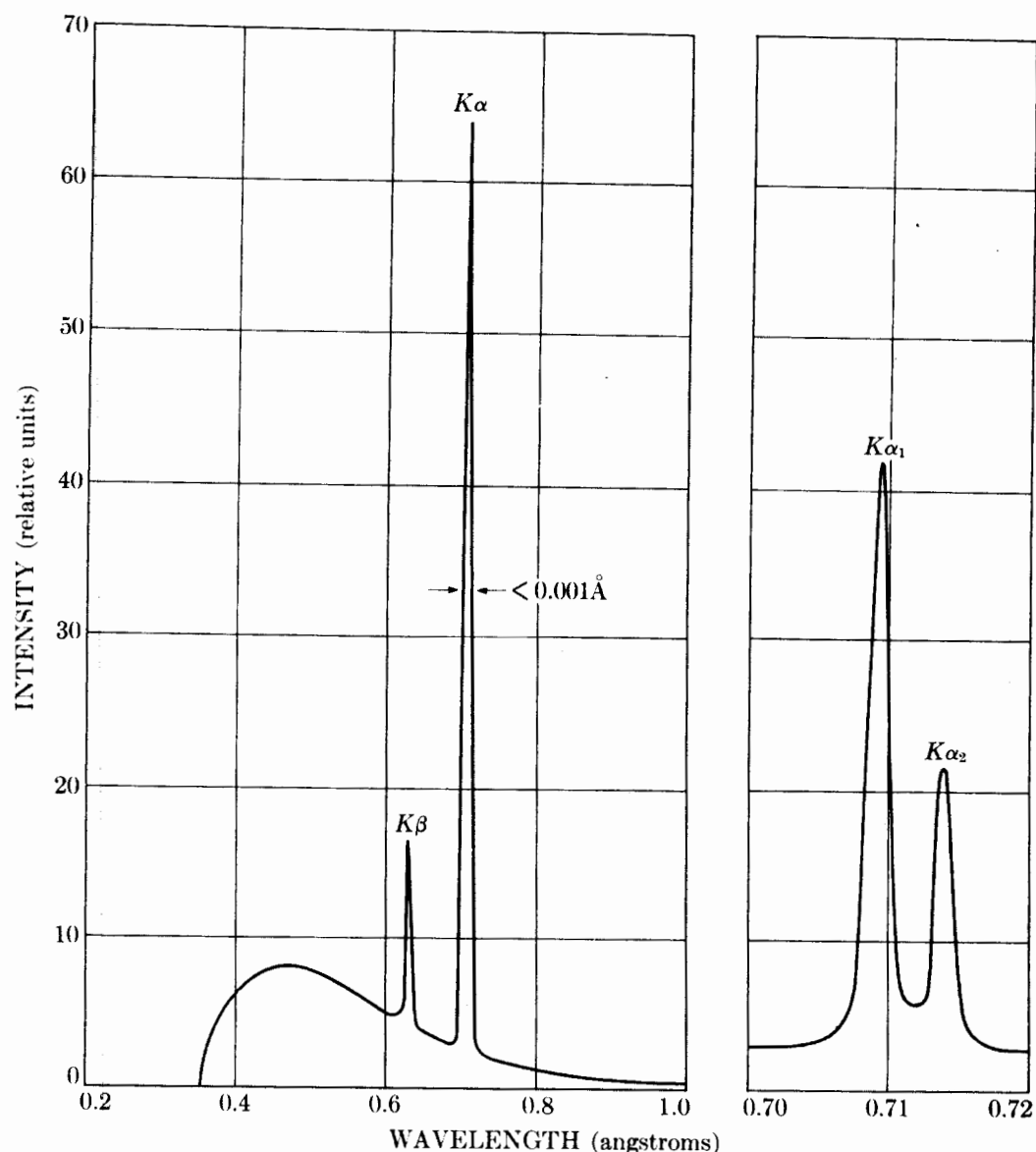


Fig. 1-5 Spectrum of Mo at 35 kV (schematic). Line widths not to scale. Resolved $K\alpha$ doublet is shown on an expanded wavelength scale at right.

experiments require the use of monochromatic or approximately monochromatic radiation.

The characteristic x-ray lines were discovered by W. H. Bragg and systematized by H. G. Moseley. The latter found that the wavelength of any particular line decreased as the atomic number of the emitter increased. In particular, he found a linear relation (Moseley's law) between the square root of the line frequency ν and the atomic number Z :

$$\sqrt{\nu} = C(Z - \sigma), \quad (1-7)$$

where C and σ are constants. This relation is plotted in Fig. 1-6 for the $K\alpha_1$ and $L\alpha_1$ lines, the latter being the strongest line in the L series. These curves show,

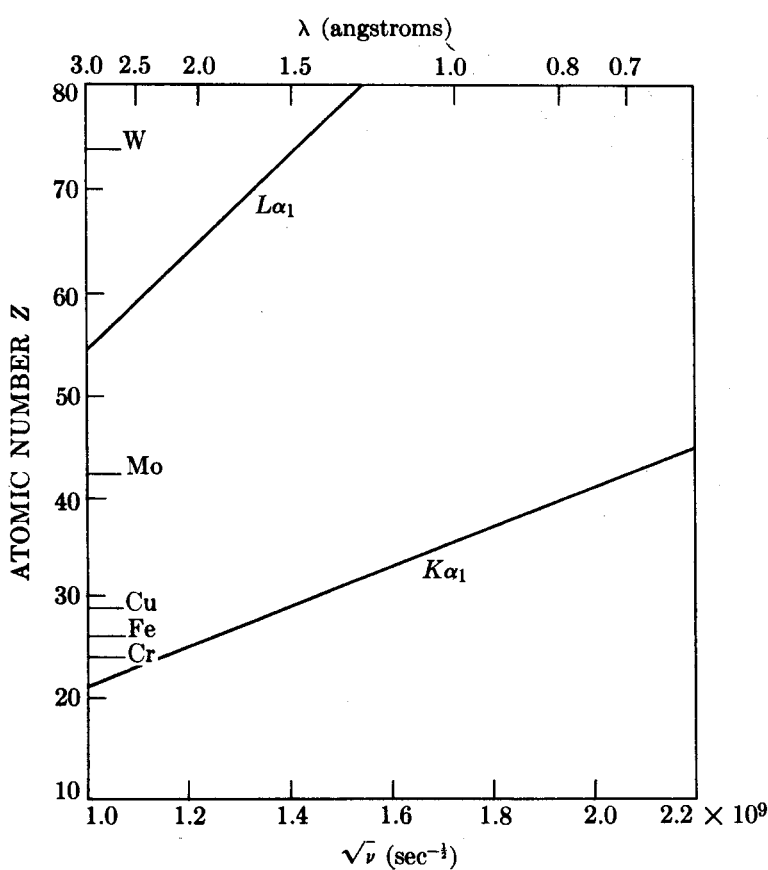


Fig. 1-6 Moseley's relation between $\sqrt{\nu}$ and Z for two characteristic lines.

incidentally, that L lines are not always of long wavelength: the $L\alpha_1$ line of a heavy metal like tungsten, for example, has about the same wavelength as the $K\alpha_1$ line of copper, namely about 1.5 Å. The wavelengths of the characteristic x-ray lines of almost all the known elements have been precisely measured, mainly by M. Siegbahn and his associates, and a tabulation of these wavelengths for the strongest lines of the K and L series will be found in Appendix 7. Data on weaker lines can be found in Vol. 4 of the *International Tables for X-Ray Crystallography* [G.11].*

While the continuous spectrum is caused by the rapid deceleration of electrons by the target, the origin of the characteristic spectrum lies in the atoms of the target material itself. To understand this phenomenon, it is enough to consider an atom as consisting of a central nucleus surrounded by electrons lying in various shells (Fig. 1-7), where the designation K, L, M, \dots corresponds to the principal quantum number $n = 1, 2, 3, \dots$. If one of the electrons bombarding the target has sufficient kinetic energy, it can knock an electron out of the K shell, leaving the atom in an excited, high-energy state. One of the outer electrons immediately falls into the vacancy in the K shell, emitting energy in the process, and the atom is

* Numbers in square brackets relate to the references at the end of the book. "G" numbers are keyed to the General References.

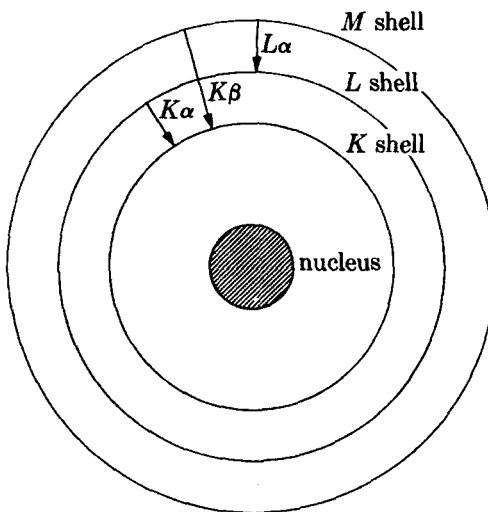


Fig. 1-7 Electronic transitions in an atom (schematic). Emission processes indicated by arrows.

once again in its normal energy state. The energy emitted is in the form of radiation of a definite wavelength and is, in fact, characteristic *K* radiation.

The *K*-shell vacancy may be filled by an electron from any one of the outer shells, thus giving rise to a series of *K* lines; $K\alpha$ and $K\beta$ lines, for example, result from the filling of a *K*-shell vacancy by an electron from the *L* or *M* shells, respectively. It is *possible* to fill a *K*-shell vacancy from either the *L* or *M* shell, so that one atom of the target may be emitting $K\alpha$ radiation while its neighbor is emitting $K\beta$; however, it is more *probable* that a *K*-shell vacancy will be filled by an *L* electron than by an *M* electron, and the result is that the $K\alpha$ line is stronger than the $K\beta$ line. It also follows that it is impossible to excite one *K* line without exciting all the others. *L* characteristic lines originate in a similar way: an electron is knocked out of the *L* shell and the vacancy is filled by an electron from some outer shell.

We now see why there should be a critical excitation voltage for characteristic radiation. *K* radiation, for example, cannot be excited unless the tube voltage is such that the bombarding electrons have enough energy to knock an electron out of the *K* shell of a target atom. If W_K is the work required to remove a *K* electron, then the necessary kinetic energy of the electrons is given by

$$\frac{1}{2}mv^2 = W_K. \quad (1-8)$$

It requires less energy to remove an *L* electron than a *K* electron, since the former is farther from the nucleus; it therefore follows that the *L* excitation voltage is less than the *K* and that *K* characteristic radiation cannot be produced without *L*, *M*, etc., radiation accompanying it.

1-5 ABSORPTION

Further understanding of the electronic transitions which can occur in atoms can be gained by considering not only the interaction of electrons and atoms, but also the interaction of x-rays and atoms. When x-rays encounter any form of matter, they are partly transmitted and partly absorbed. Experiment shows that the fractional decrease in the intensity I of an x-ray beam as it passes through any homogeneous substance is proportional to the distance traversed x . In differential form,

$$-\frac{dI}{I} = \mu dx, \quad (1-9)$$

where the proportionality constant μ is called the *linear absorption coefficient* and is dependent on the substance considered, its density, and the wavelength of the x-rays. Integration of Eq. (1-9) gives

$$I_x = I_0 e^{-\mu x}, \quad (1-10)$$

where I_0 = intensity of incident x-ray beam and I_x = intensity of transmitted beam after passing through a thickness x .

The linear absorption coefficient μ is proportional to the density ρ , which means that the quantity μ/ρ is a constant of the material and independent of its physical state (solid, liquid, or gas). This latter quantity, called the *mass absorption coefficient*, is the one usually tabulated. Equation (1-10) may then be rewritten in a more usable form:

$$I_x = I_0 e^{-(\mu/\rho)\rho x}. \quad (1-11)$$

Values of the mass absorption coefficient μ/ρ are given in Appendix 8 for various characteristic wavelengths used in diffraction.

It is occasionally necessary to know the mass absorption coefficient of a substance containing more than one element. Whether the substance is a mechanical mixture, a solution, or a chemical compound, and whether it is in the solid, liquid, or gaseous state, its mass absorption coefficient is simply the weighted average of the mass absorption coefficients of its constituent elements. If w_1, w_2 , etc., are the weight fractions of elements 1, 2, etc., in the substance and $(\mu/\rho)_1, (\mu/\rho)_2$, etc., their mass absorption coefficients, then the mass absorption coefficient of the substance is given by

$$\frac{\mu}{\rho} = w_1 \left(\frac{\mu}{\rho} \right)_1 + w_2 \left(\frac{\mu}{\rho} \right)_2 + \dots \quad (1-12)$$

The way in which the absorption coefficient varies with wavelength gives the clue to the interaction of x-rays and atoms. The lower curve of Fig. 1-8 shows this variation for a nickel absorber; it is typical of all materials. The curve consists of two similar branches separated by a sharp discontinuity called an *absorption edge*.

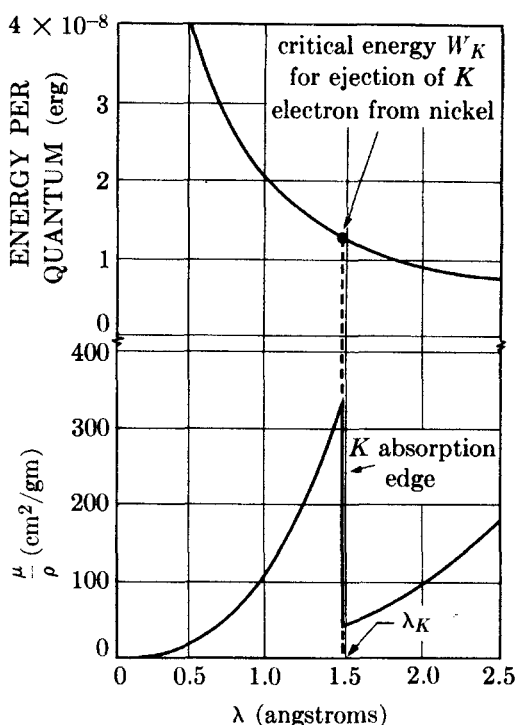


Fig. 1-8 Variation with wavelength of the energy per x-ray quantum and of the mass absorption coefficient of nickel.

Along each branch the absorption coefficient varies with wavelength approximately according to a relation of the form

$$\frac{\mu}{\rho} = k\lambda^3 Z^3, \quad (1-13)$$

where k = a constant, with a different value for each branch of the curve, and Z = atomic number of absorber. Short-wavelength x-rays are therefore highly penetrating and are termed *hard*, while long-wavelength x-rays are easily absorbed and are said to be *soft*.

Matter absorbs x-rays in two distinct ways, by scattering and by true absorption, and these two processes together make up the total absorption measured by the quantity μ/ρ . The *scattering* of x-rays by atoms is similar in many ways to the scattering of visible light by dust particles in the air. It takes place in all directions, and since the energy in the scattered beams does not appear in the transmitted beam, it is, so far as the transmitted beam is concerned, said to be absorbed (Fig. 1-9). The phenomenon of scattering will be discussed in greater detail in Chap. 4; it is enough to note here that, except for the very light elements, it is responsible for only a small fraction of the total absorption. *True absorption* is caused by electronic transitions within the atom and is best considered from the viewpoint of the quantum theory of radiation. Just as an electron of sufficient energy can knock a K electron, for example, out of an atom and thus cause the emission of K characteristic radiation, so also can an incident quantum of x-rays,

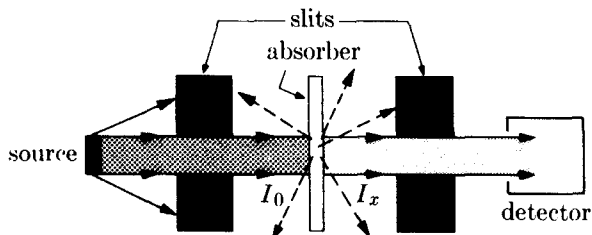


Fig. 1-9 Experimental arrangement for measuring absorption. Narrow slits or pinholes define the beam. The detector measures the intensity I_0 of the incident beam when the absorber is removed and the intensity I_x of the transmitted beam when the absorber is in place. Although the scattered radiation (dashed lines) does not represent energy absorbed in the specimen, it does constitute energy removed from the beam and accordingly forms part of the total absorption represented by the coefficient μ/ρ .

provided it has the same minimum amount of energy W_K . In the latter case, the ejected electron is called a *photoelectron* and the emitted characteristic radiation is called *fluorescent radiation*. It radiates in all directions and has exactly the same wavelength as the characteristic radiation caused by electron bombardment of a metal target. (In effect, an atom emits the same K radiation no matter how the K -shell vacancy was originally created.) This phenomenon is the x-ray counterpart of the photoelectric effect in the ultraviolet region of the spectrum; there, photoelectrons can be ejected from the outer shells of a metal atom by the action of ultraviolet radiation, provided the latter has a wavelength less than a certain critical value.

To say that the energy of the incoming quanta must exceed a certain value W_K is equivalent to saying that the wavelength must be less than a certain value λ_K , since the energy per quantum is hv and wavelength is inversely proportional to frequency. These relations may be written

$$W_K = h\nu_K = \frac{hc}{\lambda_K}, \quad (1-14)$$

where ν_K and λ_K are the frequency and wavelength, respectively, of the K absorption edge. Now consider the absorption curve of Fig. 1-8 in light of the above. Suppose that x-rays of wavelength 2.5 Å are incident on a sheet of nickel and that this wavelength is continuously decreased. At first the absorption coefficient is about $180 \text{ cm}^2/\text{gm}$, but, as the wavelength decreases, the frequency increases and so does the energy per quantum, as shown by the upper curve, thus causing the absorption coefficient to decrease, since the greater the energy of a quantum the more easily it passes through an absorber. When the wavelength is reduced just below the critical value λ_K , which is 1.488 Å for nickel, the absorption coefficient suddenly increases about eightfold in value. True K absorption is now occurring and a large fraction of the incident quanta simply disappear, their energy being converted into K fluorescent radiation and the kinetic energy of ejected photoelectrons. Since energy must be conserved in the process, it follows that the energy per quantum of the fluorescent radiation must be less than that of the incident radiation, or that the wavelength λ_K of the K absorption edge must be shorter than that

16 Properties of x-rays

of any K characteristic line. (The eight-fold increase in μ/ρ mentioned above means a tremendous decrease in transmitted intensity, because of the exponential nature of Eq. (1-11). If the transmission factor I_x/I_0 of a particular nickel sheet is 0.1 for a wavelength just longer than λ_K , then it is only 10^{-8} for a wavelength just shorter.)

As the wavelength of the incident beam is decreased below λ_K , the absorption coefficient begins to decrease again, even though the production of K fluorescent radiation and photoelectrons is still occurring. At a wavelength of 1.0 Å, for example, the incident quanta have more than enough energy to remove an electron from the K shell of nickel. But the more energetic the quanta become, the greater is their probability of passing right through the absorber, with the result that less and less of them take part in the ejection of photoelectrons.

If the absorption curve of nickel is plotted for longer wavelengths than 2.5 Å, i.e., beyond the limit of Fig. 1-8, other sharp discontinuities will be found. These are the L , M , N , etc., absorption edges; in fact, there are three closely spaced L edges (L_I , L_{II} , and L_{III}), five M edges, etc. (Fig. 1-10). Each of these discontinuities marks the wavelength of the incident beam whose quanta have just sufficient energy to eject an L , M , N , etc., electron from the atom. The right-hand branch of the curve of Fig. 1-8, for example, lies between the K and L absorption edges; in this wavelength region incident x-rays have enough energy to remove L , M , etc., electrons from nickel but not enough to remove K electrons. Absorption-edge wavelengths vary with the atomic number of the absorber in the same way, but not quite as exactly, as characteristic emission wavelengths, that is, according to Moseley's law. Values of the K and L absorption-edge wavelengths are given in Appendix 7.

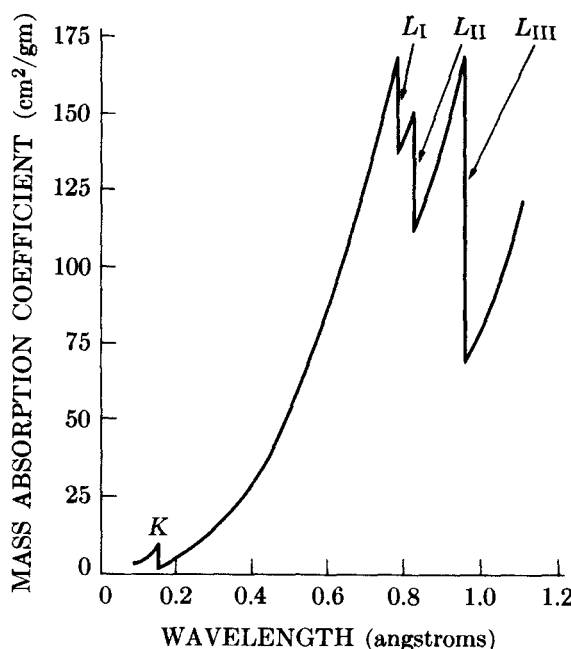


Fig. 1-10 Absorption coefficients of lead, showing K and L absorption edges [1.6].

The measured values of the absorption edges can be used to construct an energy-level diagram for the atom, which in turn can be used in the calculation of characteristic-line wavelengths. For example, if we take the energy of the neutral atom as zero, then the energy of an ionized atom (an atom in an excited state) will be some positive quantity, since work must be done to pull an electron away from the positively charged nucleus. If a K electron is removed, work equal to W_K must be done and the atom is said to be in the K energy state. The energy W_K may be calculated from the wavelength of the K absorption edge by the use of Eq. (1-14). Similarly, the energies of the L , M , etc., states can be calculated from the wavelengths of the L , M , etc., absorption edges and the results plotted in the form of an energy-level diagram for the atom (Fig. 1-11).

Although this diagram is simplified, in that the substructure of all the levels is not shown, it illustrates the main principles. The arrows show the transitions of the atom, and their directions are therefore just the opposite of the arrows in Fig. 1-7,

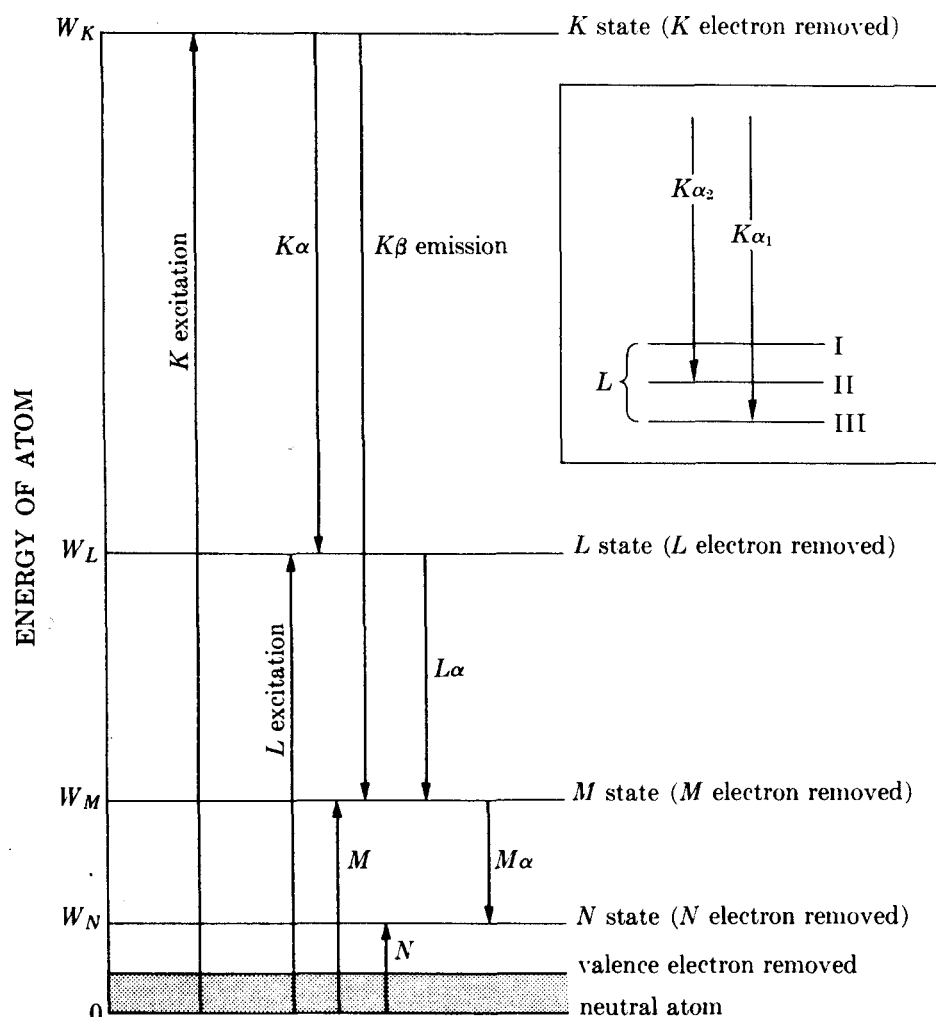


Fig. 1-11 Atomic energy levels (schematic). Excitation and emission processes indicated by arrows. The insert at top right shows the fine structure of the L state. After Barrett [1.7].

which shows the transitions of the *electron*. Thus, if a *K* electron is removed from an atom (whether by an incident electron or x-ray), the atom is raised to the *K* state. If an electron then moves from the *L* to the *K* level to fill the vacancy, the atom undergoes a transition from the *K* to the *L* state. This transition is accompanied by the emission of $K\alpha$ characteristic radiation and the arrow indicating $K\alpha$ emission is accordingly drawn from the *K* state to the *L* state.

Figure 1-11 shows clearly how the wavelengths of characteristic emission lines can be calculated, since the difference in energy between two states will equal $h\nu$, where ν is the frequency of the radiation emitted when the atom goes from one state to the other. Consider the $K\alpha_1$ characteristic line, for example. The “*L* level” of an atom is actually a group of three closely spaced levels (L_I , L_{II} , and L_{III}), and the emission of the $K\alpha_1$ line is due to a $K \rightarrow L_{III}$ transition. The frequency $\nu_{K\alpha_1}$ of this line is therefore given by the equations

$$\begin{aligned} h\nu_{K\alpha_1} &= W_K - W_{L_{III}}, \\ h\nu_{K\alpha_1} &= h\nu_K - h\nu_{L_{III}}, \\ \frac{1}{\lambda_{K\alpha_1}} &= \frac{1}{\lambda_K} - \frac{1}{\lambda_{L_{III}}}, \end{aligned} \quad (1-15)$$

where the subscripts *K* and L_{III} refer to absorption edges and the subscript $K\alpha_1$ to the emission line.

Excitation voltages can be calculated by a relation similar to Eq. (1-4). To excite *K* radiation, for example, in the target of an x-ray tube, the bombarding electrons must have energy equal to W_K . Therefore

$$\begin{aligned} eV_K &= W_K = h\nu_K = \frac{hc}{\lambda_K}, \\ V_K &= \frac{hc}{e\lambda_K}, \\ V_K &= \frac{12.40 \times 10^3}{\lambda_K}, \end{aligned} \quad (1-16)$$

where V_K is the *K* excitation voltage and λ_K is the *K* absorption edge wavelength (in angstroms).

Figure 1-12 summarizes some of the relations developed above. This curve gives the short-wavelength limit of the continuous spectrum as a function of applied voltage. Because of the similarity between Eqs. (1-4) and (1-16), the same curve also enables us to determine the critical excitation voltage from the wavelength of an absorption edge.

Auger effect [1.1, 1.2]. It might be inferred, from the last two sections, that every atom that has a vacancy in, for example, the *K* shell will always emit *K* radiation. That is not so. An atom with a *K*-shell vacancy is in an ionized, high-energy state. It can lose this excess energy and return to its normal state in two ways: (1) by emitting *K* radiation (“normal” production of characteristic radiation), or (2) by emitting an electron (*Auger effect*). In the Auger process a *K*-shell vacancy is filled from, say, the L_{II} level; the

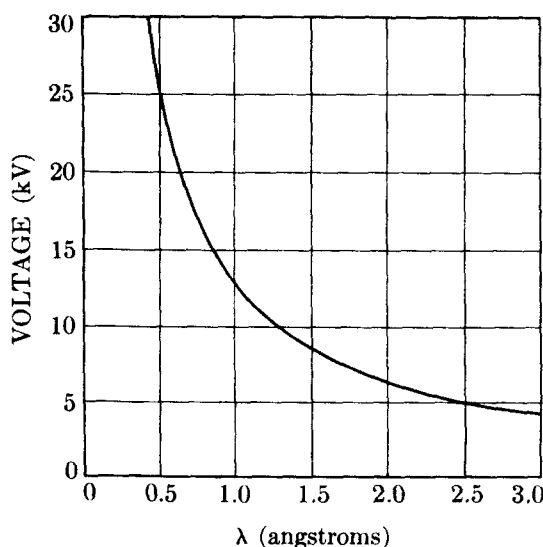


Fig. 1-12 Relation between the voltage applied to an x-ray tube and the short-wavelength limit of the continuous spectrum, and between the critical excitation voltage of any metal and the wavelength of its absorption edge.

resulting *K* radiation does not escape from the atom but ejects an electron from, say, the L_{III} level. The ejected electron, called an *Auger electron*, has a kinetic energy related to the energy difference between the *K* and L_{II} states.

The Auger effect is by no means a minor one. In fact, atoms with an atomic number *Z* less than 31 (gallium) are more likely to eject Auger electrons than to emit x-rays. The likelihood of the Auger process can be found from the fluorescence yield ω , which is defined, for the *K* shell, by

$$\omega_K = \frac{\text{number of atoms that emit } K \text{ radiation}}{\text{number of atoms with a } K\text{-shell vacancy}}. \quad (1-17)$$

(This quantity is called the *fluorescence yield*, whether the vacancy is caused by incident x-rays or by electrons.) Some values of ω_K are 0.03 for Mg (*Z* = 12), 0.41 for Cu (*Z* = 29), and 0.77 for Mo (*Z* = 42) [G.31, p. 131]. The probability of the Auger process occurring is $(1 - \omega_K)$, which amounts to some 97 percent for Mg and 23 percent for Mo.

Electrons of moderate energy like Auger electrons cannot travel very far in a solid, and an Auger electron emitted by one atom in a solid specimen cannot escape from the specimen unless the atom is situated within about 10 Å of the surface. The electrons that do escape have kinetic energies related to the differences between energy levels of the parent atom, i.e., their energies are characteristic of that atom. Means are available for measuring these energies, and we therefore have a method for chemical analysis of very thin surface layers, called *Auger electron spectroscopy*, used in studies of catalysts, corrosion, impurity segregation at surfaces, etc.

1-6 FILTERS

Many x-ray diffraction experiments require radiation which is as closely monochromatic as possible. However, the beam from an x-ray tube operated at a voltage above V_K contains not only the strong $K\alpha$ line but also the weaker $K\beta$ line and the

continuous spectrum. The intensity of these undesirable components can be decreased relative to the intensity of the $K\alpha$ line by passing the beam through a *filter* made of a material whose K absorption edge lies between the $K\alpha$ and $K\beta$ wavelengths of the target metal. Such a material will have an atomic number one less than that of the target metal, for metals with Z near 30.

A filter so chosen will absorb the $K\beta$ component much more strongly than the $K\alpha$ component, because of the abrupt change in its absorption coefficient between these two wavelengths. The effect of filtration is shown in Fig. 1-13, in which the partial spectra of the unfiltered and filtered beams from a copper target ($Z = 29$) are shown superimposed on a plot of the mass absorption coefficient of the nickel filter ($Z = 28$).

The thicker the filter the lower the ratio of intensity of $K\beta$ to $K\alpha$ in the transmitted beam. But filtration is never perfect, of course, no matter how thick the filter, and one must compromise between reasonable suppression of the $K\beta$ component and the inevitable weakening of the $K\alpha$ component which accompanies it. In practice it is found that a reduction in the intensity of the $K\alpha$ line to about half its original value will decrease the ratio of intensity of $K\beta$ to $K\alpha$ from about $\frac{1}{9}$ in the incident beam to about $\frac{1}{500}$ in the transmitted beam; this level is sufficiently low for most purposes. Table 1-1 shows the filters used in conjunction with the common target metals, the thicknesses required, and the transmission factors for the $K\alpha$ line. Filter materials are usually used in the form of thin foils. If it is not

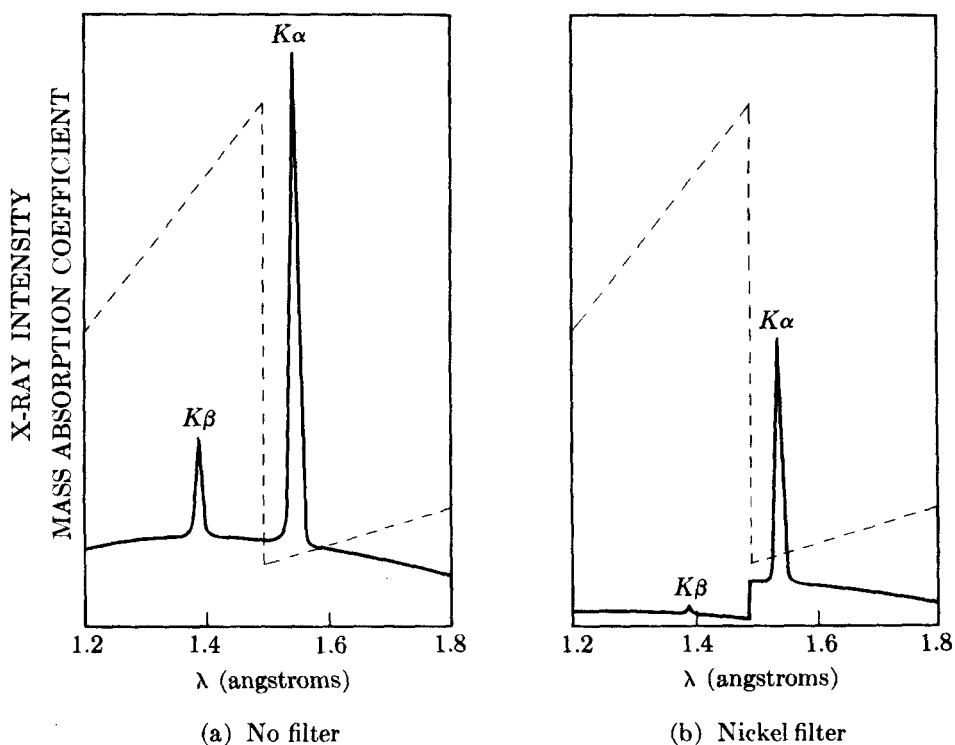


Fig. 1-13 Comparison of the spectra of copper radiation (a) before and (b) after passage through a nickel filter (schematic). The dashed line is the mass absorption coefficient of nickel.

Table 1-1
Filters for Suppression of $K\beta$ Radiation

Target	Filter	Incident beam* $\frac{I(K\alpha)}{I(K\beta)}$	Filter thickness for $\frac{I(K\alpha)}{I(K\beta)} = \frac{500}{1}$ in trans. beam		$\frac{I(K\alpha) \text{ trans.}}{I(K\alpha) \text{ incident}}$
			mg/cm ²	in.	
Mo	Zr	5.4	77	0.0046	0.29
Cu	Ni	7.5	18	0.0008	0.42
Co	Fe	9.4	14	0.0007	0.46
Fe	Mn	9.0	12	0.0007	0.48
Cr	V	8.5	10	0.0006	0.49

* This is the intensity ratio at the target [G.11, Vol. 3, p. 71]. This ratio outside the x-ray tube will be changed somewhat by the differential absorption of $K\alpha$ and $K\beta$ by the tube window, typically beryllium, 0.01 inch (0.25 mm) thick.

possible to obtain a given metal in the form of a stable foil, the oxide of the metal may be used. The powdered oxide is mixed with a suitable binder and spread on a paper backing, the required mass of metal per unit area being given in Table 1-1.

1-7 PRODUCTION OF X-RAYS

We have seen that x-rays are produced whenever high-speed electrons collide with a metal target. Any x-ray tube must therefore contain (a) a source of electrons, (b) a high accelerating voltage, and (c) a metal target. Furthermore, since most of the kinetic energy of the electrons is converted into heat in the target, the latter is almost always water-cooled to prevent its melting.

All x-ray tubes contain two electrodes, an anode (the metal target) maintained, with few exceptions, at ground potential, and a cathode, maintained at a high negative potential, normally of the order of 30,000 to 50,000 volts for diffraction work. X-ray tubes may be divided into two basic types, according to the way in which electrons are provided: gas tubes, in which electrons are produced by the ionization of a small quantity of gas (residual air in a partly evacuated tube), and filament tubes, in which the source of electrons is a hot filament.

Gas Tubes

These resemble the original x-ray tube used by Roentgen. They are now obsolete.

Filament Tubes

These were invented by Coolidge in 1913. They consist of an evacuated glass envelope which insulates the anode at one end from the cathode at the other, the cathode being a tungsten filament and the anode a water-cooled block of copper containing the desired target metal as a small insert at one end. Figure 1-14 is a photograph of such a tube, and Fig. 1-15 shows its internal construction. One lead of the high-voltage transformer is connected to the filament and the other to

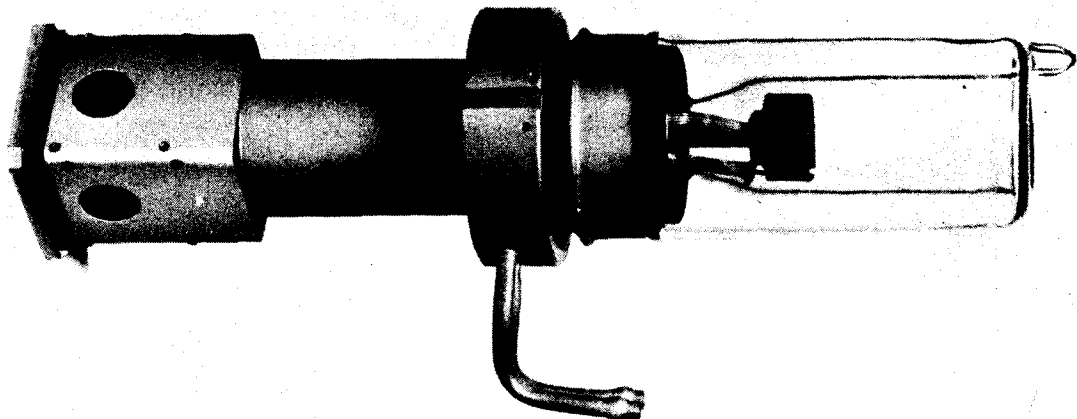


Fig. 1-14 Sealed-off filament x-ray tube. Cooling-water tubes at center connect with internal ducts leading to anode at left end. Three windows: two for projecting square focal spots and one for projecting a line focal spot. Focal spots of three sizes are available with this tube (Type A-5): 1.2×12.5 mm, 0.75×12.5 mm, and 0.45×12.5 mm. (Courtesy of Machlett Laboratories, Inc.)

ground, the target being grounded by its own cooling-water connection. The filament is heated by a *filament current* of about 3 amp and emits electrons which are rapidly drawn to the target by the high voltage across the tube. Surrounding the filament is a small metal cup maintained at the same high (negative) voltage as the filament: it therefore repels the electrons and tends to focus them into a narrow region of the target, called the *focal spot*. X-rays are emitted from the focal spot in all directions and escape from the tube through two or more windows in the tube housing. Since these windows must be vacuum tight and yet highly transparent to x-rays, they are usually made of beryllium.

Although one might think that an x-ray tube would operate only from a dc source, since the electron flow must occur only in one direction, it is actually possible to operate a tube from an ac source such as a transformer because of the rectifying properties of the tube itself. Current exists during the half-cycle in which the filament is negative with respect to the target; during the reverse half-cycle the filament is positive, but no electrons can flow since only the filament is hot enough to emit electrons. Thus a simple circuit such as shown in Fig. 1-16 suffices for many installations, although more elaborate circuits, containing rectifying tubes, smoothing capacitors, and voltage stabilizers, are often used, particularly when the x-ray intensity must be kept constant within narrow limits. In Fig. 1-16, the voltage applied to the tube is controlled by the autotransformer which controls the voltage applied to the primary of the high-voltage transformer. The voltmeter shown measures the input voltage but may be calibrated, if desired, to read the output voltage applied to the tube. The milliammeter measures the *tube current*, i.e., the flow of electrons from filament to target. This current is normally of the order of 10 to 25 mA and is controlled by the filament rheostat. The rheostat controls

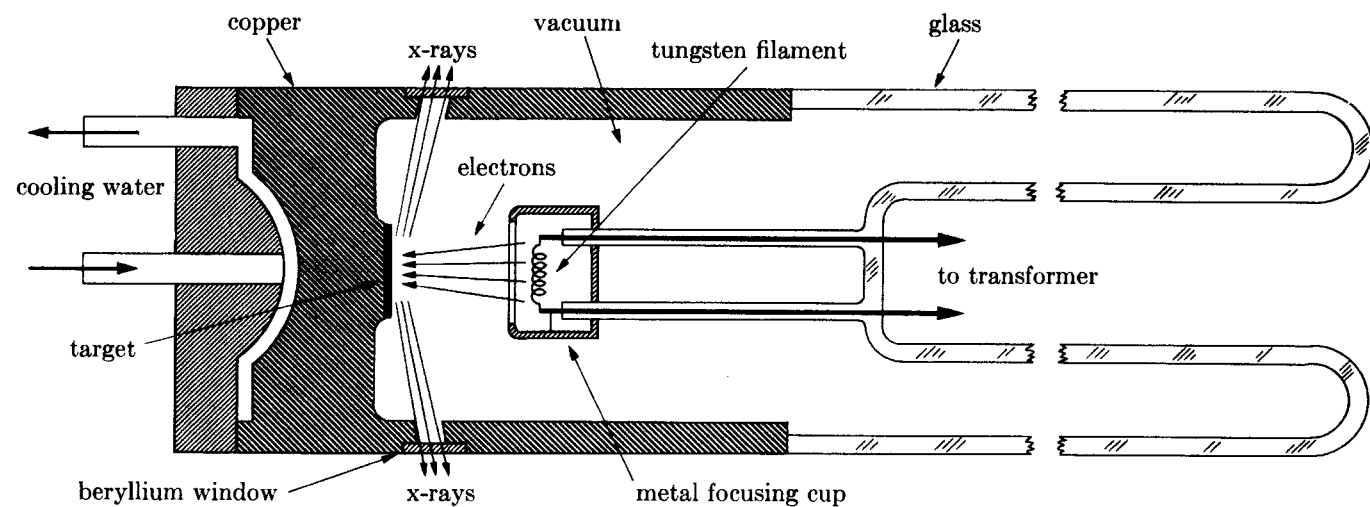


Fig. 1-15 Cross section of sealed-off filament x-ray tube (schematic).

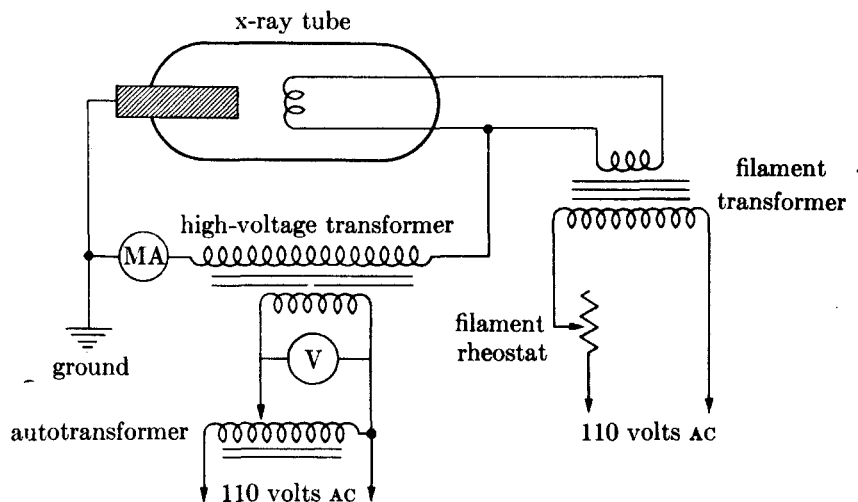


Fig. 1-16 Wiring diagram for self-rectifying filament tube.

the output voltage of the filament transformer; this voltage determines the filament current and, in turn, the temperature of the filament and the number of electrons it can emit per second. Although the filament transformer is a low-voltage step-down transformer, since it need apply only about 5 volts to the filament, it is itself at a high negative voltage relative to ground and must be well insulated.

Two kinds of filament tube exist: sealed-off and demountable. A sealed-off tube is evacuated and sealed off at the factory. It is by far the easier kind to operate, since no high-vacuum pumping equipment is needed; however, it is expensive (one needs as many tubes as there are target metals required), and the life of the tube is determined by the life of the filament. In demountable tubes, which are used nowadays only for special purposes, both the filament and the target are accessible for replacement; burned-out filaments can be replaced and targets can be interchanged at will. However, the demountable tube must be pumped out continuously during operation, and both a diffusion and a mechanical pump are necessary to obtain the high vacuum required.

The old gas tube, although tricky to operate, had the advantage of producing the purest radiation available, since the target never became contaminated with a foreign metal. In filament tubes, on the other hand, some tungsten occasionally evaporates from the filament and deposits on the target, and the tungsten then emits characteristic *L* radiation (the *L* excitation voltage of tungsten is only 10,200 volts), as well as the radiation characteristic of the target metal itself.

Focal Spot

The size and shape of the focal spot of an x-ray tube is one of its most important characteristics. Within limits, it should be as small as possible in order to concentrate the electron energy into a small area of the target and so produce an x-ray source of high intensity.

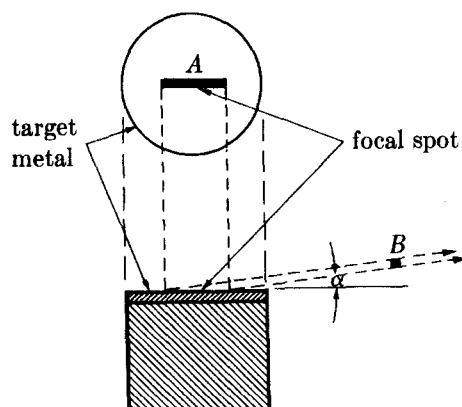


Fig. 1-17 Reduction in apparent size of focal spot.

Filament tubes usually have the filament wound in a helix in order to produce a so-called "line focus" which is actually a narrow rectangle (Fig. 1-17). The total electron energy is thus spread over a rather large focal spot *A*, which helps to dissipate the heat formed; yet the cross section *B* of the beam issuing at a small target-to-beam angle α is that of a small square, and this beam is of greater intensity than one leaving the focal spot at some larger angle α . The best value of α is about 6° , and a good tube will have a projected focal-spot size at this angle of less than 1 mm square. If the tube has a window so arranged that a beam can issue from the focal spot *A* almost normal to the plane of the drawing and at a small angle α , then the cross section of the beam will be an extremely narrow line; such a beam is quite useful in some diffraction experiments.

Power Rating

All x-ray tubes have a maximum power rating which cannot be exceeded without injury to the tube. This limit is fixed by the amount of heat that can be dissipated by the target and is usually stated by the manufacturer in terms of the maximum allowable tube current (in mA) for a given tube voltage (in kV).

Rotating-anode Tubes

Since an x-ray tube is less than 1 percent efficient in producing x-rays and since the diffraction of x-rays by crystals is far less efficient than this, it follows that the intensities of diffracted x-ray beams are extremely low. In fact, it may require as much as several hours exposure to a photographic film in order to detect them at all. Constant efforts are therefore being made to increase the intensity of the x-ray source. One solution to this problem is the rotating-anode tube, in which rotation of the anode continuously brings fresh target metal into the focal-spot area and so allows a greater power input without excessive heating of the anode. Figure 1-18 shows two designs that have been used successfully; the shafts rotate through vacuum-tight seals in the tube housing. Such tubes can operate at a power level 5 to 10 times higher than that of a fixed-focus tube, with corresponding reductions in exposure time. They are common in the area of radiography but not often used for diffraction.

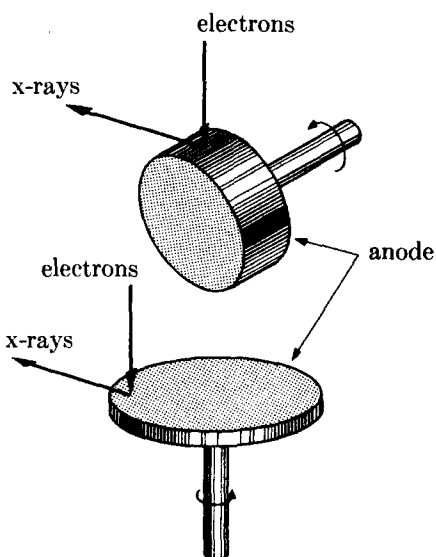


Fig. 1-18 Schematic drawings of two types of rotating anode for high-power x-ray tubes.

Microfocus Tubes

Some diffraction methods require extremely fine x-ray beams. Such beams are most efficiently produced by special demountable x-ray tubes, called microfocus tubes, in which special attention is paid to achieving a very small focal spot. The design problem—fine focusing of the electron beam—is similar to that of the electron microscope or the x-ray microprobe. One focusing method is electrostatic and consists simply in maintaining the focusing cup around the filament at a potential of a few hundred volts more negative than the filament, thus concentrating the electrons into a narrower beam.

The focal spots of these tubes have areas of less than 1 percent of those of conventional tubes. Typical sizes are 0.1×1 mm for a line focus and 0.05 mm ($= 50 \mu\text{m}$) diameter for a circular focus.

Pulsed (or Flash) Tubes

The maximum power at which an x-ray tube can operate continuously is limited by the rate at which the target can be cooled. But if the tube is operated for only a small fraction of a second, a pulse of x-rays can be obtained at a very high power level without any cooling. This can be done by slowly charging a bank of capacitors and then abruptly discharging them across a special x-ray tube. In this way an x-ray pulse lasting about 30 nanoseconds at a peak voltage of 300 kV and a peak current of 5000 amperes has been produced [1.8]. (Such a brief flash of x-rays is useful only if its results, in radiography or diffraction, can be recorded. One example of high-speed recording is described in Sec. 8-5.)

Miniature Tubes

If increased attention is given, during the design of an x-ray tube, to focusing of the electron beam and to the shape and placement of the target, the intensity of the beam issuing from the tube can be made about as large as that from a conventional tube, but with a power input of one-tenth or less. As a result, water cooling is not needed; air cooling is sufficient. This feature is important for portable apparatus.

Such tubes have been made experimentally [1.9, 1.10] and commercially [1.11]. They are small, only about 4 to 8 in. (10 to 20 cm) in length, and operate typically at a voltage of about 50 kV and a tube current of the order of 1 mA, as compared to 10 mA or more in conventional tubes.

1-8 DETECTION OF X-RAYS

The principal means used to detect x-ray beams are fluorescent screens, photographic film, and counters.

Fluorescent Screens

Fluorescent screens are made of a thin layer of zinc sulfide, containing a trace of nickel, mounted on a cardboard backing. Under the action of x-rays, this compound fluoresces in the visible region, i.e., emits visible light, in this case yellow light. Although most diffracted beams are too weak to be detected by this method, fluorescent screens are widely used in diffraction work to locate the position of the primary beam when adjusting apparatus.

Photographic Film

Photographic film is affected by x-rays in much the same way as by visible light. However, the emulsion on ordinary film is too thin to absorb much of the incident x-radiation, and only absorbed x-rays can be effective in blackening the film. For this reason, x-ray films are made with rather thick layers of emulsion on both sides in order to increase the total absorption. (Division of the total emulsion thickness into two layers permits easier penetration of the film-processing solutions.) The grain size is also made large for the same purpose: this has the unfortunate consequence that x-ray films are grainy, do not resolve fine detail, and cannot stand much enlargement.

Because the mass absorption coefficient of any substance varies with wavelength, it follows that film sensitivity, i.e., the amount of blackening caused by x-ray beams of the same intensity, depends on their wavelength. This should be borne in mind whenever white radiation is recorded photographically; for one thing, this sensitivity variation alters the effective shape of the continuous spectrum. Figure 1-19(a) shows the intensity of the continuous spectrum as a function of wavelength and (b) the variation of film sensitivity. This latter curve is merely a plot of the mass absorption coefficient of silver bromide, the active ingredient of the emulsion, and is marked by discontinuities at the *K* absorption edges of silver and bromine. (Note, incidentally, how much more sensitive the film is to the *K* radiation from copper than to the *K* radiation from molybdenum, other things being equal.) Curve (c) of Fig. 1-19 shows the net result, namely the amount of film blackening caused by the various wavelength components of the continuous spectrum, or what might be called the "effective photographic intensity" of the continuous spectrum. These curves are only approximate, however, and in practice it is almost impossible to measure photographically the relative intensities

28 Properties of x-rays

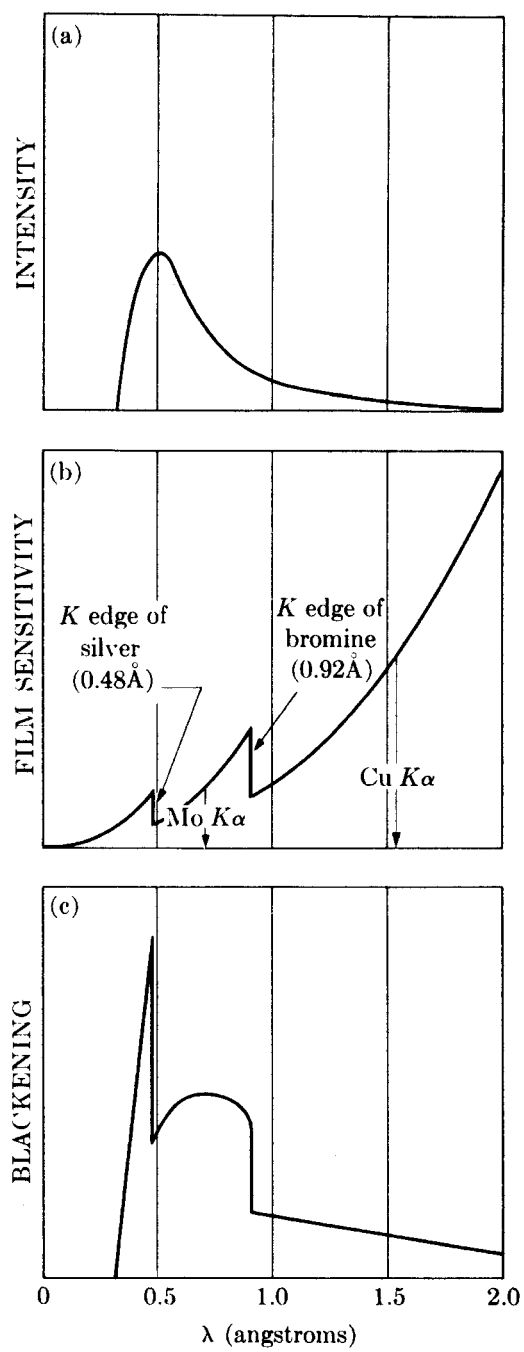


Fig. 1-19 Relation between film sensitivity and effective shape of continuous spectrum (schematic): (a) continuous spectrum from a tungsten target at 40 kV; (b) film sensitivity; (c) blackening curve for spectrum shown in (a).

of two beams of different wavelength. On the other hand, the relative intensities of beams of the *same* wavelength can be accurately measured by photographic means, and such measurements are described in Chap. 6.

The Polaroid Land rapid-process system of photography has been adapted to some kinds of diffraction equipment. The Polaroid film is backed by an intensifying screen (Sec. 5-2) which converts x-rays to visible light that can darken the film. X-ray exposures are about one tenth of those required by x-ray film, and finished prints are available about ten seconds after the x-ray exposure.

Counters

X-ray counters are devices that convert x-rays into a pulsating electric current, and the number of current pulses per unit of time is proportional to the intensity of the x-rays entering the counter. Three types are currently in use: proportional, scintillation, and semiconductor. They will be described in Chap. 7.

General

Fluorescent screens are used only for the detection of x-ray beams, while photographic film and the various kinds of counters permit both detection and measurement of intensity. Photographic film has the advantage of being able to record a number of diffracted beams at one time and their relative positions in space, and the film can be used as a basis for intensity measurements if desired. Intensities can be measured much more rapidly with counters, and these instruments are more popular for quantitative work. However, most counters record only one diffracted beam at a time.

1-9 SAFETY PRECAUTIONS

The operator of x-ray apparatus is exposed to two obvious dangers, electric shock and radiation injury, but both of these hazards can be reduced to negligible proportions by proper design of equipment and reasonable care on the part of the user. Nevertheless, it is only prudent for the x-ray worker to be continually aware of these hazards.

Electric Shock

The danger of electric shock is always present around high-voltage apparatus. The anode end of most x-ray tubes is usually grounded and therefore safe, but the cathode end is a source of danger. X-ray tubes of the nonshockproof variety (such as the one shown in Fig. 1-14) must be so mounted that their cathode end is absolutely inaccessible to the user during operation; this may be accomplished by placing the cathode end below a table top, in a box, behind a screen, etc. The installation should be so contrived that it is impossible for the operator to touch the high-voltage parts without automatically disconnecting the high voltage. Shockproof sealed-off tubes are also available: these are encased in a grounded metal covering, and an insulated, shockproof cable connects the cathode end to the

transformer. Being shockproof, such a tube has the advantage that it need not be permanently fixed in position but may be set up in various positions as required for particular experiments.

Radiation Hazard

The radiation hazard is due to the fact that x-rays can kill human tissue; in fact, it is precisely this property which is utilized in x-ray therapy for the killing of cancer cells. The biological effects of x-rays include burns (due to localized high-intensity beams), radiation sickness (due to radiation received generally by the whole body), and, at a lower level of radiation intensity, genetic mutations. The burns are painful and may be difficult, if not impossible, to heal. Slight exposures to x-rays are not cumulative, but above a certain level called the "tolerance dose," they do have a cumulative effect and can produce permanent injury. The x-rays used in diffraction are particularly harmful because they have relatively long wavelengths and are therefore easily absorbed by the body.

There is no excuse today for receiving serious injuries as early x-ray workers did through ignorance. There would probably be no accidents if x-rays were visible and produced an immediate burning sensation, but they are invisible and burns may not be immediately felt. If the body has received general radiation above the tolerance dose, the first noticeable effect will be a lowering of the white-blood-cell count, so periodic blood counts are advisable if there is any doubt about the general level of intensity in the laboratory.

Portable counters, called *radiation survey meters*, are available for surveying various areas around x-ray equipment for possible radiation leaks. Film badges should be worn on the torso or wrist of persons who spend a large fraction of their working day near x-ray equipment. Government regulations regarding radiation safety are becoming increasingly severe; Jenkins and Haas [1.3] describe some of these regulations and give useful information about radiation units, survey meters, tolerance levels, and reported accidents. Certain government booklets should also be consulted [1.4, 1.5].

The safest procedure for the experimenter to follow is: first, to locate the *primary beam* from the tube with a small fluorescent screen fixed to the end of a rod and thereafter avoid it; and second, to make sure that he is well shielded by lead or lead-glass screens from the radiation *scattered* by the camera or other apparatus which may be in the path of the primary beam. Strict and constant attention to these precautions will ensure safety.

PROBLEMS

* 1-1 What is the frequency (per second) and energy per quantum (in joules) of x-ray beams of wavelength 0.71 Å (Mo $K\alpha$) and 1.54 Å (Cu $K\alpha$)?

1-2 Calculate the velocity and kinetic energy with which the electrons strike the target

* Answers to starred problems are given at the back of the book.

of an x-ray tube operated at 50,000 volts. What is the short-wavelength limit of the continuous spectrum emitted and the maximum energy per quantum of radiation?

1-3 Show that the velocity with which electrons strike the target of an x-ray tube depends only on the voltage between anode (target) and cathode and not on the distance between them. [The force on a charge e (coulombs) by a field E (volts/m) is eE newtons.]

1-4 Graphically verify Moseley's law for the $K\beta_1$ lines of Cu, Mo, and W.

1-5 Plot the ratio of transmitted to incident intensity vs. thickness of lead sheet for Mo $K\alpha$ radiation and a thickness range of 0.00 and 0.02 mm.

* **1-6** Graphically verify Eq. (1-13) for a lead absorber and Mo $K\alpha$, Rh $K\alpha$, and Ag $K\alpha$ radiation. (The mass absorption coefficients of lead for these radiations are 122.8, 84.13, and $66.14 \text{ cm}^2/\text{gm}$, respectively.) From the curve, determine the mass absorption coefficient of lead for the shortest wavelength radiation from a tube operated at 30,000 volts.

1-7 Lead screens for the protection of personnel in x-ray diffraction laboratories are usually at least 1 mm thick. Calculate the "transmission factor" ($I_{\text{trans.}}/I_{\text{incident}}$) of such a screen for Cu $K\alpha$, Mo $K\alpha$, and the shortest wavelength radiation from a tube operated at 30,000 volts.

* **1-8** (a) Calculate the mass and linear absorption coefficients of air for Cr $K\alpha$ radiation. Assume that air contains 80 percent nitrogen and 20 percent oxygen by weight and has a density of $1.29 \times 10^{-3} \text{ g/cm}^3$. (b) Plot the transmission factor of air for Cr $K\alpha$ radiation and a path length of 0 to 20 cm.

* **1-9** Calculate the K excitation voltage of copper.

1-10 Calculate the wavelength of the L_{III} absorption edge of molybdenum.

* **1-11** Calculate the wavelength of the Cu $K\alpha_1$ line.

1-12 Plot the curve shown in Fig. 1-12 and save it for future reference.

* **1-13** What voltage must be applied to a molybdenum-target tube in order that the emitted x-rays excite K fluorescent radiation from a piece of copper placed in the x-ray beam? What is the wavelength of the fluorescent radiation?

In Problems 14 and 15 take the intensity ratios of $K\alpha$ to $K\beta$ in unfiltered radiation from Table 1-1.

1-14 Suppose that a nickel filter is required to produce an intensity ratio of Cu $K\alpha$ to Cu $K\beta$ of 100/1 in the filtered beam. Calculate the thickness of the filter and the transmission factor for the Cu $K\alpha$ line.

* **1-15** Filters for Co K radiation are usually made of iron oxide (Fe_2O_3) powder rather than iron foil. If a filter contains 5 mg $\text{Fe}_2\text{O}_3/\text{cm}^2$, what is the transmission factor for the Co $K\alpha$ line? What is the intensity ratio of Co $K\alpha$ to Co $K\beta$ in the filtered beam?

1-16 A copper-target x-ray tube is operated at 40,000 volts and 25 mA. The efficiency of an x-ray tube is so low that, for all practical purposes, one may assume that all the input energy goes into heating the target. If there were no dissipation of heat by water-cooling, conduction, radiation, etc., how long would it take a 100-gm copper target to melt? (Melting point of copper = 1083°C , mean specific heat = $6.65 \text{ cal/mole}^\circ\text{C}$, latent heat of fusion = 3220 cal/mole.)

* **1-17** Assume that the sensitivity of x-ray film is proportional to the mass absorption coefficient of the silver bromide in the emulsion for the particular wavelength involved. What, then, is the ratio of film sensitivities to Cu $K\alpha$ and Mo $K\alpha$ radiation?

2

Geometry of Crystals

2-1 INTRODUCTION

Turning from the properties of x-rays, we must now consider the geometry and structure of crystals in order to discover what there is about crystals in general that enables them to diffract x-rays. We must also consider particular crystals of various kinds and how the very large number of crystals found in nature are classified into a relatively small number of groups. Finally, we will examine the ways in which the orientation of lines and planes in crystals can be represented in terms of symbols or in graphical form.

Crystallography is a very broad subject. In this book we are concerned only with its simpler aspects: how atoms are arranged in some common crystals and how this arrangement determines the way in which a particular crystal diffracts x-rays. Readers who need a deeper knowledge of crystallography should consult such books as those by Phillips [G.38], Buerger [G.35], and Kelly and Groves [G.33].

2-2 LATTICES

A crystal may be defined as *a solid composed of atoms arranged in a pattern periodic in three dimensions*. As such, crystals differ in a fundamental way from gases and liquids because the atomic arrangements in the latter do not possess the essential requirement of periodicity. Not all solids are crystalline, however; some are *amorphous*, like glass, and do not have any regular interior arrangement of atoms. There is, in fact, no essential difference between an amorphous solid and a liquid, and the former is often referred to as an “undercooled liquid.”

In thinking about crystals, it is often convenient to ignore the actual atoms composing the crystal and their periodic arrangement in space, and to think instead of a set of imaginary points which has a fixed relation in space to the atoms of the crystal and which may be regarded as a sort of framework or skeleton on which the actual crystal is built.

This set of points can be formed as follows. Imagine space to be divided by three sets of planes, the planes in each set being parallel and equally spaced. This division of space will produce a set of cells each identical in size, shape, and orientation to its neighbors. Each cell is a parallelepiped, since its opposite faces are parallel and each face is a parallelogram. The space-dividing planes will intersect each other in a set of lines (Fig. 2-1), and these lines in turn intersect in the

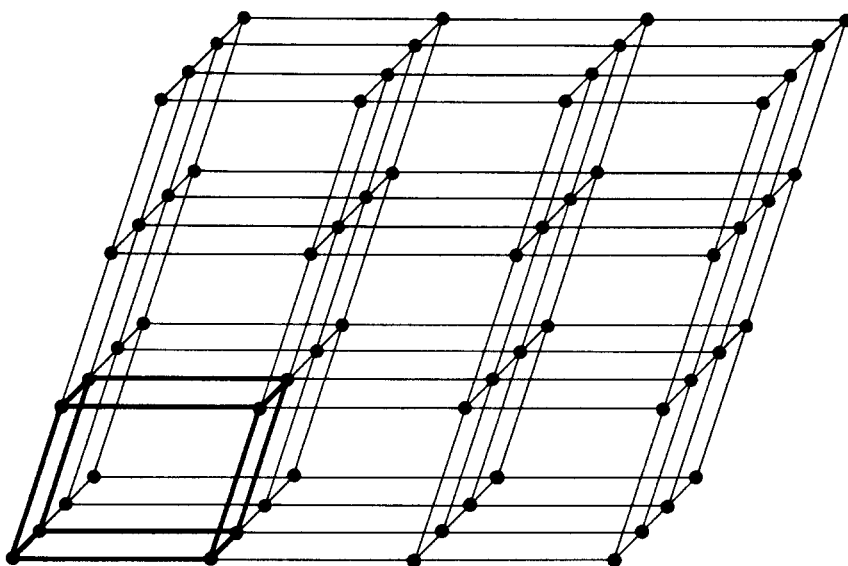


Fig. 2-1 A point lattice.

set of points referred to above. A set of points so formed has an important property: it constitutes a *point lattice*, which is defined as *an array of points in space so arranged that each point has identical surroundings*. By "identical surroundings" we mean that the lattice of points, when viewed in a particular direction from one lattice point, would have exactly the same appearance when viewed in the same direction from any other lattice point.

Since all the cells of the lattice shown in Fig. 2-1 are identical, we may choose any one, for example the heavily outlined one, as a *unit cell*. The size and shape of the unit cell can in turn be described by the three vectors* **a**, **b**, and **c** drawn from one corner of the cell taken as origin (Fig. 2-2). These vectors define the cell and are called the of the cell. They may also be described in terms of their lengths (a , b , c) and the angles between them (α , β , γ). These lengths and angles are the *lattice constants* or *lattice parameters* of the unit cell.

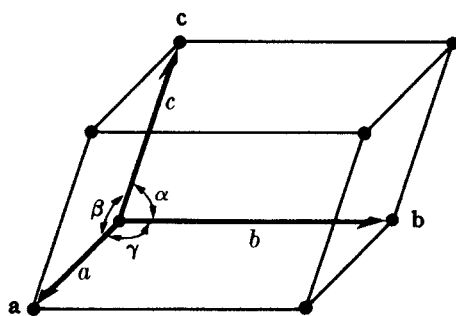


Fig. 2-2 A unit cell.

* Vectors are here represented by boldface symbols. The same symbol in italics stands for the absolute value of the vector.

Note that the vectors \mathbf{a} , \mathbf{b} , \mathbf{c} define, not only the unit cell, but also the whole point lattice through the translations provided by these vectors. In other words, the whole set of points in the lattice can be produced by repeated action of the vectors \mathbf{a} , \mathbf{b} , \mathbf{c} on one lattice point located at the origin, or, stated alternatively, the vector coordinates of any point in the lattice are $P\mathbf{a}$, $Q\mathbf{b}$, and $R\mathbf{c}$, where P , Q , and R are whole numbers. It follows that the arrangement of points in a point lattice is absolutely periodic in three dimensions, points being repeated at regular intervals along any line one chooses to draw through the lattice.

2-3 CRYSTAL SYSTEMS

In dividing space by three sets of planes, we can of course produce unit cells of various shapes, depending on how we arrange the planes. For example, if the planes in the three sets are all equally spaced and mutually perpendicular, the unit cell is cubic. In this case the vectors \mathbf{a} , \mathbf{b} , \mathbf{c} are all equal and at right angles to one another, or $a = b = c$ and $\alpha = \beta = \gamma = 90^\circ$. By thus giving special values to the axial lengths and angles, we can produce unit cells of various shapes and therefore various kinds of point lattices, since the points of the lattice are located at the cell corners. It turns out that only seven different kinds of cells are necessary to include all the possible point lattices. These correspond to the seven *crystal systems* into which all crystals can be classified. These systems are listed in Table 2-1. (Some writers consider the rhombohedral system as a subdivision of the hexagonal, thus reducing the number of crystal systems to six.)

Seven different point lattices can be obtained simply by putting points at the corners of the unit cells of the seven crystal systems. However, there are other arrangements of points which fulfill the requirements of a point lattice, namely, that each point have identical surroundings. The French crystallographer Bravais worked on this problem and in 1848 demonstrated that there are fourteen possible point lattices and no more; this important result is commemorated by our use of the terms *Bravais lattice* and *point lattice* as synonymous. For example, if a point is placed at the center of each cell of a cubic point lattice, the new array of points also forms a point lattice. Similarly, another point lattice can be based on a cubic unit cell having lattice points at each corner and in the center of each face.

The fourteen Bravais lattices are described in Table 2-1 and illustrated in Fig. 2-3, where the symbols P , F , I , etc., have the following meanings. We must first distinguish between *simple*, or *primitive*, cells (symbol P or R) and *non-primitive* cells (any other symbol): primitive cells have only one lattice point per cell while nonprimitive have more than one. A lattice point in the interior of a cell "belongs" to that cell, while one in a cell face is shared by two cells and one at a corner is shared by eight. The number of lattice points per cell is therefore given by

$$N = N_i + \frac{N_f}{2} + \frac{N_c}{8}, \quad (2-1)$$

where N_i = number of interior points, N_f = number of points on faces, and N_c = number of points on corners. Any cell containing lattice points on the

Table 2-1
Crystal Systems and Bravais Lattices

(The symbol \neq means that equality is not required by symmetry. Accidental equality may occur, as shown by an example in Sec. 2-4.)

System	Axial lengths and angles	Bravais lattice	Lattice symbol
Cubic	Three equal axes at right angles $a = b = c, \alpha = \beta = \gamma = 90^\circ$	Simple Body-centered Face-centered	P I F
Tetragonal	Three axes at right angles, two equal $a = b \neq c, \alpha = \beta = \gamma = 90^\circ$	Simple Body-centered	P I
Orthorhombic	Three unequal axes at right angles $a \neq b \neq c, \alpha = \beta = \gamma = 90^\circ$	Simple Body-centered Base-centered Face-centered	P I C F
Rhombohedral*	Three equal axes, equally inclined $a = b = c, \alpha = \beta = \gamma \neq 90^\circ$	Simple	R
Hexagonal	Two equal coplanar axes at 120° , third axis at right angles $a = b \neq c, \alpha = \beta = 90^\circ, \gamma = 120^\circ$	Simple	P
Monoclinic	Three unequal axes, one pair not at right angles $a \neq b \neq c, \alpha = \gamma = 90^\circ \neq \beta$	Simple Base-centered	P C
Triclinic	Three unequal axes, unequally inclined and none at right angles $a \neq b \neq c, \alpha \neq \beta \neq \gamma \neq 90^\circ$	Simple	P

* Also called trigonal.

corners only is therefore primitive, while one containing additional points in the interior or on faces is nonprimitive. The symbols *F* and *I* refer to face-centered and body-centered cells, respectively, while *A*, *B*, and *C* refer to base-centered cells, centered on one pair of opposite faces *A*, *B*, or *C*. (The *A* face is the face defined by the *b* and *c* axes, etc.) The symbol *R* is used especially for the rhombohedral system. In Fig. 2-3, axes of equal length in a particular system are given the same symbol to indicate their equality, e.g., the cubic axes are all marked *a*, the two equal tetragonal axes are marked *a* and the third one *c*, etc.

At first glance, the list of Bravais lattices in Table 2-1 appears incomplete. Why not, for example, a base-centered tetragonal lattice? The full lines in Fig. 2-4 delineate such a cell, centered on the *C* face, but we see that the same array of lattice points can be referred to the simple tetragonal cell shown by dashed lines, so that the base-centered arrangement of points is not a new lattice. However, the base-centered cell is a perfectly good unit cell and, if we wish, we may choose to use it rather than the simple cell. Choice of one or the other has certain consequences, which are described later (Problem 4-3).

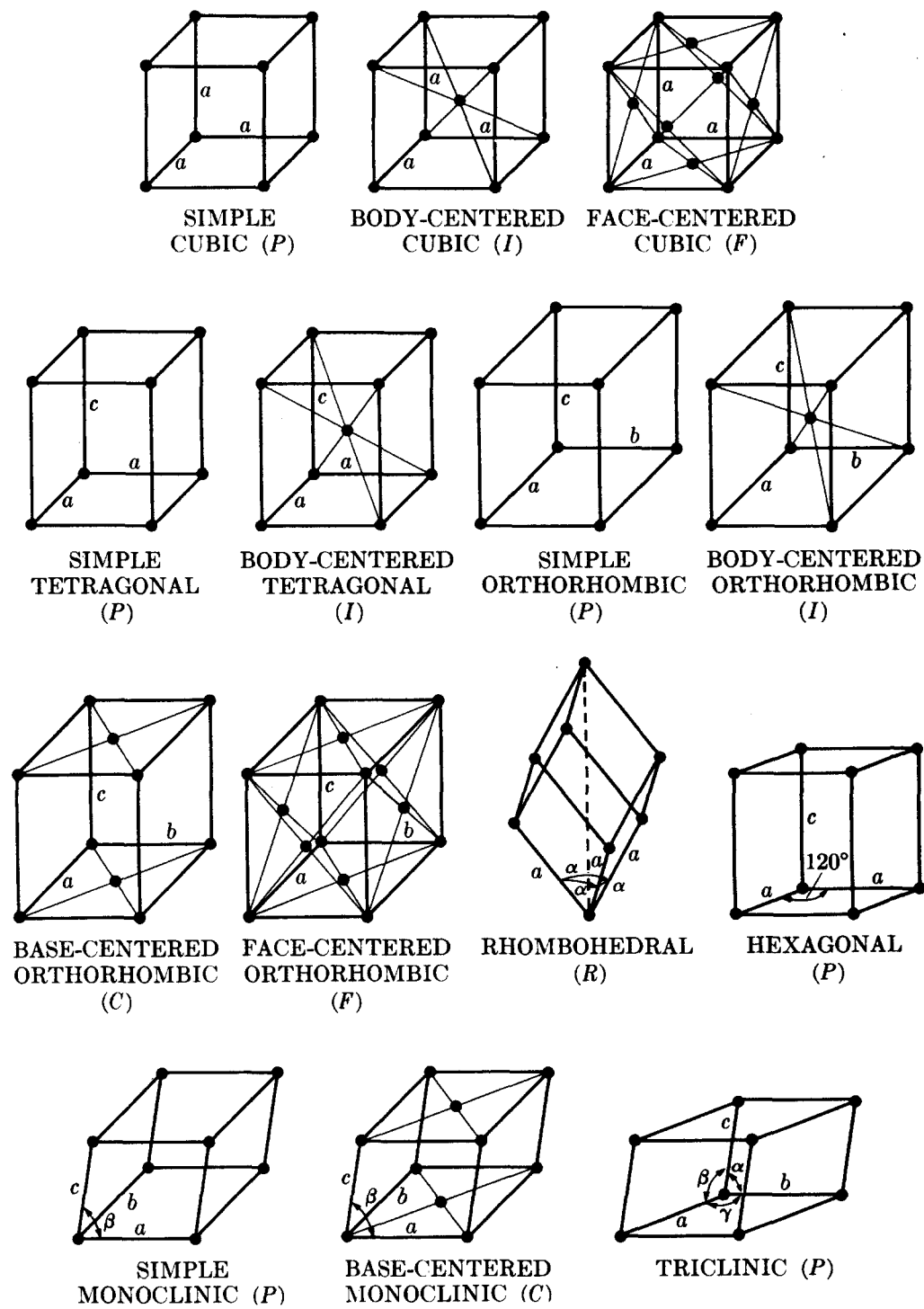


Fig. 2-3 The fourteen Bravais lattices.

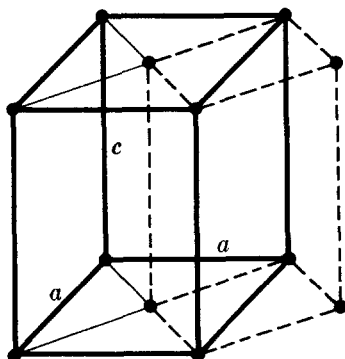


Fig. 2-4 Relation of tetragonal *C* lattice (full lines) to tetragonal *P* lattice (dashed lines).

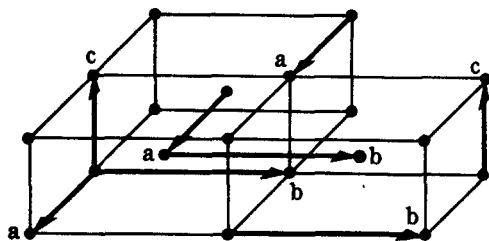


Fig. 2-5 Extension of lattice points through space by the unit cell vectors \mathbf{a} , \mathbf{b} , \mathbf{c} .

The lattice points in a nonprimitive unit cell can be extended through space by repeated applications of the unit-cell vectors \mathbf{a} , \mathbf{b} , \mathbf{c} just like those of a primitive cell. We may regard the lattice points associated with a unit cell as being translated one by one or as a group. In either case, equivalent lattice points in adjacent unit cells are separated by one of the vectors \mathbf{a} , \mathbf{b} , \mathbf{c} , wherever these points happen to be located in the cell (Fig. 2-5).

2-4 SYMMETRY

Both Bravais lattices and the real crystals which are built up on them exhibit various kinds of symmetry. A body or structure is said to be symmetrical when its component parts are arranged in such balance, so to speak, that certain operations can be performed on the body which will bring it into coincidence with itself. These are termed *symmetry operations*. For example, if a body is symmetrical with respect to a plane passing through it, then reflection of either half of the body in the plane as in a mirror will produce a body coinciding with the other half. Thus a cube has several planes of symmetry, one of which is shown in Fig. 2-6(a).

There are in all four macroscopic* symmetry operations or elements: *reflection*,

* So called to distinguish them from certain microscopic symmetry operations with which we are not concerned here. The macroscopic elements can be deduced from the angles between the faces of a well-developed crystal, without any knowledge of the atom arrangement inside the crystal. The microscopic symmetry elements, on the other hand, depend entirely on atom arrangement, and their presence cannot be inferred from the external development of the crystal.

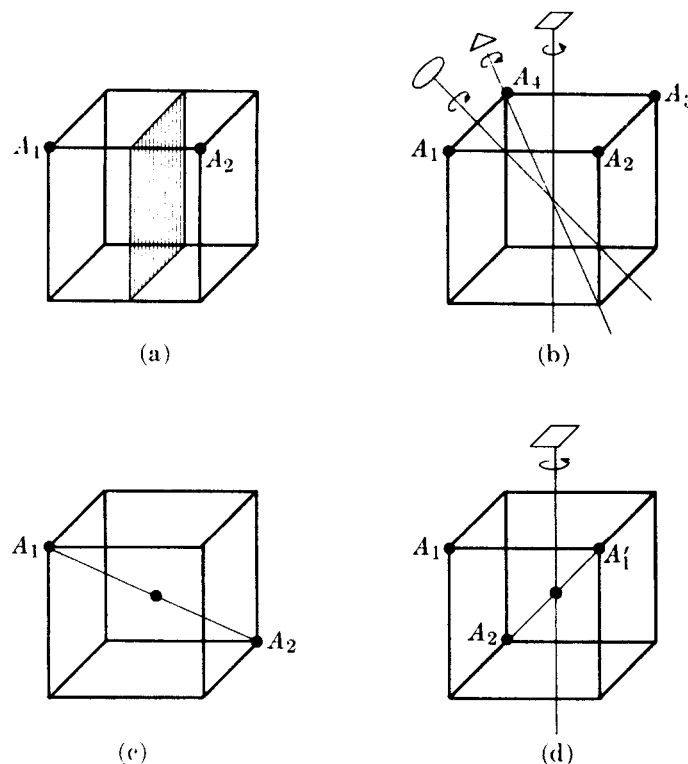


Fig. 2-6 Some symmetry elements of a cube. (a) Reflection plane. A_1 becomes A_2 . (b) Rotation axes: 4-fold axis: A_1 becomes A_2 ; 3-fold axis: A_1 becomes A_3 ; 2-fold axis: A_1 becomes A_4 . (c) Inversion center. A_1 becomes A_2 . (d) Rotation-inversion axis. 4-fold axis: A_1 becomes A'_1 ; inversion center: A'_1 becomes A_2 .

rotation, inversion, and rotation-inversion. A body has n -fold rotational symmetry about an axis if a rotation of $360^\circ/n$ brings it into self-coincidence. Thus a cube has a 4-fold rotation axis normal to each face, a 3-fold axis along each body diagonal, and 2-fold axes joining the centers of opposite edges. Some of these are shown in Fig. 2-6(b) where the small plane figures (square, triangle, and ellipse) designate the various kinds of axes. In general, rotation axes may be 1-, 2-, 3-, 4-, or 6-fold. A 1-fold axis indicates no symmetry at all, while a 5-fold axis or one of higher degree than 6 is impossible, in the sense that unit cells having such symmetry cannot be made to fill up space without leaving gaps.

A body has an inversion center if corresponding points of the body are located at equal distances from the center on a line drawn through the center. A body having an inversion center will come into coincidence with itself if every point in the body is inverted, or "reflected," in the inversion center. A cube has such a center at the intersection of its body diagonals [Fig. 2-6(c)]. Finally, a body may have a rotation-inversion axis, either 1-, 2-, 3-, 4-, or 6-fold. If it has an n -fold rotation-inversion axis, it can be brought into coincidence with itself by a rotation of $360^\circ/n$ about the axis followed by inversion in a center lying on the axis. Figure 2-6(d) illustrates the operation of a 4-fold rotation-inversion axis on a cube.

Now, the possession of a certain minimum set of symmetry elements is a

Table 2-2
Symmetry Elements

System	Minimum symmetry elements
Cubic	Four 3-fold rotation axes
Tetragonal	One 4-fold rotation (or rotation-inversion) axis
Orthorhombic	Three perpendicular 2-fold rotation (or rotation-inversion) axes
Rhombohedral	One 3-fold rotation (or rotation-inversion) axis
Hexagonal	One 6-fold rotation (or rotation-inversion) axis
Monoclinic	One 2-fold rotation (or rotation-inversion) axis
Triclinic	None

fundamental property of each crystal system, and one system is distinguished from another just as much by its symmetry elements as by the values of its axial lengths and angles. In fact, *these are interdependent*. For example, the existence of 4-fold rotation axes normal to the faces of a cubic cell *requires* that the cell edges be equal in length and at 90° to one another. On the other hand, a tetragonal cell has only one 4-fold axis, and this symmetry requires that only two cell edges be equal, namely, the two that are at right angles to the rotation axis.

The minimum number of symmetry elements possessed by each crystal system is listed in Table 2-2. Some crystals may possess more than the minimum symmetry elements required by the system to which they belong, but none may have less. The existence of certain symmetry elements often implies the existence of others. For example, a crystal with three 4-fold rotation axes necessarily has, in addition, four 3-fold axes and falls in the cubic system.

Symmetry operations apply not only to the unit cells shown in Fig. 2-3, considered merely as geometric shapes, but also to the point lattices associated with them. The latter condition rules out the possibility that the cubic system, for example, could include a base-centered point lattice, since such an array of points would not have the minimum set of symmetry elements required by the cubic system, namely four 3-fold rotation axes. Such a lattice would be classified in the tetragonal system, which has no 3-fold axes and in which accidental equality of the a and c axes is allowed.

Crystals in the rhombohedral (trigonal) system can be referred to either a rhombohedral or a hexagonal lattice. Appendix 4 gives the relation between these two lattices and the transformation equations which allow the Miller indices of a plane (see Sec. 2-6) to be expressed in terms of either set of axes.

2-5 PRIMITIVE AND NONPRIMITIVE CELLS

In any point lattice a unit cell may be chosen in an infinite number of ways and may contain one or more lattice points per cell. It is important to note that unit cells do not "exist" as such in a lattice: they are a mental construct and can

accordingly be chosen at our convenience. The conventional cells shown in Fig. 2-3 are chosen simply for convenience and to conform to the symmetry elements of the lattice.

Any of the fourteen Bravais lattices may be referred to a primitive unit cell. For example, the face-centered cubic lattice shown in Fig. 2-7 may be referred to the primitive cell indicated by dashed lines. The latter cell is rhombohedral, its axial angle α is 60° , and each of its axes is $1/\sqrt{2}$ times the length of the axes of the cubic cell. Each cubic cell has four lattice points associated with it, each rhombohedral cell has one, and the former has, correspondingly, four times the volume of the latter. Nevertheless, it is usually more convenient to use the cubic cell rather than the rhombohedral one because the former immediately suggests the cubic symmetry which the lattice actually possesses. Similarly, the other centered non-primitive cells listed in Table 2-1 are preferred to the primitive cells possible in their respective lattices.

Why then do the centered lattices appear in the list of the fourteen Bravais lattices? If the two cells in Fig. 2-7 describe the same set of lattice points, as they do, why not eliminate the cubic cell and let the rhombohedral cell serve instead? The answer is that this cell is a *particular* rhombohedral cell with an axial angle α of 60° . In the general rhombohedral lattice no restriction is placed on the angle α ; the result is a lattice of points with a single 3-fold symmetry axis. When α becomes equal to 60° , the lattice has four 3-fold axes, and this symmetry places it in the cubic system. The general rhombohedral cell is still needed.

If nonprimitive lattice cells are used, the vector from the origin to any point in the lattice will now have components which are nonintegral multiples of the unit-cell vectors \mathbf{a} , \mathbf{b} , \mathbf{c} . The position of any lattice point in a cell may be given in terms of its *coordinates*; if the vector from the origin of the unit cell to the given point has components $x\mathbf{a}$, $y\mathbf{b}$, $z\mathbf{c}$, where x , y , and z are fractions, then the coordinates of the point are x y z . Thus, point A in Fig. 2-7, taken as the origin, has coordinates $0 0 0$ while points B , C , and D , when referred to cubic axes, have coordinates $0 \frac{1}{2} \frac{1}{2}$, $\frac{1}{2} 0 \frac{1}{2}$, and $\frac{1}{2} \frac{1}{2} 0$, respectively. Point E has coordinates $\frac{1}{2} \frac{1}{2} 1$ and is equivalent to point D , being separated from it by the vector \mathbf{c} . The coordinates

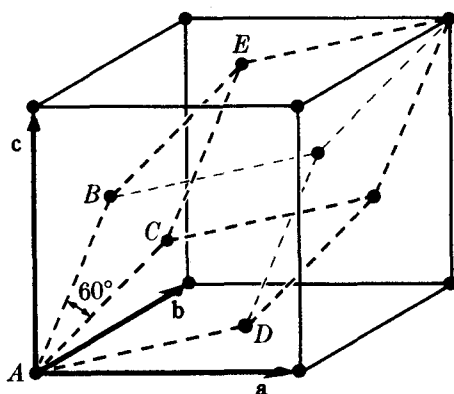


Fig. 2-7 Face-centered cubic point lattice referred to cubic and rhombohedral cells.

of equivalent points in different unit cells can always be made identical by the addition or subtraction of a set of integral coordinates; in this case, subtraction of $0\ 0\ 1$ from $\frac{1}{2}\ \frac{1}{2}\ 1$ (the coordinates of E) gives $\frac{1}{2}\ \frac{1}{2}\ 0$ (the coordinates of D).

Note that the coordinates of a body-centered point, for example, are always $\frac{1}{2}\ \frac{1}{2}\ \frac{1}{2}$ no matter whether the unit cell is cubic, tetragonal, or orthorhombic, and whatever its size. The coordinates of a point position, such as $\frac{1}{2}\ \frac{1}{2}\ \frac{1}{2}$, may also be regarded as an operator which, when "applied" to a point at the origin, will move or translate it to the position $\frac{1}{2}\ \frac{1}{2}\ \frac{1}{2}$, the final position being obtained by simple addition of the operator $\frac{1}{2}\ \frac{1}{2}\ \frac{1}{2}$ and the original position $0\ 0\ 0$. In this sense, the positions $0\ 0\ 0$, $\frac{1}{2}\ \frac{1}{2}\ \frac{1}{2}$ are called the "body-centering translations," since they will produce the two point positions characteristic of a body-centered cell when applied to a point at the origin. Similarly, the four point positions characteristic of a face-centered cell, namely, $0\ 0\ 0$, $0\ \frac{1}{2}\ \frac{1}{2}$, $\frac{1}{2}\ 0\ \frac{1}{2}$, and $\frac{1}{2}\ \frac{1}{2}\ 0$, are called the face-centering translations. The base-centering translations depend on which pair of opposite faces are centered; if centered on the C face, for example, they are $0\ 0\ 0$, $\frac{1}{2}\ \frac{1}{2}\ 0$. These centering translations, summarized below, should be memorized:

$$\begin{aligned} \text{body-centering} &= 0\ 0\ 0, \frac{1}{2}\ \frac{1}{2}\ \frac{1}{2} \\ \text{face-centering} &= 0\ 0\ 0, 0\ \frac{1}{2}\ \frac{1}{2}, \frac{1}{2}\ 0\ \frac{1}{2}, \frac{1}{2}\ \frac{1}{2}\ 0 \\ \text{base-centering} &= 0\ 0\ 0, \frac{1}{2}\ \frac{1}{2}\ 0. \end{aligned}$$

The inclusion of $0\ 0\ 0$ may appear trivial, in that it does not move the point at the origin on which it acts, but its inclusion does remind us that cells so centered contain 2, 4, and 2 lattice points, respectively.

2-6 LATTICE DIRECTIONS AND PLANES

The direction of any line in a lattice may be described by first drawing a line through the origin parallel to the given line and then giving the coordinates of any point on the line through the origin. Let the line pass through the origin of the unit cell and any point having coordinates $u\ v\ w$, where these numbers are not necessarily integral. (This line will also pass through the points $2u\ 2v\ 2w$, $3u\ 3v\ 3w$, etc.) Then $[uvw]$, written in square brackets, are the *indices* of the direction of the line. They are also the indices of any line parallel to the given line, since the lattice is infinite and the origin may be taken at any point. Whatever the values of u , v , w , they are always converted to a set of smallest integers by multiplication or division throughout: thus, $[\frac{1}{2}\ \frac{1}{2}\ 1]$, $[112]$, and $[224]$ all represent the same direction, but $[112]$ is the preferred form. Negative indices are written with a bar over the number, e.g., $[\bar{u}vw]$. Direction indices are illustrated in Fig. 2-8. Note how one can mentally shift the origin, to avoid using the adjacent unit cell, in finding a direction like $[1\bar{2}0]$.

Directions related by symmetry are called *directions of a form*, and a set of these are represented by the indices of one of them enclosed in angular brackets; for example, the four body diagonals of a cube, $[111]$, $[1\bar{1}\bar{1}]$, $[\bar{1}\bar{1}1]$, and $[\bar{1}1\bar{1}]$, may all be represented by the symbol $\langle 111 \rangle$.

The orientation of planes in a lattice may also be represented symbolically, according to a system popularized by the English crystallographer Miller. In the

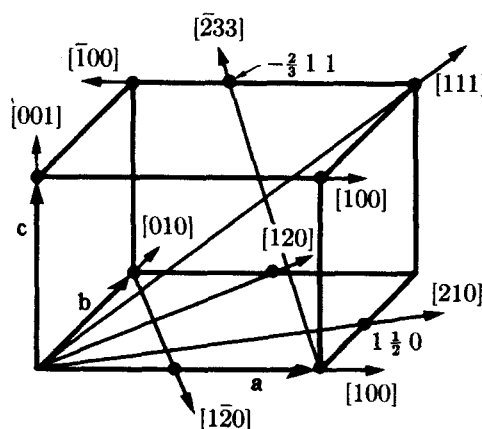


Fig. 2-8 Indices of directions.

general case, the given plane will be tilted with respect to the crystallographic axes, and, since these axes form a convenient frame of reference, we might describe the orientation of the plane by giving the actual distances, measured from the origin, at which it intercepts the three axes. Better still, by expressing these distances as fractions of the axial lengths, we can obtain numbers which are independent of the particular axial lengths involved in the given lattice. But a difficulty then arises when the given plane is parallel to a certain crystallographic axis, because such a plane does not intercept that axis, i.e., its "intercept" can only be described as "infinity." To avoid the introduction of infinity into the description of plane orientation, we can use the reciprocal of the fractional intercept, this reciprocal being zero when the plane and axis are parallel. We thus arrive at a workable symbolism for the orientation of a plane in a lattice, the *Miller indices*, which are defined as *the reciprocals of the fractional intercepts which the plane makes with the crystallographic axes*. For example, if the Miller indices of a plane are (hkl) , written in parentheses, then the plane makes fractional intercepts of $1/h$, $1/k$, $1/l$ with the axes, and, if the axial lengths are a , b , c , the plane makes actual intercepts of a/h , b/k , c/l , as shown in Fig. 2-9(a). Parallel to any plane in any lattice, there is a whole set of parallel equidistant planes, one of which passes through the origin; the Miller indices (hkl) usually refer to that plane in the set which is nearest the origin, although they may be taken as referring to any other plane in the set or to the whole set taken together.

We may determine the Miller indices of the plane shown in Fig. 2-9(b) as follows:

Axial lengths	4 Å	8 Å	3 Å
Intercept lengths	1 Å	4 Å	3 Å
Fractional intercepts	$\frac{1}{4}$	$\frac{1}{2}$	1
Miller indices	4	2	1

As stated earlier, if a plane is parallel to a given axis, its fractional intercept on that axis is taken as infinity and the corresponding Miller index is zero. If a plane cuts

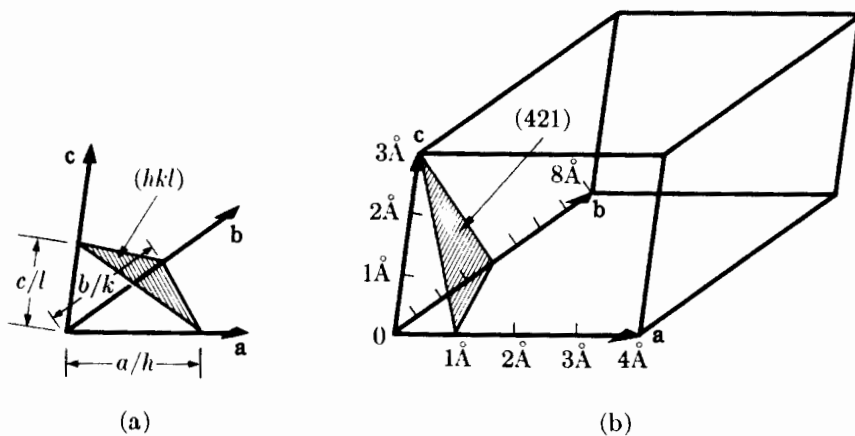


Fig. 2-9 Plane designation by Miller indices.

a negative axis, the corresponding index is negative and is written with a bar over it. Planes whose indices are the negatives of one another are parallel and lie on opposite sides of the origin, e.g., $(\bar{2}10)$ and $(2\bar{1}0)$. The planes $(nh nk nl)$ are parallel to the planes (hkl) and have $1/n$ th the spacing. The same plane may belong to two different sets, the Miller indices of one set being multiples of those of the other; thus the same plane belongs to the (210) set and the (420) set, and, in fact, the planes of the (210) set form every second plane in the (420) set. In the cubic system, it is convenient to remember that a direction $[hkl]$ is always perpendicular to a plane (hkl) of the same indices, but this is not generally true in other systems. Further familiarity with Miller indices can be gained from a study of Fig. 2-10.

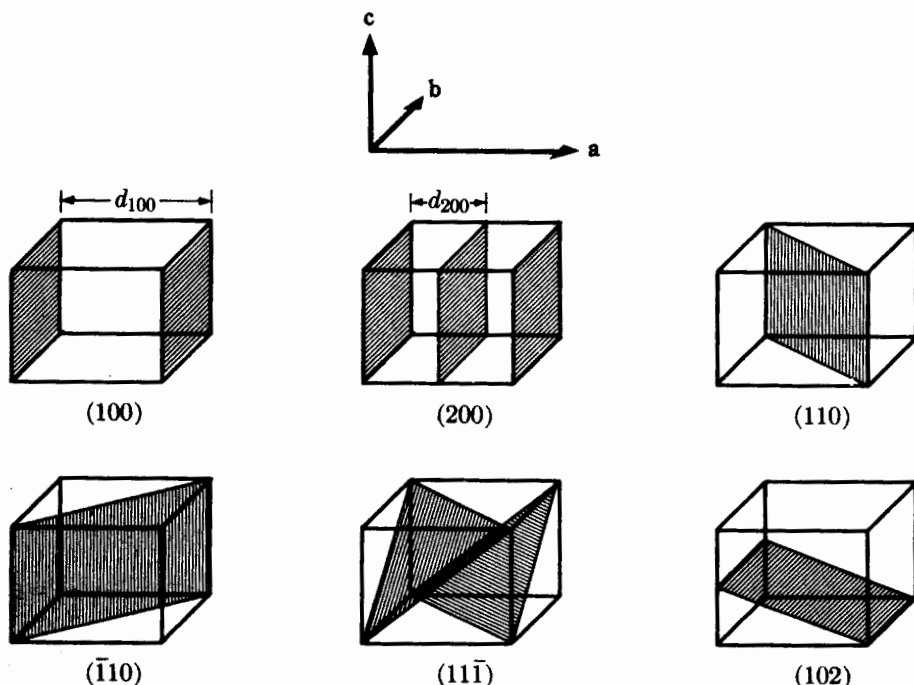


Fig. 2-10 Miller indices of lattice planes. The distance d is the plane spacing.

A slightly different system of plane indexing is used in the hexagonal system. The unit cell of a hexagonal lattice is defined by two equal and coplanar vectors \mathbf{a}_1 and \mathbf{a}_2 , at 120° to one another, and a third axis \mathbf{c} at right angles [Fig. 2-11(a)]. The complete lattice is built up, as usual, by repeated translations of the points at the unit cell corners by the vectors \mathbf{a}_1 , \mathbf{a}_2 , \mathbf{c} . Some of the points so generated are shown in the figure, at the ends of dashed lines, in order to exhibit the hexagonal symmetry of the lattice, which has a 6-fold rotation axis parallel to \mathbf{c} . The third axis \mathbf{a}_3 , lying in the basal plane of the hexagonal prism, is so symmetrically related to \mathbf{a}_1 and \mathbf{a}_2 that it is often used in conjunction with the other two. Thus the indices of a plane in the hexagonal system, called Miller-Bravais indices, refer to *four* axes and are written $(hkil)$. The index i is the reciprocal of the fractional intercept on the \mathbf{a}_3 axis. Since the intercepts of a plane on \mathbf{a}_1 and \mathbf{a}_2 determine its intercept on \mathbf{a}_3 , the value of i depends on the values of h and k . The relation is

$$h + k = -i. \quad (2-2)$$

Since i is determined by h and k , it is sometimes replaced by a dot and the plane symbol written $(hk \cdot l)$. Sometimes even the dot is omitted. However, this usage defeats the purpose for which Miller-Bravais indices were devised, namely, to give similar indices to similar planes. For example, the side planes of the hexagonal prism in Fig. 2-11(b) are all similar and symmetrically located, and their relationship is clearly shown in their full Miller-Bravais symbols: $(10\bar{1}0)$, $(01\bar{1}0)$, $(\bar{1}100)$, $(\bar{1}010)$, $(0\bar{1}10)$, $(1\bar{1}00)$. On the other hand, the abbreviated symbols of these planes, $(10 \cdot 0)$, $(01 \cdot 0)$, $(\bar{1}1 \cdot 0)$, $(\bar{1}0 \cdot 0)$, $(0\bar{1} \cdot 0)$, $(1\bar{1} \cdot 0)$ do not immediately suggest this relationship.

Directions in a hexagonal lattice are best expressed in terms of the *three* basic vectors \mathbf{a}_1 , \mathbf{a}_2 , and \mathbf{c} . Figure 2-11(b) shows several examples of both plane and direction indices. Another system, involving four indices, is sometimes used to designate directions. The required direction is broken up into four component vectors, parallel to \mathbf{a}_1 , \mathbf{a}_2 , \mathbf{a}_3 , and \mathbf{c} and so chosen that the third index is the

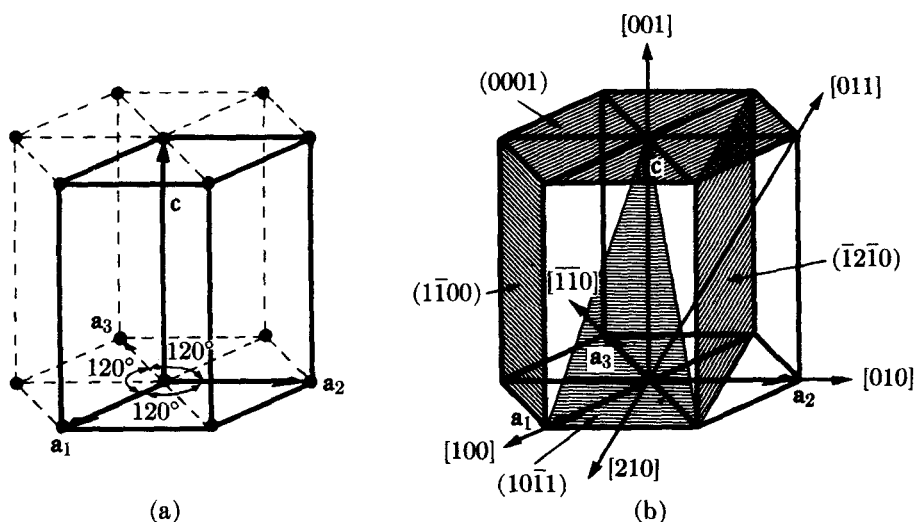


Fig. 2-11 (a) The hexagonal unit cell (heavy lines) and (b) indices of planes and directions.

negative of the sum of the first two. Then, if $[UVW]$ are the indices of a direction referred to three axes and $[uvw]$ the four-axis indices, the two are related as follows:

$$\begin{aligned} U &= u - t & u &= (2U - V)/3 \\ V &= v - t & v &= (2V - U)/3 \\ W &= w & t &= -(u + v) = -(U + V)/3 \\ && w &= W. \end{aligned}$$

Thus, $[100]$ becomes $[2\bar{1}\bar{1}0]$, $[210]$ becomes $[10\bar{1}\bar{0}]$, etc.

Note that the indices of a plane or direction are meaningless unless the orientation of the unit-cell axes is given. This means that the indices of a particular lattice plane depend on the unit cell chosen. For example, consider the right-hand vertical plane of the cell shown by full lines in Fig. 2-4; the indices of this plane are of the form $\{100\}$ for the base-centered cell and $\{110\}$ for the simple cell.

In any crystal system there are sets of equivalent lattice planes related by symmetry. These are called *planes of a form*, and the indices of any one plane, enclosed in braces $\{hkl\}$, stand for the whole set. In general, planes of a form have the same spacing but different Miller indices. For example, the faces of a cube, (100) , (010) , $(\bar{1}00)$, $(0\bar{1}0)$, (001) , and $(00\bar{1})$, are planes of the form $\{100\}$, since all of them may be generated from any one by operation of the 4-fold rotation axes perpendicular to the cube faces. In the tetragonal system, however, only the planes (100) , (010) , $(\bar{1}00)$, and $(0\bar{1}0)$ belong to the form $\{100\}$; the other two planes, (001) and $(00\bar{1})$, belong to the different form $\{001\}$; the first four planes mentioned are related by a 4-fold axis and the last two by a 2-fold axis.*

Planes of a zone are planes which are all parallel to one line, called the *zone axis*, and the zone, i.e., the set of planes, is specified by giving the indices of the zone axis. Such planes may have quite different indices and spacings, the only requirement being their parallelism to a line. Figure 2-12 shows some examples. If the axis of a zone has indices $[uvw]$, then any plane belongs to that zone whose indices (hkl) satisfy the relation

$$hu + kv + lw = 0. \quad (2-3)$$

(A proof of this relation is given in Sec. 3 of Appendix 1.) Any two nonparallel planes are planes of a zone since they are both parallel to their line of intersection. If their indices are $(h_1k_1l_1)$ and $(h_2k_2l_2)$, then the indices of their zone axis $[uvw]$ are given by the relations

$$\begin{aligned} u &= k_1l_2 - k_2l_1, \\ v &= l_1h_2 - l_2h_1, \\ w &= h_1k_2 - h_2k_1. \end{aligned} \quad (2-4)$$

* Certain important crystal planes are often referred to by name without any mention of their Miller indices. Thus, planes of the form $\{111\}$ in the cubic system are often called octahedral planes, since these are the bounding planes of an octahedron. In the hexagonal system, the (0001) plane is called the basal plane, planes of the form $\{10\bar{1}0\}$ are called prismatic planes, and planes of the form $\{10\bar{1}1\}$ are called pyramidal planes.

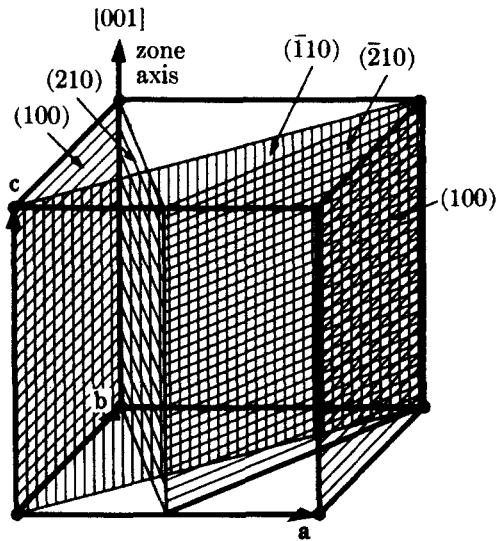


Fig. 2-12 All shaded planes in the cubic lattice shown are planes of the zone [001].

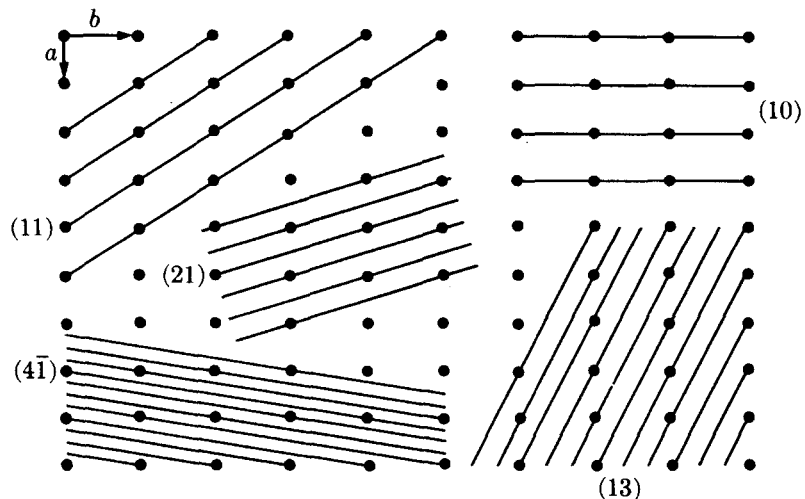


Fig. 2-13 Two-dimensional lattice, showing that lines of lowest indices have the greatest spacing and the greatest density of lattice points.

The various sets of planes in a lattice have various values of interplanar spacing. The planes of large spacing have low indices and pass through a high density of lattice points, whereas the reverse is true of planes of small spacing. Figure 2-13 illustrates this for a two-dimensional lattice, and it is equally true in three dimensions. The interplanar spacing d_{hkl} , measured at right angles to the planes, is a function both of the plane indices (hkl) and the lattice constants ($a, b, c, \alpha, \beta, \gamma$). The exact relation depends on the crystal system involved and for the cubic system takes on the relatively simple form

$$(Cubic) \quad d_{hkl} = \frac{a}{\sqrt{h^2 + k^2 + l^2}}. \quad (2-5)$$

In the tetragonal system the spacing equation naturally involves both a and c since these are not generally equal:

$$(Tetragonal) \quad d_{hkl} = \frac{a}{\sqrt{h^2 + k^2 + l^2 (a^2/c^2)}}. \quad (2-6)$$

Interplanar spacing equations for all systems are given in Appendix 3.

2-7 CRYSTAL STRUCTURE

So far we have discussed topics from the field of *mathematical (geometrical) crystallography* and have said practically nothing about actual crystals and the atoms of which they are composed. In fact, all of the above was well known long before the discovery of x-ray diffraction, i.e., long before there was any certain knowledge of the interior arrangements of atoms in crystals.

It is now time to describe the structure of some actual crystals and to relate this structure to the point lattices, crystal systems, and symmetry elements discussed above. The cardinal principle of crystal structure is that *the atoms of a crystal are set in space either on the points of a Bravais lattice or in some fixed relation to those points*. It follows from this that the atoms of a crystal will be arranged periodically in three dimensions and that this arrangement of atoms will exhibit many of the properties of a Bravais lattice, in particular many of its symmetry elements.

The simplest crystals one can imagine are those formed by placing atoms of the same kind *on* the points of a Bravais lattice. Not all such crystals exist but, fortunately for metallurgists, many metals crystallize in this simple fashion, and Fig. 2-14 shows two common structures based on the body-centered cubic (BCC) and face-centered cubic (FCC) lattices. The former has two atoms per unit cell and the latter four, as we can find by rewriting Eq. (2-1) in terms of the number of atoms, rather than lattice points, per cell and applying it to the unit cells shown.

The next degree of complexity is encountered when two or more atoms of the same kind are “associated with” each point of a Bravais lattice, as exemplified by the hexagonal close-packed (HCP) structure common to many metals. This structure is simple hexagonal and is illustrated in Fig. 2-15. There are two atoms per unit cell, as shown in (a), one at 0 0 0 and the other at $\frac{2}{3} \frac{1}{3} \frac{1}{2}$ (or at $\frac{1}{3} \frac{2}{3} \frac{1}{2}$, which is an equivalent position). Figure 2-15(b) shows the same structure with the origin of the unit cell shifted so that the point 1 0 0 in the new cell is midway between

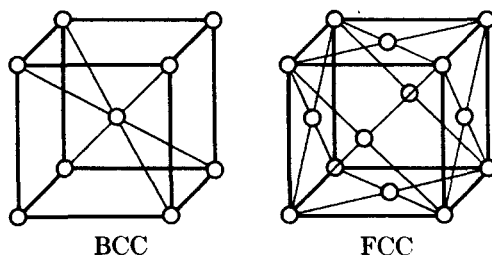


Fig. 2-14 Structures of some common metals. Body-centered cubic: α -Fe, Cr, Mo, V, etc.; face-centered cubic: γ -Fe, Cu, Pb, Ni, etc.

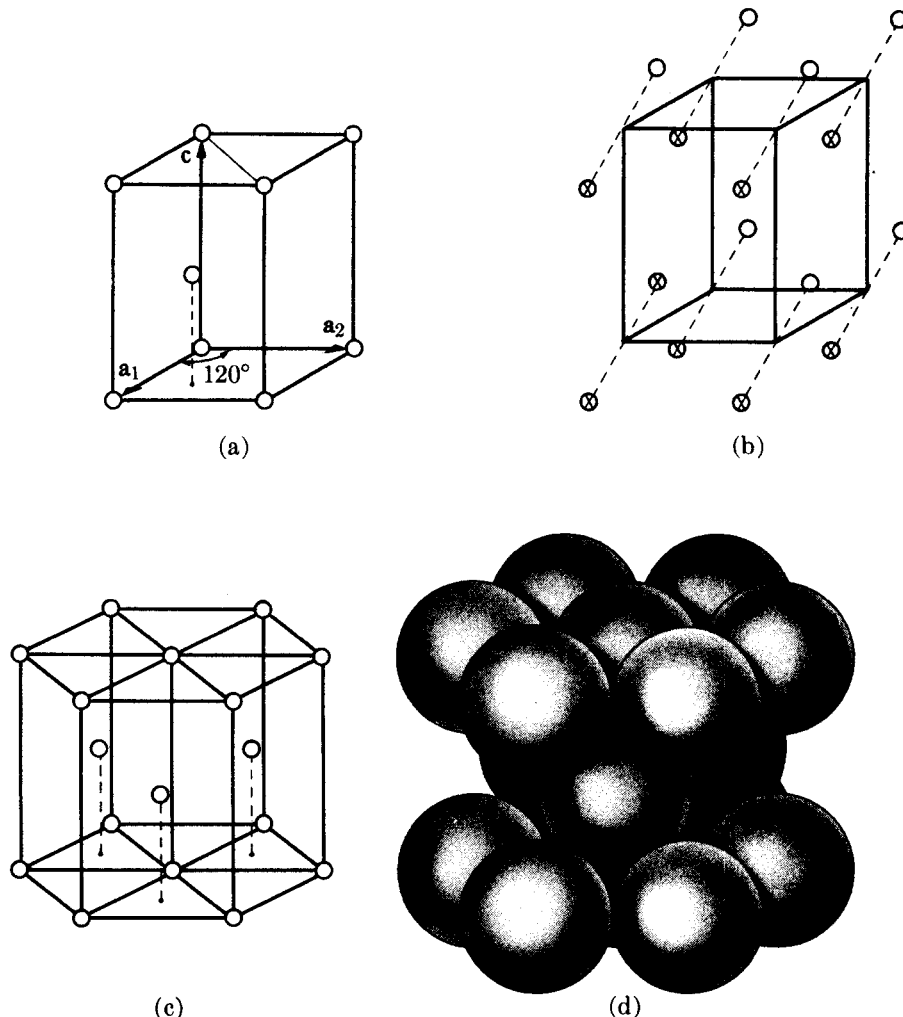


Fig. 2-15 The hexagonal close-packed structure, shared by Zn, Mg, Be, α -Ti, etc.

the atoms at $1\ 0\ 0$ and $\frac{2}{3}\ \frac{1}{3}\ \frac{1}{2}$ in (a), the nine atoms shown in (a) corresponding to the nine atoms marked with an X in (b). The “association” of pairs of atoms with the points of a simple hexagonal Bravais lattice is suggested by the dashed lines in (b). Note, however, that the atoms of a close-packed hexagonal structure do not themselves form a point lattice, the surroundings of an atom at $0\ 0\ 0$ being different from those of an atom at $\frac{2}{3}\ \frac{1}{3}\ \frac{1}{2}$. Figure 2-15(c) shows still another representation of the HCP structure: the three atoms in the interior of the hexagonal prism are directly above the centers of alternate triangles in the base and, if repeated through space by the vectors a_1 and a_2 , would also form a hexagonal array just like the atoms in the layers above and below.

The HCP structure is so called because it is one of the two ways in which spheres can be packed together in space with the greatest possible density and still have a periodic arrangement. Such an arrangement of spheres in contact is shown in Fig. 2-15(d). If these spheres are regarded as atoms, then the resulting picture of an HCP metal is much closer to physical reality than is the relatively open

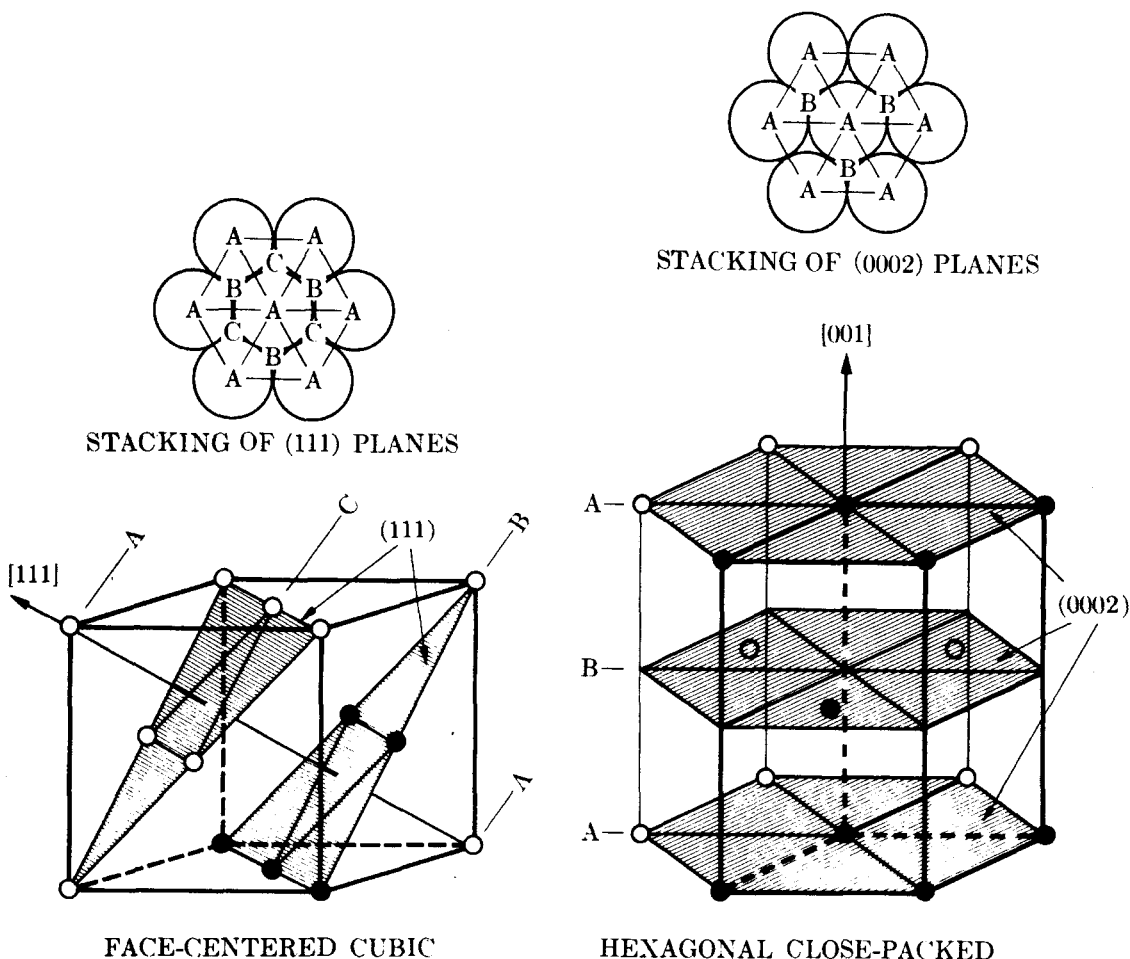


Fig. 2-16 Comparison of FCC and HCP structures. The black atoms in the FCC drawing delineate half a hexagon, which is completed on the same plane extended into the next unit cell below (not shown).

structure suggested by the drawing of Fig. 2-15(c), and this is true, generally, of all crystals. On the other hand, it may be shown that the ratio of c to a in an HCP structure formed of spheres in contact is 1.633 whereas the c/a ratio of metals having this structure varies from about 1.58 (Be) to 1.89 (Cd). As there is no reason to suppose that the atoms in these crystals are not in contact, it follows that they must be ellipsoidal in shape rather than spherical.

The FCC structure is an equally close-packed arrangement. Its relation to the HCP structure is not immediately obvious, but Fig. 2-16 shows that the atoms on the (111) planes of the FCC structure are arranged in a hexagonal pattern just like the atoms on the (0002) planes of the HCP structure. The only difference between the two structures is the way in which these hexagonal sheets of atoms are arranged above one another. In an HCP metal, the atoms in the second layer are above the hollows in the first layer and the atoms in the third layer are above the atoms in the first layer, so that the layer stacking sequence can be summarized as $A\ B\ A\ B\ A\ B\ \dots$. The first two atom layers of an FCC metal are put down in the same way, but the atoms of the third layer are so placed in the hollows of the second

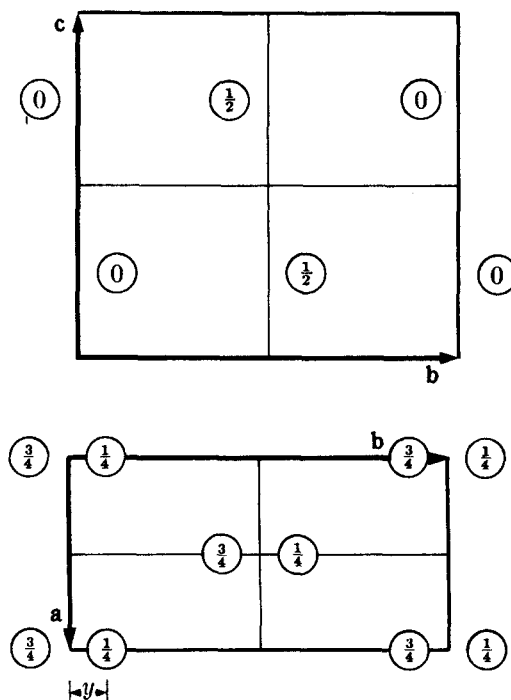


Fig. 2-17 The structure of α -uranium, after Jacob and Warren [2.1].

layer that not until the fourth layer does a position repeat. FCC stacking therefore has the sequence $A B C A B C \dots$. These stacking schemes are indicated in the plan views shown in Fig. 2-16.

Another example of the “association” of more than one atom with each point of a Bravais lattice is given by uranium. The structure of the form stable at room temperature, α -uranium, is illustrated in Fig. 2-17 by plan and elevation drawings. In such drawings, the height of an atom (expressed as a fraction of the axial length) above the plane of the drawing (which includes the origin of the unit cell and two of the cell axes) is given by the numbers marked on each atom. The Bravais lattice is base-centered orthorhombic, centered on the C face, and Fig. 2-17 shows how the atoms occur in pairs through the structure, each pair associated with a lattice point. There are four atoms per unit cell, located at $0 y \frac{1}{4}$, $0 \bar{y} \frac{3}{4}$, $\frac{1}{2} (\frac{1}{2} + y) \frac{1}{4}$, and $\frac{1}{2} (\frac{1}{2} - y) \frac{3}{4}$. Here we have an example of a variable parameter y in the atomic coordinates. Crystals often contain such variable parameters, which may have any fractional value without destroying any of the symmetry elements of the structure. A quite different substance might have exactly the same structure as uranium except for slightly different values of a , b , c , and y . For uranium y is 0.105 ± 0.005 .

Turning to the crystal structure of *compounds* of unlike atoms, we find that the structure is built up on the skeleton of a Bravais lattice but that certain other rules must be obeyed, precisely because there are unlike atoms present. Consider, for example, a crystal of A_xB_y , which might be an ordinary chemical compound, an intermediate phase of relatively fixed composition in some alloy system, or an ordered solid solution. Then the arrangement of atoms in A_xB_y must satisfy the

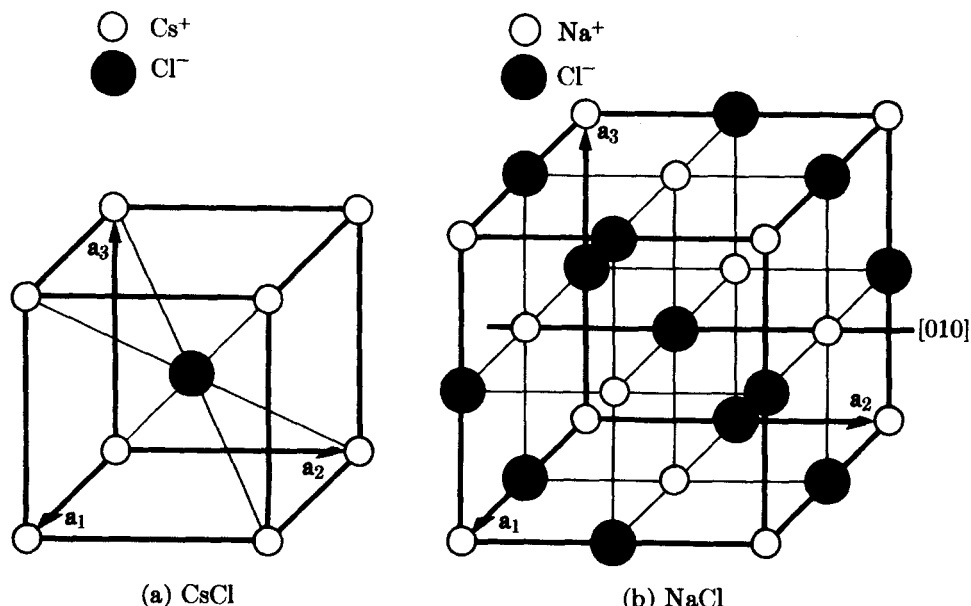


Fig. 2-18 The structures of (a) CsCl (common to CsBr, NiAl, ordered β -brass, ordered CuPd, etc.) and (b) NaCl (common to KCl, CaSe, PbTe, etc.).

following conditions:

1. Body-, face-, or base-centering translations, if present, must begin and end on atoms of the same kind. For example, if the structure is based on a body-centered Bravais lattice, then it must be possible to go from an A atom, say, to *another* A atom by the translation $\frac{1}{2} \frac{1}{2} \frac{1}{2}$.
 2. The set of A atoms in the crystal and the set of B atoms must separately possess the same symmetry elements as the crystal as a whole, since in fact they make up the crystal. In particular, the operation of any symmetry element present must bring a given atom, A for example, into coincidence with another atom of the same kind, namely A.

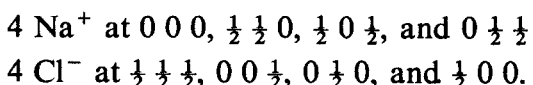
Suppose we consider the structures of a few common crystals in light of the above requirements. Figure 2-18 illustrates the unit cells of two ionic compounds, CsCl and NaCl. These structures, both cubic, are common to many other crystals and, wherever they occur, are referred to as the "CsCl structure" and the "NaCl structure." In considering a crystal structure, one of the most important things to determine is its Bravais lattice, since that is the basic framework on which the crystal is built and because, as we shall see later, it has a profound effect on the way in which that crystal diffracts x-rays.

What is the Bravais lattice of CsCl? Figure 2-18(a) shows that the unit cell contains two atoms, ions really, since this compound is completely ionized even in the solid state: a caesium ion at $0\ 0\ 0$ and a chlorine ion at $\frac{1}{2}\ \frac{1}{2}\ \frac{1}{2}$. The Bravais lattice is obviously not face-centered, but we note that the body-centering translation $\frac{1}{2}\ \frac{1}{2}\ \frac{1}{2}$ connects two atoms. However, these are unlike atoms and the lattice is therefore *not* body-centered. It is, by elimination, simple cubic. If one wishes, one may think of both ions, the caesium at $0\ 0\ 0$ and the chlorine at $\frac{1}{2}\ \frac{1}{2}\ \frac{1}{2}$, as being

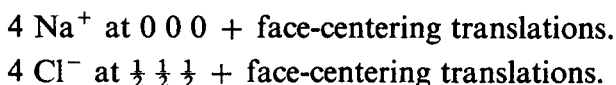
52 Geometry of crystals

associated with the lattice point at 0 0 0. It is not possible, however, to associate any one caesium ion with any particular chlorine ion and refer to them as a CsCl molecule; the term "molecule" therefore has no real physical significance in such a crystal, and the same is true of most inorganic compounds and alloys.

Close inspection of Fig. 2-18(b) will show that the unit cell of NaCl contains 8 ions, located as follows:

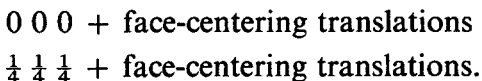


The sodium ions are clearly face-centered, and we note that the face-centering translations ($0\ 0\ 0, \frac{1}{2}\ \frac{1}{2}\ 0, \frac{1}{2}\ 0\ \frac{1}{2}, 0\ \frac{1}{2}\ \frac{1}{2}$), when applied to the chlorine ion at $\frac{1}{2}\ \frac{1}{2}\ \frac{1}{2}$, will reproduce all the chlorine-ion positions. The Bravais lattice of NaCl is therefore face-centered cubic. The ion positions, incidentally, may be written in summary form as:



Note also that in these, as in all other structures, the operation of any symmetry element possessed by the lattice must bring similar atoms or ions into coincidence. For example, in Fig. 2-18(b), 90° rotation about the 4-fold [010] rotation axis shown brings the chlorine ion at $0\ 1\ \frac{1}{2}$ into coincidence with the chlorine ion at $\frac{1}{2}\ 1\ 1$, the sodium ion at $0\ 1\ 1$ with the sodium ion at $1\ 1\ 1$, etc.

Elements and compounds often have closely similar structures. Figure 2-19 shows the unit cells of diamond and the zinc-blende form of ZnS. Both are face-centered cubic. Diamond has 8 atoms per unit cell, located at



The atom positions in zinc blende are identical with these, but the first set of positions is now occupied by one kind of atom (S) and the other by a different kind (Zn).

Note that diamond and a metal like copper have quite dissimilar structures, although both are based on a face-centered cubic Bravais lattice. To distinguish between these two, the terms "diamond cubic" and "face-centered cubic" are usually used. The industrially important semiconductors, silicon and germanium, have the diamond cubic structure.

Instead of referring to a structure by name, such as the "NaCl structure," one can use the designations introduced years ago in *Strukturbericht* [G.1]. These consist of a letter and a number: the letter A indicates an element, B an AB compound, C an AB_2 compound, etc. The structure of copper, for example, is called the A1 structure, α -Fe is A2, zinc is A3, diamond is A4, NaCl is B1, etc. A full list is given by Pearson [G.16, Vol. 1, p. 85].

Some rather complex crystals can be built on a cubic lattice. For example, the ferrites, which are magnetic and are used as memory cores in digital computers, have the formula $\text{MO} \cdot \text{Fe}_2\text{O}_3$, where M is a divalent metal ion like Mn, Ni, Fe, Co, etc. Their structure is related to that of the mineral spinel. The Bravais lattice of the ferrites is face-centered cubic, and the unit cell contains 8 "molecules" or a

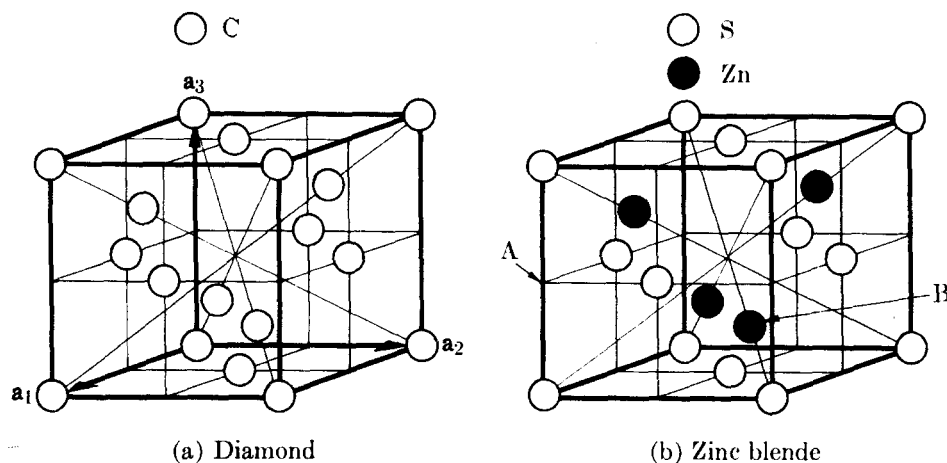


Fig. 2-19 The structures of (a) diamond (common to Si, Ge, and gray Sn) and (b) the zinc-blende form of ZnS (common to HgS, CuI, AlSb, BeSe, etc.).

total of $8 \times 7 = 56$ ions. There are therefore $56/4$ or 14 ions associated with each lattice point.

The number of atoms per unit cell in any crystal is partially dependent on its Bravais lattice. For example, the number of atoms per unit cell in a crystal based on a body-centered lattice must be a multiple of 2, since there must be, for any atom in the cell, a corresponding atom of the same kind at a translation of $\frac{1}{2} \frac{1}{2} \frac{1}{2}$ from the first. The number of atoms per cell in a base-centered lattice must also be a multiple of 2, as a result of the base-centering translations. Similarly, the number of atoms per cell in a face-centered lattice must be a multiple of 4.

The reverse of these propositions is not true. It would be a mistake to assume, for example, that if the number of atoms per cell is a multiple of 4, then the lattice is necessarily face-centered. The unit cell of the intermediate phase AuBe, for example (Fig. 2-20), contains 8 atoms and yet it is based on a simple cubic Bravais lattice. The atoms are located as follows:

4 Au at

$$u \, u \, u, (\tfrac{1}{2} + u) (\tfrac{1}{2} - u) \bar{u}, \bar{u} (\tfrac{1}{2} + u) (\tfrac{1}{2} - u), (\tfrac{1}{2} - u) \bar{u} (\tfrac{1}{2} + u),$$

4 Be at

$$w w w, (\tfrac{1}{2} + w) (\tfrac{1}{2} - w) \bar{w}, \bar{w} (\tfrac{1}{2} + w) (\tfrac{1}{2} - w), (\tfrac{1}{2} - w) \bar{w} (\tfrac{1}{2} + w),$$

where $u = 0.100$ and $w = 0.406$, each ± 0.005 . If the parameter u is put equal to zero, the atomic coordinates of the gold atoms become those of a face-centered cubic cell. The structure of AuBe may therefore be regarded as distorted face-centered cubic, in which the presence of the beryllium atoms has forced the gold atoms out of their original positions by a distance $\pm u$, $\pm u$, $\pm u$. These translations are all in directions of the form $\langle 111 \rangle$, i.e., parallel to body diagonals of the cube, and are shown as dotted lines in Fig. 2-20.

It should now be apparent that the term "simple," when applied to a Bravais lattice, is used in a very special, technical sense and that some very complex structures can be built up on a "simple" lattice. In fact, they may contain more than a hundred atoms per unit cell. The only workable definition of a simple

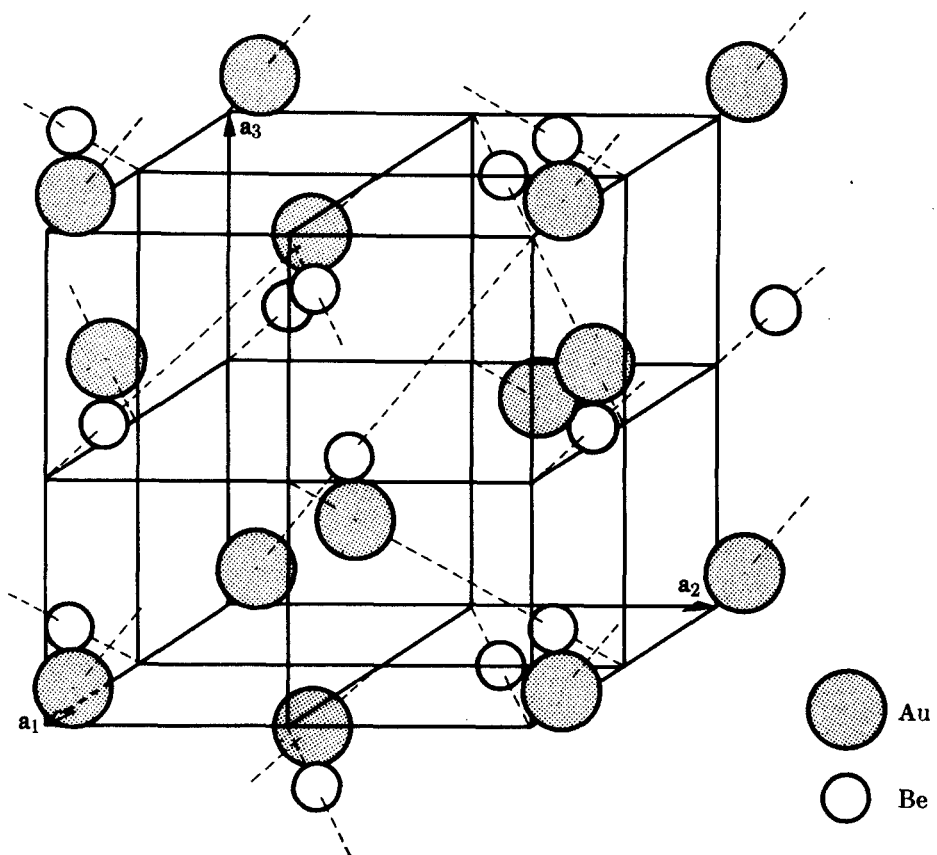


Fig. 2–20 The structure of AuBe, shared by FeSi, NiSi, CoSi, MnSi, etc. It is known as the FeSi structure [2.2].

lattice is a negative one: a given lattice is simple if it is neither body-, base-, nor face-centered; these latter possibilities can be ruled out by showing that the set of atomic positions does not contain the body-, base-, or face-centering translations. There is no rule governing the allowable number of atoms per cell in a simple lattice: this number may take on any one of the values 1, 2, 3, 4, 5, etc., although not in every crystal system and not every higher integer is permitted. Incidentally, not every theoretical possibility known to mathematical crystallography is realized in nature; for example, no known element crystallizes with a simple hexagonal lattice containing one atom per unit cell.

There is one other way of arranging unlike atoms on a point lattice besides those considered so far and that is exemplified by the structure of *solid solutions*. These solutions are of two types, substitutional and interstitial; in the former, solute atoms substitute for, or replace, solvent atoms on the lattice of the solvent, while in the latter, solute atoms fit into the interstices of the solvent lattice. The interesting feature of these structures is that the solute atoms are distributed more or less at random. For example, consider a 10 atomic percent solution of molybdenum in chromium, which has a BCC structure. The molybdenum atoms can occupy either the corner or body-centered positions of the cube in a random, irregular manner, and a small portion of the crystal might have the appearance of Fig. 2-21(a). Five adjoining unit cells are shown there, with a total of 29 atoms,

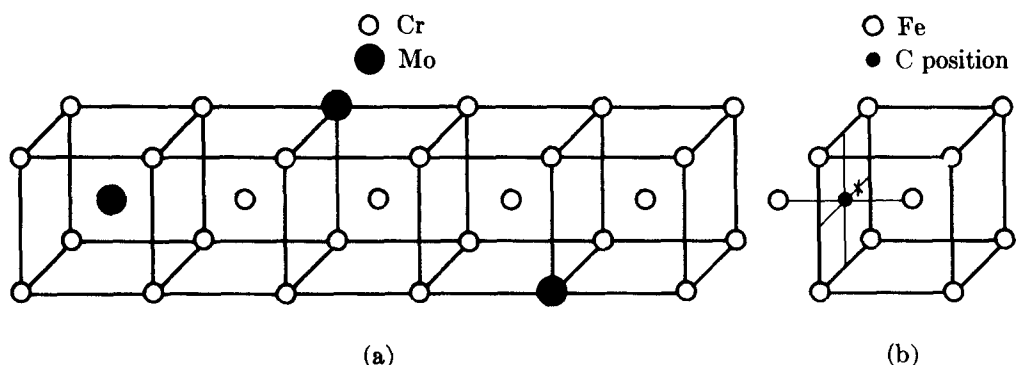


Fig. 2-21 Structure of solid solutions: (a) Mo in Cr (substitutional); (b) C in α -Fe (interstitial).

3 of which are molybdenum. This section of the crystal therefore contains somewhat more than 10 atomic percent molybdenum, but the next five cells would probably contain somewhat less. Such a structure does not obey the ordinary rules of crystallography: for example, the right-hand cell of the group shown does not have cubic symmetry, and one finds throughout the structure that the translation given by one of the unit cell vectors may begin on an atom of one kind and end on an atom of another kind. All that can be said of this structure is that it is BCC *on the average*, and experimentally we find that it displays the x-ray diffraction effects proper to a BCC lattice. This is not surprising since the x-ray beam used to examine the crystal is so large compared to the size of a unit cell that it observes, so to speak, millions of unit cells at the same time and so obtains only an average “picture” of the structure.

The above remarks apply equally well to interstitial solid solutions. These form whenever the solute atom is small enough to fit into the solvent lattice without causing too much distortion. Ferrite, the solid solution of carbon in α -iron, is a good example.* In the unit cell shown in Fig. 2-21(b), there are two kinds of "holes" in the lattice: one at $\frac{1}{2} 0 \frac{1}{2}$ (marked •) and equivalent positions in the centers of the cube faces and edges, and one at $\frac{1}{4} 0 \frac{1}{2}$ (marked x) and equivalent positions. All the evidence at hand points to the fact that the carbon atoms in ferrite are located in the holes at $\frac{1}{2} 0 \frac{1}{2}$ and equivalent positions. On the average, however, no more than about 1 of these positions in 500 unit cells is occupied, since the maximum solubility of carbon in ferrite is only about 0.1 atomic percent.

Still another type of structure worth noting is that of *ordered solid solutions*. As described above, a typical substitutional solid solution has solute atoms distributed more or less at random on the lattice points of the solvent.[†] On the other hand, there are solutions in which this is true only at elevated temperatures; when cooled to lower temperatures, the solute atoms take up an orderly, periodic

* Note the double meaning of the word *ferrite*: (1) metallurgical, for the metallic solid solution mentioned above, and (2) mineralogical, for the oxide $\text{MO} \cdot \text{Fe}_2\text{O}_3$ previously described.

† Of course, when the solution becomes concentrated, there is no real distinction between "solvent" and "solute." There is only one lattice, with two or more kinds of atoms distributed on it.

arrangement while still remaining on the lattice points of the solvent. The solid solution is then said to be *ordered* and to possess a *superlattice*. The alloy AuCu₃ is a classic example: at high temperatures the copper and gold atoms are located more or less at random on face-centered cubic lattice sites, while at low temperature the gold atoms occupy only the cube corner positions and the copper atoms only the face-centered positions. In its temperature range of stability then, an ordered solid solution resembles a chemical compound, with atoms of one kind on one set of lattice sites and atoms of a different kind on another set. But an ordered solid solution is a "half-hearted compound" because, when heated, it disorders before it melts; a real compound, like NaCl, remains ordered right up to the melting point. Crystallographically, the structures of the disordered and ordered solid solutions are quite different; disordered AuCu₃ is, on the average, face-centered cubic while the ordered form is simple cubic. Such structures will be discussed more fully in Chap. 13.

2-8 ATOM SIZES AND COORDINATION

When two or more unlike atoms unite to form a chemical compound, intermediate phase, or solid solution, the kind of structure formed is dependent, in part, on the relative sizes of the atoms involved. But what is meant by the size of an atom? To regard an atom as something like a billiard ball with a sharply defined bounding surface is surely an oversimplification, since we know that the electron density decreases gradually at the "surface" of the atom and that there is a small but finite probability of finding an electron at quite large distances from the nucleus. And yet the only practical way we have of defining atomic size lies in considering a crystal as a collection of rigid spheres in contact. The size of an atom, then, is given by the distance of closest approach of atom centers in a crystal of the element, and this distance can be calculated from the lattice parameters.

For example, the lattice parameter a of α -iron is 2.87 Å, and in a BCC lattice the atoms are in contact only along the diagonals of the unit cube. The diameter of an iron atom is therefore equal to one half the length of the cube diagonal, or $(\sqrt{3}/2)a = 2.48$ Å. The following formulas give the distance of closest approach in the three common metal structures:

$$\begin{aligned} \text{BCC} &= \frac{\sqrt{3}}{2} a, \\ \text{FCC} &= \frac{\sqrt{2}}{2} a, \\ \text{HCP} &= a \quad (\text{between atoms in basal plane}), \\ &= \sqrt{\frac{a^2}{3} + \frac{c^2}{4}} \quad (\text{between atom in basal plane and neighbors above or below}). \end{aligned} \tag{2-7}$$

Values of the distance of closest approach, together with the crystal structures and lattice parameters of the elements, are tabulated in Appendix 5.

To a first approximation, the size of an atom is a constant. In other words, an iron atom has about the same size whether it occurs in pure iron, an intermediate phase, or a solid solution. This is a very useful fact to remember when investigating unknown crystal structures, for it enables us to predict roughly how large a hole is necessary in a proposed structure to accommodate a given atom. More precisely, it is known that the size of an atom has a slight dependence on its *coordination number*, which is the number of nearest neighbors of the given atom and which depends on crystal structure. The coordination number of an atom in the FCC or HCP structures is 12, in BCC 8, and diamond cubic 4. The smaller the coordination number, the smaller the volume occupied by a given atom, and the approximate amount of contraction to be expected with decrease in coordination number is found to be:

Change in coordination	Size contraction, percent
12 → 8	3
12 → 6	4
12 → 4	12

This means, for example, that the diameter of an iron atom is greater if the iron is dissolved in FCC copper than if it exists in a crystal of BCC α -iron or is dissolved in BCC vanadium. If it were dissolved in copper, its diameter would be approximately $2.48/0.97$, or 2.56 \AA .

The size of an atom in a crystal also depends on whether its binding is ionic, covalent, metallic, or van der Waals, and on its state of ionization. The more electrons are removed from a neutral atom the smaller it becomes, as shown strikingly for iron, whose atoms and ions Fe , Fe^{++} , Fe^{+++} have diameters of 2.48, 1.66, and 1.34 \AA , respectively.

The spatial arrangement of atoms about a given point is often described by words such as *octahedral* and *tetrahedral*. For example, in the NaCl structure of Fig. 2-18(b) the central Cl^- ion at $\frac{1}{2} \frac{1}{2} \frac{1}{2}$ is said to be octahedrally surrounded by Na^+ ions, because the six Na^+ ions in the face-centered positions lie on the corners of an octahedron, a solid bounded by eight triangular sides. In the zinc blende structure of Fig. 2-19(b) the empty position marked *A* is octahedrally surrounded by sulphur atoms, of which only four are in the cell shown, and would be referred to as an octahedral hole in the structure. This group of atoms is shown separately in Fig. 2-22. In the same structure the Zn atom at $\frac{3}{4} \frac{3}{4} \frac{1}{4}$, marked *B* in Fig. 2-19(b), is surrounded by four S atoms at the corners of a tetrahedron, a solid bounded by four triangular sides (Fig. 2-22). In fact, all four of the Zn atoms in the unit cell have tetrahedral S surroundings. Also in the ZnS structure the reader can demonstrate, by sketching three cells adjacent to the one shown, that the hole at *A* is tetrahedrally surrounded by Zn atoms. Thus, the hole at *A* has both octahedral (S) and tetrahedral (Zn) surroundings, an unusual circumstance.

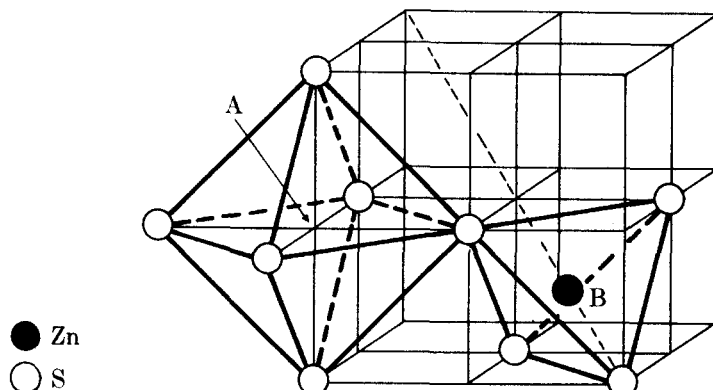


Fig. 2-22 Portion of the zinc blende structure. Compare Fig. 2-19(b). The hole at *A* has octahedral surroundings. The Zn atom at *B* has tetrahedral surroundings.

2-9 CRYSTAL SHAPE

We have said nothing so far about the shape of crystals, preferring to concentrate instead on their interior structure. However, the shape of crystals is, to the layman, perhaps their most characteristic property, and nearly everyone is familiar with the beautifully developed flat faces exhibited by natural minerals or crystals artificially grown from a supersaturated salt solution. In fact, it was with a study of these faces and the angles between them that the science of crystallography began.

Nevertheless, the shape of crystals is really a secondary characteristic, since it depends on, and is a consequence of, the interior arrangement of atoms. Sometimes the external shape of a crystal is rather obviously related to its smallest building block, the unit cell, as in the little cubical grains of ordinary table salt (NaCl has a cubic lattice) or the six-sided prisms of natural quartz crystals (hexagonal lattice). In many other cases, however, the crystal and its unit cell have quite different shapes; gold, for example, has a cubic lattice, but natural gold crystals are octahedral in form, i.e., bounded by eight planes of the form {111}.

An important fact about crystal faces was known long before there was any knowledge of crystal interiors. It is expressed as the *law of rational indices*, which states that the indices of naturally developed crystal faces are always composed of small whole numbers, rarely exceeding 3 or 4. Thus, faces of the form {100}, {111}, {1100}, {210}, etc., are observed but not such faces as {510}, {719}, etc. We know today that planes of low indices have the largest density of lattice points, and it is a law of crystal growth that such planes develop at the expense of planes with high indices and few lattice points.

To a metallurgist, however, crystals with well-developed faces are in the category of things heard of but rarely seen. They occur occasionally on the free surface of castings, in some electrodeposits, or under other conditions of no external constraint. To a metallurgist, a crystal is most usually a "grain," seen through a microscope in the company of many other grains on a polished section. If he has an isolated single crystal, it will have been artificially grown either from the melt, and thus have the shape of the crucible in which it solidified, or by re-

crystallization, and thus have the shape of the starting material, whether sheet, rod, or wire.

The shapes of the grains in a polycrystalline mass of metal are the result of several kinds of forces, all of which are strong enough to counteract the natural tendency of each grain to grow with well-developed flat faces. The result is a grain roughly polygonal in shape with no obvious aspect of crystallinity. Nevertheless, that grain is a crystal and just as "crystalline" as, for example, a well-developed prism of natural quartz, since the essence of crystallinity is a periodicity of inner atomic arrangement and not any regularity of outward form.

2-10 TWINNED CRYSTALS

Some crystals have two parts symmetrically related to one another. These, called twinned crystals, are fairly common both in minerals and in metals and alloys. For a detailed discussion of twinning, see Kelly and Groves [G.33] and Barrett and Massalski [G.25].

The relationship between the two parts of a twinned crystal is described by the symmetry operation which will bring one part into coincidence with the other or with an extension of the other. Two main kinds of twinning are distinguished, depending on whether the symmetry operation is 180° rotation about an axis, called the twin axis, or reflection across a plane, called the twin plane. The plane on which the two parts of a twinned crystal are united is called the composition plane. In the case of a reflection twin, the composition plane may or may not coincide with the twin plane.

Of most interest to metallurgists, who deal mainly with FCC, BCC, and HCP structures, are the following kinds of twins:

1. Annealing twins, such as occur in FCC metals and alloys (Cu, Ni, α -brass, Al, etc.), which have been cold-worked and then annealed to cause recrystallization.
2. Deformation twins, such as occur in deformed HCP metals (Zn, Mg, Be, etc.) and BCC metals (α -Fe, W, etc.).

Annealing Twins

Annealing twins in FCC metals are rotation twins, in which the two parts are related by a 180° rotation about a twin axis of the form $\langle 111 \rangle$. Because of the high symmetry of the cubic lattice, this orientation relationship is also given by a 60° rotation about the twin axis or by reflection across the $\{111\}$ plane normal to the twin axis. In other words, FCC annealing twins may also be classified as reflection twins. The twin plane is also the composition plane.

Occasionally, annealing twins appear under the microscope as in Fig. 2-23(a), with one part of a grain (B) twinned with respect to the other part (A). The two parts are in contact on the composition plane (111) which makes a straight-line trace on the plane of polish. More common, however, is the kind shown in Fig. 2-23(b). The grain shown consists of three parts: two parts (A_1 and A_2) of identical orientation separated by a third part (B) which is twinned with respect to A_1 and A_2 . B is known as a twin band.

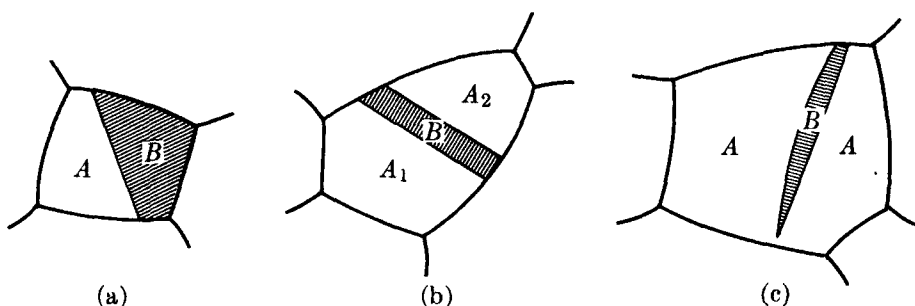
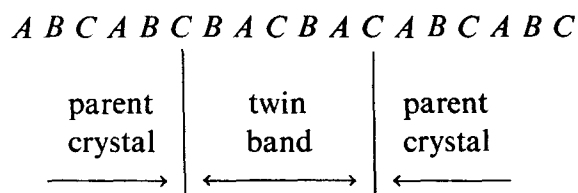


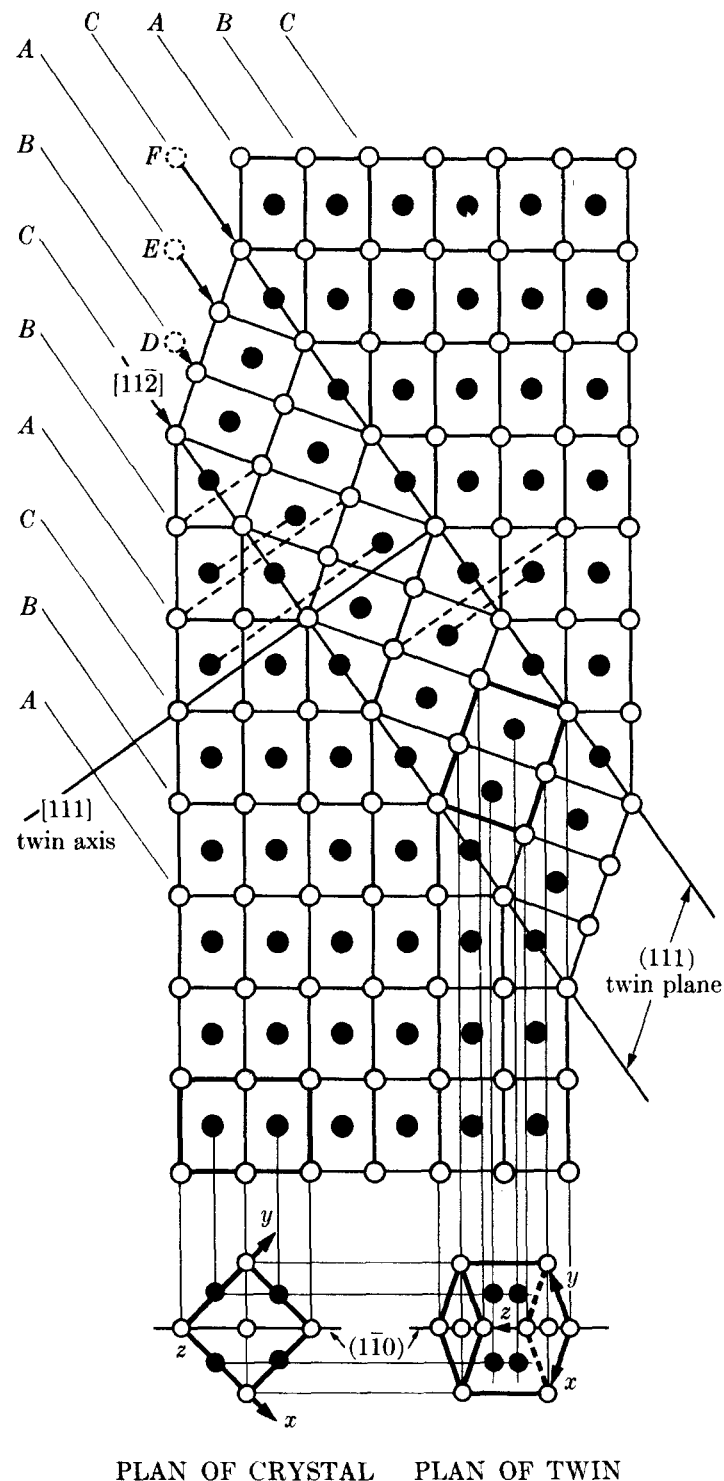
Fig. 2-23 Twinned grains: (a) and (b) FCC annealing twins; (c) HCP deformation twin.

Figure 2-24 illustrates the structure of an FCC twin band. The plane of the main drawing is $(1\bar{1}0)$, the (111) twin plane is perpendicular to this plane, and the $[111]$ twin axis lies in it. Open circles represent atoms in the plane of the drawing and filled circles those in the layers immediately above or below. The reflection symmetry across the twin plane is suggested by the dashed lines connecting several pairs of atoms.

The statement that a rotation twin of this kind is related to the parent crystal by a 180° rotation about the twin axis is merely an expression of the orientation relationship between the two and is not meant to suggest that a twin is formed by a physical rotation of one part of the crystal with respect to another. Actually, FCC annealing twins are formed by a change in the normal growth mechanism. Suppose that, during normal grain growth following recrystallization, a grain boundary is roughly parallel to (111) and is advancing in a direction approximately normal to this boundary, namely $[111]$. To say that the boundary is advancing is to say that atoms are leaving the lattice of the consumed grain and joining that of the growing grain. The grain is therefore growing by the addition of layers of atoms parallel to (111) , and we already know that these layers are piled up in the sequence $A\ B\ C\ A\ B\ C\dots$ in an FCC crystal. If, however, a mistake should occur and this sequence become altered to $C\ B\ A\ C\ B\ A\dots$, the crystal so formed would still be FCC but it would be a twin of the former. If a similar mistake occurred later, a crystal of the original orientation would start growing and a twin band would be formed. With this symbolism, we may indicate a twin band as follows:



In this terminology, the symbols themselves are imaged in the mirror C , the twin plane. At the left of Fig. 2-24 the positional symbols A , B , C are attached to various (111) planes to show the change in stacking which occurs at the boundaries of the twin band. Parenthetically, it should be remarked that twin bands visible under the light microscope are thousands of times thicker than the one shown in this drawing.



PLAN OF CRYSTAL PLAN OF TWIN

Fig. 2-24 Twin band in FCC lattice. Plane of main drawing is $(1\bar{1}0)$.

There is still another way of *describing* the orientation relationship between an FCC crystal and its twin: the {111} layers of the twin are in positions which would result from homogeneous shear in a [112] direction, each layer moving by an amount proportional to its distance from the twin plane. In Fig. 2-24, this shear is indicated by the arrows going from initial positions *D*, *E*, *F* to final positions in the twin. Although it has been frequently suggested that such twins are *formed* by deformation, no convincing evidence for this view has been advanced and it is generally held that annealing twins are the result of the growth process described above. Nevertheless, this hypothetical shear is sometimes a useful way of describing the orientation relationship between a crystal and its twin.

Deformation Twins

Deformation twins are found in both BCC and HCP lattices and are all that their name implies, since, in both cases, the cause of twinning is deformation. In each case, the orientation relationship between parent crystal and twin is that of reflection across a plane.

In BCC structures, the twin plane is {112} and the twinning shear is in the direction [111]. The only common example of such twins is in α -iron (ferrite) deformed by impact, where they occur as extremely narrow twin bands called Neumann bands. It should be noted that, in cubic lattices, both {112} and {111} reflection twinning produce the same orientation relationship; however, they differ in the interatomic distances produced, and an FCC lattice can twin by reflection on {111} with less distortion than on {112}, while for the same reason {112} is the preferred plane for BCC lattices.

In HCP metals, the twin plane is normally (1012). The twinning shear is not well understood; in a gross sense, it takes place in the direction [211] for metals with c/a ratios less than $\sqrt{3}$ (Be, Ti, Mg) and in the reverse direction [211] for metals with c/a larger than $\sqrt{3}$ (Zn, Cd), but the direction of motion of individual atoms during shear is not definitely known. Figure 2-23(c) illustrates the usual form of a twin band in HCP metals, and it will be noted that the composition "plane," although probably parallel or nearly parallel to the twin plane, is not quite flat but often exhibits appreciable curvature.

General

Twins, in general, can form on different planes in the same crystal. For example, there are four {111} planes of different orientation on which twinning can take place in an FCC crystal. Accordingly, in the microstructure of recrystallized copper, for example, one often sees twin bands running in more than one direction in the same grain.

A crystal may also twin repeatedly, producing several new orientations. If crystal *A* twins to form *B*, which twins to form *C*, etc., then *B*, *C*, etc., are said to be first-order, second-order, etc., twins of the parent crystal *A*. Not all these orientations are new. In Fig. 2-23(b), for example, *B* may be regarded as the first-order twin of *A*₁, and *A*₂ as the first-order twin of *B*. *A*₂ is therefore the second-order twin of *A*₁ but has the same orientation as *A*₁.

2-11 THE STEREOGRAPHIC PROJECTION

Crystal drawings made in perspective or in the form of plan and elevation, while they have their uses, are not suitable for displaying the angular relationship between lattice planes and directions. But frequently we are more interested in these angular relationships than in any other aspect of the crystal, and we then need a kind of drawing on which the angles between planes can be accurately measured and which will permit graphical solution of problems involving such angles. The stereographic projection fills this need. For details not given below, see Barrett and Massalski [G.25], Kelly and Groves [G.33], and Johari and Thomas [G.28].

The orientation of any plane in a crystal can be just as well represented by the inclination of the normal to that plane relative to some reference plane as by the inclination of the plane itself. All the planes in a crystal can thus be represented by a set of plane normals radiating from some one point within the crystal. If a reference sphere is now described about this point, the plane normals will intersect the surface of the sphere in a set of points called *poles*. This procedure is illustrated in Fig. 2-25, which is restricted to the {100} planes of a cubic crystal. The pole of a plane represents, by its position on the sphere, the orientation of that plane.

A plane may also be represented by the trace the extended plane makes in the surface of the sphere, as illustrated in Fig. 2-26, where the trace $ABCD A$ represents the plane whose pole is P_1 . This trace is a *great circle*, i.e., a circle of maximum diameter, if the plane passes through the center of the sphere. A plane not passing through the center will intersect the sphere in a *small circle*. On a ruled globe, for example, the longitude lines (meridians) are great circles, while the latitude lines, except the equator, are small circles.

The angle α between two planes is evidently equal to the angle between their great circles or to the angle between their normals (Fig. 2-26). But this angle, in degrees, can also be measured on the surface of the sphere along the great circle $KLMNK$ connecting the poles P_1 and P_2 of the two planes, if this circle has been divided into 360 equal parts. The measurement of an angle has thus been transferred from the planes themselves to the surface of the reference sphere.

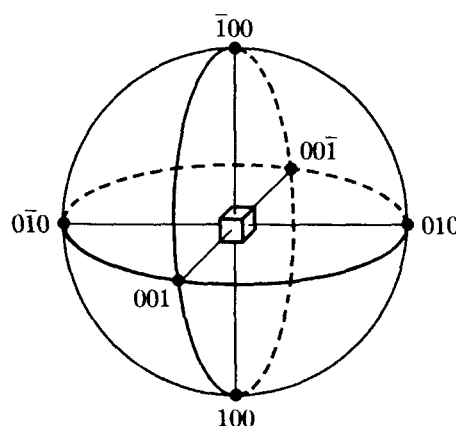


Fig. 2-25 {100} poles of a cubic crystal.

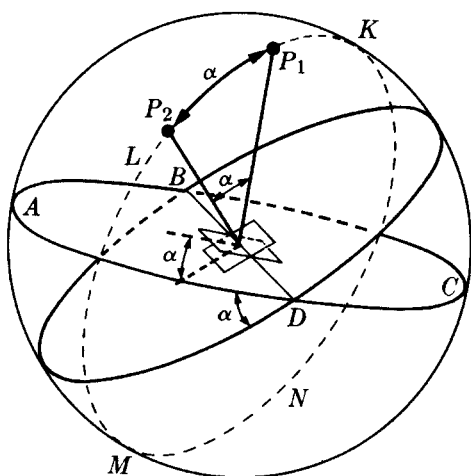


Fig. 2-26 Angle between two planes.

Preferring, however, to measure angles on a flat sheet of paper rather than on the surface of a sphere, we find ourselves in the position of the geographer who wants to transfer a map of the world from a globe to a page of an atlas. Of the many known kinds of projections, he usually chooses a more or less equal-area projection so that countries of equal area will be represented by equal areas on the map. In crystallography, however, we prefer the equiangular stereographic projection since it preserves angular relationships faithfully although distorting areas. It is made by placing a plane of projection normal to the end of any chosen diameter of the sphere and using the other end of that diameter as the point of projection. In Fig. 2-27 the projection plane is normal to the diameter AB , and the projection is made from the point B . If a plane has its pole at P , then the stereographic projection of P is at P' , obtained by drawing the line BP and extending it until it meets the projection plane. Alternately stated, the stereographic projection of the pole P is the shadow cast by P on the projection plane when a light source is placed at B . The observer, incidentally, views the projection from the side opposite the light source.

The plane $NESW$ is normal to AB and passes through the center C . It therefore cuts the sphere in half and its trace in the sphere is a great circle. This great circle projects to form the *basic circle* $N'E'S'W'$ on the projection, and all poles on the left-hand hemisphere will project within this basic circle. Poles on the right-hand hemisphere will project outside this basic circle, and those near B will have projections lying at very large distances from the center. If we wish to plot such poles, we move the point of projection to A and the projection plane to B and distinguish the new set of points so formed by minus signs, the previous set (projected from B) being marked with plus signs. Note that movement of the projection plane along AB or its extension merely alters the magnification; we usually make it tangent to the sphere, as illustrated, but we can also make it pass through the center of the sphere, for example, in which case the basic circle becomes identical with the great circle $NESW$.

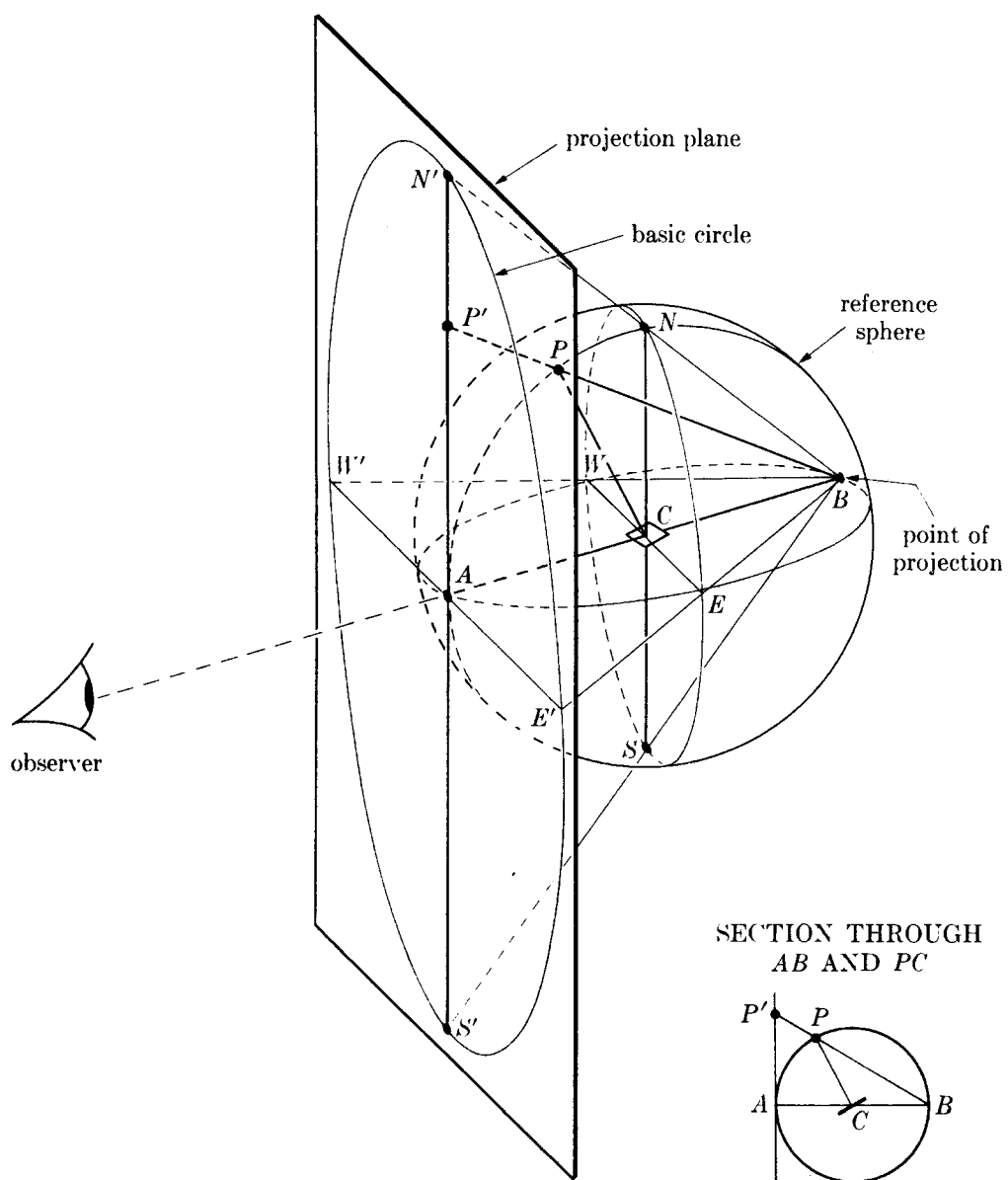


Fig. 2-27 The stereographic projection.

A lattice plane in a crystal is several steps removed from its stereographic projection, and it may be worth-while at this stage to summarize these steps:

1. The plane C is represented by its normal CP .
2. The normal CP is represented by its pole P , which is its intersection with the reference sphere.
3. The pole P is represented by its stereographic projection P' .

After gaining some familiarity with the stereographic projection, the student will be able mentally to omit these intermediate steps and he will then refer to the projected point P' as the pole of the plane C or, even more directly, as the plane C itself.

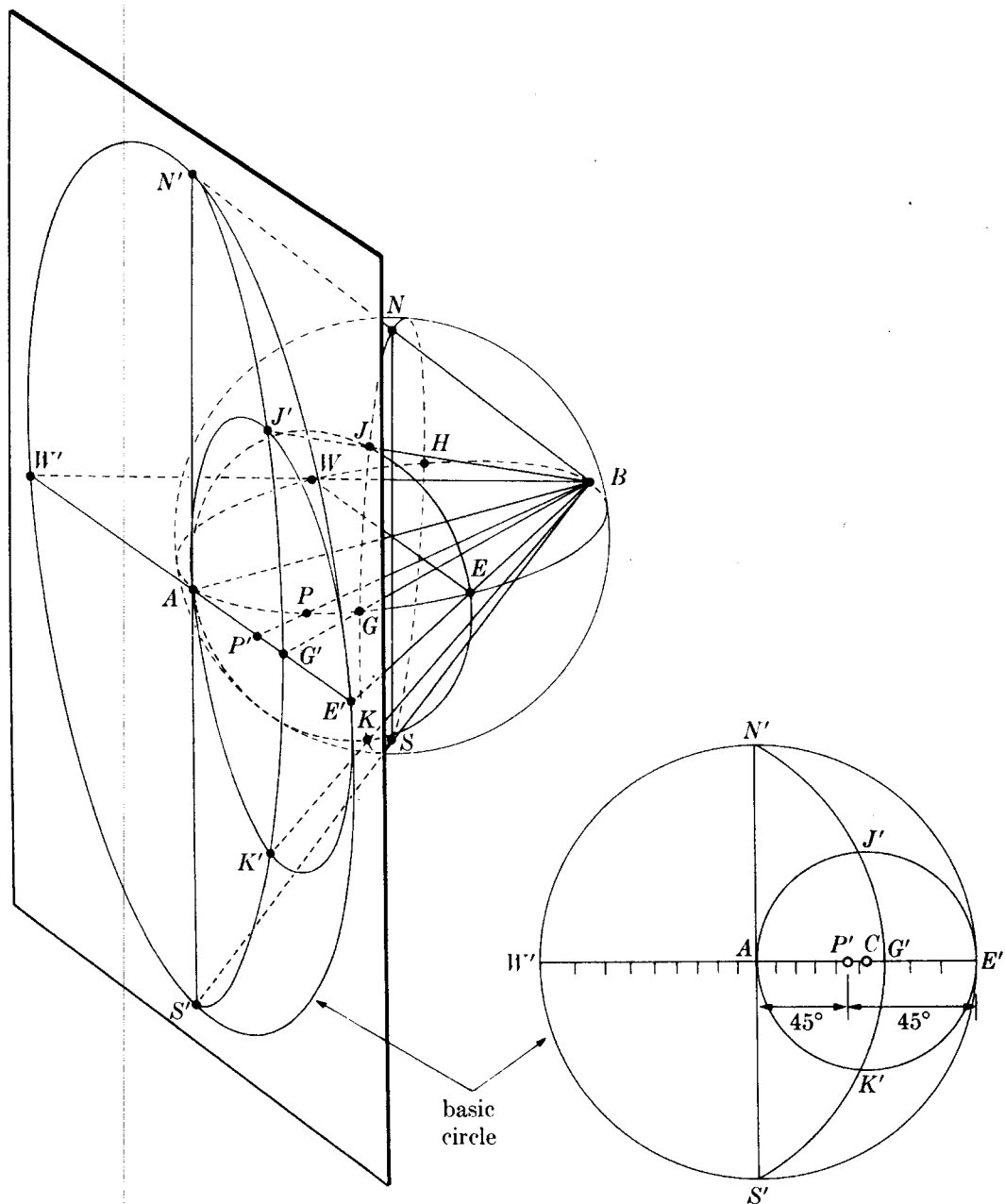


Fig. 2-28 Stereographic projection of great and small circles.

Great circles on the reference sphere project as circular arcs on the projection or, if they pass through the points A and B (Fig. 2-28), as straight lines through the center of the projection. Projected great circles always cut the basic circle in diametrically opposite points, since the locus of a great circle on the sphere is a set of diametrically opposite points. Thus the great circle $ANBS$ in Fig. 2-28 projects as the straight line $N'S'$ and $AWBE$ as $W'E'$; the great circle $NGSH$, which is inclined to the plane of projection, projects as the circle arc $N'G'S'$. If the half great circle WAE is divided into 18 equal parts and these points of division projected on $W'A'E'$, we obtain a graduated scale, at 10° intervals, on the equator of the basic circle.

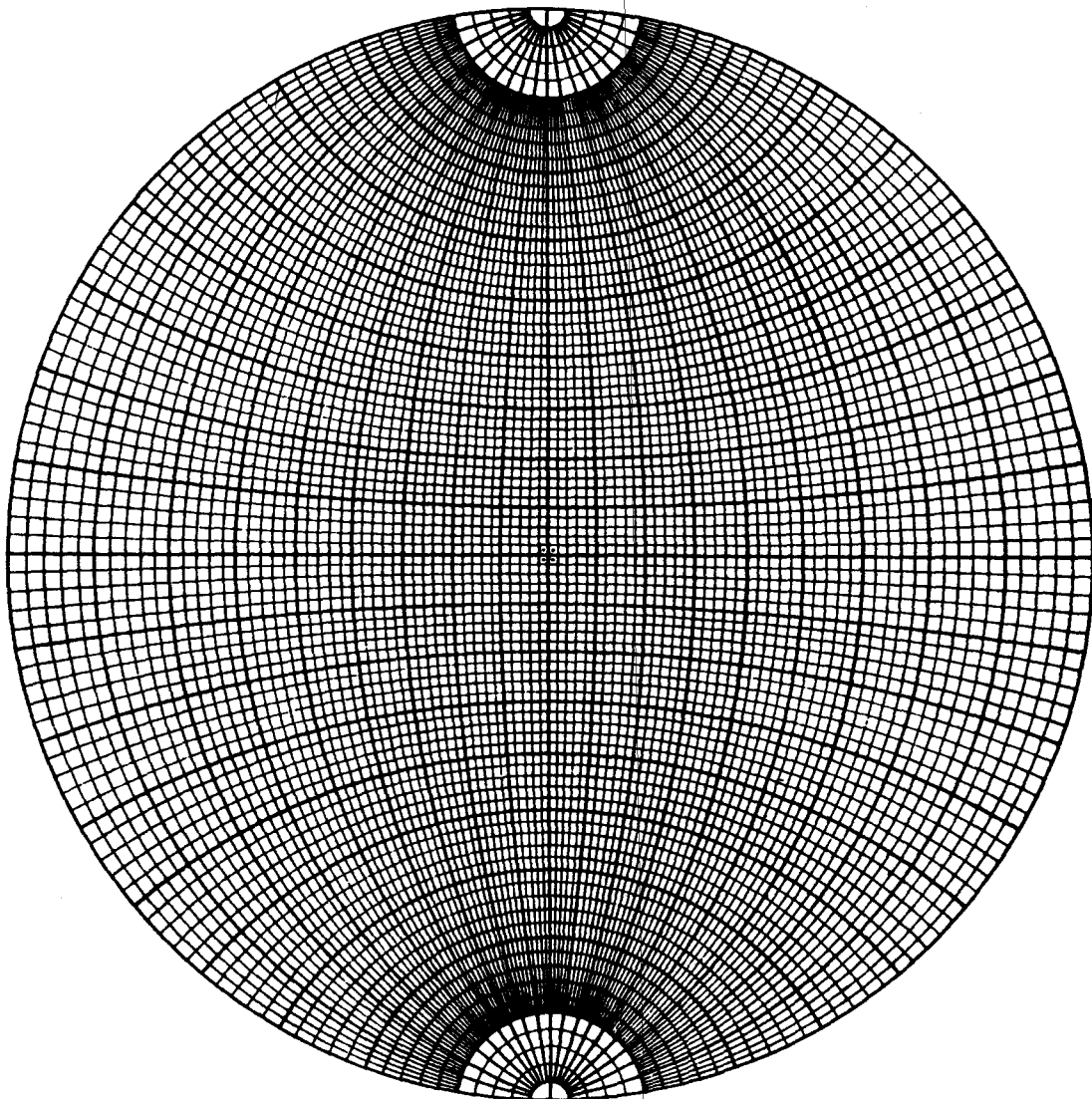


Fig. 2-29 Wulff net drawn to 2° intervals.

Small circles on the sphere also project as circles, but their projected center does not coincide with their center on the projection. For example, the circle $AJEK$ whose center P lies on $AEBW$ projects as $AJ'E'K'$. Its center *on the projection* is at C , located at equal distances from A and E' , but its *projected center* is at P' , located an equal number of degrees (45° in this case) from A and E' .

The device most useful in solving problems involving the stereographic projection is the *Wulff net* shown in Fig. 2-29. It is the projection of a sphere ruled with parallels of latitude and longitude on a plane parallel to the north-south axis of the sphere. The latitude lines on a Wulff net are small circles extending from side to side and the longitude lines (meridians) are great circles connecting the north and south poles of the net. These nets are available in various sizes [2.3], one of 18-cm diameter giving an accuracy of about one degree, which is satisfactory for most problems; to obtain greater precision, either a larger net or mathematical calculation must be used. Wulff nets are used by making the stereographic pro-

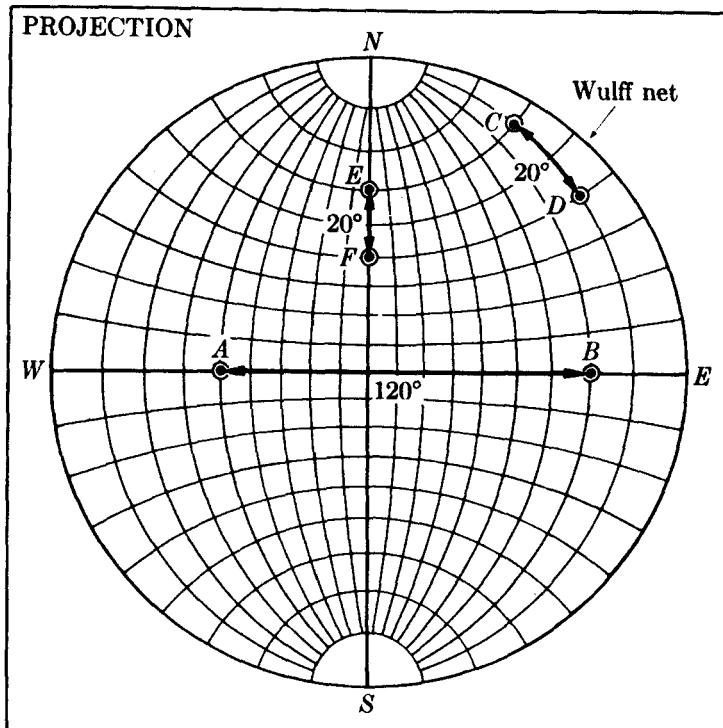


Fig. 2-30 Stereographic projection superimposed on Wulff net for measurement of angle between poles. For illustrative purposes this net is graduated at 10° intervals.

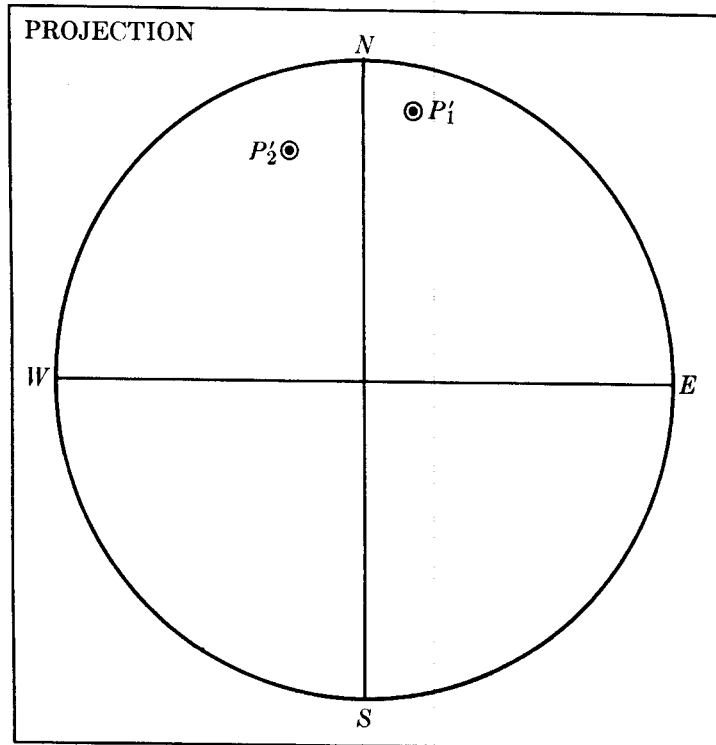
jection on tracing paper and with the basic circle of the same diameter as that of the Wulff net; the projection is then superimposed on the Wulff net, with the centers always coinciding.

To return to our problem of the measurement of the angle between two crystal planes, we saw in Fig. 2-26 that this angle could be measured on the surface of the sphere along the great circle connecting the poles of the two planes. This measurement can also be carried out on the stereographic projection *if, and only if, the projected poles lie on a great circle*. In Fig. 2-30, for example, the angle between the planes* *A* and *B* or *C* and *D* can be measured directly, simply by counting the number of degrees separating them along the great circle on which they lie. Note that the angle *C-D* equals the angle *E-F*, there being the same difference in latitude between *C* and *D* as between *E* and *F*.

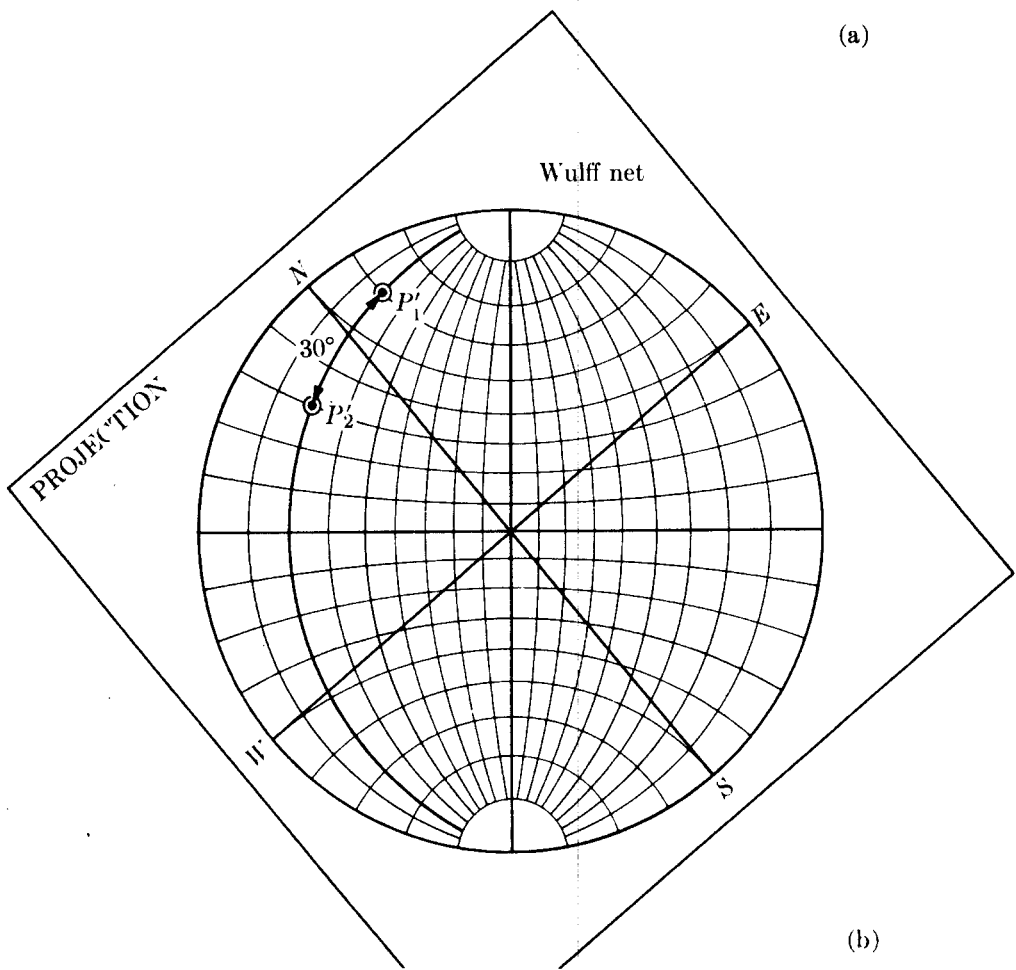
If the two poles do not lie on a great circle, then the projection is rotated relative to the Wulff net until they do lie on a great circle, where the desired angle measurement can then be made. Figure 2-31(a) is a projection of the two poles P_1 and P_2 shown in perspective in Fig. 2-26, and the angle between them is found by the rotation illustrated in Fig. 2-31(b). This rotation of the projection is equivalent to rotation of the poles on latitude circles of a sphere whose north-south axis is perpendicular to the projection plane.

As shown in Fig. 2-26, a plane may be represented by its trace in the reference

* We are here using the abbreviated terminology referred to above.



(a)



(b)

Fig. 2-31 (a) Stereographic projection of poles P_1 and P_2 of Fig. 2-26. (b) Rotation of projection to put poles on same great circle of Wulff net. Angle between poles = 30° .

sphere. This trace becomes a great circle in the stereographic projection. Since every point on this great circle is 90° from the pole of the plane, the great circle may be found by rotating the projection until the pole falls on the equator of the underlying Wulff net and tracing that meridian which cuts the equator 90° from the pole, as illustrated in Fig. 2-32. If this is done for two poles, as in Fig. 2-33, the angle between the corresponding planes may also be found from the angle of intersection of the two great circles corresponding to these poles; it is in this sense that the stereographic projection is said to be angle-true. This method of angle measurement is not as accurate, however, as that shown in Fig. 2-31(b).

We often wish to rotate poles around various axes. We have already seen that rotation about an axis normal to the projection is accomplished simply by rotation of the projection around the center of the Wulff net. Rotation about an axis lying in the plane of the projection is performed by, first, rotating the *axis* about the center of the Wulff net until it coincides with the north-south axis if it does not already do so, and, second, moving the poles involved along their respective latitude circles the required number of degrees. Suppose it is required to rotate the poles A_1 and B_1 shown in Fig. 2-34 by 60° about the *NS* axis, the direction of motion being from *W* to *E* on the projection. Then A_1 moves to A_2 along its

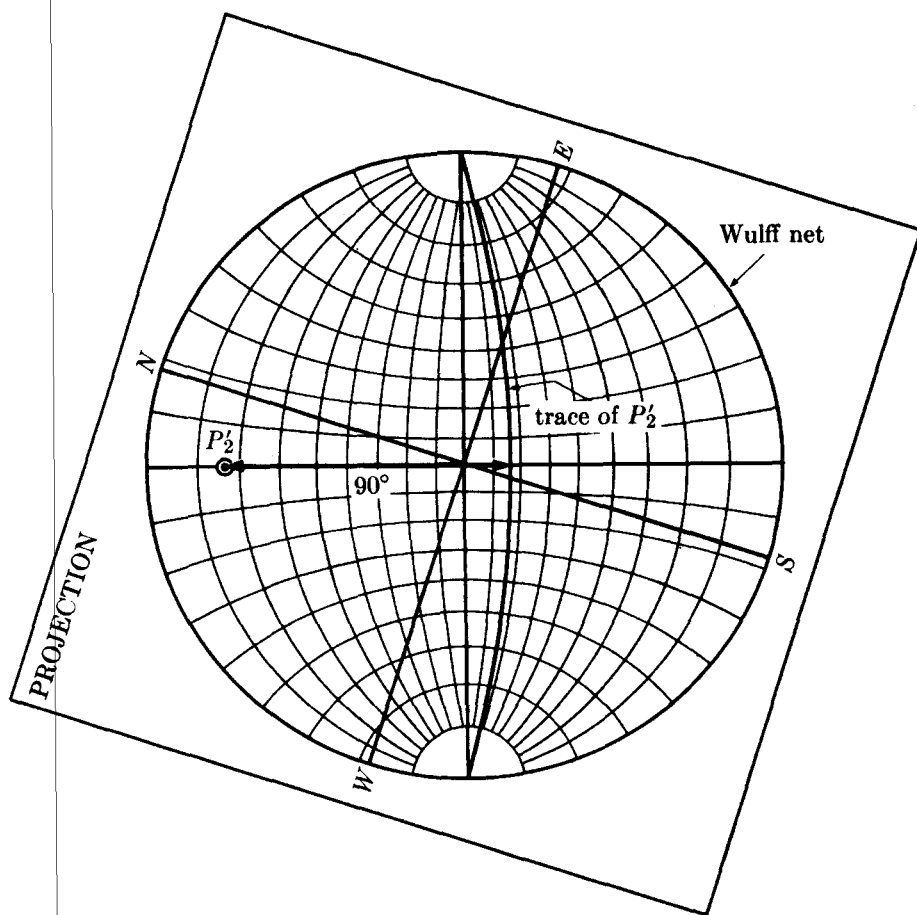


Fig. 2-32 Method of finding the trace of a pole (the pole P'_2 in Fig. 2-31).

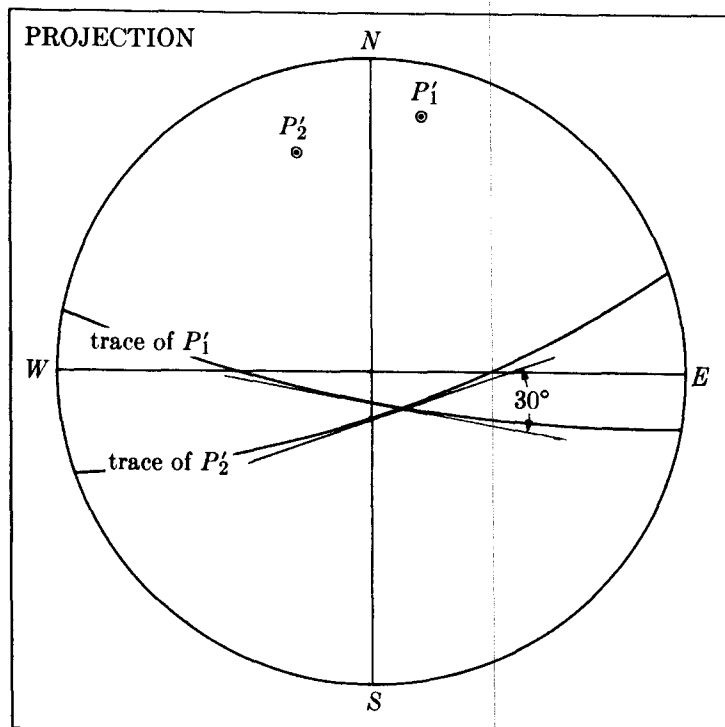


Fig. 2-33 Measurement of an angle between two poles (P_1 and P_2 of Fig. 2-26) by measurement of the angle of intersection of the corresponding traces.

latitude circle as shown. B_1 , however, can rotate only 40° before finding itself at the edge of the projection; we must then imagine it to move 20° in from the edge to the point B'_1 on the other side of the projection, staying always on its own latitude circle. The final position of this pole on the positive side of the projection is at B_2 diametrically opposite B'_1 .

(The student should carefully note that the angle between A_1 and A_2 , for example, in Fig. 2-34 is *not* 60° . The pole A_2 is the position of A_1 after a 60° rotation about NS , which is not the same thing. Consider the two great circles NA_1S and NA_2S ; these are the traces of two planes between which there is a true dihedral angle of 60° . Any pole initially on NA_1S will be on NA_2S after a 60° rotation about NS , but the angle between the initial and final positions of the poles will be less than 60° , unless they lie on the equator, and will approach zero as the poles approach N .)

Rotation about an axis inclined to the plane of projection is accomplished by compounding rotations about axes lying in and perpendicular to the projection plane. In this case, the given axis must first be rotated into coincidence with one or the other of the two latter axes, the given rotation performed, and the axis then rotated back to its original position. Any movement of the given axis must be accompanied by a similar movement of all the poles on the projection.

For example, we may be required to rotate A_1 about B_1 by 40° in a clockwise direction (Fig. 2-35). In (a) the pole to be rotated A_1 and the rotation axis B_1 are shown in their initial position. In (b) the projection has been rotated to bring B_1

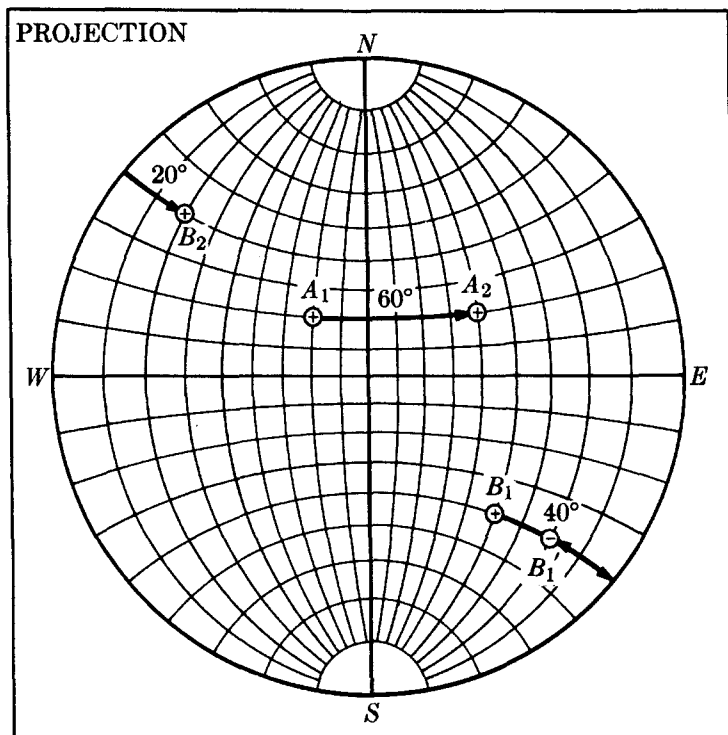


Fig. 2-34 Rotation of poles about NS axis of projection.

to the equator of a Wulff net. A rotation of 48° about the NS axis of the net brings B_1 to the point B_2 at the center of the net; at the same time A_1 must go to A_2 along a parallel of latitude. The rotation axis is now perpendicular to the projection plane, and the required rotation of 40° brings A_2 to A_3 along a circular path centered on B_2 . The operations which brought B_1 to B_2 must now be reversed in order to return B_2 to its original position. Accordingly, B_2 is brought to B_3 and A_3 to A_4 , by a 48° reverse rotation about the NS axis of the net. In (c) the projection has been rotated back to its initial position, construction lines have been omitted, and only the initial and final positions of the rotated pole are shown. During its rotation about B_1 , A_1 moves along the small circle shown. This circle is centered at C on the projection and not at its projected center B_1 . To find C we use the fact that all points on the circle must lie at equal *angular* distances from B_1 ; in this case, measurement on a Wulff net shows that both A_1 and A_4 are 76° from B_1 . Accordingly, we locate any other point, such as D , which is 76° from B_1 , and, knowing three points on the required circle, we can locate its center C by the methods of plane geometry.

In dealing with problems of crystal orientation a *standard projection* is of very great value, since it shows at a glance the relative orientation of all the important planes in the crystal. Such a projection is made by selecting some important crystal plane of low indices as the plane of projection [e.g., (100), (110), (111), or (0001)] and projecting the poles of various crystal planes onto the selected plane. The construction of a standard projection of a crystal requires a knowledge of the

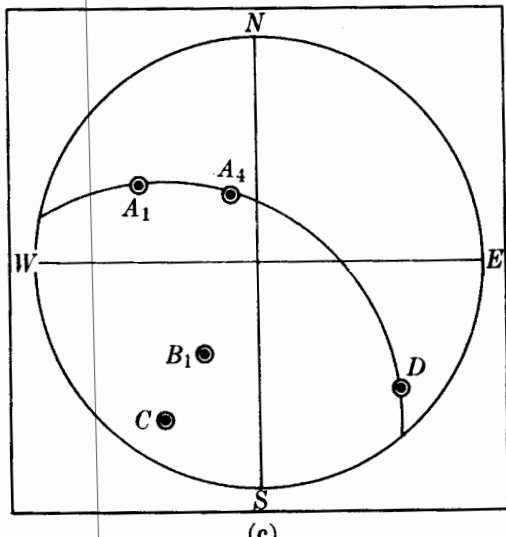
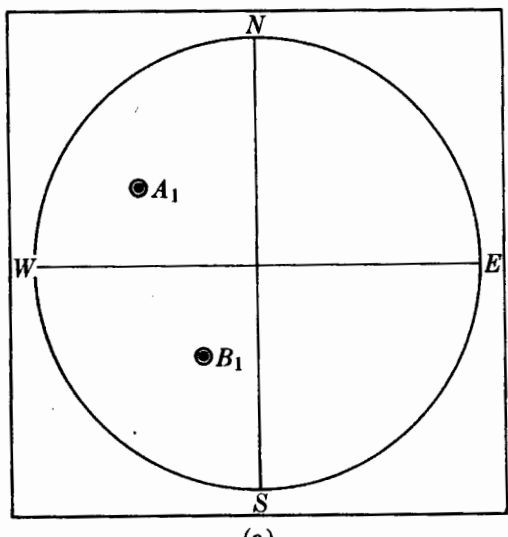
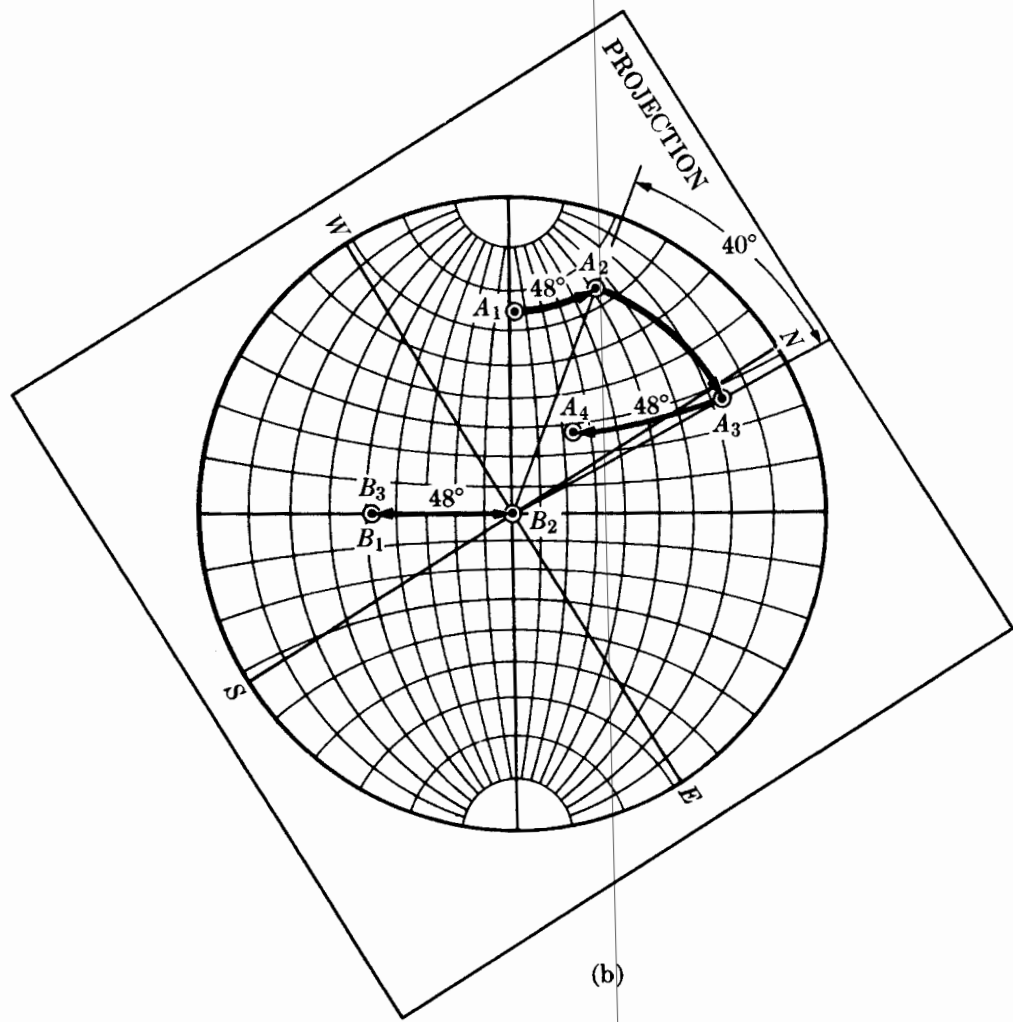


Fig. 2-35 Rotation of a pole about an inclined axis.

interplanar angles for all the principal planes of the crystal. A set of values applicable to all crystals in the cubic system is given in Table 2-3, but those for crystals of other systems depend on the particular axial ratios involved and must be calculated for each case by the equations given in Appendix 3. Much time can be saved in making standard projections by making use of the zonal relation: the normals to all planes belonging to one zone are coplanar and at right angles to the zone axis. Consequently, the poles of planes of a zone will all lie on the same great circle on the projection, and the axis of the zone will be at 90° from this great circle. Furthermore, important planes usually belong to more than one zone and their poles are therefore located at the intersection of zone circles. It is also helpful to remember that important directions, which in the cubic system are normal to planes of the same indices, are usually the axes of important zones.

Figure 2-36(a) shows the principal poles of a cubic crystal projected on the (001) plane of the crystal or, in other words, a standard (001) projection. The location of the {100} cube poles follows immediately from Fig. 2-25. To locate the {110} poles we first note from Table 2-3 that they must lie at 45° from {100} poles, which are themselves 90° apart. In this way we locate (011), for example, on the great circle joining (001) and (010) and at 45° from each. After all the {110} poles are plotted, we can find the {111} poles at the intersection of zone circles. Inspection of a crystal model or drawing or use of the zone relation given by Eq. (2-3) will show that (111), for example, belongs to both the zone [101] and the zone [011]. The pole of (111) is thus located at the intersection of the zone circle through (010), (101), and (010) and the zone circle through (100), (011), and (100). This location may be checked by measurement of its angular distance from (010) or (100), which should be 54.7° . The (011) standard projection shown in Fig. 2-36(b) is plotted in the same manner. Alternatively, it may be constructed by rotating all the poles in the (001) projection 45° to the left about the NS axis of the projection, since this operation will bring the (011) pole to the center. In both of these projections symmetry symbols have been given each pole in conformity with Fig. 2-6(b), and it will be noted that the projection itself has the symmetry of the axis perpendicular to its plane, Figs. 2-36(a) and (b) having 4-fold and 2-fold symmetry, respectively.

Figure 2-37 is a standard (001) projection of a cubic crystal with considerably more detail and a few important zones indicated. A standard (0001) projection of a hexagonal crystal (zinc) is given in Fig. 2-38.

It is sometimes necessary to determine the *Miller indices of a given pole* on a crystal projection, for example the pole *A* in Fig. 2-39(a), which applies to a cubic crystal. If a detailed standard projection is available, the projection with the unknown pole can be superimposed on it and its indices will be disclosed by its coincidence with one of the known poles on the standard. Alternatively, the method illustrated in Fig. 2-39 may be used. The pole *A* defines a direction in space, normal to the plane (*hkl*) whose indices are required, and this direction makes angles ρ , σ , τ with the coordinate axes *a*, *b*, *c*. These angles are measured on the projection as shown in (a). Let the perpendicular distance between the origin and the (*hkl*) plane nearest the origin be *d* [Fig. 2-39(b)], and let the

Table 2-3
 Interplanar Angles (in degrees) in Cubic Crystals between Planes
 of the Form $\{h_1k_1l_1\}$ and $\{h_2k_2l_2\}$

$\{h_2k_2l_2\}$	$\{h_1k_1l_1\}$						
	100	110	111	210	211	221	310
100	0						
	90						
110	45	0					
	90	60					
111	54.7	35.3	0				
		90	70.5				
210	26.6	18.4	39.2	0			
	63.4	50.8	75.0	36.9			
211	90	71.6		53.1			
	35.3	30	19.5	24.1	0		
221	65.9	54.7	61.9	43.1	33.6		
		73.2	90	56.8	48.2		
310	90						
	48.2	19.5	15.8	26.6	17.7	0	
311	70.5	45	54.7	41.8	35.3	27.3	
		76.4	78.9	53.4	47.1	39.0	
320	90						
	18.4	26.6	43.1	8.1	25.4	32.5	0
321	71.6	47.9	68.6	58.1	49.8	42.5	25.9
		90	63.4	45	58.9	58.2	36.9
331	77.1						
	25.2	31.5	29.5	19.3	10.0	25.2	17.6
510	72.5	64.8	58.5	47.6	42.4	45.3	40.3
		90	80.0	66.1	60.5	59.8	55.1
511	33.7	11.3	36.9	7.1	25.2	22.4	15.3
	56.3	54.0	80.8	29.8	37.6	42.3	37.9
711	90	66.9		41.9	55.6	49.7	52.1
	36.7	19.1	22.2	17.0	10.9	11.5	21.6
721	57.7	40.9	51.9	33.2	29.2	27.0	32.3
		74.5	55.5	72.0	53.3	40.2	36.7
731	90						
	46.5	13.1	22.0				
510	11.4						
511	15.6						
711	11.3						

Largely from R. M. Bozorth, *Phys. Rev.* **26**, 390 (1925); rounded off to the nearest 0.1°. A much longer list is given on p. 120–122 of Vol. 2 of [G.11].

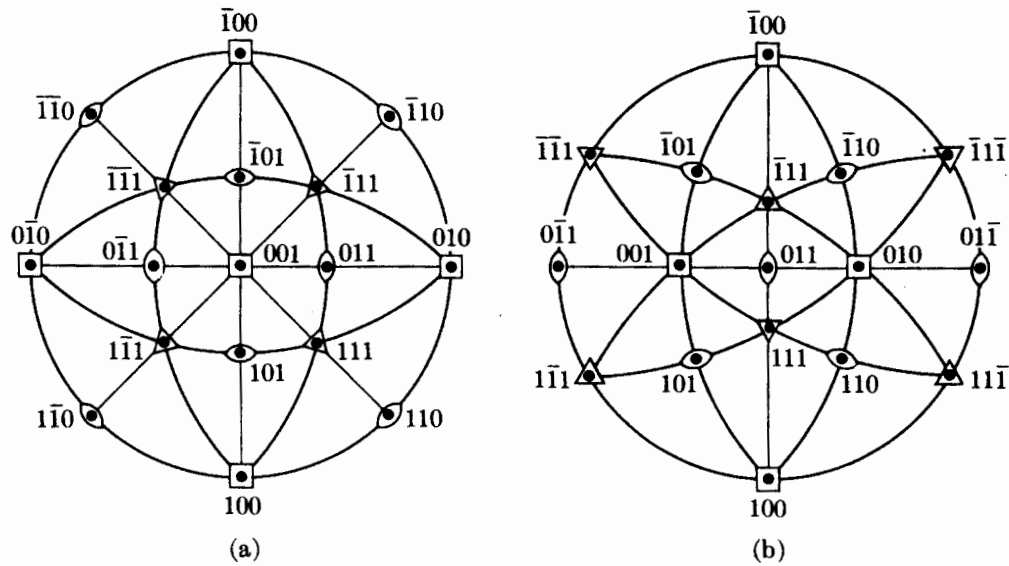


Fig. 2-36 Standard projections of cubic crystals, (a) on (001) and (b) on (011).

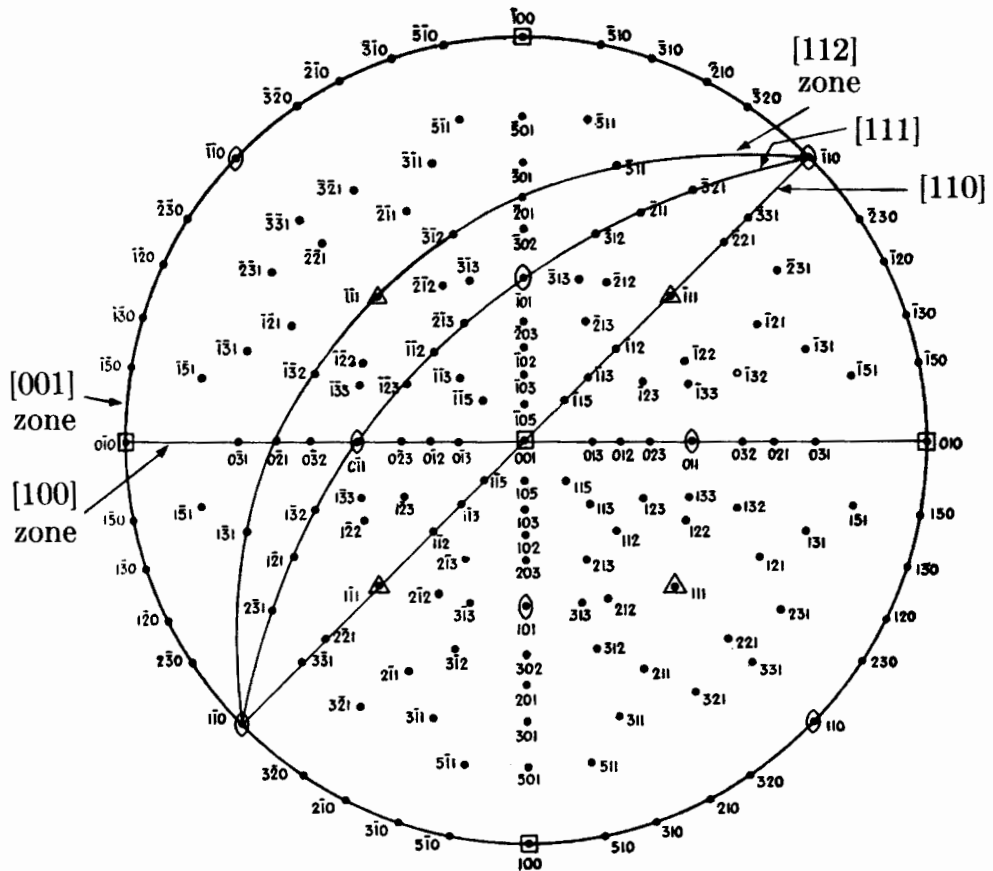


Fig. 2-37 Standard (001) projection of a cubic crystal, after Barrett [1.7].

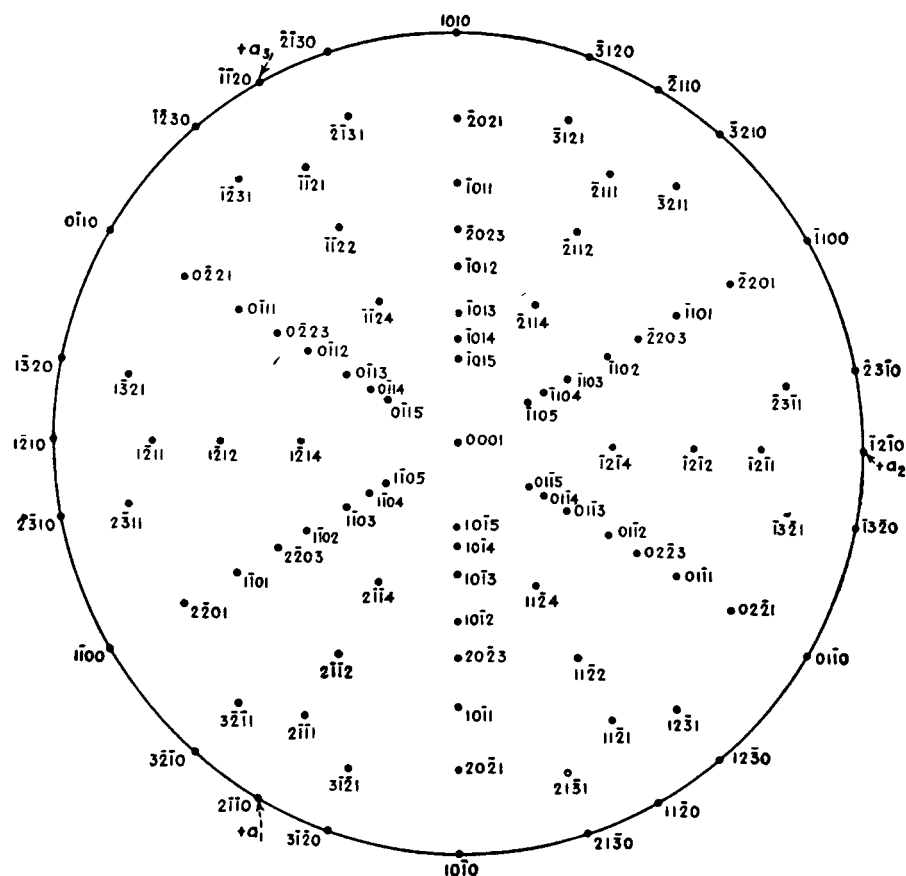


Fig. 2-38 Standard (0001) projection for zinc (hexagonal, $c/a = 1.86$) after Barrett [1.7].

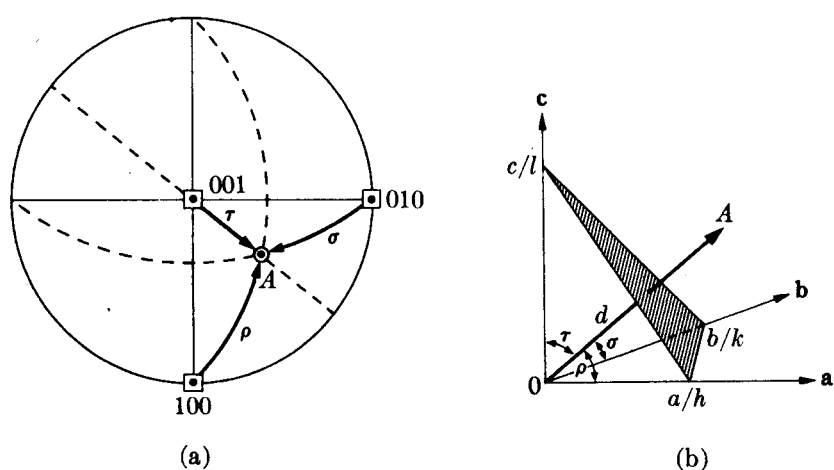


Fig. 2-39 Determination of the Miller indices of a pole.

direction cosines of the line A be p, q, r . Therefore

$$p = \cos \rho = \frac{d}{a/h}, \quad q = \cos \sigma = \frac{d}{b/k}, \quad r = \cos \tau = \frac{d}{c/l},$$

$$h:k:l = pa:qb:rc. \quad (2-8)$$

For the cubic system we have the simple result that the Miller indices required are in the same ratio as the direction cosines.

The lattice reorientation caused by *twinning* can be clearly shown on the stereographic projection. In Fig. 2-40 the open symbols are the $\{100\}$ poles of a cubic crystal projected on the (001) plane. If this crystal is FCC, then one of its possible twin planes is $(\bar{1}\bar{1}1)$, represented on the projection both by its pole and its trace. The cube poles of the twin formed by reflection in this plane are shown as solid symbols; these poles are located by rotating the projection on a Wulff net until the pole of the twin plane lies on the equator, after which the cube poles of the crystal can be moved along latitude circles of the net to their final position.

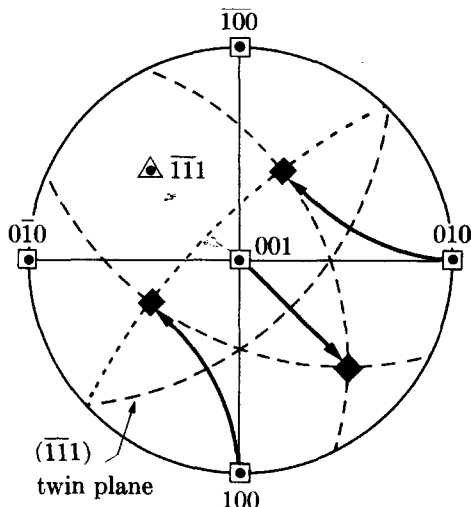


Fig. 2-40 Stereographic projection of an FCC crystal and its twin.

The main principles of the stereographic projection have now been presented, and we will have occasion to use them later in dealing with various practical problems in x-ray crystallography. The student is reminded, however, that a mere reading of this section is not sufficient preparation for such problems. In order to gain real familiarity with the stereographic projection, he must practice, with Wulff net and tracing paper, the operations described above and solve problems of the kind given below. Only in this way will he be able to read and manipulate the stereographic projection with facility and think in three dimensions of what is represented in two.

PROBLEMS

2-1 Draw the following planes and directions in a tetragonal unit cell: (001), (011), (113), [110], [201], [101]. Show cell axes.

2-2 Show by means of a (110) sectional drawing that [111] is perpendicular to (111) in the cubic system, but not, in general, in the tetragonal system.

2-3 In a drawing of a hexagonal prism, indicate the following planes and directions: (1210), (1012), (1011), [110], [111], [021]. Show cell axes.

2-4 Derive Eq. (2-2) of the text.

2-5 Show that the planes (110), (121), and (312) belong to the zone [111].

2-6 Do the following planes all belong to the same zone: (110), (311), (132)? If so, what is the zone axis? Give the indices of any other plane belonging to this zone.

* **2-7** Prepare a cross-sectional drawing of an HCP structure which will show that all atoms do not have identical surroundings and therefore do not lie on a point lattice.

2-8 Show that c/a for hexagonal close packing of spheres is 1.633.

2-9 Show that the HCP structure (with $c/a = 1.633$) and the FCC structure are equally close-packed, and that the BCC structure is less closely packed than either of the former.

2-10 The unit cells of several orthorhombic crystals are described below. What is the Bravais lattice of each and how do you know? Do not change axes. (In solving this kind of problem, examining the given atom positions for the existence or nonexistence of centering translations is generally more helpful than making a drawing of the structure.)

- Two atoms of the same kind per unit cell located at $0 \frac{1}{2} 0, \frac{1}{2} 0 \frac{1}{2}$.
- Four atoms of the same kind per unit cell located at $0 0 z, 0 \frac{1}{2} z, 0 \frac{1}{2} (\frac{1}{2} + z), 0 0 (\frac{1}{2} + z)$.
- Four atoms of the same kind per unit cell located at $x y z, \bar{x} \bar{y} z, (\frac{1}{2} + x)(\frac{1}{2} - y) \bar{z}, (\frac{1}{2} - x)(\frac{1}{2} + y) \bar{z}$.
- Two atoms of one kind *A* located at $\frac{1}{2} 0 0, 0 \frac{1}{2} \frac{1}{2}$; and two atoms of another kind *B* located at $0 0 \frac{1}{2}, \frac{1}{2} \frac{1}{2} 0$.

***2-11** Make a drawing, similar to Fig. 2-23, of a (112) twin in a BCC lattice and show the shear responsible for its formation. Obtain the magnitude of the shear strain graphically.

2-12 Construct a Wulff net, 18 cm in diameter and graduated at 30° intervals, by the use of compass, dividers, and straightedge only. Show all construction lines.

In some of the following problems, the coordinates of a point on a stereographic projection are given in terms of its latitude and longitude, measured from the center of the projection. Thus, the N pole is $90^\circ N, 0^\circ E$, the E pole is $0^\circ N, 90^\circ E$, etc.

2-13 Plane *A* is represented on a stereographic projection by a great circle passing through the N and S poles and the point $0^\circ N, 70^\circ W$. The pole of plane *B* is located at $30^\circ N, 50^\circ W$.

- Find the angle between the two planes by measuring the angle between the poles of *A* and *B*.
- Draw the great circle of plane *B* and demonstrate that the stereographic projection is angle-true by measuring with a protractor the angle between the great circles of *A* and *B*.

***2-14** Pole *A*, whose coordinates are 20°N , 50°E , is to be rotated about the axes described below. In each case, find the coordinates of the final position of pole *A* and show the path traced out during its rotation.

- 100° rotation about the *NS* axis, counterclockwise looking from *N* to *S*.
- 60° rotation about an axis normal to the plane of projection, clockwise to the observer.
- 60° rotation about an inclined axis *B*, whose coordinates are 10°S , 30°W , clockwise to the observer.

2-15 Draw a standard (111) projection of a cubic crystal, showing all poles of the form $\{100\}$, $\{110\}$, $\{111\}$ and the important zone circles between them. Compare with Figs. 2-36(a) and (b).

2-16 Draw a standard (001) projection of white tin (tetragonal, $c/a = 0.545$), showing all poles of the form $\{001\}$, $\{100\}$, $\{110\}$, $\{011\}$, $\{111\}$ and the important zone circles between them. Compare with Fig. 2-36(a).

2-17 Draw a standard (0001) projection of beryllium (hexagonal, $c/a = 1.57$), showing all poles of the form $\{2\bar{1}\bar{1}0\}$, $\{10\bar{1}0\}$, $\{2\bar{1}\bar{1}1\}$, $\{10\bar{1}1\}$ and the important zone circles between them. Compare with Fig. 2-38.

2-18 On a standard (001) projection of a cubic crystal, in the orientation of Fig. 2-36(a), the pole of a certain plane has coordinates 53.3°S , 26.6°E . What are its Miller indices? Verify your answer by comparison of measured angles with those given in Table 2-3.

***2-19** Duplicate the operations shown in Fig. 2-40 and thus find the locations of the cube poles of a $(\bar{1}\bar{1}1)$ reflection twin in a cubic crystal. What are their coordinates?

2-20 Show that the twin orientation found in Prob. 2-19 can also be obtained by

- Reflection in a $\{112\}$ plane. Which one?
- 180° rotation about a $\langle 111 \rangle$ axis. Which one?
- 60° rotation about a $\langle 111 \rangle$ axis. Which one?

In (c), show the paths traced out by the cube poles during their rotation.

***2-21** Plot the great-circle route from Washington, D.C. (39°N , 77°W) to Moscow (56°N , 38°E).

- What is the distance between the two cities? (Radius of the earth = 6360 km.)
- What is the true bearing of an airplane flying from Washington to Moscow at the beginning, midpoint, and end of the trip? (The bearing is the angle measured clockwise from north to the flight direction. Thus east is 90° and west is 270° .)

Diffraction I: Directions of Diffracted Beams

3-1 INTRODUCTION

After our preliminary survey of the physics of x-rays and the geometry of crystals, we can now proceed to fit the two together and discuss the phenomenon of x-ray diffraction, which is an interaction of the two. Historically, this is exactly the way this field of science developed. For many years, mineralogists and crystallographers had accumulated knowledge about crystals, chiefly by measurement of interfacial angles, chemical analysis, and determination of physical properties. There was little knowledge of interior structure, however, although some very shrewd guesses had been made, namely, that crystals were built up by periodic repetition of some unit, probably an atom or molecule, and that these units were situated some 1 or 2 Å apart. On the other hand, there were indications, but only indications, that x-rays might be electromagnetic waves about 1 or 2 Å in wavelength. In addition, the phenomenon of diffraction was well understood, and it was known that diffraction, as of visible light by a ruled grating, occurred whenever wave motion encountered a set of regularly spaced scattering objects, provided that the wavelength of the wave motion was of the same order of magnitude as the repeat distance between the scattering centers.

Such was the state of knowledge in 1912 when the German physicist von Laue (1879–1960) took up the problem. He reasoned that, *if* crystals were composed of regularly spaced atoms which might act as scattering centers for x-rays, and *if* x-rays were electromagnetic waves of wavelength about equal to the interatomic distance in crystals, then it should be possible to diffract x-rays by means of crystals. Under his direction, experiments to test this hypothesis were carried out: a crystal of copper sulfate was set up in the path of a narrow beam of x-rays and a photographic plate was arranged to record the presence of diffracted beams, if any. The second attempt was successful and showed without doubt that x-rays *were* diffracted by the crystal out of the primary beam to form a pattern of spots on the photographic plate. These experiments proved, at one and the same time, the wave nature of x-rays and the periodicity of the arrangement of atoms within a crystal. Hindsight is always easy and these ideas appear quite simple to us now, when viewed from the vantage point of more than sixty years' development of the subject, but they were not at all obvious in 1912, and von Laue's hypothesis and its experimental verification must stand as a great intellectual achievement [3.1].

The account of these experiments was read with great interest by two English physicists, W. H. Bragg (1862–1942) and his son W. L. Bragg (1890–1971). The

latter, although only a young student at the time—it was still the year 1912—successfully analyzed the Laue experiment and was able to express the necessary conditions for diffraction in a considerably simpler mathematical form than that used by von Laue. He also attacked the problem of crystal structure with the new tool of x-ray diffraction and, in the following year, solved the structures of NaCl, KCl, KBr, and KI, all of which have the NaCl structure; these were the first complete crystal-structure determinations ever made [3.2]. The simpler structures of metals like iron and copper were not determined until later.

3-2 DIFFRACTION

Diffraction is due essentially to the existence of certain phase relations between two or more waves, and it is advisable, at the start, to get a clear notion of what is meant by phase relations. Consider a beam of x-rays, such as beam 1 in Fig. 3-1, proceeding from left to right. For convenience only, this beam is assumed to be plane-polarized in order that we may draw the electric field vector \mathbf{E} always in one plane. We may imagine this beam to be composed of two equal parts, ray 2 and ray 3, each of half the amplitude of beam 1. These two rays, on the wave front AA' , are said to be completely *in phase* or *in step*; i.e., their electric-field vectors have the same magnitude and direction at the same instant at any point x measured along the direction of propagation of the wave. A *wave front* is a surface perpendicular to this direction of propagation.

Now consider an imaginary experiment, in which ray 3 is allowed to continue in a straight line but ray 2 is diverted by some means into a curved path before

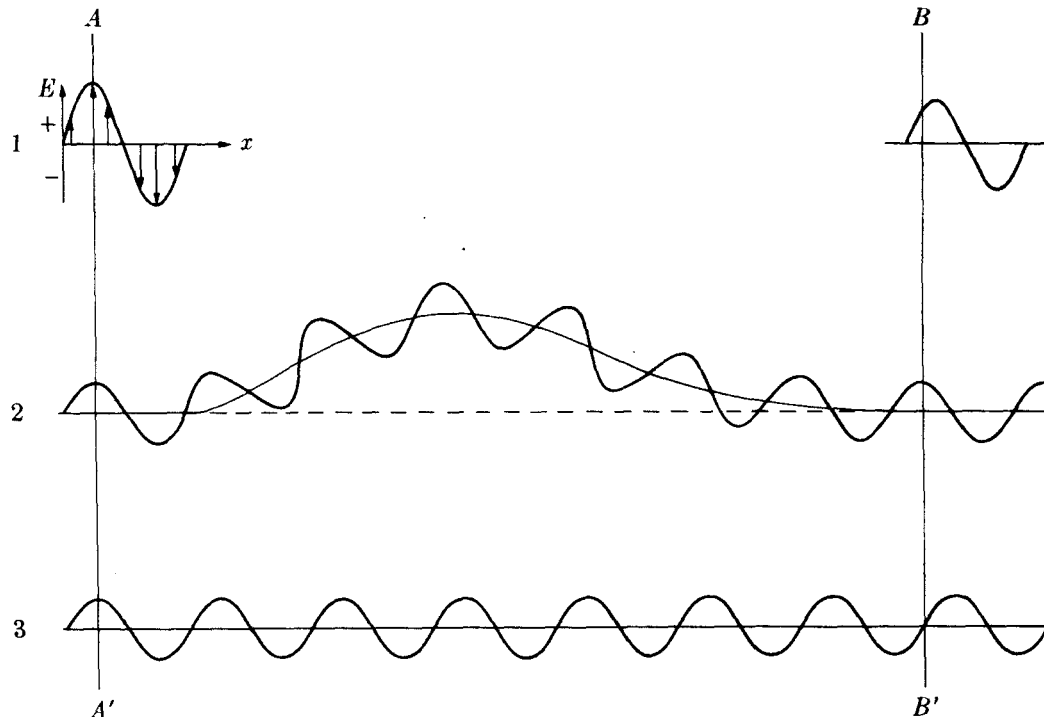


Fig. 3-1 Effect of path difference on relative phase.

rejoining ray 3. What is the situation on the wave front BB' where both rays are proceeding in the original direction? On this front, the electric vector of ray 2 has its maximum value at the instant shown, but that of ray 3 is zero. The two rays are therefore *out of phase*. If we add these two imaginary components of the beam together, we find that beam 1 now has the form shown in the upper right of the drawing. If the amplitudes of rays 2 and 3 are each 1 unit, then the amplitude of beam 1 at the left is 2 units and that of beam 1 at the right is 1.4 units, if a sinusoidal variation of \mathbf{E} with x is assumed.

Two conclusions may be drawn from this illustration:

1. Differences in the length of the path traveled lead to differences in phase.
2. The introduction of phase differences produces a change in amplitude.

The greater the path difference, the greater the difference in phase, since the path difference, measured in wavelengths, exactly equals the phase difference, also measured in wavelengths. If the diverted path of ray 2 in Fig. 3-1 were a quarter wavelength longer than shown, the phase difference would be a half wavelength. The two rays would then be completely out of phase on the wave front BB' and beyond, and they would therefore annul each other, since at any point their electric vectors would be either both zero or of the same magnitude and opposite in direction. If the difference in path length were made three quarters of a wavelength greater than shown, the two rays would be one complete wavelength out of phase, a condition indistinguishable from being completely in phase since in both cases the two waves would combine to form a beam of amplitude 2 units, just like the original beam. We may conclude that two rays are completely in phase whenever their path lengths differ either by zero or by a whole number of wavelengths.

Differences in the path length of various rays arise quite naturally when we consider how a crystal diffracts x-rays. Figure 3-2 shows a section of a crystal, its atoms arranged on a set of parallel planes A, B, C, D, \dots , normal to the plane of the drawing and spaced a distance d' apart. Assume that a beam of perfectly parallel, perfectly monochromatic x-rays of wavelength λ is incident on this crystal at an angle θ , called the Bragg angle, where θ is measured between the incident beam and the particular crystal planes under consideration.

We wish to know whether this incident beam of x-rays will be diffracted by the crystal and, if so, under what conditions. *A diffracted beam may be defined as a beam composed of a large number of scattered rays mutually reinforcing one another.* Diffraction is, therefore, essentially a scattering phenomenon and not one involving any "new" kind of interaction between x-rays and atoms. We saw in Sec. 1-5 that atoms scatter incident x-rays in all directions, and we shall see presently that in some of these directions the scattered beams will be completely in phase and so reinforce each other to form diffracted beams.

For the particular conditions described by Fig. 3-2 the only diffracted beam formed is that shown, namely one making an angle θ of reflection* equal to the

* Note that these angles are defined differently in x-ray diffraction and in general optics. In the latter, the angles of incidence and reflection are the angles which the incident and reflected beams make with the *normal* to the reflecting surface.

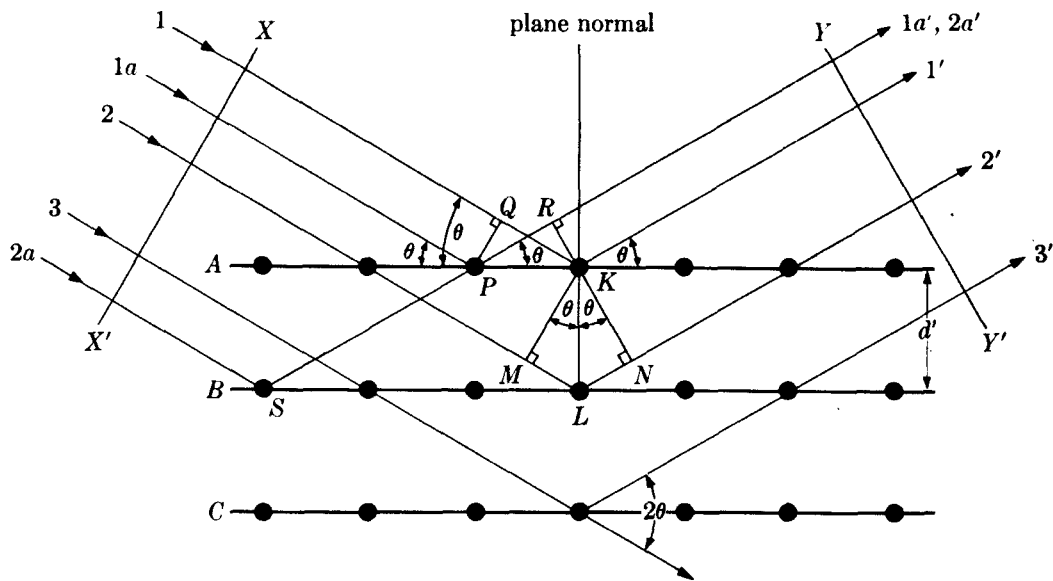


Fig. 3-2 Diffraction of x-rays by a crystal.

angle θ of incidence. We will show this, first, for one plane of atoms and, second, for all the atoms making up the crystal. Consider rays 1 and 1a in the incident beam; they strike atoms K and P in the first plane of atoms and are scattered in all directions. Only in the directions 1' and 1a', however, are these scattered beams completely in phase and so capable of reinforcing one another; they do so because the difference in their length of path between the wave fronts XX' and YY' is equal to

$$QK - PR = PK \cos \theta - PK \cos \theta = 0.$$

Similarly, the rays scattered by all the atoms in the first plane in a direction parallel to 1' are in phase and add their contributions to the diffracted beam. This will be true of all the planes separately, and it remains to find the condition for reinforcement of rays scattered by atoms in different planes. Rays 1 and 2, for example, are scattered by atoms K and L, and the path difference for rays 1K1' and 2L2' is

$$ML + LN = d' \sin \theta + d' \sin \theta.$$

This is also the path difference for the overlapping rays scattered by S and P in the direction shown, since in this direction there is no path difference between rays scattered by S and L or P and K. Scattered rays 1' and 2' will be completely in phase if this path difference is equal to a whole number n of wavelengths, or if

$$n\lambda = 2d' \sin \theta. \quad (3-1)$$

This relation was first formulated by W. L. Bragg and is known as the Bragg law. It states the essential condition which must be met if diffraction is to occur. n is called the order of reflection; it may take on any integral value consistent with $\sin \theta$ not exceeding unity and is equal to the number of wavelengths in the path difference between rays scattered by adjacent planes. Therefore, for fixed values of λ and d' , there may be several angles of incidence $\theta_1, \theta_2, \theta_3, \dots$ at which diffraction may occur, corresponding to $n = 1, 2, 3, \dots$. In a first-order reflection

($n = 1$), the scattered rays $1'$ and $2'$ of Fig. 3-2 would differ in length of path (and in phase) by one wavelength, rays $1'$ and $3'$ by two wavelengths, rays $1'$ and $4'$ by three wavelengths, and so on throughout the crystal. The rays scattered by all the atoms in all the planes are therefore completely in phase and reinforce one another (constructive interference) to form a diffracted beam in the direction shown. In all other directions of space the scattered beams are out of phase and annul one another (destructive interference). The diffracted beam is rather strong compared to the sum of all the rays scattered in the same direction, simply because of the reinforcement which occurs,* but extremely weak compared to the incident beam since the atoms of a crystal scatter only a small fraction of the energy incident on them.

It is helpful to distinguish three scattering modes:

1. By atoms arranged randomly in space, as in a monatomic gas. This scattering occurs in *all* directions and is weak. Intensities add.
2. By atoms arranged periodically in space, as in a perfect crystal:
 - a) In a very few directions, those satisfying the Bragg law, the scattering is strong and is called diffraction. Amplitudes add.
 - b) In most directions, those not satisfying the Bragg law, there is *no* scattering because the scattered rays cancel one another.

At first glance, the diffraction of x-rays by crystals and the reflection of visible light by mirrors appear very similar, since in both phenomena the angle of incidence is equal to the angle of reflection. It seems that we might regard the planes of atoms as little mirrors which "reflect" the x-rays. Diffraction and reflection, however, differ fundamentally in at least three aspects:

1. The diffracted beam from a crystal is built up of rays scattered by all the atoms of the crystal which lie in the path of the incident beam. The reflection of visible light takes place in a thin surface layer only.
2. The diffraction of monochromatic x-rays takes place only at those particular angles of incidence which satisfy the Bragg law. The reflection of visible light takes place at any angle of incidence.

* If the scattering atoms were not arranged in a regular, periodic fashion but in some independent manner, then the rays scattered by them would have a random phase relationship to one another. In other words, there would be an equal probability of the phase difference between any two scattered rays having any value between zero and one wavelength. Neither constructive nor destructive interference takes place under these conditions, and the intensity of the beam scattered in a particular direction is simply *the sum of the intensities* of all the rays scattered in that direction. If there are N scattered rays each of amplitude A and therefore of intensity A^2 in arbitrary units, then the intensity of the scattered beam is NA^2 . On the other hand, if the rays are scattered by the atoms of a crystal in a direction satisfying the Bragg law, then they are all in phase and the amplitude of the scattered beam is *the sum of the amplitudes* of the scattered rays. The total amplitude is then N times the amplitude A of each scattered ray, or NA . The intensity of the scattered beam is therefore N^2A^2 , or N times as large as if reinforcement had not occurred. Since N is very large for the scattering of x-rays from even a small bit of crystal, ($N = 1.1 \times 10^{19}$ atoms for 1 mg of iron), the role of reinforcement in producing a strong diffracted beam is considerable.

3. The reflection of visible light by a good mirror is almost 100 percent efficient. The intensity of a diffracted x-ray beam is extremely small compared to that of the incident beam.

Despite these differences, we often speak of "reflecting planes" and "reflected beams" when we really mean diffracting planes and diffracted beams. This is common usage and, from now on, we will frequently use these terms without quotation marks but with the tacit understanding that we really mean diffraction and not reflection.*

To sum up, diffraction is essentially a scattering phenomenon in which a large number of atoms cooperate. Since the atoms are arranged periodically on a lattice, the rays scattered by them have definite phase relations between them; these phase relations are such that destructive interference occurs in most directions of scattering, but in a few directions constructive interference takes place and diffracted beams are formed. The two essentials are a wave motion capable of interference (x-rays) and a set of periodically arranged scattering centers (the atoms of a crystal).

3-3 THE BRAGG LAW

Two geometrical facts are worth remembering: (1) The incident beam, the normal to the reflecting plane, and the diffracted beam are always coplanar. (2) The angle between the diffracted beam and the transmitted beam is always 2θ . This is known as the diffraction angle, and it is this angle, rather than θ , which is usually measured experimentally.

As previously stated, diffraction in general occurs only when the wavelength of the wave motion is of the same order of magnitude as the repeat distance between scattering centers. This requirement follows from the Bragg law. Since $\sin \theta$ cannot exceed unity, we may write

$$\frac{n\lambda}{2d'} = \sin \theta < 1. \quad (3-2)$$

Therefore, $n\lambda$ must be less than $2d'$. For diffraction, the smallest value of n is 1. ($n = 0$ corresponds to the beam diffracted in the same direction as the transmitted beam. It cannot be observed.) Therefore the condition for diffraction at any observable angle 2θ is

$$\lambda < 2d'. \quad (3-3)$$

For most sets of crystal planes d' is of the order of 3 Å or less, which means that λ cannot exceed about 6 Å. A crystal could not possibly diffract ultraviolet radiation, for example, of wavelength about 500 Å. On the other hand, if λ is very small, the diffraction angles are too small to be conveniently measured.

* For the sake of completeness, it should be mentioned that x-rays *can* be totally reflected by a solid surface, just as visible light is by a mirror, but only at very small angles of incidence (below about one degree).

The Bragg law may be written in the form

$$\lambda = 2 \frac{d'}{n} \sin \theta. \quad (3-4)$$

Since the coefficient of λ is now unity, we can consider a reflection of any order as a first-order reflection from planes, real or fictitious, spaced at a distance $1/n$ of the previous spacing. This turns out to be a real convenience, so we set $d = d'/n$ and write the Bragg law in the form

$$\boxed{\lambda = 2d \sin \theta}. \quad (3-5)$$

This form will be used throughout this book.

This usage is illustrated by Fig. 3-3. Consider the second-order 100 reflection* shown in (a). Since it is second-order, the path difference ABC between rays scattered by adjacent (100) planes must be two whole wavelengths. If there is no real plane of atoms between the (100) planes, we can always imagine one as in Fig. 3-3(b), where the dotted plane midway between the (100) planes forms part of the (200) set of planes. For the same reflection as in (a), the path difference DEF between rays scattered by adjacent (200) planes is now only one whole wavelength, so that this reflection can properly be called a first-order 200 reflection. Similarly, 300, 400, etc., reflections are equivalent to reflections of the third, fourth, etc., orders from the (100) planes. In general, an n th-order reflection from (hkl) planes of spacing d' may be considered as a first-order reflection from the $(nh nk nl)$ planes of spacing $d = d'/n$. Note that this convention is in accord with the definition of Miller indices since $(nh nk nl)$ are the Miller indices of planes parallel to the (hkl) planes but with $1/n$ th the spacing of the latter.

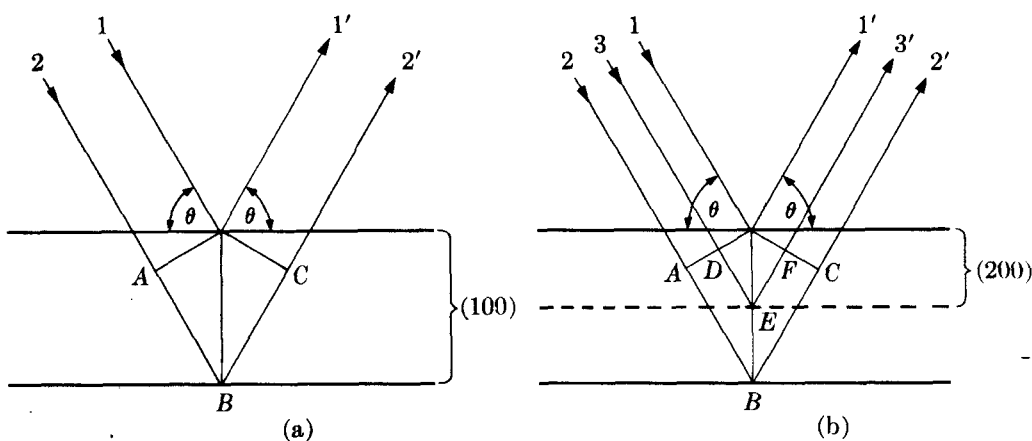


Fig. 3-3 Equivalence of (a) a second-order 100 reflection and (b) a first-order 200 reflection.

* This means the reflection from the (100) planes. Conventionally, the Miller indices of a reflecting plane hkl , written without parentheses, stand for the reflected beam from the plane (hkl) .

3-4 X-RAY SPECTROSCOPY

Experimentally, the Bragg law can be applied in two ways. By using x-rays of known wavelength λ and measuring θ , we can determine the spacing d of various planes in a crystal: this is *structure analysis* and is the subject, in one way or another, of the greater part of this book. Alternatively, we can use a crystal with planes of known spacing d , measure θ , and thus determine the wavelength λ of the radiation used: this is *x-ray spectroscopy*.

The essential features of an x-ray spectrometer are shown in Fig. 3-4. X-rays from the tube T are incident on a crystal C which may be set at any desired angle to the incident beam by rotation about an axis through O , the center of the spectrometer circle. D is a counter which measures the intensity of the diffracted x-rays; it can also be rotated about O and set at any desired angular position. The crystal is usually cut or cleaved so that a particular set of reflecting planes of known spacing is parallel to its surface, as suggested by the drawing. In use, the crystal is positioned so that its reflecting planes make some particular angle θ with the incident beam, and D is set at the corresponding angle 2θ . The intensity of the diffracted beam is then measured and its wavelength calculated from the Bragg law, this procedure being repeated for various angles θ . It is in this way that curves such as Fig. 1-5 and the characteristic wavelengths tabulated in Appendix 7 were obtained. W. H. Bragg designed and used the first x-ray spectrometer, and the Swedish physicist Siegbahn developed it into an instrument of very high precision.

Except for one application, the subject of chemical analysis described in Chap. 15, we are here concerned with x-ray spectroscopy only insofar as it concerns certain units of wavelength. Wavelength measurements made in the way just described are obviously relative, and their accuracy is no greater than the accuracy with which the plane spacing of the crystal is known.

Before considering how the first plane spacing was determined, we must digress to consider the subject of *x-ray density*. Normally the density of a solid is found by measuring the volume, usually of the order of a few cubic centimeters, and the weight of a particular specimen. But x-ray diffraction allows us to determine the lattice parameters of a crystal's unit cell, and therefore its volume, together with the number of atoms in the cell. We can therefore base a density

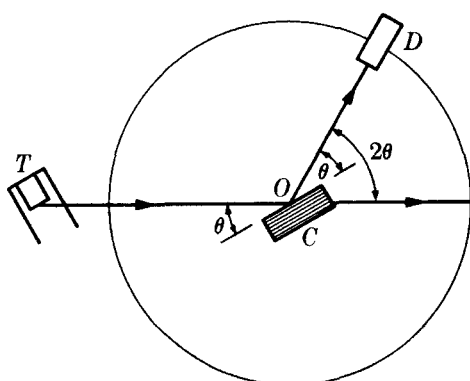


Fig. 3-4 The x-ray spectrometer.

determination, not on a few cubic centimeters but on the volume of a single unit cell, by defining the

$$\text{x-ray density} = \frac{\text{weight of atoms in unit cell}}{\text{volume of unit cell}}.$$

$$\rho = \frac{\sum A/N}{V} \quad (3-6)$$

where ρ = density (gm/cm^3), $\sum A$ = sum of the atomic weights of all the atoms in the unit cell, N = Avogadro's number, and V = volume of unit cell (cm^3). Inserting the current value of N , we have

$$\rho = \frac{\sum A}{NV} = \frac{\sum A}{(6.02257 \times 10^{23})(V' \times 10^{-24})} = \frac{1.66042 \sum A}{V'} \quad (3-7)$$

where ρ is in gm/cm^3 and V' is the unit-cell volume in \AA^3 .

The macroscopic density of a particular specimen, determined from the weight and volume of that specimen, is usually less than, and cannot exceed, the x-ray density, because the macroscopic specimen will usually contain minute cracks and pores. The x-ray density is therefore a useful quantity to know. By comparing it to the macroscopic density of, for example, a pressed and sintered metal or ceramic compact, one can calculate the percent porosity in the compact. X-ray densities are sometimes loosely called "theoretical densities"; they are not theoretical because they are determined experimentally.

To return to the problem of wavelength determination, it is an interesting and crucial fact that Bragg was able to solve the crystal structure of NaCl without knowing the wavelength of the x-rays being diffracted. All he knew—all he needed to know—was that there was one *single*, strong wavelength in the radiation from the x-ray tube, namely, the strong $K\alpha$ line of the tube target. Once the NaCl structure is known [Fig. 2-18(b)], it follows that there are four sodium and four chlorine atoms per unit cell, and that

$$\sum A = 4(\text{at. wt. Na}) + 4(\text{at. wt. Cl}).$$

If this value is inserted into Eq. (3-7) together with the macroscopic density ρ , the volume V' of the unit cell can be found. Because NaCl is cubic, the lattice parameter a is given simply by the cube root of V' . From this value of a and the cubic plane-spacing equation (Eq. 2-5), the spacing of any set of planes can be found.

In this way, Siegbahn obtained a value of 2.814 \AA for the spacing of the (200) planes of rock salt (NaCl), which he could use as a basis for wavelength measurements. This spacing was known to only four significant figures, because it was derived from a macroscopic density of that precision. However, Siegbahn was able to measure wavelengths in terms of this spacing much more accurately, namely, to six significant figures. Not wishing to throw away the high relative precision he could attain, he wisely decided to arbitrarily define a new unit in which relative wavelengths could be expressed. This was the X unit (XU), so called because its true value in absolute units (angstroms) was unknown. By defining the

(200) spacing of rock salt to six significant figures as 2814.00 XU, the new unit was made as nearly as possible equal to 0.001 Å.

Once a particular wavelength was determined in terms of this spacing, the spacing of a given set of planes in any other crystal could be measured. Siegbahn thus measured the (211) spacing of calcite (CaCO_3), which he found more suitable as a standard crystal, and thereafter based all his wavelength measurements on this spacing. Its value is 3029.45 XU. Later on, the kilo X unit (kX) was introduced, a thousand times as large as the X unit and nearly equal to an angstrom. The kX unit is therefore *defined* by the relation

$$1 \text{ kX} = \frac{(211) \text{ plane spacing of calcite}}{3.02945}. \quad (3-8)$$

On this basis, Siegbahn and his associates made very accurate measurements of wavelength in relative (kX) units and these measurements form the basis of most published wavelength tables.

It was found later that x-rays could be diffracted by a ruled grating such as is used in the spectroscopy of visible light, provided that the angle of incidence (the angle between the incident beam and the plane of the grating) is kept below the critical angle for total reflection. Gratings thus offer a means of making absolute wavelength measurements, independent of any knowledge of crystal structure. By a comparison of values so obtained with those found by Siegbahn from crystal diffraction, it was possible to calculate the following relation between the relative and absolute units:

$$1 \text{ kX} = 1.00202 \text{ Å}.$$

This conversion factor was decided on in 1946 by international agreement. Later work improved the accuracy of this factor, and the relation is now believed to be

$$1 \text{ kX} = 1.002056 \text{ Å}^*. \quad (3-9)$$

Note that this relation is stated in terms of still another unit, the Å* unit, which was introduced because of the still remaining uncertainty in the conversion factor. The difference between Å and Å* is only some five parts per million, and the distinction between the two units is negligible except in work of the very highest accuracy.

The present situation is not entirely clear, but the wavelength tables published in 1974 by the International Union of Crystallography [Vol. 4, G.11], which are reproduced in Appendix 7, are based on Eq. (3-9).

The distinction between kX and Å is unimportant if no more than about three significant figures are involved, because the kX unit is only about 0.2 percent larger than the angstrom. In precise work, on the other hand, units must be correctly stated, and on this point there has been considerable confusion in the past. Some wavelength values published prior to about 1946 are stated to be in angstrom units but are actually in kX units. Some crystallographers have used such a value as the basis for a precise measurement of the lattice parameter of a crystal and the result has been stated, again incorrectly, in angstrom units. Many

published parameters are therefore in error, and it is unfortunately not always easy to determine which ones are and which ones are not. The only safe rule to follow, in stating a precise parameter, is to give the wavelength of the radiation used in its determination. Similarly, any published table of wavelengths can be tested for the correctness of its units by noting the wavelength given for a particular characteristic line, Cu $K\alpha_1$ for example. The wavelength of this line is 1.540562 Å* (1974 value, 1.002056 as conversion factor), 1.54051 Å (1946 value, 1.00202 factor), or 1.53740 kX. See Appendix 7 for the estimated accuracy of the wavelengths listed there.

3-5 DIFFRACTION DIRECTIONS

What determines the possible directions, i.e., the possible angles 2θ , in which a given crystal can diffract a beam of monochromatic x-rays? Referring to Fig. 3-3, we see that various diffraction angles $2\theta_1$, $2\theta_2$, $2\theta_3$, ... can be obtained from the (100) planes by using a beam incident at the correct angle θ_1 , θ_2 , θ_3 , ... and producing first-, second-, third-, ... order reflections. But diffraction can also be produced by the (110) planes, the (111) planes, the (213) planes, and so on. We obviously need a general relation which will predict the diffraction angle for *any* set of planes. This relation is obtained by combining the Bragg law and the plane-spacing equation (Appendix 3) applicable to the particular crystal involved.

For example, if the crystal is cubic, then

$$\lambda = 2d \sin \theta$$

and

$$\frac{1}{d^2} = \frac{(h^2 + k^2 + l^2)}{a^2}.$$

Combining these equations, we have

$$\sin^2 \theta = \frac{\lambda^2}{4a^2} (h^2 + k^2 + l^2). \quad (3-10)$$

This equation predicts, for a particular incident wavelength λ and a particular cubic crystal of unit cell size a , all the possible Bragg angles at which diffraction can occur from the planes (hkl) . For (110) planes, for example, Eq. (3-10) becomes

$$\sin^2 \theta_{110} = \frac{\lambda^2}{2a^2}.$$

If the crystal is tetragonal, with axes a and c , then the corresponding general equation is

$$\sin^2 \theta = \frac{\lambda^2}{4} \left(\frac{h^2 + k^2}{a^2} + \frac{l^2}{c^2} \right), \quad (3-11)$$

and similar equations can readily be obtained for the other crystal systems.

These examples show that the directions in which a beam of given wavelength is diffracted by a given set of lattice planes are determined by the crystal system to which the crystal belongs and its lattice parameters. In short, *diffraction directions are determined solely by the shape and size of the unit cell*. This is an important

point and so is its converse: all we can possibly determine about an unknown crystal by measurements of the *directions* of diffracted beams are the shape and size of its unit cell. We will find, in the next chapter, that the *intensities* of diffracted beams are determined by the positions of the atoms within the unit cell, and it follows that we must measure intensities if we are to obtain any information at all about atom positions. We will find, for many crystals, that there are particular atomic arrangements which reduce the intensities of some diffracted beams to zero. In such a case, there is simply no diffracted beam at the angle predicted by an equation of the type of Eqs. (3-10) and (3-11). It is in this sense that equations of this kind predict all *possible* diffracted beams.

3-6 DIFFRACTION METHODS

Diffraction can occur whenever the Bragg law, $\lambda = 2d \sin \theta$, is satisfied. This equation puts very stringent conditions on λ and θ for any given crystal. With monochromatic radiation, an arbitrary setting of a single crystal in a beam of x-rays will not in general produce *any* diffracted beams. Some way of satisfying the Bragg law must be devised, and this can be done by continuously varying either λ or θ during the experiment. The ways in which these quantities are varied distinguish the three main diffraction methods:

	λ	θ
Laue method	Variable	Fixed
Rotating-crystal method	Fixed	Variable (in part)
Powder method	Fixed	Variable

Laue Method

The Laue method was the first diffraction method ever used, and it reproduces von Laue's original experiment. A beam of white radiation, the continuous spectrum from an x-ray tube, is allowed to fall on a fixed single crystal. The Bragg angle θ is therefore fixed for every set of planes in the crystal, and each set picks out and diffracts that particular wavelength which satisfies the Bragg law for the particular values of d and θ involved. Each diffracted beam thus has a different wavelength.

There are two variations of the Laue method, depending on the relative positions of source, crystal, and film (Fig. 3-5). In each, the film is flat and placed perpendicular to the incident beam. The film in the *transmission Laue method* (the original Laue method) is placed behind the crystal so as to record the beams diffracted in the forward direction. This method is so called because the diffracted beams are partially transmitted through the crystal. In the *back-reflection Laue method* the film is placed between the crystal and the x-ray source, the incident beam passing through a hole in the film, and the beams diffracted in a backward direction are recorded.

In either method, the diffracted beams form an array of spots on the film as shown in Fig. 3-6. This array of spots is commonly called a *pattern*, but the term is not used in any strict sense and does not imply any periodic arrangement of the

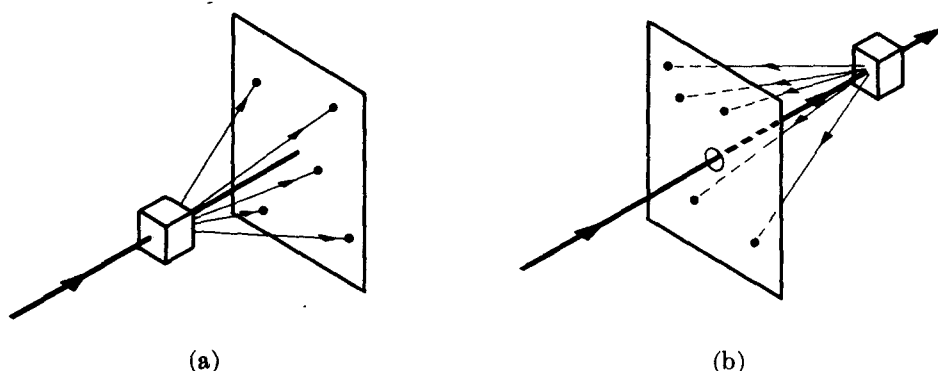


Fig. 3-5 (a) Transmission and (b) back-reflection Laue methods.

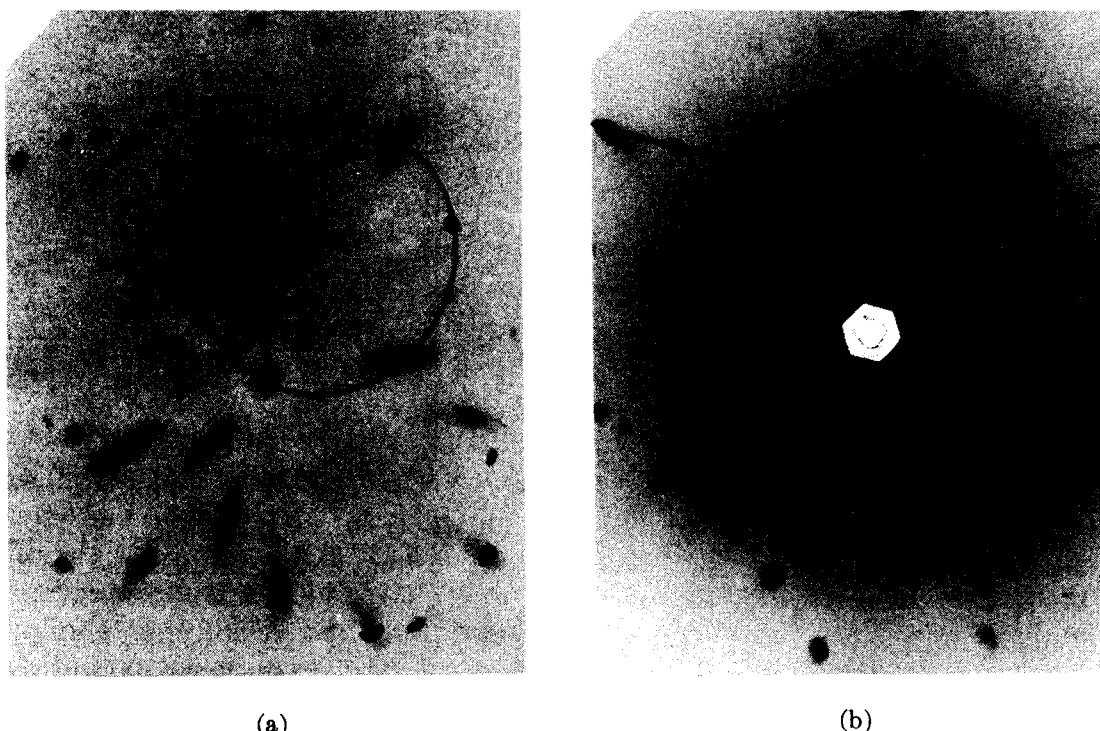


Fig. 3-6 (a) Transmission and (b) back-reflection Laue patterns of an aluminum crystal (cubic). Tungsten radiation, 30 kV, 19 mA.

spots. On the contrary, the spots are seen to lie on certain curves, as shown by the lines drawn on the photographs. These curves are generally ellipses or hyperbolas for transmission patterns [Fig. 3-6(a)] and hyperbolas for back-reflection patterns [Fig. 3-6(b)].

The spots lying on any one curve are reflections from planes belonging to one zone. This is due to the fact that the Laue reflections from planes of a zone all lie on the surface of an imaginary cone whose axis is the zone axis. As shown in Fig. 3-7(a), one side of the cone is tangent to the transmitted beam, and the angle of inclination ϕ of the zone axis (Z.A.) to the transmitted beam is equal to the semi-apex angle of the cone. A film placed as shown intersects the cone in an

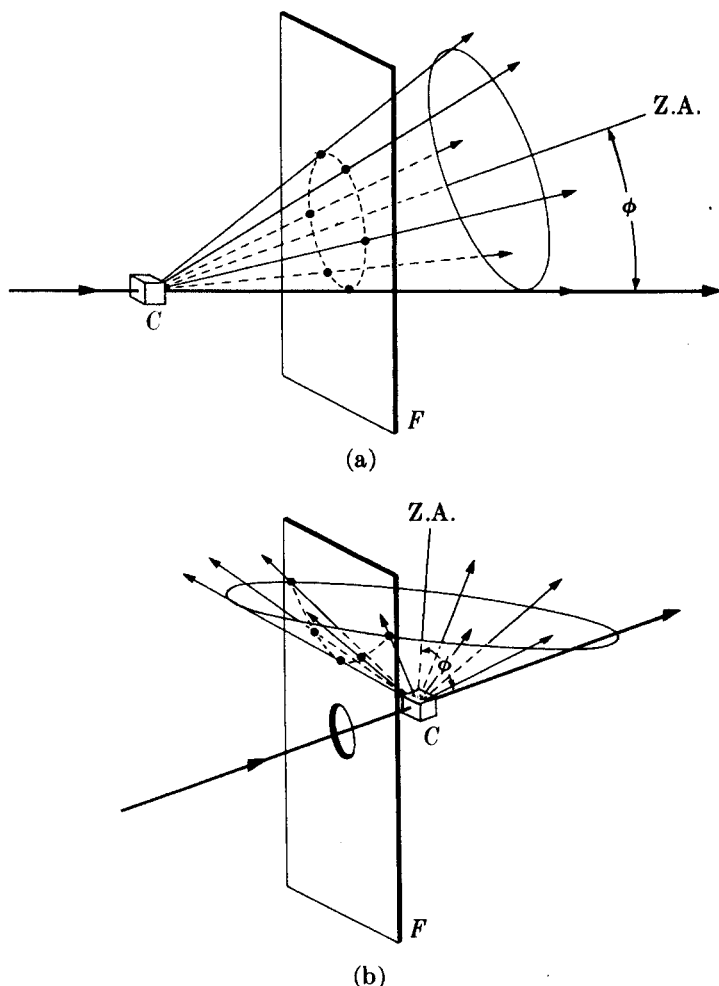


Fig. 3-7 Location of Laue spots (a) on ellipses in transmission method and (b) on hyperbolas in back-reflection method. (C = crystal, F = film, Z.A. = zone axis.)

imaginary ellipse passing through the center of the film, the diffraction spots from planes of a zone being arranged on this ellipse. When the angle ϕ exceeds 45° , a film placed between the crystal and the x-ray source to record the back-reflection pattern will intersect the cone in a hyperbola, as shown in Fig. 3-7(b).

The fact that the Laue reflections from planes of a zone lie on the surface of a cone can be nicely demonstrated with the stereographic projection. In Fig. 3-8, the crystal is at the center of the reference sphere, the incident beam I enters at the left, and the transmitted beam T leaves at the right. The point representing the zone axis lies on the circumference of the basic circle and the poles of five planes belonging to this zone, P_1 to P_5 , lie on the great circle shown. The direction of the beam diffracted by any one of these planes, for example the plane P_2 , can be found as follows. I , P_2 , D_2 (the diffraction direction required), and T are all coplanar. Therefore D_2 lies on the great circle through I , P_2 , and T . The angle between I and P_2 is $(90^\circ - \theta)$, and D_2 must lie at an equal angular distance on the other side of P_2 , as shown. The diffracted beams so found, D_1 to D_5 , are seen

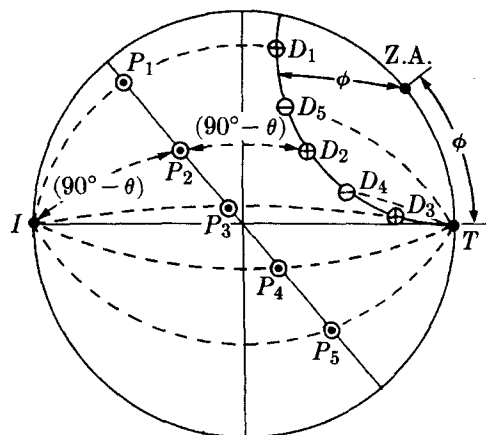


Fig. 3-8 Stereographic projection of transmission Laue method.

to lie on a small circle, the intersection with the reference sphere of a cone whose axis is the zone axis.

The positions of the spots on the film, for both the transmission and the back-reflection method, depend on the orientation of the crystal relative to the incident beam, and the spots themselves become distorted and smeared out if the crystal has been bent or twisted in any way. These facts account for the two main uses of the Laue methods: the determination of crystal orientation and the assessment of crystal quality.

Rotating-crystal Method

In the rotating-crystal method a single crystal is mounted with one of its axes, or some important crystallographic direction, normal to a monochromatic x-ray beam. A cylindrical film is placed around it and the crystal is rotated about the chosen direction, the axis of the film coinciding with the axis of rotation of the crystal (Fig. 3-9). As the crystal rotates, a particular set of lattice planes will, for an instant, make the correct Bragg angle for reflection of the monochromatic incident beam, and at that instant a reflected beam will be formed. The reflected beams are again located on imaginary cones but now the cone axes coincide with the rotation axis. The result is that the spots on the film, when the film is laid out flat, lie on imaginary horizontal lines, as shown in Fig. 3-10. Since the crystal is rotated about only one axis, the Bragg angle does not take on all possible values between 0° and 90° for every set of planes. Not every set, therefore, is able to produce a diffracted beam; sets perpendicular or almost perpendicular to the rotation axis are examples.

The chief use of the rotating-crystal method and its variations is in the determination of unknown crystal structures, and for this purpose it is the most powerful tool the x-ray crystallographer has at his disposal. However, the complete determination of complex crystal structures is a subject beyond the scope of this book and outside the province of the average metallurgist who uses x-ray diffraction as a laboratory tool. For this reason the rotating-crystal method will not be described in any further detail, except for a brief discussion in Appendix 1.

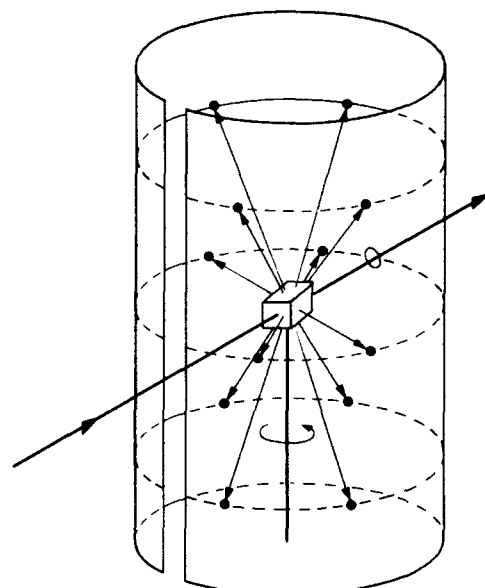


Fig. 3-9 Rotating-crystal method.

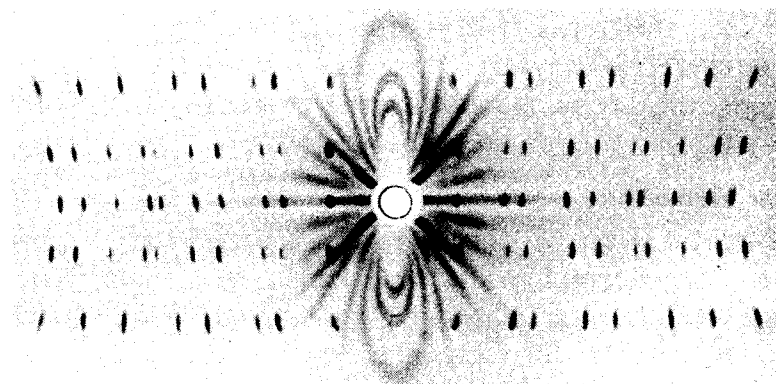


Fig. 3-10 Rotating-crystal pattern of a quartz crystal (hexagonal) rotated about its c axis. Filtered copper radiation. (The streaks are due to the white radiation not removed by the filter.) (Courtesy of B. E. Warren.)

Powder Method

In the powder method, the crystal to be examined is reduced to a very fine powder and placed in a beam of monochromatic x-rays. Each particle of the powder is a tiny crystal, or assemblage of smaller crystals, oriented at random with respect to the incident beam. Just by chance, some of the crystals will be correctly oriented so that their (100) planes, for example, can reflect the incident beam. Other crystals will be correctly oriented for (110) reflections, and so on. The result is that every set of lattice planes will be capable of reflection. The mass of powder is equivalent, in fact, to a single crystal rotated, not about one axis, but about all possible axes.

Consider one particular hkl reflection. One or more little crystals will, by

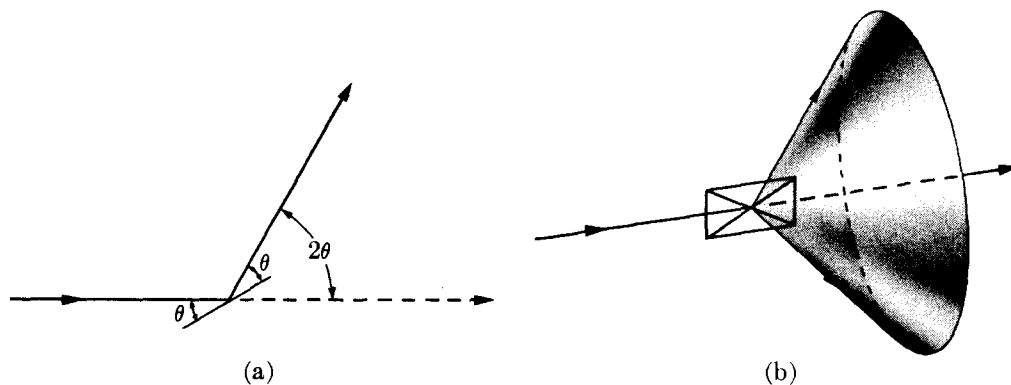


Fig. 3-11 Formation of a diffracted cone of radiation in the powder method.

chance, be so oriented that their (hkl) planes make the correct Bragg angle for reflection; Fig. 3-11(a) shows one plane in this set and the diffracted beam formed. If this plane is now rotated about the incident beam as axis in such a way that θ is kept constant, then the reflected beam will travel over the surface of a cone as shown in Fig. 3-11(b), the axis of the cone coinciding with the transmitted beam. This rotation does not actually occur in the powder method, but the presence of a large number of crystal particles having all possible orientations is equivalent to this rotation, since among these particles there will be a certain fraction whose (hkl) planes make the right Bragg angle with the incident beam and which at the same time lie in all possible rotational positions about the axis of the incident beam. The hkl reflection from a stationary mass of powder thus has the form of a conical sheet of diffracted radiation, and a separate cone is formed for each set of differently spaced lattice planes.

Figure 3-12 shows three such cones and also illustrates the most common powder-diffraction method. In this, the Debye-Scherrer method, a narrow strip of film is curved into a short cylinder with the specimen placed on its axis and the incident beam directed at right angles to this axis. The cones of diffracted radiation intersect the cylindrical strip of film in lines and, when the strip is unrolled and laid out flat, the resulting pattern has the appearance of the one illustrated in Fig. 3-12(b). Actual patterns, produced by various metal powders, are shown in Fig. 3-13. Each diffraction line is made up of a large number of small spots, each from a separate crystal particle, the spots lying so close together that they appear as a continuous line. The lines are generally curved, unless they occur exactly at $2\theta = 90^\circ$ when they will be straight. From the measured position of a given diffraction line on the film, θ can be determined, and, knowing λ , we can calculate the spacing d of the reflecting lattice planes which produced the line.

Conversely, if the shape and size of the unit cell of the crystal are known, we can predict the position of all possible diffraction lines on the film. The line of lowest 2θ value is produced by reflection from planes of the greatest spacing. In the cubic system, for example, d is a maximum when $(h^2 + k^2 + l^2)$ is a minimum, and the minimum value of this term is 1, corresponding to (hkl) equal to (100). The 100 reflection is accordingly the one of lowest 2θ value. The next possible

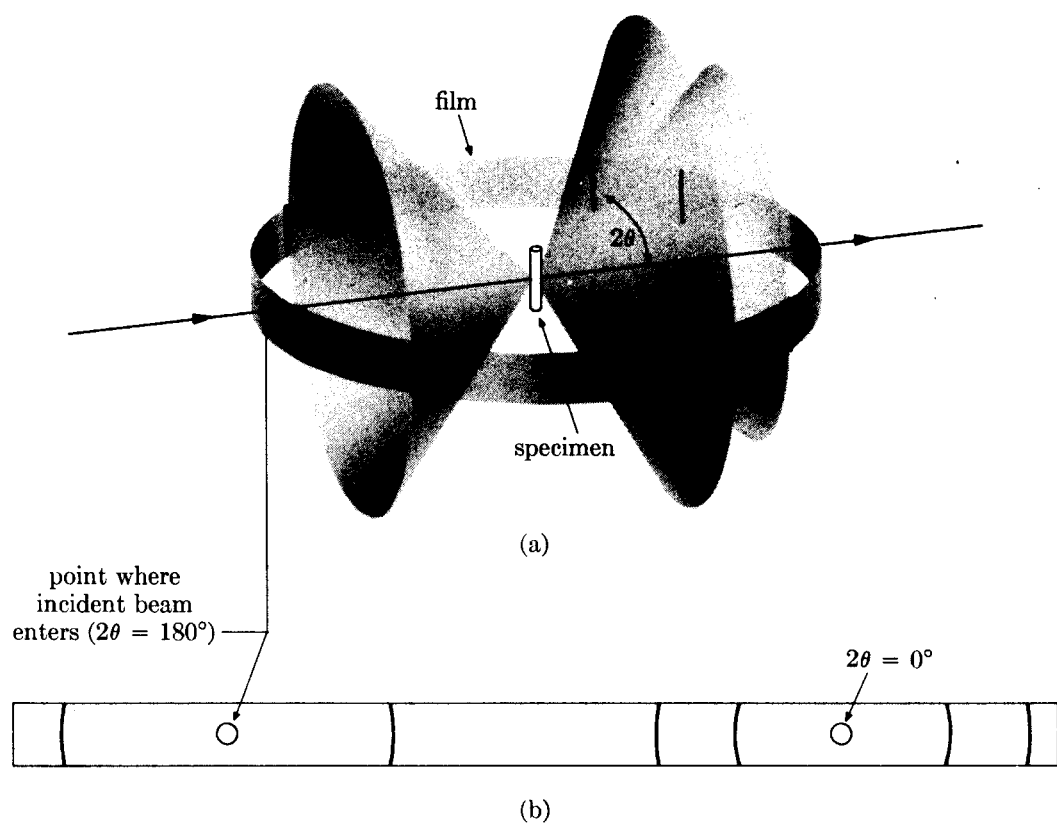


Fig. 3-12 Debye-Scherrer powder method: (a) relation of film to specimen and incident beam; (b) appearance of film when laid out flat.

reflection will have indices hkl corresponding to the next higher value of $(h^2 + k^2 + l^2)$, namely 2, in which case (hkl) equals (110), and so on.

The Debye-Scherrer and other variations of the powder method are very widely used, especially in metallurgy. The powder method is, of course, the only method that can be employed when a single-crystal specimen is not available, and this is the case more often than not in metallurgical work. The method is especially suited for determining lattice parameters with high precision and for the identification of phases, whether they occur alone or in mixtures such as polyphase alloys, corrosion products, refractories, and rocks. These and other uses of the powder method will be fully described in later chapters.

Diffractometer Method

The x-ray spectrometer can also be used as a tool in diffraction analysis. This instrument is known as a *diffractometer* when it is used with x-rays of *known* wavelength to determine the *unknown* spacing of crystal planes, and as a spectrometer in the reverse case, when crystal planes of *known* spacing are used to determine *unknown* wavelengths. The diffractometer is always used with monochromatic radiation and measurements may be made on either single crystals or polycrystalline specimens; in the latter case, it functions much like a Debye-Scherrer camera.

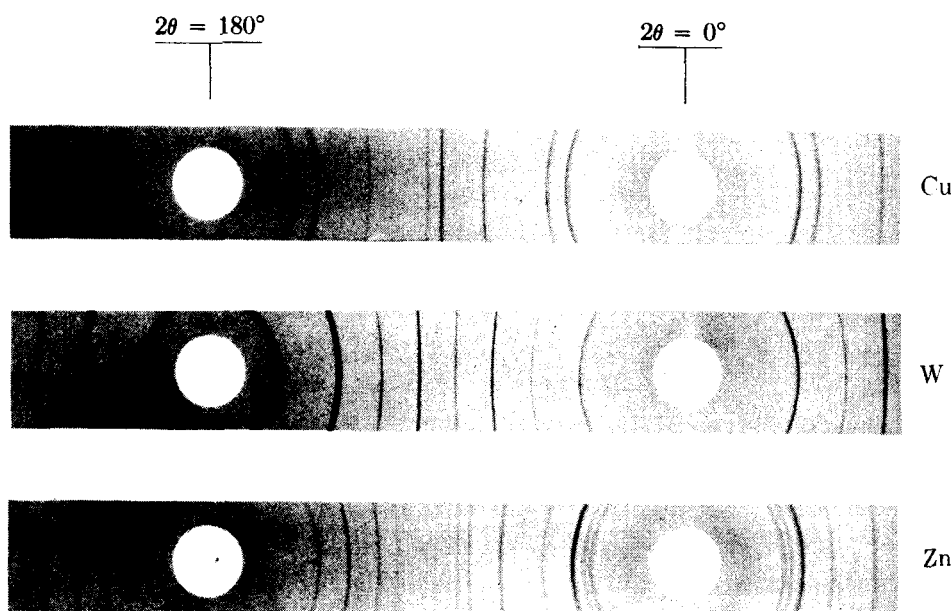


Fig. 3-13 Debye-Scherrer powder patterns of copper (FCC), tungsten (BCC), and zinc (HCP). Filtered copper radiation, camera diameter = 5.73 cm.

in that the counter intercepts and measures only a short arc of any one cone of diffracted rays.

3-7 DIFFRACTION UNDER NONIDEAL CONDITIONS

Before going any further, it is important to stop and consider with some care the derivation of the Bragg law given in Sec. 3-2 in order to understand precisely under what conditions it is strictly valid. In our derivation we assumed certain ideal conditions, namely a perfect crystal and an incident beam composed of perfectly parallel and strictly monochromatic radiation. These conditions never actually exist, so we must determine the effect on diffraction of various kinds of departure from the ideal.

In particular, the way in which destructive interference is produced in all directions except those of the diffracted beams is worth examining in some detail, both because it is fundamental to the theory of diffraction and because it will lead us to a method for estimating the size of very small crystals. We will find that only the infinite crystal is really perfect and that small size alone, of an otherwise perfect crystal, can be considered a crystal imperfection.

The condition for reinforcement used in Sec. 3-2 is that the waves involved must differ in path length, that is, in phase, by exactly an integral number of wavelengths. But suppose that the angle θ in Fig. 3-2 is such that the path difference for rays scattered by the first and second planes is only a quarter wavelength. These rays do not annul one another but, as we saw in Fig. 3-1, simply unite to form a beam of smaller amplitude than that formed by two rays which are completely in phase. How then does destructive interference take place? The answer lies in the contributions from planes deeper in the crystal. Under the assumed

conditions, the rays scattered by the second and third planes would also be a quarter wavelength out of phase. But this means that the rays scattered by the first and third planes are exactly half a wavelength out of phase and would completely cancel one another. Similarly, the rays from the second and fourth planes, third and fifth planes, etc., throughout the crystal, are completely out of phase; the result is destructive interference and no diffracted beam. *Destructive interference is therefore just as much a consequence of the periodicity of atom arrangement as is constructive interference.*

This is an extreme example. If the path difference between rays scattered by the first two planes differs only slightly from an integral number of wavelengths, then the plane scattering a ray exactly out of phase with the ray from the first plane will lie deep within the crystal. If the crystal is so small that this plane does not exist, then complete cancellation of all the scattered rays will not result. It follows that there is a connection between the amount of "out-of-phasesness" that can be tolerated and the size of the crystal. We will find that very small crystals cause broadening (a small angular divergence) of the diffracted beam, i.e., diffraction (scattering) at angles near to, but not equal to, the exact Bragg angle. We must therefore consider the scattering of rays incident on the crystal planes at angles deviating slightly from the exact Bragg angle.

Suppose, for example, that the crystal has a thickness t measured in a direction perpendicular to a particular set of reflecting planes (Fig. 3-14). Let there be $(m + 1)$ planes in this set. We will regard the Bragg angle θ as a variable and call θ_B the angle which exactly satisfies the Bragg law for the particular values of λ and d involved, or

$$\lambda = 2d \sin \theta_B.$$

In Fig. 3-14, rays A, D, ..., M make exactly this angle θ_B with the reflecting planes. Ray D', scattered by the first plane below the surface, is therefore one

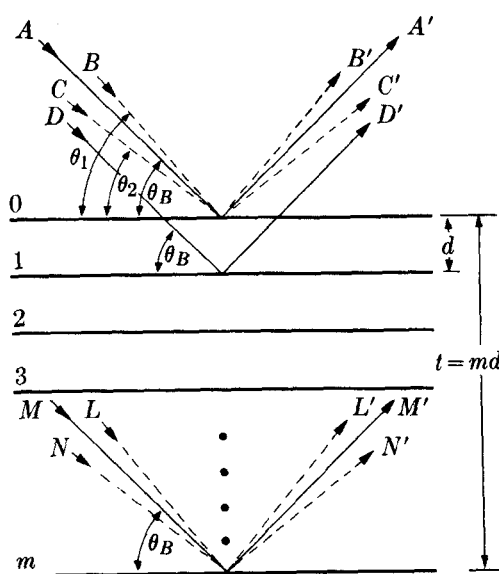


Fig. 3-14 Effect of crystal size on diffraction.

wavelength out of phase with A' ; and ray M' , scattered by the m th plane below the surface, is m wavelengths out of phase with A' . Therefore, at a diffraction angle $2\theta_B$, rays A', D', \dots, M' are completely in phase and unite to form a diffracted beam of maximum amplitude, i.e., a beam of maximum intensity, since the intensity is proportional to the square of the amplitude.

When we consider incident rays that make Bragg angles only slightly different from θ_B , we find that destructive interference is not complete. Ray B , for example, makes a slightly larger angle θ_1 , such that ray L' from the m th plane below the surface is $(m + 1)$ wavelengths out of phase with B' , the ray from the surface plane. This means that midway in the crystal there is a plane scattering a ray which is one-half (actually, an integer plus one-half) wavelength out of phase with ray B' from the surface plane. These rays cancel one another, and so do the other rays from similar pairs of planes throughout the crystal, the net effect being that rays scattered by the top half of the crystal annul those scattered by the bottom half. The intensity of the beam diffracted at an angle $2\theta_1$ is therefore zero. It is also zero at an angle $2\theta_2$ where θ_2 is such that ray N' from the m th plane below the surface is $(m - 1)$ wavelengths out of phase with ray C' from the surface plane. We have therefore found two limiting angles, $2\theta_1$ and $2\theta_2$, at which the diffracted intensity must drop to zero. It follows that the diffracted intensity at angles near $2\theta_B$, but not greater than $2\theta_1$ or less than $2\theta_2$, is *not zero* but has a value intermediate between zero and the maximum intensity of the beam diffracted at an angle $2\theta_B$. The curve of diffracted intensity vs. 2θ will thus have the form of Fig. 3-15(a) in contrast to Fig. 3-15(b), which illustrates the hypothetical case of diffraction occurring only at the exact Bragg angle.

The width of the diffraction curve of Fig. 3-15(a) increases as the thickness of the crystal decreases, because the angular range $(2\theta_1 - 2\theta_2)$ increases as m

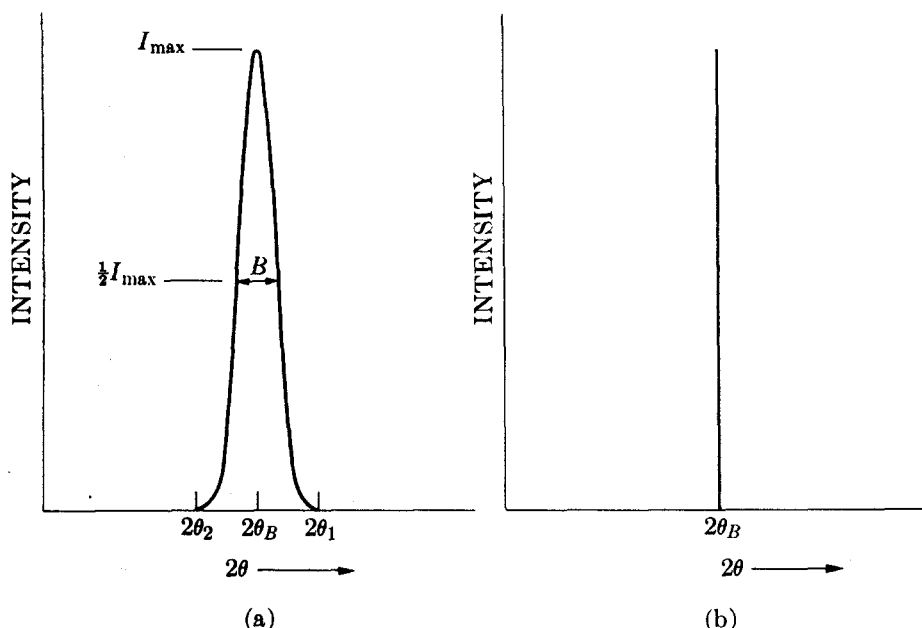


Fig. 3-15 Effect of fine particle size on diffraction curves (schematic).

decreases. The width B is usually measured, in radians, at an intensity equal to half the maximum intensity. [Note that B is an angular width, in terms of 2θ (not θ), and not a linear width.] As a rough measure of B , we can take half the difference between the two extreme angles at which the intensity is zero, which amounts to assuming that the diffraction line is triangular in shape. Therefore,

$$B = \frac{1}{2}(2\theta_1 - 2\theta_2) = \theta_1 - \theta_2.$$

We now write path-difference equations for these two angles, similar to Eq. (3-1) but related to the entire thickness of the crystal rather than to the distance between adjacent planes:

$$2t \sin \theta_1 = (m + 1)\lambda,$$

$$2t \sin \theta_2 = (m - 1)\lambda.$$

By subtraction we find

$$t(\sin \theta_1 - \sin \theta_2) = \lambda,$$

$$2t \cos \left(\frac{\theta_1 + \theta_2}{2} \right) \sin \left(\frac{\theta_1 - \theta_2}{2} \right) = \lambda.$$

But θ_1 and θ_2 are both very nearly equal to θ_B , so that

$$\theta_1 + \theta_2 = 2\theta_B \quad (\text{approx.})$$

and

$$\sin \left(\frac{\theta_1 - \theta_2}{2} \right) = \left(\frac{\theta_1 - \theta_2}{2} \right) \quad (\text{approx.}).$$

Therefore

$$2t \left(\frac{\theta_1 - \theta_2}{2} \right) \cos \theta_B = \lambda,$$

$$t = \frac{\lambda}{B \cos \theta_B}. \quad (3-12)$$

A more exact treatment of the problem gives

$$t = \frac{0.9\lambda}{B \cos \theta_B}, \quad (3-13)$$

which is known as the Scherrer formula. It is used to estimate the *particle size* of very small crystals from the measured width of their diffraction curves. What is the order of magnitude of this effect? Suppose $\lambda = 1.5 \text{ \AA}$, $d = 1.0 \text{ \AA}$, and $\theta = 49^\circ$. Then for a crystal 1 mm in diameter the breadth B , due to the small crystal effect alone, would be about 2×10^{-7} radian (10^{-5} degree), or too small to be observable. Such a crystal would contain some 10^7 parallel lattice planes of the spacing assumed above. However, if the crystal were only 500 \AA thick, it would contain only 500 planes, and the diffraction curve would be relatively broad, namely about 4×10^{-3} radian (0.2°), which is easily measurable.

Nonparallel incident rays, such as **B** and **C** in Fig. 3-14, actually exist in any real diffraction experiment, since the "perfectly parallel beam" assumed in Fig. 3-2 has never been produced in the laboratory. As will be shown in Sec. 5-4, any actual beam of x-rays contains divergent and convergent rays as well as parallel

rays, so that the phenomenon of diffraction at angles not exactly satisfying the Bragg law actually takes place.

Neither is any real beam ever strictly monochromatic. The usual "monochromatic" beam is simply one containing the strong $K\alpha$ component superimposed on the continuous spectrum. But the $K\alpha$ line itself has a width of about 0.001 Å and this narrow range of wavelengths in the nominally monochromatic beam is a further cause of line broadening, i.e., of measurable diffraction at angles close, but not equal, to $2\theta_B$, since for each value of λ there is a corresponding value of θ . (Translated into terms of diffraction line width, a range of wavelengths extending over 0.001 Å leads to an increase in line width, for $\lambda = 1.5$ Å and $\theta = 45^\circ$, of about 0.08° over the width one would expect if the incident beam were strictly monochromatic.) Line broadening due to this natural "spectral width" is proportional to $\tan \theta$ and becomes quite noticeable as θ approaches 90° .

Finally, there is a kind of crystal imperfection known as *mosaic structure* which is possessed by all real crystals to a greater or lesser degree and which has a decided effect on diffraction phenomena. It is a kind of substructure into which a "single" crystal is broken up and is illustrated in Fig. 3-16 in an enormously exaggerated fashion. A crystal with mosaic structure does not have its atoms arranged on a perfectly regular lattice extending from one side of the crystal to the other; instead, the lattice is broken up into a number of tiny blocks, each slightly disoriented one from another. The size of these blocks is of the order of 1000 Å, while the maximum angle of disorientation between them may vary from a very small value to as much as one degree, depending on the crystal. If this angle is ε , then diffraction of a parallel monochromatic beam from a "single" crystal will occur not only at an angle of incidence θ_B but at all angles between θ_B and $\theta_B + \varepsilon$. Another effect of mosaic structure is to increase the integrated intensity of the reflected beam relative to that theoretically calculated for an ideally perfect crystal (Sec. 4-12).

The notion of the mosaic crystal dates from the early years of x-ray diffraction and depends on much indirect evidence, both theoretical and experimental. In the 1960s the electron microscope provided direct evidence. It showed that real crystals, whether single crystals or individual grains in a polycrystalline aggregate,

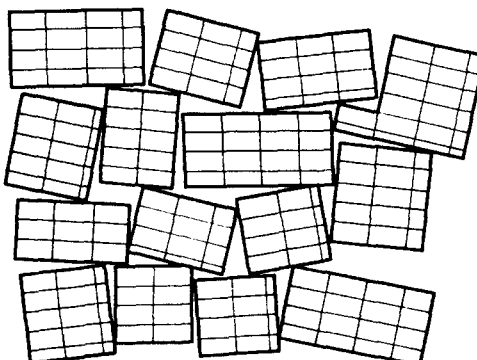
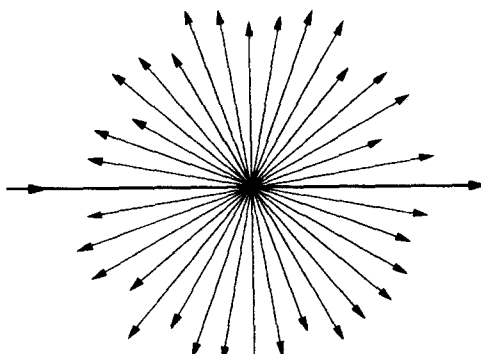


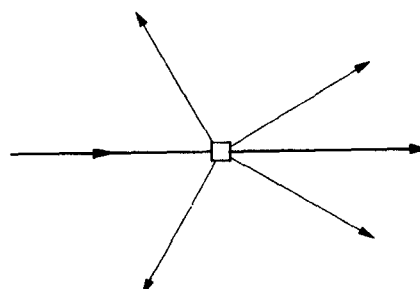
Fig. 3-16 The mosaic structure of a real crystal.

had a substructure defined by the dislocations present. The density of these dislocations is not uniform; they tend to group themselves into walls (sub-grain boundaries) surrounding small volumes having a low dislocation density (sub-grains or cells). Today the term "mosaic structure" is seldom used, but the little blocks of Fig. 3-16 are identical with sub-grains and the regions between the blocks are the dislocation walls.

These, then, are some examples of diffraction under nonideal conditions, that is, of diffraction as it actually occurs. We should not regard these as "deviations" from the Bragg law, and we will not as long as we remember that this law is derived for certain ideal conditions and that diffraction is only a special kind of scattering. This latter point cannot be too strongly emphasized. A single atom scatters an incident beam of x-rays in all directions in space, but a large number of atoms arranged in a perfectly periodic array in three dimensions to form a crystal scatters (diffracts) x-rays in relatively few directions, as illustrated schematically in Fig. 3-17. It does so precisely because the periodic arrangement of atoms causes destructive interference of the scattered rays in all directions *except* those predicted by the Bragg law, and in these directions constructive interference (reinforcement) occurs. It is not surprising, therefore, that measurable diffraction (scattering) occurs at non-Bragg angles whenever any crystal imperfection results in the partial



(a)



(b)

Fig. 3-17 (a) Scattering by an atom. (b) Diffraction by a crystal.

absence of one or more of the necessary conditions for perfect destructive interference at these angles. These imperfections are generally slight compared to the over-all regularity of the lattice, with the result that diffracted beams are confined to very narrow angular ranges centered on the angles predicted by the Bragg law for ideal conditions.

This relation between destructive interference and structural periodicity can be further illustrated by a comparison of x-ray scattering by solids, liquids, and gases (Fig. 3-18). The curve of scattered intensity vs. 2θ for a crystalline solid is almost zero everywhere except at certain angles where high sharp maxima occur: these are the diffracted beams. Both amorphous solids and liquids have structures characterized by an almost complete lack of periodicity and a tendency to "order" only in the sense that the atoms are fairly tightly packed together and show a statistical preference for a particular interatomic distance; the result is an x-ray scattering curve showing nothing more than one or two broad maxima. Finally, there are the monatomic gases, which have no structural periodicity whatever; in such gases, the atoms are arranged perfectly at random and their relative positions

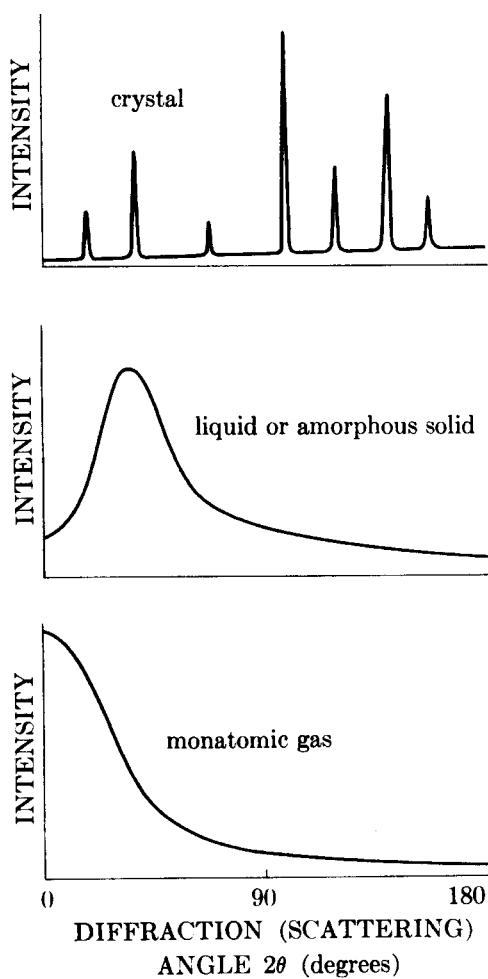


Fig. 3-18 Comparative x-ray scattering by crystalline solids, amorphous solids, liquids, and monatomic gases (schematic). The three vertical scales are not equal.

change constantly with time. The corresponding scattering curve shows no maxima, merely a regular decrease of intensity with increase in scattering angle. This curve would be entirely featureless, i.e., horizontal, if it were not for the fact that isolated atoms scatter x-rays more intensely at low 2θ angles than at high (Sec. 4-3).

PROBLEMS

3-1 A transmission Laue pattern is made of a cubic crystal having a lattice parameter of 4.00 Å. The x-ray beam is horizontal. The [010] axis of the crystal points along the beam towards the x-ray tube, the [100] axis points vertically upward, and the [001] axis is horizontal and parallel to the photographic film. The film is 5.00 cm from the crystal.

- What is the wavelength of the radiation diffracted from the (310) planes?
- Where will the 310 reflection strike the film?

***3-2** A transmission Laue pattern is made of a cubic crystal in the orientation of Prob. 3-1. By means of a stereographic projection similar to Fig. 3-8, show that the beams diffracted by the planes (210), (213), and (211), all of which belong to the zone [120], lie on the surface of a cone whose axis is the zone axis. What is the angle ϕ between the zone axis and the transmitted beam?

3-3 Determine, and list in order of increasing angle, the values of 2θ and (hkl) for the first three lines (those of lowest 2θ values) on the powder patterns of substances with the following structures, the incident radiation being Cu $K\alpha$:

- simple cubic ($a = 3.00$ Å),
- simple tetragonal ($a = 2.00$ Å, $c = 3.00$ Å),
- simple tetragonal ($a = 3.00$ Å, $c = 2.00$ Å),
- simple rhombohedral ($a = 3.00$ Å, $\alpha = 80^\circ$).

3-4 In Fig. 3-14, put $m = 10$. (a) Write down a complete list of the path differences, in wavelengths λ , between the ray scattered by each plane below the surface and the ray scattered by the surface plane, for a scattering angle of $2\theta_1$. What plane scatters a ray exactly out of phase with the ray scattered by the third plane below the surface? What is the path difference for these two rays? (b) Write down a similar list of path differences for rays scattered at an angle halfway between $2\theta_B$ and $2\theta_1$ in order to convince yourself that these rays do *not* cancel one another.

***3-5** In Fig. 3-14, assume that the incident beam is perfectly parallel, instead of convergent, and incident at the angle θ_B . Does broadening of the diffracted beam still occur? If so, derive the relation between t and B .

***3-6** Calculate the breadth B (in degrees of 2θ), due to the small crystal effect alone, of the powder pattern lines of particles of diameter 1000, 750, 500, and 250 Å. Assume $\theta = 45^\circ$ and $\lambda = 1.5$ Å. For particles 250 Å in diameter, calculate the breadth B for $\theta = 10$, 45, and 80° .

3-7 Check the value given in Sec. 3-7 for the increase in breadth of a diffraction line due to the natural width of the $K\alpha$ emission line. [Hint: Differentiate the Bragg law and find an expression for the rate of change of 2θ with λ .]

Diffraction II: Intensities of Diffracted Beams

4-1 INTRODUCTION

As stated earlier, the positions of the atoms in the unit cell affect the intensities but not the directions of the diffracted beams. That this must be so may be seen by considering the two structures shown in Fig. 4-1. Both are orthorhombic with two atoms of the same kind per unit cell, but the one on the left is base-centered and the one on the right body-centered. Either is derivable from the other by a simple shift of one atom by the vector $\frac{1}{2}\mathbf{c}$.

Consider reflections from the (001) planes which are shown in profile in Fig. 4-2. For the base-centered lattice shown in (a), suppose that the Bragg law is satisfied for the particular values of λ and θ employed. This means that the path difference ABC between rays 1' and 2' is one wavelength, so that rays 1' and 2' are in phase and diffraction occurs in the direction shown. Similarly, in the body-centered lattice shown in (b), rays 1' and 2' are in phase, since their path difference ABC is one wavelength. However, in this case, there is another plane of atoms midway between the (001) planes, and the path difference DEF between rays 1' and 3' is exactly half of ABC , or one-half wavelength. Thus rays 1' and 3' are completely out of phase and annul each other. Similarly, ray 4' from the next plane down (not shown) annuls ray 2', and so on throughout the crystal. There is no 001 reflection from the body-centered lattice.

This example shows how a simple rearrangement of atoms within the unit cell can eliminate a reflection completely. More generally, the intensity of a diffracted beam is changed, not necessarily to zero, by any change in atomic positions, and, conversely, we can determine atomic positions only by observations of diffracted intensities. To establish an exact relation between atom position and intensity is the main purpose of this chapter. The problem is complex because of the many variables involved, and we will have to proceed step by step: we will consider how x-rays are scattered first by a single electron, then by an atom, and finally by all the atoms in the unit cell. We will apply these results to the powder method of x-ray diffraction only, and, to obtain an expression for the intensity of a powder pattern line, we will have to consider a number of other factors which affect the way in which a crystalline powder diffracts x-rays.

4-2 SCATTERING BY AN ELECTRON

We have seen in Chap. 1 that an x-ray beam is an electromagnetic wave characterized by an electric field whose strength varies sinusoidally with time at any one

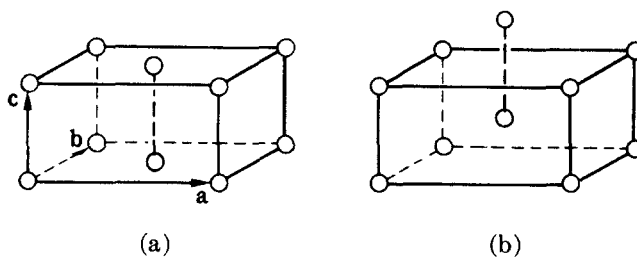


Fig. 4-1 (a) Base-centered and (b) body-centered orthorhombic unit cells.

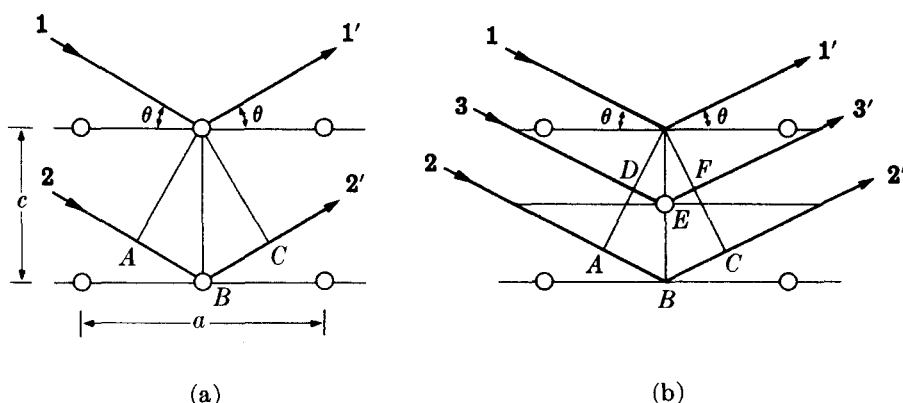


Fig. 4-2 Diffraction from the (001) planes of (a) base-centered and (b) body-centered orthorhombic lattices.

point in the beam. Since an electric field exerts a force on a charged particle such as an electron, the oscillating electric field of an x-ray beam will set any electron it encounters into oscillatory motion about its mean position.

Now an accelerating or decelerating electron emits an electromagnetic wave. We have already seen an example of this phenomenon in the x-ray tube, where x-rays are emitted because of the rapid deceleration of the electrons striking the target. Similarly, an electron which has been set into oscillation by an x-ray beam is continuously accelerating and decelerating during its motion and therefore emits an electromagnetic wave. In this sense, an electron is said to *scatter x-rays*, the scattered beam being simply the beam radiated by the electron under the action of the incident beam. The scattered beam has the same wavelength and frequency as the incident beam and is said to be *coherent* with it, since there is a definite relationship between the phase of the scattered beam and that of the incident beam which produced it. (The phase change on scattering from an electron is $\lambda/2$. Because it is exactly the same for all the electrons in a crystal, it cancels out in any consideration of phase differences between rays scattered by different atoms, as in Fig. 3-2, and so does not affect the derivation of the Bragg law given in Sec. 3-2.)

Although x-rays are scattered in all directions by an electron, the intensity of the scattered beam depends on the angle of scattering, in a way which was first

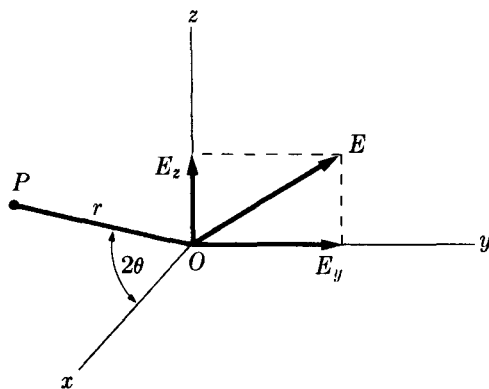


Fig. 4-3 Coherent scattering of x-rays by a single electron.

worked out by J. J. Thomson. He found that the intensity I of the beam scattered by a single electron of charge e coulombs (C) and mass m kg, at a distance r meters from the electron, is given by

$$I = I_0 \left(\frac{\mu_0}{4\pi} \right)^2 \left(\frac{e^4}{m^2 r^2} \right) \sin^2 \alpha = I_0 \frac{K}{r^2} \sin^2 \alpha \quad (4-1)$$

where I_0 = intensity of the incident beam, $\mu_0 = 4\pi \times 10^{-7}$ m kg C⁻², K = constant, and α = angle between the scattering direction and the direction of acceleration of the electron. Suppose the incident beam is traveling in the direction Ox (Fig. 4-3) and encounters an electron at O . We wish to know the scattered intensity at P in the xz plane where OP is inclined at a scattering angle of 2θ to the incident beam. An unpolarized incident beam, such as that issuing from an x-ray tube, has its electric vector E in a random direction in the yz plane. This beam may be resolved into two plane-polarized components, having electric vectors E_y and E_z where

$$\mathbf{E}^2 = \mathbf{E}_y^2 + \mathbf{E}_z^2.$$

On the average, E_y will be equal to E_z , since the direction of E is perfectly random. Therefore

$$\mathbf{E}_y^2 = \mathbf{E}_z^2 = \frac{1}{2}\mathbf{E}^2.$$

The intensity of these two components of the incident beam is proportional to the square of their electric vectors, since E measures the amplitude of the wave and the intensity of a wave is proportional to the square of its amplitude. Therefore

$$I_{0y} = I_{0z} = \frac{1}{2}I_0.$$

The y component of the incident beam accelerates the electron in the direction Oy . It therefore gives rise to a scattered beam whose intensity at P is found from Eq. (4-1) to be

$$I_{Py} = I_{0y} \frac{K}{r^2},$$

since $\alpha = \Delta y OP = \pi/2$. Similarly, the intensity of the scattered z component is given by

$$I_{Pz} = I_{0z} \frac{K}{r^2} \cos^2 2\theta,$$

since $\alpha = \pi/2 - 2\theta$. The total scattered intensity at P is obtained by summing the intensities of these two scattered components:

$$\begin{aligned} I_P &= I_{Py} + I_{Pz} \\ &= \frac{K}{r^2} (I_{0y} + I_{0z} \cos^2 2\theta) \\ &= \frac{K}{r^2} \left(\frac{I_0}{2} + \frac{I_0}{2} \cos^2 2\theta \right) \\ &= I_0 \frac{K}{r^2} \left(\frac{1 + \cos^2 2\theta}{2} \right). \end{aligned} \quad (4-2)$$

This is the Thomson equation for the scattering of an x-ray beam by a single electron. The intensity of the scattered beam is only a minute fraction of the intensity of the incident beam; the value of K is $7.94 \times 10^{-30} \text{ m}^2$, so that I_P/I_0 is only 7.94×10^{-26} in the forward direction at 1 cm from the electron. The equation also shows that the scattered intensity decreases as the inverse square of the distance from the scattering electron, as one would expect, and that the scattered beam is stronger in forward or backward directions than in a direction at right angles to the incident beam.

The Thomson equation gives the absolute intensity (in ergs/sq cm/sec) of the scattered beam in terms of the absolute intensity of the incident beam. These absolute intensities are both difficult to measure and difficult to calculate, so it is fortunate that relative values are sufficient for our purposes in practically all diffraction problems. In most cases, all factors in Eq. (4-2) except the last are constant during the experiment and can be omitted. This last factor, $\frac{1}{2}(1 + \cos^2 2\theta)$, is called the *polarization factor*; this is a rather unfortunate term because, as we have just seen, this factor enters the equation simply because the incident beam is unpolarized. The polarization factor is common to all intensity calculations, and we will use it later in our equation for the intensity of a beam diffracted by a crystalline powder.

There is another and quite different way in which an electron can scatter x-rays, and that is manifested in the *Compton effect*. This effect, discovered by A. H. Compton in 1923, occurs whenever x-rays encounter loosely bound or free electrons and can be understood only by considering the incident beam not as a wave motion, but as a stream of x-ray quanta or photons, each of energy $h\nu_1$. When such a photon strikes a loosely bound electron, the collision is an elastic one like that of two billiard balls (Fig. 4-4). The electron is knocked aside and the photon is deviated through an angle 2θ . Since some of the energy of the incident photon is used in providing kinetic energy for the electron, the energy $h\nu_2$ of the photon after impact is less than its energy $h\nu_1$ before impact. The wavelength λ_2 of the

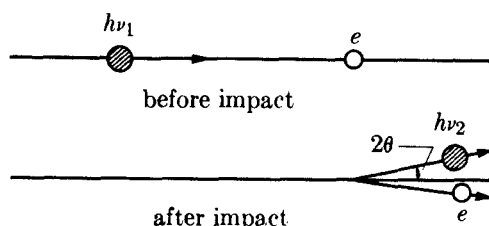


Fig. 4-4 Elastic collision of photon and electron (Compton effect).

scattered radiation is thus slightly greater than the wavelength λ_1 of the incident beam, the magnitude of the change being given by the equation

$$\Delta\lambda(\text{\AA}) = \lambda_2 - \lambda_1 = 0.0486 \sin^2 \theta. \quad (4-3)$$

The increase in wavelength depends only on the scattering angle, and it varies from zero in the forward direction ($2\theta = 0$) to 0.05 \AA in the extreme backward direction ($2\theta = 180^\circ$).

Radiation so scattered is called *Compton modified radiation*, and, besides having its wavelength increased, it has the important characteristic that *its phase has no fixed relation to the phase of the incident beam*. For this reason it is also known as incoherent radiation. It cannot take part in diffraction because its phase is only randomly related to that of the incident beam and cannot therefore produce any interference effects. Compton modified scattering cannot be prevented, however, and it has the undesirable effect of darkening the background of diffraction patterns.

(It should be noted that the quantum theory can account for both the coherent and the incoherent scattering, whereas the wave theory is applicable only to the former. In terms of the quantum theory, coherent scattering occurs when an incident photon bounces off an electron which is so tightly bound that the electron receives no momentum from the impact. The scattered photon therefore has the same energy, and hence wavelength, as it had before.)

4-3 SCATTERING BY AN ATOM

When an x-ray beam encounters an atom, each electron in it scatters part of the radiation coherently in accordance with the Thomson equation. One might also expect the nucleus to take part in the coherent scattering, since it also bears a charge and should be capable of oscillating under the influence of the incident beam. However, the nucleus has an extremely large mass relative to that of the electron and cannot be made to oscillate to any appreciable extent; in fact, the Thomson equation shows that the intensity of coherent scattering is inversely proportional to the square of the mass of the scattering particle. The net effect is that coherent scattering by an atom is due only to the electrons contained in that atom.

The following question then arises: is the wave scattered by an atom simply the sum of the waves scattered by its component electrons? More precisely, does an atom of atomic number Z , i.e., an atom containing Z electrons, scatter a wave

whose amplitude is Z times the amplitude of the wave scattered by a single electron? The answer is yes, if the scattering is in the forward direction ($2\theta = 0$), because the waves scattered by all the electrons of the atom are then in phase and the amplitudes of all the scattered waves can be added directly.

This is not true for other directions of scattering. The fact that the electrons of an atom are situated at different points in space introduces differences in phase between the waves scattered by different electrons. Consider Fig. 4-5, in which, for simplicity, the electrons are shown as points arranged around the central nucleus. The waves scattered in the forward direction by electrons A and B are exactly in phase on a wave front such as XX' , because each wave has traveled the same distance before and after scattering. The other scattered waves shown in the figure, however, have a path difference equal to $(CB - AD)$ and are thus somewhat out of phase along a wave front such as YY' , the path difference being less than one wavelength. Partial interference occurs between the waves scattered by A and B , with the result that the net amplitude of the wave scattered in this direction is less than that of the wave scattered by the same electrons in the forward direction.

A quantity f , the *atomic scattering factor*, is used to describe the "efficiency" of scattering of a given atom in a given direction. It is defined as a ratio of amplitudes:

$$f = \frac{\text{amplitude of the wave scattered by an atom}}{\text{amplitude of the wave scattered by one electron}}.$$

From what has been said already, it is clear that $f = Z$ for any atom scattering in the forward direction. As θ increases, however, the waves scattered by individual electrons become more and more out of phase and f decreases. The atomic scattering factor depends also on the wavelength of the incident beam: at a fixed

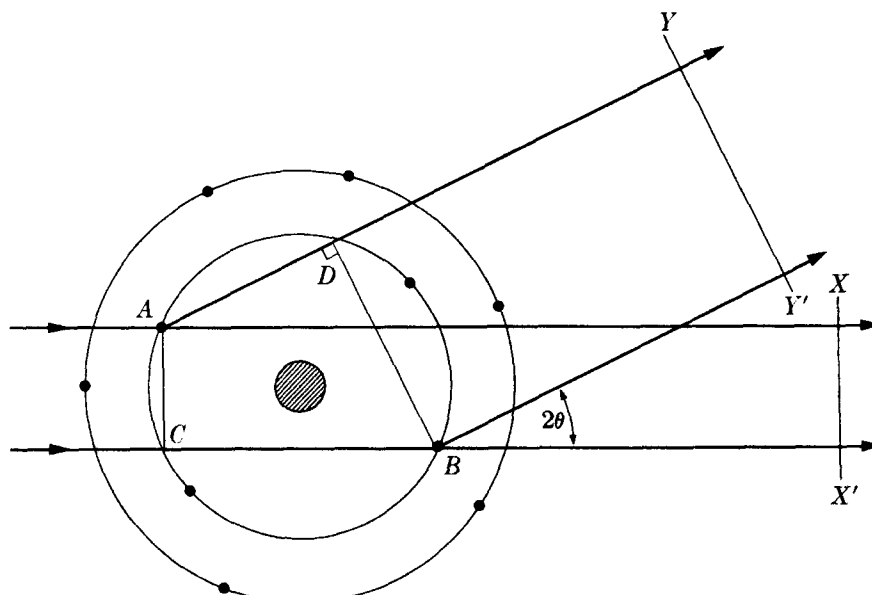


Fig. 4-5 X-ray scattering by an atom.

value of θ , f will be smaller the shorter the wavelength, since the path differences will be larger relative to the wavelength, leading to greater interference between the scattered beams. The actual calculation of f involves $\sin \theta$ rather than θ , so that the net effect is that f decreases as the quantity $(\sin \theta)/\lambda$ increases. The scattering factor f is sometimes called the *form factor*, because it depends on the way in which the electrons are distributed around the nucleus.

Calculated values of f for various atoms and various values of $(\sin \theta)/\lambda$ are tabulated in Appendix 12, and a curve showing the typical variation of f , in this case for copper, is given in Fig. 4-6. Note again that the curve begins at the atomic number of copper, 29, and decreases to very low values for scattering in the backward direction (θ near 90°) or for very short wavelengths. Since the intensity of a wave is proportional to the square of its amplitude, a curve of scattered intensity from an atom can be obtained simply by squaring the ordinates of a curve such as Fig. 4-6. (The resulting curve closely approximates the observed scattered intensity per atom of a monatomic gas, as shown in Fig. 3-18.)

Strictly, the scattering factors f tabulated in Appendix 12 apply only when the scattered radiation has a wavelength much shorter than that of an absorption edge of the scattering atom. When these two wavelengths are nearly the same, a small correction to f must be applied in precise work. An example is given in Sec. 13-4. Ordinarily we neglect this effect, called *anomalous dispersion*.

The scattering just discussed, whose amplitude is expressed in terms of the atomic scattering factor, is coherent, or unmodified, scattering, which is the only kind capable of being diffracted. On the other hand, incoherent, or Compton modified, scattering is occurring at the same time. Since the latter is due to collisions of quanta with loosely bound electrons, its intensity relative to that of the

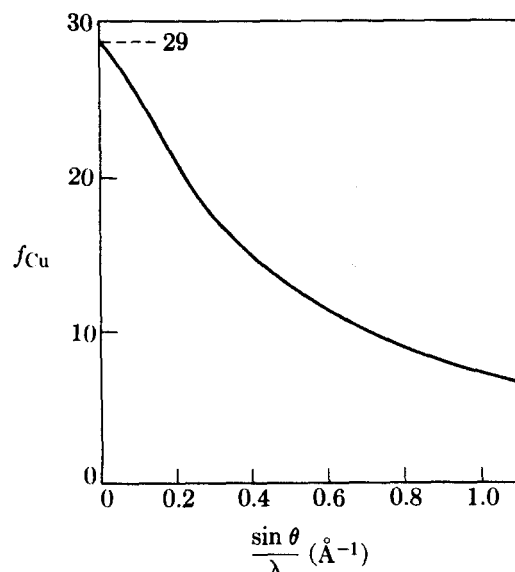


Fig. 4-6 The atomic scattering factor of copper.

unmodified radiation increases as the proportion of loosely bound electrons increases. The intensity of Compton modified radiation thus increases as the atomic number Z decreases. It is for this reason that it is difficult to obtain good diffraction photographs of organic materials, which contain light elements such as carbon, oxygen, and hydrogen, since the strong Compton modified scattering from these substances darkens the background of the photograph and makes it difficult to see the diffraction lines formed by the unmodified radiation. It is also found that the intensity of the modified radiation increases as the quantity $(\sin \theta)/\lambda$ increases. The intensities of modified scattering and of unmodified scattering therefore vary in opposite ways with Z and with $(\sin \theta)/\lambda$.

To summarize, when a monochromatic beam of x-rays strikes an atom, two scattering processes occur. Tightly bound electrons are set into oscillation and radiate x-rays of the same wavelength as that of the incident beam. More loosely bound electrons scatter part of the incident beam and slightly increase its wavelength in the process, the exact amount of increase depending on the scattering angle. The former is called coherent or unmodified scattering and the latter incoherent or modified; both kinds occur simultaneously and in all directions. If the atom is a part of a large group of atoms arranged in space in a regular periodic fashion as in a crystal, then another phenomenon occurs. The coherently scattered radiation from all the atoms undergoes reinforcement in certain directions and cancellation in other directions, thus producing diffracted beams. Diffraction is, essentially, reinforced coherent scattering.

We are now in a position to summarize, from the preceding sections and from Chap. 1, the chief effects associated with the passage of x-rays through matter. This is done schematically in Fig. 4-7. The incident x-rays are assumed to be of high enough energy, i.e., of short enough wavelength, to cause the emission of photoelectrons and characteristic fluorescent radiation. The Compton recoil electrons shown in the diagram are the loosely bound electrons knocked out of

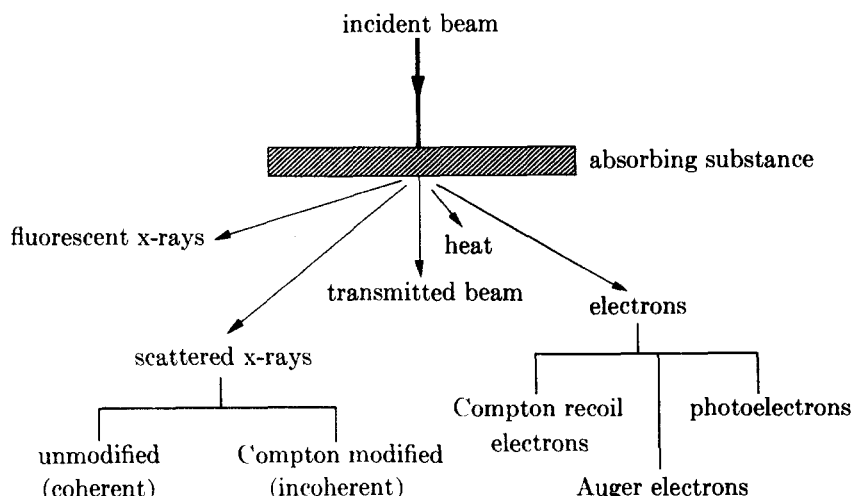


Fig. 4-7 Effects produced by the passage of x-rays through matter, after Henry, Lipson, and Wooster [G.8].

the atom by x-ray quanta, the interaction giving rise to Compton modified radiation. Auger electrons are those ejected from an atom by characteristic x-rays produced within the atom.

4-4 SCATTERING BY A UNIT CELL

To arrive at an expression for the intensity of a diffracted beam, we must now restrict ourselves to a consideration of the coherent scattering, not from an isolated atom but from all the atoms making up the crystal. The mere fact that the atoms are arranged in a periodic fashion in space means that the scattered radiation is now severely limited to certain definite directions and is now referred to as a set of diffracted beams. The directions of these beams are fixed by the Bragg law, which is, in a sense, a negative law. If the Bragg law is not satisfied, no diffracted beam can occur; however, the Bragg law may be satisfied for a certain set of atomic planes and yet no diffraction may occur, as in the example given at the beginning of this chapter, because of a particular arrangement of atoms within the unit cell [Fig. 4-2(b)].

Assuming that the Bragg law is satisfied, we wish to find the intensity of the beam diffracted by a crystal as a function of atom position. Since the crystal is merely a repetition of the fundamental unit cell, it is enough to consider the way in which the arrangement of atoms within a single unit cell affects the diffracted intensity.

Qualitatively, the effect is similar to the scattering from an atom, discussed in the previous section. There we found that phase differences occur in the waves scattered by the individual electrons, for any direction of scattering except the extreme forward direction. Similarly, the waves scattered by the individual atoms of a unit cell are not necessarily in phase except in the forward direction, and we must now determine how the phase difference depends on the arrangement of the atoms.

This problem is most simply approached by finding the phase difference between waves scattered by an atom at the origin and another atom whose position is variable in the x direction only. For convenience, consider an orthogonal unit cell, a section of which is shown in Fig. 4-8. Take atom A as the origin and let diffraction occur from the $(h00)$ planes shown as heavy lines in the drawing. This means that the Bragg law is satisfied for this reflection and that $\delta_{2'1'}$, the path difference between ray $2'$ and ray $1'$, is given by

$$\delta_{2'1'} = MCN = 2d_{h00} \sin \theta = \lambda.$$

From the definition of Miller indices,

$$d_{h00} = AC = \frac{a}{h}.$$

How is this reflection affected by x-rays scattered in the same direction by atom B , located at a distance x from A ? Note that only this direction need be considered since only in this direction is the Bragg law satisfied for the $h00$ reflection. Clearly, the path difference between ray $3'$ and ray $1'$, $\delta_{3'1'}$, will be less

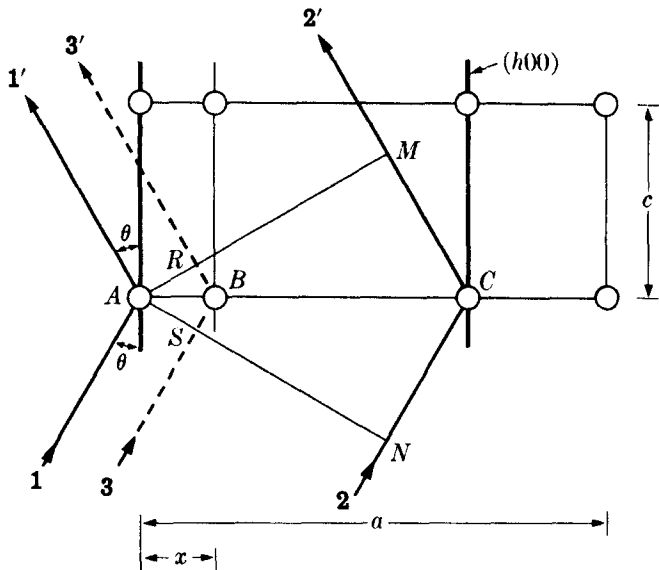


Fig. 4-8 The effect of atom position on the phase difference between diffracted rays.

than λ ; by simple proportion it is found to be

$$\delta_{3'1'} = RBS = \frac{AB}{AC} (\lambda) = \frac{x}{a/h} (\lambda).$$

Phase differences may be expressed in angular measure as well as in wavelength: two rays, differing in path length by one whole wavelength, are said to differ in phase by 360° , or 2π radians. If the path difference is δ , then the phase difference ϕ in radians is given by

$$\phi = \frac{\delta}{\lambda} (2\pi).$$

The use of angular measure is convenient because it makes the expression of phase differences independent of wavelength, whereas the use of a path difference to describe a phase difference is meaningless unless the wavelength is specified.

The phase difference, then, between the wave scattered by atom *B* and that scattered by atom *A* at the origin is given by

$$\phi_{3'1'} = \frac{\delta_{3'1'}}{\lambda} (2\pi) = \frac{2\pi h x}{a}.$$

If the position of atom *B* is specified by its fractional coordinate $u = x/a$, then the phase difference becomes

$$\phi_{3'1'} = 2\pi h u.$$

This reasoning may be extended to three dimensions, as in Fig. 4-9, in which atom *B* has actual coordinates $x y z$ or fractional coordinates $\frac{x}{a} \frac{y}{b} \frac{z}{c}$ equal to $u v w$, respectively. We then arrive at the following important relation for the

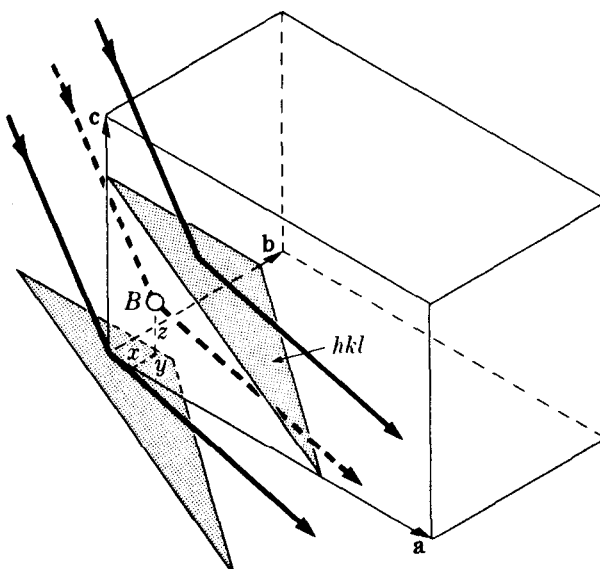


Fig. 4-9 The three-dimensional analogue of Fig. 4-8.

phase difference between the wave scattered by atom *B* and that scattered by atom *A* at the origin, for the hkl reflection:

$$\phi = 2\pi(hu + kv + lw). \quad (4-4)$$

This relation is general and applicable to a unit cell of any shape.

These two waves may differ, not only in phase, but also in amplitude if atom *B* and the atom at the origin are of different kinds. In that case, the amplitudes of these waves are given, relative to the amplitude of the wave scattered by a single electron, by the appropriate values of *f*, the atomic scattering factor.

We now see that the problem of scattering from a unit cell resolves itself into one of adding waves of different phase and amplitude in order to find the resultant wave. Waves scattered by all the atoms of the unit cell, including the one at the origin, must be added. The most convenient way of carrying out this summation is by expressing each wave as a complex exponential function.

The two waves shown as full lines in Fig. 4-10 represent the variations in electric field intensity \mathbf{E} with time *t* of two rays on any given wave front in a diffracted x-ray beam. Their equations may be written

$$\mathbf{E}_1 = A_1 \sin(2\pi vt - \phi_1), \quad (4-5)$$

$$\mathbf{E}_2 = A_2 \sin(2\pi vt - \phi_2). \quad (4-6)$$

These waves are of the same frequency *v* and therefore of the same wavelength λ , but differ in amplitude *A* and in phase ϕ . The dotted curve shows their sum \mathbf{E}_3 , which is also a sine wave, but of different amplitude and phase.

Waves differing in amplitude and phase may also be added by representing them as vectors. In Fig. 4-11, each component wave is represented by a vector whose length is equal to the amplitude of the wave and which is inclined to the x-axis at an angle equal to the phase angle. The amplitude and phase of the

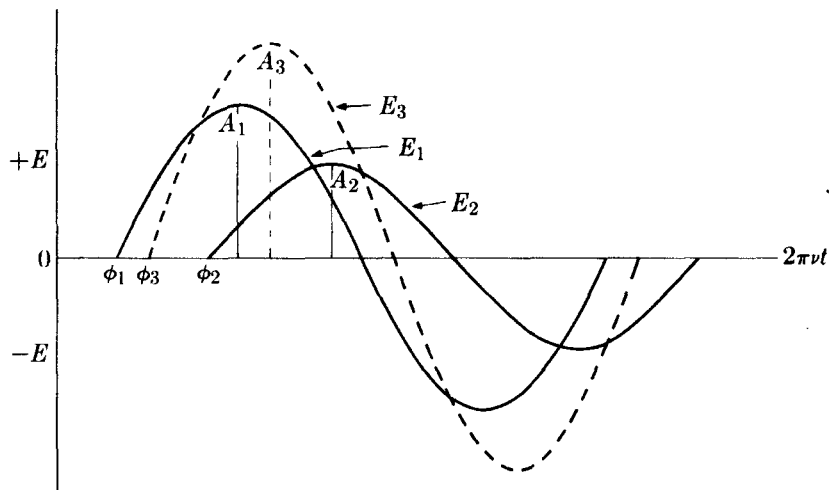


Fig. 4-10 The addition of sine waves of different phase and amplitude.

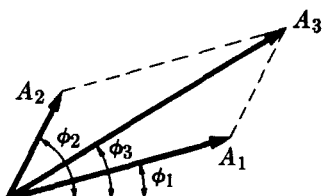


Fig. 4-11 Vector addition of waves.

resultant wave are then found simply by adding the vectors by the parallelogram law.

This geometrical construction may be avoided by use of the following analytical treatment, in which complex numbers are used to represent the vectors. A complex number is the sum of a real and an imaginary number, such as $(a + bi)$, where a and b are real and $i = \sqrt{-1}$ is imaginary. Such numbers may be plotted in the "complex plane," in which real numbers are plotted as abscissae and imaginary numbers as ordinates. Any point in this plane, or the vector drawn from the origin to this point, then represents a particular complex number $(a + bi)$.

To find an analytical expression for a vector representing a wave, we draw the wave vector in the complex plane as in Fig. 4-12. Here again the amplitude and phase of the wave are given by A , the length of the vector, and ϕ , the angle between the vector and the axis of real numbers. The analytical expression for the wave is now the complex number $(A \cos \phi + iA \sin \phi)$, since these two terms are the horizontal and vertical components OM and ON of the vector. Note that multiplication of a vector by i rotates it counterclockwise by 90° ; thus multiplication by i converts the horizontal vector 2 into the vertical vector $2i$. Multiplication twice by i , that is, by $i^2 = -1$, rotates a vector through 180° or reverses its sense; thus multiplication twice by i converts the horizontal vector 2 into the horizontal vector -2 pointing in the opposite direction.

If we write down the power-series expansions of e^{ix} , $\cos x$, and $\sin x$ and

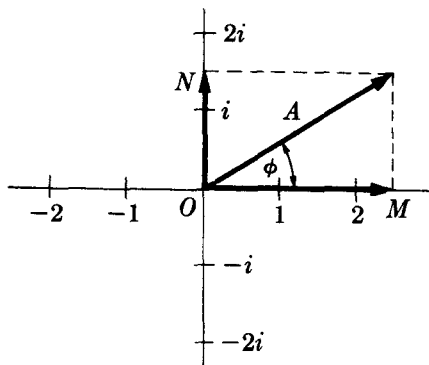


Fig. 4-12 A wave vector in the complex plane.

compare them, we find that

$$e^{ix} = \cos x + i \sin x \quad (4-7)$$

or

$$Ae^{i\phi} = A \cos \phi + Ai \sin \phi. \quad (4-8)$$

Thus the wave vector may be expressed analytically by either side of Eq. (4-8). The expression on the left is called a complex exponential function.

Since the intensity of a wave is proportional to the square of its amplitude, we now need an expression for A^2 , the square of the absolute value of the wave vector. When a wave is expressed in complex form, this quantity is obtained by multiplying the complex expression for the wave by its complex conjugate, which is obtained simply by replacing i by $-i$. Thus, the complex conjugate of $Ae^{i\phi}$ is $Ae^{-i\phi}$. We have

$$|Ae^{i\phi}|^2 = Ae^{i\phi}Ae^{-i\phi} = A^2, \quad (4-9)$$

which is the quantity desired. Or, using the other form given by Eq. (4-8), we have

$$A(\cos \phi + i \sin \phi)A(\cos \phi - i \sin \phi) = A^2(\cos^2 \phi + \sin^2 \phi) = A^2.$$

We return now to the problem of adding the scattered waves from each of the atoms in the unit cell. The amplitude of each wave is given by the appropriate value of f for the scattering atom considered and the value of $(\sin \theta)/\lambda$ involved in the reflection. The phase of each wave is given by Eq. (4-4) in terms of the hkl reflection considered and the uvw coordinates of the atom. Using our previous relations, we can then express any scattered wave in the complex exponential form

$$Ae^{i\phi} = fe^{2\pi i(hu+kv+lw)}. \quad (4-10)$$

The resultant wave scattered by all the atoms of the unit cell is called the *structure factor*, because it describes how the atom arrangement, given by uvw for each atom, affects the scattered beam. The structure factor, designated by the symbol F , is obtained by simply adding together all the waves scattered by the individual atoms. If a unit cell contains atoms 1, 2, 3, ..., N , with fractional coordinates $u_1 v_1 w_1, u_2 v_2 w_2, u_3 v_3 w_3, \dots$ and atomic scattering factors f_1, f_2, f_3, \dots , then the structure factor for the hkl reflection is given by

$$F = f_1 e^{2\pi i(hu_1+kv_1+lw_1)} + f_2 e^{2\pi i(hu_2+kv_2+lw_2)} + f_3 e^{2\pi i(hu_3+kv_3+lw_3)} + \dots$$

This equation may be written more compactly as

$$F_{hkl} = \sum_1^N f_n e^{2\pi i(hu_n + kv_n + lw_n)}, \quad (4-11)$$

where the summation extends over all the N atoms of the unit cell.

F is, in general, a complex number, and it expresses both the amplitude and phase of the resultant wave. Its absolute value $|F|$ gives the amplitude of the resultant wave in terms of the amplitude of the wave scattered by a single electron. Like the atomic scattering factor f , $|F|$ is defined as a ratio of amplitudes:

$$|F| = \frac{\text{amplitude of the wave scattered by all the atoms of a unit cell}}{\text{amplitude of the wave scattered by one electron}}.$$

The intensity of the beam diffracted by all the atoms of the unit cell in a direction predicted by the Bragg law is proportional simply to $|F|^2$, the square of the amplitude of the resultant beam, and $|F|^2$ is obtained by multiplying the expression given for F in Eq. (4-11) by its complex conjugate. Equation (4-11) is therefore a very important relation in x-ray crystallography, since it permits a calculation of the intensity of any hkl reflection from a knowledge of the atomic positions.

We have found the resultant scattered wave by adding together waves, differing in phase, scattered by individual atoms in the unit cell. Note that the phase difference between rays scattered by any two atoms, such as A and B in Fig. 4-8, is *constant* for every unit cell. There is no question here of these rays becoming increasingly out of phase as we go deeper in the crystal as there was when we considered diffraction at angles not exactly equal to the Bragg angle θ_B . In the direction predicted by the Bragg law, the rays scattered by all the atoms A in the crystal are exactly in phase and so are the rays scattered by all the atoms B , but between these two sets of rays there is a definite phase difference which depends on the relative positions of atoms A and B in the unit cell and which is given by Eq. (4-4).

Although it is more unwieldy, the following trigonometric equation may be used instead of Eq. (4-11):

$$F = \sum_1^N f_n [\cos 2\pi(hu_n + kv_n + lw_n) + i \sin 2\pi(hu_n + kv_n + lw_n)].$$

One such term must be written down for each atom in the unit cell. In general, the summation will be a complex number of the form

$$F = a + ib,$$

where

$$a = \sum_1^N f_n \cos 2\pi(hu_n + kv_n + lw_n),$$

$$b = \sum_1^N f_n \sin 2\pi(hu_n + kv_n + lw_n),$$

$$|F|^2 = (a + ib)(a - ib) = a^2 + b^2.$$

Substitution for a and b gives the final form of the equation:

$$|F|^2 = [f_1 \cos 2\pi(hu_1 + kv_1 + lw_1) + f_2 \cos 2\pi(hu_2 + kv_2 + lw_2) + \dots]^2 + [f_1 \sin 2\pi(hu_1 + kv_1 + lw_1) + f_2 \sin 2\pi(hu_2 + kv_2 + lw_2) + \dots]^2.$$

Equation (4-11) is much easier to manipulate, compared to this trigonometric form, particularly if the structure is at all complicated, since the exponential form is more compact.

4-5 SOME USEFUL RELATIONS

In calculating structure factors by complex exponential functions, many particular relations occur often enough to be worthwhile stating here. They may be verified by means of Eq. (4-7).

- a) $e^{\pi i} = e^{3\pi i} = e^{5\pi i} = -1,$
- b) $e^{2\pi i} = e^{4\pi i} = e^{6\pi i} = +1,$
- c) in general, $e^{n\pi i} = (-1)^n,$ where n is any integer,
- d) $e^{n\pi i} = e^{-n\pi i},$ where n is any integer,
- e) $e^{ix} + e^{-ix} = 2 \cos x.$

4-6 STRUCTURE-FACTOR CALCULATIONS

Facility in the use of Eq. (4-11) can be gained only by working out some actual examples, and we shall consider a few such problems here and again in Chap. 10.

a) The simplest case is that of a unit cell containing only one atom at the origin, i.e., having fractional coordinates 0 0 0. Its structure factor is

$$F = fe^{2\pi i(0)} = f$$

and

$$F^2 = f^2.$$

F^2 is thus independent of h , k , and l and is the same for all reflections.

b) Consider now the base-centered cell discussed at the beginning of this chapter and shown in Fig. 4-1(a). It has two atoms of the same kind per unit cell located at 0 0 0 and $\frac{1}{2} \frac{1}{2} 0$.

$$\begin{aligned} F &= fe^{2\pi i(0)} + fe^{2\pi i(h/2+k/2)} \\ &= f[1 + e^{\pi i(h+k)}]. \end{aligned}$$

This expression may be evaluated without multiplication by the complex conjugate,

since $(h + k)$ is always integral, and the expression for F is thus real and not complex. If h and k are both even or both odd, i.e., "unmixed," then their sum is always even and $e^{\pi i(h+k)}$ has the value 1. Therefore

$$F = 2f \quad \text{for } h \text{ and } k \text{ unmixed;} \\ F^2 = 4f^2.$$

On the other hand, if h and k are one even and one odd, i.e., "mixed," then their sum is odd and $e^{\pi i(h+k)}$ has the value -1. Therefore

$$F = 0 \quad \text{for } h \text{ and } k \text{ mixed;} \\ F^2 = 0.$$

Note that, in either case, the value of the l index has no effect on the structure factor. For example, the reflections 111, 112, 113, and 021, 022, 023 all have the same value of F , namely $2f$. Similarly, the reflections 011, 012, 013, and 101, 102, 103 all have a zero structure factor.

c) The structure factor of the body-centered cell shown in Fig. 4-1(b) may also be calculated. This cell has two atoms of the same kind located at 0 0 0 and $\frac{1}{2} \frac{1}{2} \frac{1}{2}$.

$$F = fe^{2\pi i(0)} + fe^{2\pi i(h/2+k/2+l/2)} \\ = f[1 + e^{\pi i(h+k+l)}]. \\ F = 2f \quad \text{when } (h + k + l) \text{ is even;} \\ F^2 = 4f^2. \\ F = 0 \quad \text{when } (h + k + l) \text{ is odd;} \\ F^2 = 0.$$

We had previously concluded from geometrical considerations that the base-centered cell would produce a 001 reflection but that the body-centered cell would not. This result is in agreement with the structure-factor equations for these two cells. A detailed examination of the geometry of all possible reflections, however, would be a very laborious process compared to the straightforward calculation of the structure factor, a calculation that yields a set of rules governing the value of F^2 for all possible values of plane indices.

d) A face-centered cubic cell, such as that shown in Fig. 2-14, may now be considered. Assume it to contain four atoms of the same kind, located at 0 0 0, $\frac{1}{2} \frac{1}{2} 0$, $\frac{1}{2} 0 \frac{1}{2}$, and $0 \frac{1}{2} \frac{1}{2}$.

$$F = fe^{2\pi i(0)} + fe^{2\pi i(h/2+k/2)} + fe^{2\pi i(h/2+l/2)} + fe^{2\pi i(k/2+l/2)} \\ = f[1 + e^{\pi i(h+k)} + e^{\pi i(h+l)} + e^{\pi i(k+l)}].$$

If h , k , and l are unmixed, then all three sums $(h + k)$, $(h + l)$, and $(k + l)$ are even integers, and each term in the above equation has the value 1.

$$F = 4f \quad \text{for unmixed indices;} \\ F^2 = 16f^2.$$

If h , k , and l are mixed, then the sum of the three exponentials is -1 , whether two of the indices are odd and one even, or two even and one odd. Suppose, for example, that h and l are even and k is odd, e.g., 012. Then $F = f(1 - 1 + 1 - 1) = 0$, and no reflection occurs.

$$\begin{aligned} F &= 0 \quad \text{for mixed indices;} \\ F^2 &= 0 \end{aligned}$$

Thus, reflections will occur for such planes as (111), (200), and (220) but not for the planes (100), (210), (112), etc.

The reader may have noticed in the previous examples that some of the information given was not used in the calculations. In (a), for example, the cell was said to contain only one atom, but the shape of the cell was not specified; in (b) and (c), the cells were described as orthorhombic and in (d) as cubic, but this information did not enter into the structure-factor calculations. This illustrates the important point that *the structure factor is independent of the shape and size of the unit cell*. For example, *any* body-centered cell will have missing reflections for those planes which have $(h + k + l)$ equal to an odd number, whether the cell is cubic, tetragonal, or orthorhombic. The rules we have derived in the above examples are therefore of wider applicability than would at first appear and demonstrate the close connection between the Bravais lattice of a substance and its diffraction pattern. They are summarized in Table 4-1. These rules are subject to

Table 4-1

Bravais lattice	Reflections possibly present	Reflections necessarily absent
Simple	all	none
Base-centered	h and k unmixed*	h and k mixed*
Body-centered	$(h + k + l)$ even	$(h + k + l)$ odd
Face-centered	h , k , and l unmixed	h , k , and l mixed

* These relations apply to a cell centered on the C face. If reflections are present only when h and l are unmixed, or when k and l are unmixed, then the cell is centered on the B or A face, respectively.

some qualification, since some cells may contain more atoms than the ones given in examples (a) through (d), and these atoms may be in such positions that reflections normally present are now missing. For example, diamond has a face-centered cubic lattice, but it contains eight carbon atoms per unit cell. All the reflections present have unmixed indices, but reflections such as 200, 222, 420, etc., are missing. The fact that the only reflections *present* have unmixed indices proves that the lattice is face-centered, while the extra missing reflections are a clue to the actual atom arrangement in this crystal.

e) This point may be further illustrated by the structure of NaCl (Fig. 2-18). This crystal has a cubic lattice with 4 Na and 4 Cl atoms per unit cell, located as follows:

Na	0 0 0	$\frac{1}{2} \frac{1}{2} 0$	$\frac{1}{2} 0 \frac{1}{2}$	$0 \frac{1}{2} \frac{1}{2}$
Cl	$\frac{1}{2} \frac{1}{2} \frac{1}{2}$	0 0 $\frac{1}{2}$	$0 \frac{1}{2} 0$	$\frac{1}{2} 0 0$

In this case, the proper atomic scattering factors for each atom* must be inserted in the structure-factor equation, which will have eight terms:

$$\begin{aligned} F &= f_{\text{Na}}e^{2\pi i(0)} + f_{\text{Na}}e^{2\pi i(h/2+k/2)} + f_{\text{Na}}e^{2\pi i(h/2+l/2)} + f_{\text{Na}}e^{2\pi i(k/2+l/2)} \\ &\quad + f_{\text{Cl}}e^{2\pi i(h/2+k/2+l/2)} + f_{\text{Cl}}e^{2\pi i(l/2)} + f_{\text{Cl}}e^{2\pi i(k/2)} + f_{\text{Cl}}e^{2\pi i(h/2)}, \\ F &= f_{\text{Na}}[1 + e^{\pi i(h+k)} + e^{\pi i(h+l)} + e^{\pi i(k+l)}] \\ &\quad + f_{\text{Cl}}[e^{\pi i(h+k+l)} + e^{\pi il} + e^{\pi ik} + e^{\pi ih}]. \end{aligned}$$

As discussed in Sec. 2-7, the sodium-atom positions are related by the face-centering translations and so are the chlorine-atom positions. *Whenever a lattice contains common translations, the corresponding terms in the structure-factor equation can always be factored out*, leading to considerable simplification. In this case we proceed as follows:

$$\begin{aligned} F &= f_{\text{Na}}[1 + e^{\pi i(h+k)} + e^{\pi i(h+l)} + e^{\pi i(k+l)}] \\ &\quad + f_{\text{Cl}}e^{\pi i(h+k+l)}[1 + e^{\pi i(-h-k)} + e^{\pi i(-h-l)} + e^{\pi i(-k-l)}]. \end{aligned}$$

The signs of the exponents in the second bracket may be changed, by relation (d) of Sec. 4-5. Therefore

$$F = [1 + e^{\pi i(h+k)} + e^{\pi i(h+l)} + e^{\pi i(k+l)}][f_{\text{Na}} + f_{\text{Cl}}e^{\pi i(h+k+l)}].$$

Here the terms corresponding to the face-centering translations appear in the first factor; the second factor contains the terms that describe the “basis” of the unit cell, namely, the Na atom at 0 0 0 and the Cl atom at $\frac{1}{2} \frac{1}{2} \frac{1}{2}$. The terms in the first bracket, describing the face-centering translations, have already appeared in example (d), and they were found to have a total value of zero for mixed indices and 4 for unmixed indices. This shows at once that NaCl has a face-centered lattice and that

$$F = 0 \quad \text{for mixed indices};$$

$$F^2 = 0.$$

For unmixed indices,

$$F = 4[f_{\text{Na}} + f_{\text{Cl}}e^{\pi i(h+k+l)}].$$

$$F = 4(f_{\text{Na}} + f_{\text{Cl}}) \quad \text{if } (h + k + l) \text{ is even};$$

$$F^2 = 16(f_{\text{Na}} + f_{\text{Cl}})^2.$$

$$F = 4(f_{\text{Na}} - f_{\text{Cl}}) \quad \text{if } (h + k + l) \text{ is odd};$$

$$F^2 = 16(f_{\text{Na}} - f_{\text{Cl}})^2.$$

In this case, there are more than four atoms per unit cell, but the lattice is still face-centered. The introduction of additional atoms has not eliminated any reflections present in the case of the four-atom cell, but it has decreased some in intensity. For example, the 111 reflection now involves the difference, rather than the sum, of the scattering powers of the two atoms.

* Strictly, and if the calculation of F is to be made to the highest accuracy, scattering factors f for the ions Na^+ and Cl^- must be used, rather than the f values for the neutral atoms Na and Cl, because NaCl is ionized.

The student should carefully note that a lot of algebra can be eliminated, whenever a lattice is known to be centered in any way, by factoring common translations out of the structure-factor equation and inserting immediately the known values of the terms representing these translations. This shortcut procedure is illustrated for NaCl:

1. Write down the atom positions in abbreviated form:

4 Na at 0 0 0 + face-centering translations,

4 Cl at $\frac{1}{2} \frac{1}{2} \frac{1}{2}$ + face-centering translations.

2. Write down the equation for F as a product of two factors. The first is the value of the terms representing the common translations; the second has terms corresponding to the "basis" atoms of the cell. The equation is

$$F = \begin{bmatrix} 4 \\ 0 \end{bmatrix} [f_{\text{Na}} + f_{\text{Cl}} e^{\pi i(h+k+l)}] \quad \begin{array}{l} \text{unmixed indices} \\ \text{mixed indices.} \end{array}$$

3. Simplify further, as necessary. In all structure-factor calculations the aim is to obtain a set of *general* equations that will give the value of F for *any* value of hkl .

This shortcut procedure is illustrated again, for the ZnS structure, in Sec. 4-13.

- One other example of structure factor calculation will be given here. The close-packed hexagonal cell shown in Fig. 2-15 has two atoms of the same kind located at 0 0 0 and $\frac{1}{3} \frac{2}{3} \frac{1}{2}$.

$$\begin{aligned} F &= fe^{2\pi i(0)} + fe^{2\pi i(h/3+2k/3+l/2)} \\ &= f[1 + e^{2\pi i[(h+2k)/3+l/2]}]. \end{aligned}$$

For convenience, put $[(h+2k)/3+l/2] = g$.

$$F = f(1 + e^{2\pi ig}).$$

Since g may have fractional values, such as $\frac{1}{3}, \frac{2}{3}, \frac{5}{6}$, etc., this expression is still complex. Multiplication by the complex conjugate, however, will give the square of the absolute value of the resultant wave amplitude F .

$$\begin{aligned} |F|^2 &= f^2(1 + e^{2\pi ig})(1 + e^{-2\pi ig}) \\ &= f^2(2 + e^{2\pi ig} + e^{-2\pi ig}). \end{aligned}$$

By relation (e) of Sec. 4-5, this becomes

$$\begin{aligned} |F|^2 &= f^2(2 + 2 \cos 2\pi g) \\ &= f^2[2 + 2(2 \cos^2 \pi g - 1)] \\ &= f^2(4 \cos^2 \pi g) \\ &= 4f^2 \cos^2 \pi \left(\frac{h+2k}{3} + \frac{l}{2} \right) \\ &= 0 \quad \text{when } (h+2k) \text{ is a multiple of 3 and } l \text{ is odd.} \end{aligned}$$

It is by these missing reflections, such as $11 \cdot 1$, $11 \cdot 3$, $22 \cdot 1$, $22 \cdot 3$, that a hexagonal structure is recognized as being close-packed. Not all the reflections present have the same structure factor. For example, if $(h + 2k)$ is a multiple of 3 and l is even, then

$$\left(\frac{h+2k}{3} + \frac{l}{2} \right) = n, \quad \text{where } n \text{ is an integer;}$$

$$\cos \pi n = \pm 1,$$

$$\cos^2 \pi n = 1,$$

$$|F|^2 = 4f^2.$$

When all possible values of h , k , and l are considered, the results may be summarized as follows, where m is an integer:

$h + 2k$	l	$ F ^2$
$3m$	odd	0
$3m$	even	$4f^2$
$3m \pm 1$	odd	$3f^2$
$3m \pm 1$	even	f^2

4-7 APPLICATION TO POWDER METHOD

Any calculation of the intensity of a diffracted beam must always begin with the structure factor. The remainder of the calculation, however, varies with the particular diffraction method involved. For the Laue method, intensity calculations are so difficult that they are rarely made, since each diffracted beam has a different wavelength and blackens the film by a variable amount, depending on both the intensity and the film sensitivity for that particular wavelength. The factors governing diffracted intensity in the rotating-crystal and powder methods are somewhat similar, in that monochromatic radiation is used in each, but they differ in detail. The remainder of this chapter will be devoted to the powder method, since it is of most general utility in metallurgical work.

There are six factors affecting the relative intensity of the diffraction lines on a powder pattern:

1. polarization factor,
2. structure factor,
3. multiplicity factor,
4. Lorentz factor,
5. absorption factor,
6. temperature factor.

The first two of these have already been described, and the others will be discussed in the following sections.

4-8 MULTIPLICITY FACTOR

Consider the 100 reflection from a cubic lattice. In the powder specimen, some of the crystals will be so oriented that reflection can occur from their (100) planes. Other crystals of different orientation may be in such a position that reflection can occur from their (010) or (001) planes. Since all these planes have the same spacing, the beams diffracted by them all form part of the same cone. Now consider the 111 reflection. There are four sets of planes of the form {111} which have the same spacing but different orientation, namely, (111), (1 $\bar{1}$ $\bar{1}$), (1 $\bar{1}$ 1), and (11 $\bar{1}$), whereas there are only three sets of the form {100}. Therefore, the probability that {111} planes will be correctly oriented for reflection is $\frac{4}{3}$ the probability that {100} planes will be correctly oriented. It follows that the intensity of the 111 reflection will be $\frac{4}{3}$ that of the 100 reflection, other things being equal.

This relative proportion of planes contributing to the same reflection enters the intensity equation as the quantity p , the *multiplicity factor*, which may be defined as the number of different planes in a form having the same spacing. Parallel planes with different Miller indices, such as (100) and (100), are counted separately as different planes, yielding numbers which are double those given in the preceding paragraph. Thus the multiplicity factor for the {100} planes of a cubic crystal is 6 and for the {111} planes 8.

The value of p depends on the crystal system: in a tetragonal crystal, the (100) and (001) planes do not have the same spacing, so that the value of p for {100} planes is reduced to 4 and the value for {001} planes to 2. Values of the multiplicity factor as a function of hkl and crystal system are given in Appendix 13.

4-9 LORENTZ FACTOR

We must now consider certain trigonometrical factors which influence the intensity of the reflected beam. Suppose there is incident on a crystal [Fig. 4-13(a)] a narrow beam of parallel monochromatic rays, and let the crystal be rotated at a uniform angular velocity about an axis through O and normal to the drawing, so that a particular set of reflecting planes, assumed for convenience to be parallel to the crystal surface, passes through the angle θ_B , at which the Bragg law is exactly satisfied. As mentioned in Sec. 3-7, the intensity of reflection is greatest at the exact Bragg angle but still appreciable at angles deviating slightly from the Bragg angle, so that a curve of intensity vs. 2θ is of the form shown in Fig. 4-13(b). If all the diffracted beams sent out by the crystal as it rotates through the Bragg angle are received on a photographic film or in a counter, the total energy of the diffracted beam can be measured. This energy is called the *integrated intensity* of the reflection and is given by the area under the curve of Fig. 4-13(b). The integrated intensity is of much more interest than the maximum intensity, since the former is characteristic of the specimen while the latter is influenced by slight adjustments of the experimental apparatus. Moreover, in the visual comparison of the intensities of diffraction lines, it is the integrated intensity of the line rather than the maximum intensity which the eye evaluates.

The integrated intensity of a reflection depends on the particular value of θ_B

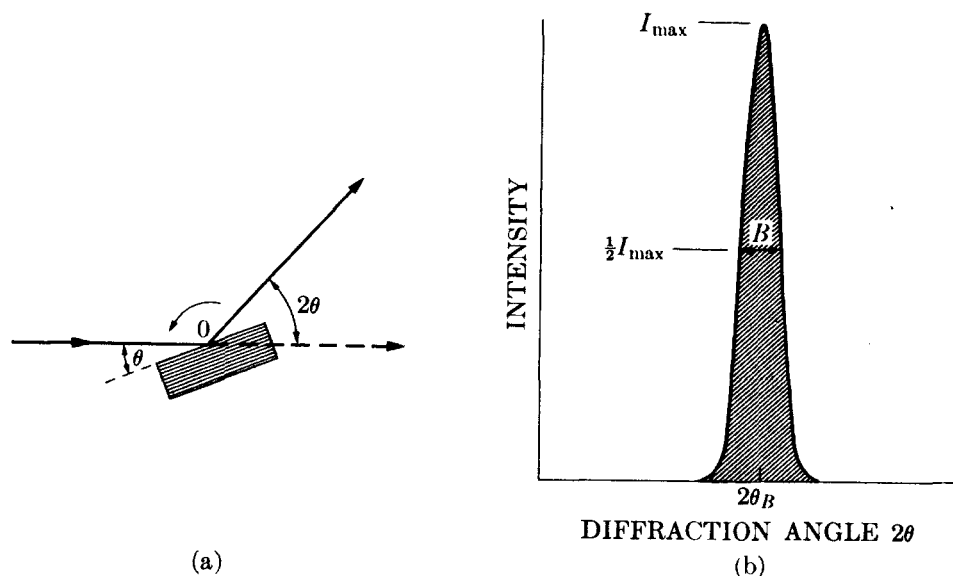


Fig. 4-13 Diffraction by a crystal rotated through the Bragg angle.

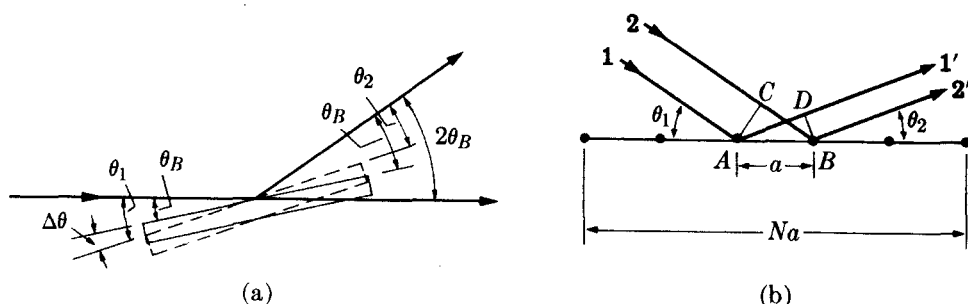


Fig. 4-14 Scattering in a fixed direction during crystal rotation.

involved, even though all other variables are held constant. We can find this dependence by considering, separately, two aspects of the diffraction curve: the maximum intensity and the breadth. When the reflecting planes make an angle θ_B with the incident beam, the Bragg law is exactly satisfied and the intensity diffracted in the direction $2\theta_B$ is a maximum. But some energy is still diffracted in this direction when the angle of incidence differs slightly from θ_B , and the total energy diffracted in the direction $2\theta_B$ as the crystal is rotated through the Bragg angle is given by the value of I_{\max} of the curve of Fig. 4-13(b). The value of I_{\max} therefore depends on the angular range of crystal rotation over which the energy diffracted in the direction $2\theta_B$ is appreciable. In Fig. 4-14(a), the dashed lines show the position of the crystal after rotation through a small angle $\Delta\theta$ from the Bragg position. The incident beam and the diffracted beam under consideration now make unequal angles with the reflecting planes, the former making an angle $\theta_1 = \theta_B + \Delta\theta$ and the latter an angle $\theta_2 = \theta_B - \Delta\theta$. The situation on an atomic scale is shown in Fig. 4-14(b). Here we need only consider a single plane of atoms, since the rays scattered by all other planes are in phase with the corresponding rays

scattered by the first plane. Let a equal the atom spacing in the plane and Na the total length* of the plane. The difference in path length for rays 1' and 2' scattered by adjacent atoms is given by

$$\begin{aligned}\delta_{1'2'} &= AD - CB \\ &= a \cos \theta_2 - a \cos \theta_1 \\ &= a[\cos(\theta_B - \Delta\theta) - \cos(\theta_B + \Delta\theta)].\end{aligned}$$

By expanding the cosine terms and setting $\sin \Delta\theta$ equal to $\Delta\theta$, since the latter is small, we find:

$$\delta_{1'2'} = 2a \Delta\theta \sin \theta_B,$$

and the path difference between the rays scattered by atoms at either end of the plane is simply N times this quantity. When the rays scattered by the two end atoms are one wavelength out of phase, the diffracted intensity will be zero. (The argument here is exactly analogous to that used in Sec. 3-7.) The condition for zero diffracted intensity is therefore

$$2Na \Delta\theta \sin \theta_B = \lambda,$$

or

$$\Delta\theta = \frac{\lambda}{2Na \sin \theta_B}.$$

This equation gives the maximum angular range of crystal rotation over which appreciable energy will be diffracted in the direction $2\theta_B$. Since I_{\max} depends on this range, we can conclude that I_{\max} is proportional to $1/\sin \theta_B$. Other things being equal, I_{\max} is therefore large at low scattering angles and small in the back-reflection region.

The breadth of the diffraction curve varies in the opposite way, being larger at large values of $2\theta_B$, as was shown in Sec. 3-7, where the half-maximum breadth B was found to be proportional to $1/\cos \theta_B$. The integrated intensity of the reflection is given by the area under the diffraction curve and is therefore proportional to the product $I_{\max} B$, which is in turn proportional to $(1/\sin \theta_B)(1/\cos \theta_B)$ or to $1/\sin 2\theta_B$. Thus, as a crystal is rotated through the Bragg angle, the integrated intensity of a reflection, which is the quantity of most experimental interest, turns out to be greater for large and small values of $2\theta_B$ than for intermediate values, other things being equal.

The preceding remarks apply just as well to the powder method as they do to the case of a rotating crystal, since the range of orientations available among the powder particles, some satisfying the Bragg law exactly, some not so exactly, are the equivalent of single-crystal rotation.

However, in the powder method, a second geometrical factor arises when we consider that the integrated intensity of a reflection at any particular Bragg angle depends on the number of crystals oriented at or near that angle. This number is

* If the crystal is larger than the incident beam, then Na is the irradiated length of the plane; if it is smaller, Na is the actual length of the plane.

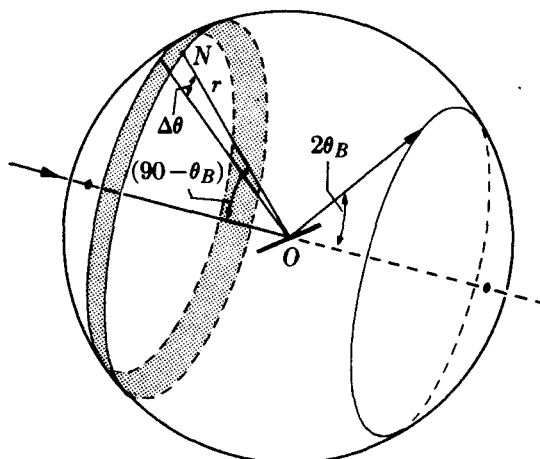


Fig. 4-15 The distribution of plane normals for a particular cone of reflected rays.

not constant even though the crystals are oriented completely at random. In Fig. 4-15 a reference sphere of radius r is drawn around the powder specimen located at O . For the particular hkl reflection shown, ON is the normal to this set of planes in one crystal of the powder. Suppose that the range of angles near the Bragg angle over which reflection is appreciable is $\Delta\theta$. Then, for this particular reflection, only those crystals will be in a reflecting position which have the ends of their plane normals lying in a band of width $r \Delta\theta$ on the surface of the sphere. Since the crystals are assumed to be oriented at random, the ends of their plane normals will be uniformly distributed over the surface of the sphere; the fraction favorably oriented for a reflection will be given by the ratio of the area of the strip to that of the whole sphere. If ΔN is the number of such crystals and N the total number, then

$$\frac{\Delta N}{N} = \frac{r \Delta\theta \cdot 2\pi r \sin (90^\circ - \theta_B)}{4\pi r^2} = \frac{\Delta\theta \cos \theta_B}{2}.$$

The number of crystals favorably oriented for reflection is thus proportional to $\cos \theta_B$ and is quite small for reflections in the backward direction.

In assessing relative intensities, we do not compare the total diffracted energy in one cone of rays with that in another but rather the integrated intensity per unit length of one diffraction line with that of another. For example, in the most common arrangement of specimen and film, the Debye-Scherrer method, shown in Fig. 4-16, the film obviously receives a greater proportion of a diffraction cone when the reflection is in the forward or backward direction than it does near $2\theta = 90^\circ$. Inclusion of this effect thus leads to a third geometrical factor affecting the intensity of a reflection. The length of any diffraction line being $2\pi R \sin 2\theta_B$, where R is the radius of the camera, the relative intensity per unit length of line is proportional to $1/\sin 2\theta_B$.

In intensity calculations, the three factors just discussed are combined into one and called the Lorentz factor. Dropping the subscript on the Bragg angle, we have:

$$\text{Lorentz factor} = \left(\frac{1}{\sin 2\theta}\right) (\cos \theta) \left(\frac{1}{\sin 2\theta}\right) = \frac{\cos \theta}{\sin^2 2\theta} = \frac{1}{4 \sin^2 \theta \cos \theta}.$$

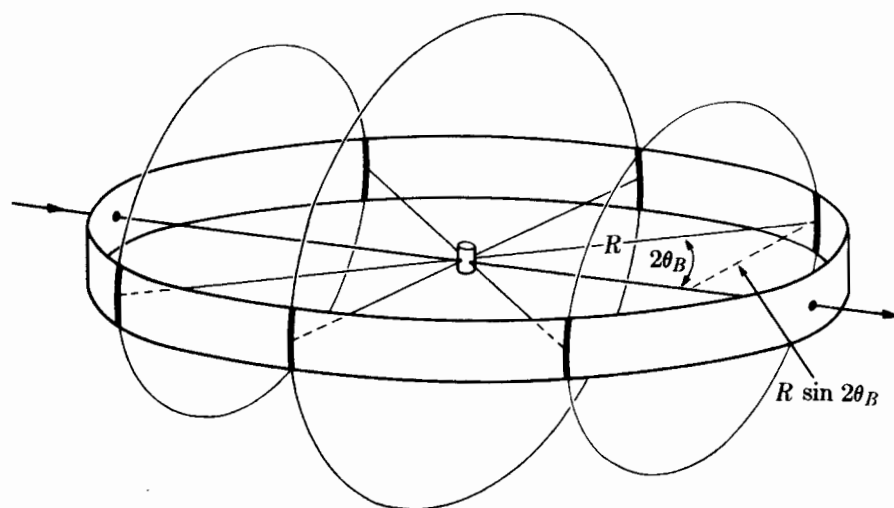


Fig. 4-16 Intersection of cones of diffracted rays with Debye-Scherrer film.

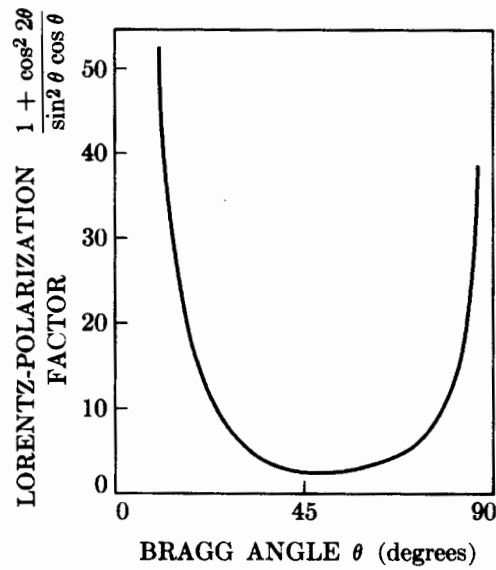


Fig. 4-17 Lorentz-polarization factor.

This in turn is combined with the polarization factor $\frac{1}{2}(1 + \cos^2 2\theta)$ of Sec. 4-2 to give the combined Lorentz-polarization factor which, with a constant factor of $\frac{1}{8}$ omitted, is given by

$$\text{Lorentz-polarization factor} = \frac{1 + \cos^2 2\theta}{\sin^2 \theta \cos \theta}.$$

Values of this factor are given in Appendix 14 and plotted in Fig. 4-17 as a function of θ . The overall effect of these geometrical factors is to decrease the intensity of reflections at intermediate angles compared to those in forward or backward directions.

4-10 ABSORPTION FACTOR

Still another factor affecting the intensities of the diffracted rays must be considered, and that is the absorption which takes place in the specimen itself. We allow for this effect in intensity calculations by introducing the *absorption factor A*, which is a number by which the calculated intensity is to be multiplied to allow for absorption. The calculation of *A* depends on the geometry of the diffraction method involved, and we will consider below the two most-used methods.

Debye-Scherrer Camera

The specimen in the Debye-Scherrer method has the form of a very thin cylinder of powder placed on the camera axis, and Fig. 4-18(a) shows the cross section of such a specimen. For the low-angle reflection shown, absorption of a particular ray in the incident beam occurs along a path such as *AB*; at *B* a small fraction of the incident energy is diffracted by a powder particle, and absorption of this diffracted beam occurs along the path *BC*. Similarly, for a high-angle reflection, absorption of both the incident and diffracted beams occurs along a path such as (*DE + EF*). The net result is that the diffracted beam is of lower intensity than one would expect for a specimen of no absorption.

A calculation of this effect shows that the relative absorption increases as θ decreases, for any given cylindrical specimen. That this must be so can be seen from Fig. 4-18(b) which applies to a specimen (for example, tungsten) of very high absorption. The incident beam is very rapidly absorbed, and most of the diffracted beams originate in the thin surface layer on the left side of the specimen; backward-reflected beams then undergo very little absorption, but forward-reflected beams have to pass through the whole specimen and are greatly absorbed. Actually, the forward-reflected beams in this case come almost entirely from the top and bottom

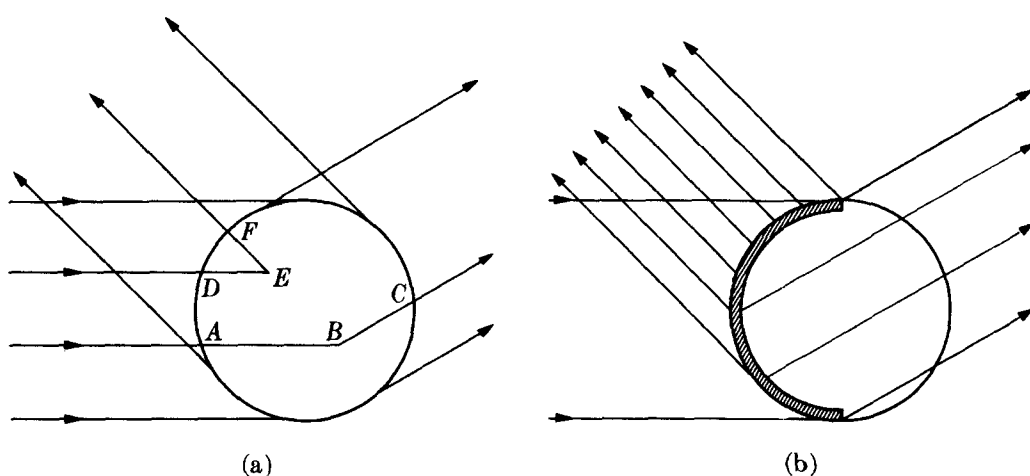


Fig. 4-18 Absorption in Debye-Scherrer specimens: (a) general case, (b) highly absorbing specimen.

edges of the specimen.* This difference in absorption between high- θ and low- θ reflections decreases as the linear absorption coefficient decreases, but the absorption is always greater for the low- θ reflections. We therefore write the Debye-Scherrer absorption factor as $A(\theta)$ to emphasize the fact that it varies with θ . Qualitatively, we conclude that $A(\theta)$ for any specimen increases as 2θ increases.

Exact calculation of the absorption factor for a cylindrical specimen is often difficult, so it is fortunate that this effect can usually be neglected in the calculation of diffracted intensities, when the Debye-Scherrer method is used. Justification of this omission will be found in Sec. 4-11.

The calculation of $A(\theta)$ for a cylindrical specimen proceeds as follows. In Fig. 4-18(a) the path length ($AB + BC$), for a given value of θ , is expressed as a function of the position x, y of the point B relative to coordinate axes fixed relative to the specimen. The absorption factor $A(\theta)$ is then given by the function $e^{-\mu(AB+BC)}$ integrated over the entire cross-sectional area of the specimen. This integration can only be performed numerically. The result is a table of values of $A(\theta)$ as a function of θ and of the product μr , where μ is the linear absorption coefficient of the specimen and r is its radius. The specimen is usually a powder compact, with an absorption coefficient given by

$$\mu_{\text{compact}} = \mu_{\text{solid}} \left(\frac{\rho_{\text{compact}}}{\rho_{\text{solid}}} \right) \quad (4-12)$$

where ρ is density.

Values of $A(\theta)$ have been calculated and tabulated by Bradley [4.1]. Tables of values can also be found in [G.11, Vol. 2, p. 295-299] and in [G.13, p. 663-666].

Diffractometer

A diffractometer specimen usually has the form of a flat plate making equal angles with the incident and diffracted beams as in Fig. 3-4, if one imagines a polycrystalline plate substituted for the single crystal indicated there. It is shown below that the absorption factor A is equal to $1/2\mu$, *independent of θ* . This independence of θ is due to the exact balancing of two opposing effects. When θ is small, the specimen area irradiated by an incident beam of fixed cross section is large, but the effective depth of x-ray penetration is small; when θ is large, the irradiated area is small, but the penetration depth is relatively large. The net effect is that the effective irradiated volume is constant and independent of θ . Absorption occurs in any case, however, and the larger the absorption coefficient of the specimen, the lower the intensity of the diffracted beams, other things being equal. The important fact to note is that absorption decreases the intensities of all diffracted beams by the same factor and therefore does not enter into the calculation of *relative* intensities.

* The powder patterns reproduced in Fig. 3-13 show this effect, at least on the original films. The lowest-angle line in each pattern is split in two, because the beam diffracted through the center of the specimen is so highly absorbed. It is important to keep the possibility of this phenomenon in mind when examining Debye-Scherrer photographs, or split low-angle lines may be incorrectly interpreted as separate diffraction lines from two different sets of planes.

The calculation of A proceeds as follows. The incident beam in the diffractometer is actually divergent (Sec. 7-2), but we will assume here that the beam is composed of parallel rays, because the divergence angle is very small (3° or less). We will calculate the effect of absorption in the specimen on the intensity of the diffracted beam, and, since this effect will come up again in later parts of this book, we will make our calculation quite general. In Fig. 4-19, the incident beam has intensity I_0 (ergs/cm²/sec), is 1 cm square in cross section, and is incident on the powder plate at an angle γ . We consider the energy diffracted from this beam by a layer of the powder of length l and thickness dx , located at a depth x below the surface. Since the incident beam undergoes absorption by the specimen over the path length AB , the energy incident per second on the layer considered is $I_0 e^{-\mu(AB)}$ (ergs/sec), where μ is the linear absorption coefficient of the powder compact, given by Eq. (4-12). Let a be the volume fraction of the specimen containing particles having the correct orientation for reflection of the incident beam, and b the fraction of the incident energy which is diffracted by unit volume. Then the energy diffracted per second by the layer considered, which has a volume $l dx$, is given by $ab l I_0 e^{-\mu(AB)} dx$. But this diffracted energy is also decreased by absorption, by a factor of $e^{-\mu(BC)}$, since the diffracted rays have a path length of BC in the specimen. The energy flux per second in the diffracted beam outside the specimen, i.e., the integrated intensity, is therefore given by

$$dI_D = ab l I_0 e^{-\mu(AB+BC)} dx \quad (\text{ergs/sec}). \quad (4-13)$$

But

$$l = \frac{1}{\sin \gamma}, \quad AB = \frac{x}{\sin \gamma}, \quad BC = \frac{x}{\sin \beta}.$$

Therefore,

$$dI_D = \frac{I_0 ab}{\sin \gamma} e^{-\mu x(1/\sin \gamma + 1/\sin \beta)} dx. \quad (4-14)$$

(The reader might note that the analogous absorption effect in transmission, rather than reflection, is given later as Eq. (9-7).)

For the particular specimen arrangement used in the diffractometer, $\gamma = \beta = \theta$, and the above equation becomes

$$dI_D = \frac{I_0 ab}{\sin \theta} e^{-2\mu x/\sin \theta} dx. \quad (4-15)$$

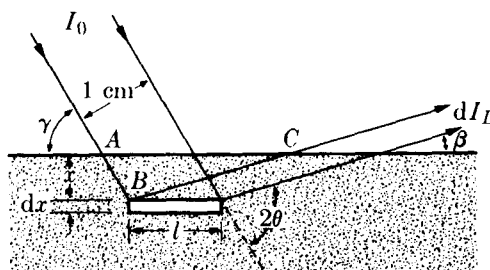


Fig. 4-19 Diffraction from a flat plate: incident and diffracted beams have a thickness of 1 cm in a direction normal to the plane of the drawing.

The total diffracted intensity is obtained by integrating over an infinitely thick specimen:

$$I_D = \int_{x=0}^{x=\infty} dI_D = \frac{I_0 ab}{2\mu}. \quad (4-16)$$

Here I_0 , b , and μ are constant for all reflections (independent of θ) and we may also regard a as constant. Actually, a varies with θ , but this variation is already taken care of by the $\cos \theta$ portion of the Lorentz factor (see Sec. 4-9) and need not concern us here. We conclude that the absorption factor $1/2\mu$ is independent of θ for a flat specimen making equal angles with the incident and diffracted beams, provided the specimen fills the incident beam at all angles and is effectively of infinite thickness.

The criterion adopted for "infinite thickness" depends on the sensitivity of our intensity measurements or on what we regard as negligible diffracted intensity. For example, we might arbitrarily but quite reasonably define infinite thickness as that thickness t which a specimen must have in order that the intensity diffracted by a thin layer on the back side be $\frac{1}{1000}$ of the intensity diffracted by a thin layer on the front side. Then, from Eq. (4-15) we have

$$\frac{dI_D \text{ (at } x = 0)}{dI_D \text{ (at } x = t)} = e^{2\mu t / \sin \theta} = 1000,$$

from which

$$t = \frac{3.45 \sin \theta}{\mu}.$$

This expression shows that "infinite thickness," for a metal specimen, is very small indeed. For example, suppose a specimen of nickel powder is being examined with Cu $K\alpha$ radiation at θ values approaching 90° . The density of the powder compact may be taken as about 0.6 the density of bulk nickel, which is 8.9 gm/cm^3 , leading to a value of μ for the compact of 261 cm^{-1} . The value of t is therefore $1.32 \times 10^{-2} \text{ cm}$, or about five thousandths of an inch.

4-11 TEMPERATURE FACTOR

So far we have considered a crystal as a collection of atoms located at fixed points in the lattice. Actually, the atoms undergo thermal vibration about their mean positions even at the absolute zero of temperature, and the amplitude of this vibration increases as the temperature increases. In aluminum at room temperature, the average displacement of an atom from its mean position is about 0.17 \AA , which is by no means negligible, being about 6 percent of the distance of closest approach of the mean atom positions in this crystal.

Increased thermal vibration of the atoms, as the result of an increase in temperature, has three main effects:

1. The unit cell expands, causing changes in plane spacings d and therefore in the 2θ positions of the diffraction lines. If the positions of one or more lines are

measured as a function of temperature (Sections 6-5 and 7-2), the thermal expansion coefficient of the specimen can be determined by x-ray diffraction.

2. The intensities of the diffraction lines decrease.
3. The intensity of the background scattering between lines increases.

The second and third effects are described below. Here we are usually interested not in intensity changes with temperature, but in variations in intensity with 2θ at constant temperature (usually room temperature).

Thermal agitation decreases the intensity of a diffracted beam because it has the effect of smearing out the lattice planes; atoms can be regarded as lying no longer on mathematical planes but rather in platelike regions of ill-defined thickness. Thus the reinforcement of waves scattered at the Bragg angle by various parallel planes, the reinforcement which is called a diffracted beam, is not as perfect as it is for a crystal with fixed atoms. This reinforcement requires that the path difference, which is a function of the plane spacing d , between waves scattered by adjacent planes be an integral number of wavelengths. Now the thickness of the platelike "planes" in which the vibrating atoms lie is, on the average, $2u$, where u is the average displacement of an atom from its mean position. Under these conditions reinforcement is no longer perfect, and it becomes more imperfect as the ratio u/d increases, i.e., as the temperature increases, since that increases u , or as θ increases, since high- θ reflections involve planes of low d value. Thus the intensity of a diffracted beam decreases as the temperature is raised, and, for a constant temperature, thermal vibration causes a greater decrease in the reflected intensity at high angles than at low angles. In intensity calculations we allow for this effect by introducing the *temperature factor* e^{-2M} , which is a number by which the calculated intensity is to be multiplied to allow for thermal vibration of the atoms. Qualitatively, we conclude that e^{-2M} decreases as 2θ increases. A method of calculating e^{-2M} when it is needed is outlined later, and Fig. 4-20 shows the result of such a calculation for iron.

The temperature effect and the previously discussed absorption effect in cylindrical specimens depend on angle in opposite ways and, to a first approximation, cancel each other in the Debye-Scherrer method. In back reflection, for

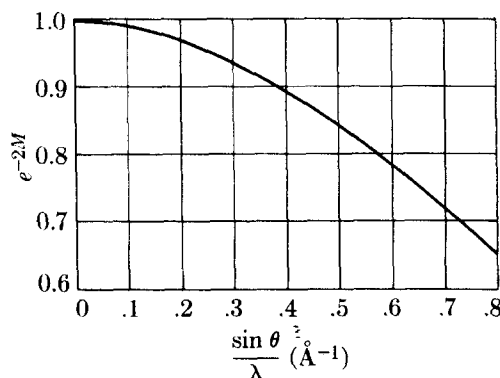


Fig. 4-20 Temperature factor e^{-2M} of iron at 20°C as a function of $(\sin \theta)/\lambda$.

example, the intensity of a diffracted beam is decreased very little by absorption but very greatly by thermal agitation, while in the forward direction the reverse is true. The two effects do not exactly cancel one another at all angles; however, if the comparison of line intensities is restricted to lines not differing too greatly in θ values, the absorption and temperature effects can be safely ignored in the Debye-Scherrer method. This is a fortunate circumstance, since both of these effects are rather difficult to calculate exactly.

Theoretically, thermal vibration of the atoms causes a very slight increase in the breadth B , measured at half-maximum intensity, of the diffraction lines. However, this expected effect has never been detected [4.2], and diffraction lines are observed to be sharp right up to the melting point, but their maximum intensity gradually decreases.

It is also worth noting that the mean amplitude of atomic vibration is not a function of the temperature alone but depends also on the elastic constants of the crystal. At any given temperature, the less "stiff" the crystal, the greater the vibration amplitude u . This means that u is much greater at any one temperature for a soft, low-melting-point metal like lead than it is for, say, tungsten. Substances with low melting points have quite large values of u even at room temperature and therefore yield rather poor back-reflection photographs. For example, thermal atomic vibration in lead at 20°C reduces the intensity of the highest-angle line observed with Cu $K\alpha$ radiation (at about $161^\circ 2\theta$) to only 18 percent ($e^{-2M} = 0.18$) of the value for atoms at rest.

In only one application described in this book (Sec. 14-10) will we need any quantitative information about the temperature factor e^{-2M} , but it is convenient to describe the calculation here. Formally, we allow for the effect by defining f as the atomic scattering factor of an atom undergoing thermal vibration, f_0 as the same quantity for an atom at rest, and relating the two by

$$f = f_0 e^{-M}.$$

(The quantity f_0 is then the scattering factor as usually tabulated, for example in Appendix 12.) Because the intensity of any line depends on f^2 , calculated intensities must be multiplied by e^{-2M} to allow for thermal vibration. The quantity M depends on both the amplitude u of thermal vibration and the scattering angle 2θ :

$$M = 2\pi^2 \left(\frac{\overline{u^2}}{d^2} \right) = 8\pi^2 \overline{u^2} \left(\frac{\sin \theta}{\lambda} \right)^2 = B \left(\frac{\sin \theta}{\lambda} \right)^2 \quad (4-17)$$

where $\overline{u^2}$ is the mean square displacement of the atom in a direction normal to the reflecting planes. The exact calculation of $\overline{u^2}$ as a function of temperature is extremely difficult, which means that M or B is hard to determine accurately. Debye has given the following expression:

$$M = \frac{6h^2 T}{mk\Theta^2} \left[\phi(x) + \frac{x}{4} \right] \left(\frac{\sin \theta}{\lambda} \right)^2, \quad (4-18)$$

where h is Planck's constant, T the absolute temperature, m the mass of the vibrating atom, k Boltzmann's constant, Θ the Debye characteristic temperature of the substance

in °K, $x = \Theta/T$, and $\phi(x)$ is a function tabulated, along with values of Θ , in Appendix 15. Because $m = A/N$, where A = atomic weight and N = Avogadro's number, the coefficient of the bracketed terms above becomes

$$\frac{6h^2T}{mk\Theta^2} = \frac{(6)(6.02 \times 10^{26})(6.63 \times 10^{-34})^2 T}{A\Theta^2(1.38 \times 10^{-23})(10^{-20})} = \frac{1.15 \times 10^4 T}{A\Theta^2}$$

if λ is in angstroms. Equation (4-18) is approximate and applies only to elements with cubic crystal structure.

For thorough treatments of the effect of thermal vibration on the diffraction pattern, see James [G.7] and Warren [G.30].

The thermal vibration of atoms has another effect on diffraction patterns. Besides decreasing the intensity of diffraction lines, it causes some general coherent scattering in all directions. This is called *temperature-diffuse scattering*; it contributes only to the general background of the pattern and its intensity gradually increases with 2θ . Contrast between lines and background naturally suffers, so this effect is a very undesirable one, leading in extreme cases to diffraction lines in the back-reflection region scarcely distinguishable from the background. Figure 4-21 illustrates this effect. In (a) is shown an extremely hypothetical pattern (only three lines, equally spaced, equally strong, with no background whatever) for atoms at rest; in (b) the lines, decreased in intensity by the factor e^{-2M} , are superimposed on a background of thermal diffuse scattering.

In the phenomenon of temperature-diffuse scattering we have another example, beyond those alluded to in Sec. 3-7, of scattering at non-Bragg angles. Here again it is not surprising that such scattering should occur, since the displacement of atoms from their mean positions constitutes a kind of crystal imperfection and leads to a partial breakdown of the conditions necessary for perfect destructive interference between rays scattered at non-Bragg angles.

The effect of thermal vibration also illustrates what has been called "the approximate law of conservation of diffracted energy." This law states that the total energy diffracted by a particular specimen under particular experimental conditions is roughly constant. Therefore, anything done to alter the physical condition of the specimen does not alter the total amount of diffracted energy but

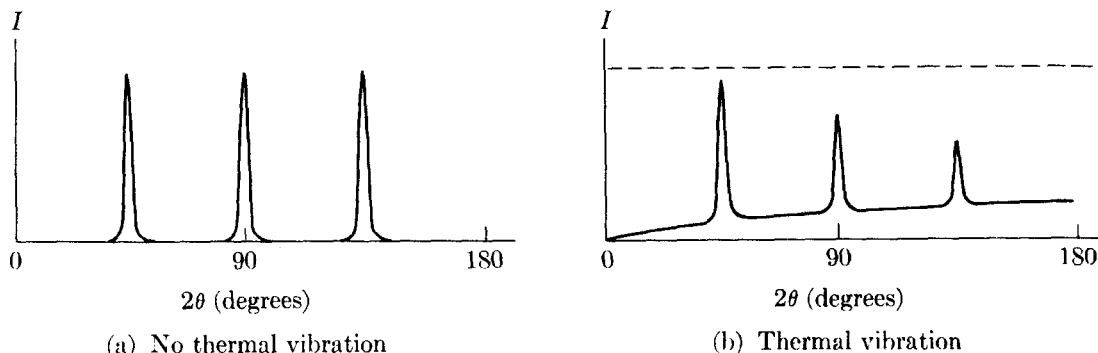


Fig. 4-21 Effect of thermal vibration of the atoms on a powder pattern. Very schematic, see text.

only its distribution in space. This "law" is not at all rigorous, but it does prove helpful in considering many diffraction phenomena. For example, at low temperatures there is very little background scattering due to thermal agitation and the diffraction lines are relatively intense; if the specimen is now heated to a high temperature, the lines will become quite weak and the energy which is lost from the lines will appear in a spread-out form as temperature-diffuse scattering.

4-12 INTENSITIES OF POWDER PATTERN LINES

We are now in a position to gather together the factors discussed in preceding sections into an equation for the relative intensity of powder pattern lines.

Debye-Scherrer Camera

(Approximate)

$$I = |F|^2 p \left(\frac{1 + \cos^2 2\theta}{\sin^2 \theta \cos \theta} \right), \quad (4-19)$$

where I = relative integrated intensity (arbitrary units), F = structure factor, p = multiplicity factor, and θ = Bragg angle. The trigonometric terms in parentheses are the Lorentz-polarization factor. In arriving at this equation, we have omitted factors which are constant for all lines of the pattern. For example, all that is retained of the Thomson equation (Eq. 4-2) is the polarization factor $(1 + \cos^2 2\theta)$, with constant factors, such as the intensity of the incident beam and the charge and mass of the electron, omitted. The intensity of a diffraction line is also directly proportional to the irradiated volume of the specimen and inversely proportional to the camera radius, but these factors are again constant for all diffraction lines and may be neglected. Omission of the temperature and absorption factors means that Eq. (4-19) is valid only for lines fairly close together on the pattern; this latter restriction is not as serious as it may sound. Finally, it should be remembered that this equation gives the relative *integrated* intensity, i.e., the relative area under the curve of intensity vs. 2θ .

If an exact expression is required, the absorption factor $A(\theta)$ and the temperature factor e^{-2M} must be inserted:

$$(Exact) \quad I = |F|^2 p \left(\frac{1 + \cos^2 2\theta}{\sin^2 \theta \cos \theta} \right) A(\theta) e^{-2M}. \quad (4-20)$$

Diffractometer

Here the absorption factor is independent of θ and so does not enter into the calculation of relative intensities. Equation (4-19) becomes still less precise, because there is no longer any approximate cancellation of the absorption and temperature factors. Equation (4-19) may still be used, for adjacent lines on the pattern, but the calculated intensity of the higher-angle line, relative to that of the lower-angle line, will always be somewhat too large because of the omission of the temperature factor.

The exact equation for the diffractometer is

$$(Exact) \quad I = |F|^2 p \left(\frac{1 + \cos^2 2\theta}{\sin^2 \theta \cos \theta} \right) e^{-2M}. \quad (4-21)$$

Qualifications

The two following effects can make the above intensity equations invalid:

1) *Preferred orientation.* From the way in which the $\cos \theta$ portion of the Lorentz factor was determined in Sec. 4-9, it follows that Eqs. (4-19) through (4-21) are valid only when the crystals making up the specimen are randomly oriented in space. Preferred orientation of the crystal grains causes radical disagreement between calculated and observed intensities and, when such disagreement exists, preferred orientation should be the first possible cause to be suspected. It is relatively easy to prepare powder-compact specimens from ground powders or metal filings so that the ideal of perfect randomness of orientation is closely approached, but virtually all polycrystalline specimens of metal wire, metal sheet, manufactured ceramics, and even natural rocks or minerals will exhibit more or less preferential orientation of the grains.

2) *Extinction* [G.7, G.30]. As mentioned in Sec. 3-7, all real crystals are imperfect, in the sense that they have a mosaic structure, and the degree of imperfection can vary greatly from one crystal to another. Equations (4-19) through (4-21) are derived on the basis of the so-called "ideally imperfect" crystal, one in which the mosaic blocks are quite small (of the order of 10^{-4} cm to 10^{-5} cm in thickness) and so disoriented that they are all essentially nonparallel. Such a crystal has maximum reflecting power. A crystal made up of large mosaic blocks, some or all of which are accurately parallel to one another, is more nearly perfect and has a lower reflecting power. This *decrease* in the integrated intensity of the diffracted beam as the crystal becomes more nearly perfect is called *extinction*. Extinction is absent for the ideally imperfect crystal, and the presence of extinction invalidates Eqs. (4-19) through (4-21). Any treatment that will make a crystal more imperfect will reduce extinction and, for this reason alone, powder specimens should be ground as fine as possible. Grinding not only reduces the crystal size but also tends to decrease the mosaic block size, disorient the mosaic blocks, and strain them nonuniformly. (The theory of the extinction effect is difficult. To prove that imperfections in a crystal increase its reflecting power would take us too far afield, but an experimental proof is given in Sec. 8-7.)

The extinction effect can operate, not only in single-crystal specimens, but also in the individual grains of polycrystalline specimens. Extinction may be assumed to be absent in ground or filed powders and is usually negligible in fine-grained polycrystalline specimens. If its presence is suspected in the latter, the specimen can always be reduced to powder by grinding or filing.

4-13 EXAMPLES OF INTENSITY CALCULATIONS

The use of Eq. (4-19) will be illustrated by the calculation of the position and relative intensities of the diffraction lines on a Debye-Scherrer pattern of copper, made with $Cu K\alpha$ radiation. The calculations are most readily carried out in tabular form, as in Table 4-2.

Remarks

Column 2: Since copper is face-centered cubic, F is equal to $4f_{Cu}$ for lines of unmixed indices and zero for lines of mixed indices. The reflecting plane indices, all unmixed, are

Table 4-2

1	2	3	4	5	6	7	8
Line	hkl	$h^2 + k^2 + l^2$	$\sin^2 \theta$	$\sin \theta$	θ	$\frac{\sin \theta}{\lambda} (\text{\AA}^{-1})$	f_{Cu}
1	111	3	0.1365	0.369	21.7°	0.24	22.1
2	200	4	0.1820	0.427	25.3	0.27	20.9
3	220	8	0.364	0.603	37.1	0.39	16.8
4	311	11	0.500	0.707	45.0	0.46	14.8
5	222	12	0.546	0.739	47.6	0.48	14.2
6	400	16	0.728	0.853	58.5	0.55	12.5
7	331	19	0.865	0.930	68.4	0.60	11.5
8	420	20	0.910	0.954	72.6	0.62	11.1

1	9	10	11	12	13	14
Line	F^2	p	$\frac{1 + \cos^2 2\theta}{\sin^2 \theta \cos \theta}$	Relative integrated intensity		
				Calc.	Calc.	Obs.
1	7810	8	12.03	7.52×10^5	10.0	vs
2	6990	6	8.50	3.56	4.7	s
3	4520	12	3.70	2.01	2.7	s
4	3500	24	2.83	2.38	3.2	s
5	3230	8	2.74	0.71	0.9	m
6	2500	6	3.18	0.48	0.6	w
7	2120	24	4.81	2.45	3.3	s
8	1970	24	6.15	2.91	3.9	s

written down in this column in order of increasing values of $(h^2 + k^2 + l^2)$, from Appendix 10.

Column 4: For a cubic crystal, values of $\sin^2 \theta$ are given by Eq. (3-10):

$$\sin^2 \theta = \frac{\lambda^2}{4a^2} (h^2 + k^2 + l^2).$$

In this case, $\lambda = 1.542 \text{ \AA}$ (Cu $K\alpha$) and $a = 3.615 \text{ \AA}$ (lattice parameter of copper). Therefore, multiplication of the integers in column 3 by $\lambda^2/4a^2 = 0.0455$ gives the values of $\sin^2 \theta$ listed in column 4. In this and similar calculations, three-figure accuracy is ample.

Column 6: Needed to determine the Lorentz-polarization factor and $(\sin \theta)/\lambda$.

Column 7: Obtained from Appendix 11. Needed to determine f_{Cu} .

Column 8: Obtained from Appendix 12.

Column 9: Obtained from the relation $F^2 = 16f_{\text{Cu}}^2$.

Column 10: Obtained from Appendix 13.

Column 11: Obtained from Appendix 14.

Column 12: These values are the product of the values in columns 9, 10, and 11, according to Eq. (4-19).

Column 13: Values from column 12 recalculated to give the first line an arbitrary intensity of 10, i.e., "normalized" to 10 for the first line.

Column 14: These entries give the observed intensities, visually estimated according to the following simple scale, from the original film for copper in Fig. 3-13 (vs = very strong, s = strong, m = medium, w = weak).

The agreement obtained here between observed and calculated intensities is satisfactory. Note how the value of the multiplicity p exerts a strong control over the line intensity. The values of $|F|^2$ and of the Lorentz-polarization factor vary smoothly with θ , but the values of p , and therefore of I , vary quite irregularly.

A more complicated structure may now be considered, namely, that of the zinc-blende form of ZnS, shown in Fig. 2-19(b). This form of ZnS is cubic and has a lattice parameter of 5.41 Å. We will calculate the relative intensities of the first six lines on a Debye-Scherrer pattern made with Cu $K\alpha$ radiation.

As always, the first step is to work out the structure factor. ZnS has four zinc and four sulfur atoms per unit cell, located in the following positions:

Zn: $\frac{1}{4} \frac{1}{4} \frac{1}{4}$ + face-centering translations,

S: 0 0 0 + face-centering translations.

Since the structure is face-centered, we know that the structure factor will be zero for planes of mixed indices. We also know, from example (e) of Sec. 4-6, that the terms in the structure-factor equation corresponding to the face-centering translations can be factored out and the equation for unmixed indices written down at once:

$$F = 4[f_S + f_{Zn}e^{(\pi i/2)(h+k+l)}].$$

$|F|^2$ is obtained by multiplication of the above by its complex conjugate:

$$|F|^2 = 16[f_S + f_{Zn}e^{(\pi i/2)(h+k+l)}][f_S + f_{Zn}e^{-(\pi i/2)(h+k+l)}].$$

This equation reduces to the following form:

$$|F|^2 = 16 \left[f_S^2 + f_{Zn}^2 + 2f_S f_{Zn} \cos \frac{\pi}{2}(h+k+l) \right].$$

Further simplification is possible for various special cases:

$$|F|^2 = 16(f_S^2 + f_{Zn}^2) \quad \text{when } (h+k+l) \text{ is odd}; \quad (4-22)$$

$$|F|^2 = 16(f_S - f_{Zn})^2 \quad \text{when } (h+k+l) \text{ is an odd multiple of 2}; \quad (4-23)$$

$$|F|^2 = 16(f_S + f_{Zn})^2 \quad \text{when } (h+k+l) \text{ is an even multiple of 2}. \quad (4-24)$$

The intensity calculations are carried out in Table 4-3, with some columns omitted for the sake of brevity.

Remarks

Columns 5 and 6: These values are read from scattering-factor curves plotted from the data of Appendix 12.

Column 7: $|F|^2$ is obtained by the use of Eq. (4-22), (4-23), or (4-24), depending on the particular values of hkl involved. Thus, Eq. (4-22) is used for the 111 reflection and Eq. (4-24) for the 220 reflection.

Columns 10 and 11: The agreement obtained here between calculated and observed intensities is again satisfactory. In this case, both the values of $|F|^2$ and of p vary irregularly with θ , leading to an irregular variation of I .

One further remark on intensity calculations is necessary. In the powder method, two sets of planes with different Miller indices can reflect to the same

Table 4-3

1	2	3	4	5	6
Line	hkl	θ	$\frac{\sin \theta}{\lambda} (\text{\AA}^{-1})$	f_S	f_{Zn}
1	111	14.3°	0.16	12.3	25.8
2	200	16.6	0.19	11.4	24.6
3	220	23.8	0.26	9.7	22.1
4	311	28.2	0.30	9.0	20.7
5	222	29.6	0.32	8.8	20.0
6	400	34.8	0.37	8.2	18.4

1	7	8	9	10	11
Line	$ F ^2$	p	$\frac{1 + \cos^2 2\theta}{\sin^2 \theta \cos \theta}$	Relative intensity	
				Calc.	Obs.
1	13070	8	30.0	10.0	vs
2	2790	6	21.7	1.2	w
3	16180	12	9.76	6.1	vs
4	8150	24	6.64	4.1	vs
5	2010	8	5.95	0.3	vw
6	11320	6	4.19	0.9	w

point on the film: for example, the planes (411) and (330) in the cubic system, since they have the same value of $(h^2 + k^2 + l^2)$ and hence the same spacing, or the planes (501) and (431) of the tetragonal system, since they have the same values of $(h^2 + k^2)$ and l^2 . In such a case, the intensity of each reflection must be calculated separately, since in general the two will have different multiplicity and structure factors, and then added to find the total intensity of the line.

4-14 MEASUREMENT OF X-RAY INTENSITY

In the examples just given, the observed intensity was estimated simply by visual comparison of one line with another. Although this simple procedure is satisfactory in a surprisingly large number of cases, there are problems in which a more precise measurement of diffracted intensity is necessary. Two methods are available for making such measurements, one dependent on the photographic effect of x-rays and the other on the ability of x-rays to activate an electronic counter. These methods have already been mentioned briefly in Sec. 1-8 and will be described more fully in Chaps. 6 and 7, respectively.

PROBLEMS

- * 4-1 Derive an expression for the absorption factor of a diffractometer specimen in the form of a flat plate of finite thickness t . (Note that the absorption factor now depends on θ .)

* 4-2 Consider the highest-angle line on the diffraction pattern of Cu and of Pb, measured at 20°C with Cu $K\alpha$ radiation. By what percentage is the intensity of each of these lines reduced by thermal vibration of the atoms?

4-3 Consider a hypothetical element whose structure can be based on either of the following:

- Cell A, base-centered tetragonal containing two atoms per cell, at $0\ 0\ 0$ and $\frac{1}{2}\ \frac{1}{2}\ 0$, for which $a = 2\text{ \AA}$ and $c = 3\text{ \AA}$;
- Cell B, simple tetragonal with one atom per cell at $0\ 0\ 0$.

Determine simplified structure-factor equations for each cell and the positions (2θ values) of the first four lines that would be *observed* ($F^2 \neq 0$) on a powder pattern made with Cu $K\alpha$ radiation. Plot the 2θ values of these lines in the manner of Fig. 10-2, and label each line with its indices relative to Cell A and Cell B. Draw the two cells in the proper relation to one another, and show that the indices of any one observed line, other than obvious ones of the form $0\ 0\ l$, refer to the same plane of atoms.

[This problem illustrates several points: (1) we can choose any unit cell we wish, (2) the Miller indices of any given plane of atoms depend on the choice of cell, and (3) the diffraction pattern of the material is independent of the choice of cell.]

* 4-4 Derive simplified expressions for F^2 for diamond, including the rules governing observed reflections. This crystal is cubic and contains 8 carbon atoms per unit cell, located in the following positions:

$$\begin{array}{cccc} 0\ 0\ 0 & \frac{1}{2}\ \frac{1}{2}\ 0 & \frac{1}{2}\ 0\ \frac{1}{2} & 0\ \frac{1}{2}\ \frac{1}{2} \\ \frac{1}{4}\ \frac{1}{4}\ \frac{1}{4} & \frac{3}{4}\ \frac{3}{4}\ \frac{1}{4} & \frac{3}{4}\ \frac{1}{4}\ \frac{3}{4} & \frac{1}{4}\ \frac{3}{4}\ \frac{3}{4} \end{array}$$

4-5 A certain tetragonal crystal has four atoms of the same kind per unit cell, located at $0\ \frac{1}{2}\ \frac{1}{4}$, $\frac{1}{2}\ 0\ \frac{1}{4}$, $\frac{1}{2}\ 0\ \frac{3}{4}$, $0\ \frac{1}{2}\ \frac{3}{4}$. (Do not change axes.)

- Derive simplified expressions for F^2 .
- What is the Bravais lattice of this crystal?
- What are the values of F^2 for the 100, 002, 111, and 011 reflections?

* 4-6 Derive simplified expressions for F^2 for the wurtzite form of ZnS, including the rules governing observed reflections. This crystal is hexagonal and contains 2 ZnS per unit cell, located in the following positions:

$$\text{Zn: } 0\ 0\ 0, \frac{1}{3}\ \frac{2}{3}\ \frac{1}{2},$$

$$\text{S: } 0\ 0\ \frac{2}{3}, \frac{1}{3}\ \frac{2}{3}\ \frac{7}{6}.$$

Note that these positions involve a common translation, which may be factored out of the structure-factor equation.

Ignore the absorption and temperature factors in all of the following problems.

* 4-7 A Debye-Scherrer pattern of tungsten (BCC) is made with Cu $K\alpha$ radiation. The first four lines on this pattern were observed to have the following θ values:

Line	θ
1	20.3°
2	29.2
3	36.7
4	43.6

Index these lines (i.e., determine the Miller indices of each reflection by the use of Eq. (3-10) and Appendix 10) and calculate their relative integrated intensities.

4-8 A Debye-Scherrer pattern is made of silicon, which has the same structure as diamond, with $\text{Cu } K\alpha$ radiation. What are the indices of the first two lines on the pattern, and what is the ratio of the integrated intensity of the first to that of the second?

* **4-9** A Debye-Scherrer pattern is made of the intermediate phase InSb with $\text{Cu } K\alpha$ radiation. This phase has the zinc-blende structure and a lattice parameter of 6.46 Å. What are the indices of the first two lines on the pattern, and what is the ratio of the integrated intensity of the first to the second?

4-10 Calculate the relative integrated intensities of the first six lines of the Debye-Scherrer pattern of zinc, made with $\text{Cu } K\alpha$ radiation. The indices and observed θ values of these lines are:

Line	hkl	θ
1	00 · 2	18.8°
2	10 · 0	20.2
3	10 · 1	22.3
4	10 · 2	27.9
5	11 · 0, 10 · 3	36.0
6	00 · 4	39.4

(Line 5 is made up of two unresolved lines from planes of very nearly the same spacing.) Compare your results with the intensities observed in the pattern shown in Fig. 3-13.